

Microbial adaptations towards utilisation of the explosive RDX in soil

Dana Khdr Sabir

PhD

University of York
Biology

March 2015

Abstract

Hexahydro-1,3,5-trinitro-1,3,5-triazine (RDX) is a synthetic toxic explosive compound which was introduced into the environment during the Second World War. Microorganisms have adapted to degrade RDX and the enzymes involved include an unusual cytochrome P450, termed XplA, that is N-terminally-fused to a flavodoxin domain, and a flavodoxin reductase partner, XplB.

To discover new RDX-degrading enzymes, selective enrichments were performed on explosive-contaminated soil samples from the United Kingdom, Belgium, Germany, Czech Republic, Ukraine and Moldova. Thirteen RDX-degrading bacteria were isolated and all identified as *Rhodococcus* spp. The *xplA* gene was identified in all isolates and TNT found to inhibit RDX-degradation.

The evolutionary origin of *xplA* was analysed in eleven aerobic RDX-degrading bacteria belonging to four different genera: *Rhodococcus* spp., *Microbacterium*, *Gordonia* and *Williamsia*. Only six single nucleotide polymorphisms were found in the *xplA/xplB* region, emphasising the recent evolution of these genes. Additionally, genes flanking *xplA/xplB* were nearly identical between the four genera and together comprise a genomic island approximately 36 kbp in size which has been transmitted horizontally within a transposable element.

In *Gordonia* sp. KTR9 several gene re-arrangements were found on the *xplA/xplB*-containing plasmid, including the fusion of *xplB* to *glnA*. The XplB portion of the fusion was found to be inactive due to a serine to tryptophan substitution, whereas the GS portion, encoded by *glnA*, has activity, despite missing 15 % of the C-terminal region.

Finally, the evolutionary origin of *xplA* was investigated by characterising three putative cytochromes P450: Gt-XplA from *Gordonia terrae* strain NBRC 100016; and CYPA and CYPB from *Gordonia polyisoprenivorans* NBRC 16320. Although purified Gt-XplA, CYPA and CYPB did not have activity towards RDX, activity was detected following the substitution of amino acids into the putative active site of GT-XplA and truncated-CYPA.

List of Contents

| | |
|--|-------------|
| ABSTRACT | II |
| LIST OF CONTENTS | III |
| LIST OF FIGURES | VI |
| LIST OF TABLES | XIII |
| ACKNOWLEDGEMENTS | XIV |
| AUTHOR'S DECLARATION | XVI |
| CHAPTER 1: INTRODUCTION | 17 |
| 1.1 Microbial adaptation to xenobiotic compounds | 18 |
| 1.2 Molecular mechanisms of microbial evolution | 19 |
| 1.2.1 Microbial evolution through small scale mutation in existing DNA | 19 |
| 1.1.2 Large scale cellular DNA manipulation | 21 |
| 1.1.3 DNA acquisition through horizontal gene transfer | 26 |
| 1.3 Explosives as xenobiotic compounds | 30 |
| 1.3.1 Overview of explosives | 30 |
| 1.3.2 Environmental contamination by explosives | 33 |
| 1.3.3 Microbial transformation of TNT | 34 |
| 1.3.4 Microbial degradation of RDX | 37 |
| 1.3.5 RDX denitration by cytochrome P450 XplA | 42 |
| 1.3.6 Application of XplA and XplB for environmental remediation | 45 |
| 1.3.7 Aims of the project | 47 |
| CHAPTER 2: MATERIALS AND METHODS | 48 |
| 2.1 Chemicals and reagents | 49 |
| 2.2 Bacterial strains | 49 |
| 2.3 Plasmids | 49 |
| 2.4 Media | 55 |
| 2.4.1 Minimal medium | 55 |
| 2.4.2 Luria Bertani Broth (LB) medium | 55 |
| 2.4.3 MacConkey Broth | 56 |
| 2.4.4 SOC media | 56 |
| 2.4.5 RDX dispersion agar plates | 56 |
| 2.4.6 <i>Gordonia terrae</i> strain NBRC 100016 growth medium | 56 |
| 2.4.7 <i>Gordonia polyisoprenivorans</i> NBRC 16320 growth medium | 56 |
| 2.4.8 Y medium | 57 |
| 2.5 Microbiological techniques | 57 |
| 2.5.1 Bacterial growth on RDX medium | 57 |
| 2.5.2 Resting cell experiments | 57 |
| 2.5.3 Effect of TNT on RDX degradation by bacteria | 58 |
| 2.6 Molecular biology techniques | 58 |
| 2.6.1 Bacterial total genome extraction | 58 |
| 2.6.2 Total genome sequencing | 58 |
| 2.6.3 Polymerase chain reaction | 58 |
| 2.6.4 Agarose gel electrophoresis | 59 |
| 2.6.5 Purification of DNA fragments for sequencing | 59 |
| 2.6.6 Short fragment of DNA sequencing and analysis | 60 |

| | |
|---|------------|
| 2.2.7 Phylogenetic analysis | 60 |
| 2.6.8 Generating competent <i>E. coli</i> cells | 60 |
| 2.6.9 Plasmid transformation by heat shock method | 61 |
| 2.6.10 Plasmid extraction | 61 |
| 2.6.11 Restriction endonuclease digestion of DNA | 61 |
| 2.6.12 DNA Cloning | 61 |
| 2.6.13 Site directed mutagenesis | 62 |
| 2.6.14 Colony PCR | 62 |
| 2.7 Protein Techniques | 63 |
| 2.7.1 Protein quantification | 63 |
| 2.7.2 Cell lysis by sonication | 64 |
| 2.7.3 Expression and purification of XplA and XplB from <i>R. rhodochrous</i> 11Y | 64 |
| 2.7.4 Sodium Dodecyl Sulphate – PolyAcrylamide Gel Electrophoresis (SDS-PAGE) with the Bio-Rad system | 64 |
| 2.7.5 Protein identification by MALDI-MS analysis | 64 |
| 2.7.6 Western blot analysis | 65 |
| 2.7.7 Homology modelling | 66 |
| 2.8 Analytical Techniques | 66 |
| 2.8.1 High-performance liquid chromatography (HPLC) | 66 |
| 2.8.2 Griess (nitrite) assay | 67 |
| CHAPTER 3: ISOLATION OF RDX-DEGRADING BACTERIA FROM DIFFERENT GEOGRAPHICAL LOCATIONS | 69 |
| 3.1 Introduction | 70 |
| 3.2 Materials and Methods | 71 |
| 3.2.1 Sample collections | 71 |
| 3.2.2 RDX and TNT extraction from the soil | 71 |
| 3.2.3 Enrichment cultures | 71 |
| 3.2.4 Identification and characterisation of RDX-degrading bacteria | 73 |
| 3.2.5 Effect of TNT on the growth of <i>R. rhodochrous</i> 11Y | 74 |
| 3.2.6 Effect of dinitrotoluenes on the activity of purified XplA | 74 |
| 3.3 Results | 75 |
| 3.3.1 RDX and TNT extraction from soil samples | 75 |
| 3.3.2 Identification and characterisation of the RDX-degrading bacteria | 80 |
| 3.4 Discussion | 90 |
| CHAPTER 4: CHARACTERISATION OF THE RDX-DEGRADING GENOMIC ISLAND | 94 |
| 4.1 Introduction | 95 |
| 4.2 Materials and Methods | 97 |
| 4.3 Results | 99 |
| 4.3.1 Characterisation of RDX-degrading isolates | 99 |
| 4.3.2 Analysis of the sequence flanking <i>xplA</i> in the RDX-degraders | 104 |
| 4.3.3 Total genome sequencing | 113 |
| 4.3.3.1 Analysis of the total genome sequence of <i>R. rhodochrous</i> 11Y | 114 |
| 4.3.3.2 Analysis of the total genome sequence of <i>Williamsia</i> sp. EG1 | 117 |
| 4.4 Discussion | 121 |
| CHAPTER 5: EXPRESSION, PURIFICATION AND CHARACTERISATION OF THE XPLB-GLUTAMINE SYNTHETASE FUSION PROTEIN | 126 |
| 5.1 Introduction | 127 |

| | |
|--|------------|
| 5. 2 Materials and Methods | 129 |
| 5.2.1 Cloning <i>xplB-glnA</i> | 129 |
| 5.2.2 Expression of <i>xplB-glnA</i> | 129 |
| 5.2.3 Reductase assay for XplB and XplB-GS | 130 |
| 5.2.4 Determination of the amount of FAD in XplB | 130 |
| 5.2.5 Activity assay for glutamine synthetase | 131 |
| 5.3 Results | 132 |
| 5.3.1 Cloning and expression of <i>xplB-glnA</i> | 132 |
| 5.3.2 Characterisation of XplB-GS | 137 |
| 5.3.3 Characterization of GS portion of XplB-GS | 146 |
| 5.4 Discussion | 151 |
| 5.4.1 The XplB portion of the XplB-GS fusion | 151 |
| 5.4.2 The GS portion of the XplB-GS fusion | 152 |
| CHAPTER 6: EXPRESSION, PURIFICATION AND CHARACTERISATION OF XPLA-HOMOLOGUES FROM NON-RDX DEGRADING BACTERIA | 154 |
| 6.1 Introduction | 155 |
| 6.2 Materials and Methods | 160 |
| 6.2.1 Cloning of the cytochrome P450 genes | 160 |
| 6.2.2 Expression of the cytochromes P450 | 161 |
| 6.2.3 Purification of the cytochromes P450 | 161 |
| 6.2.4 Spectra analysis of purified protein | 162 |
| 6.2.5 Whole cell assays | 162 |
| 6.3 Results | 164 |
| 6.3.1 Sequence analysis of the XplA homologues | 164 |
| 6.3.2 Cloning and expression of putative ancestral XplA cytochromes P450 | 169 |
| 6.3.2 Spectrophotometric analysis of the putative cytochromes P450 | 179 |
| 6.3.3 Mutagenesis study and whole cell activity assay | 182 |
| 6.4 Discussion | 186 |
| Ancestral XplA cytochromes P450 | 186 |
| Origin of the <i>xplA</i> and <i>xplB</i> genes | 190 |
| CHAPTER 7: FINAL DISCUSSION | 191 |
| 7.1 Final discussion | 192 |
| LIST OF ABBREVIATIONS | 199 |
| REFERENCES | 202 |

List of Figures

| | |
|--|----|
| Figure 1.1: Physiological and lifestyle diversity of number of enteric bacteria.. | 18 |
| Figure 1.2: Photos of the pioneer scientists of modern molecular evolution - Motoo Kimura and Tomoko Ohta.. | 20 |
| Figure 1.3: Transposition of Class II (Tn3) transposable element..... | 23 |
| Figure 1.4: Transposition of the Integrative and Conjugative Elements (ICEs). | 24 |
| Figure 1.5: Life cycle of Integrative and Conjugative Elements (ICEs) lifecycle | 25 |
| Figure 1.6: Example of distribution of the horizontally acquired genes amongst the genome of various bacteria. | 26 |
| Figure 1.7: Examples of explosives and explosives transformation products of the explosives in the explosive contaminated sites..... | 31 |
| Figure 1.8: Biotransformation pathways of TNT..... | 36 |
| Figure 1.9: Biodegradation of RDX under anaerobic conditions. | 40 |
| Figure 1.10: Aerobic denitration pathway of RDX in <i>Rhodococcus</i> sp. DN22..... | 41 |
| Figure 1.11: The 7.5 kbp fragment flanking the <i>xplA/xplB</i> region from <i>R. rhodochrous</i> 11Y..... | 42 |
| Figure 1.12: Spectrophotometric analysis of the purified XplA from <i>R. rhodochrous</i> 11Y | 43 |
| Figure 1.13: Growth of eight week old transgenic and wild-type plants in uncontaminated and soil contaminated soil with RDX..... | 46 |
| Figure 2.1: Vector map of pET-16b..... | 50 |
| Figure 2.2: Vector map of pET-28a(+) | 51 |
| Figure 2.3: Vector map of pGEX-2T. | 51 |
| Figure 2.4: Standard curve of the protein concentration versus absorbance at 595 nm.. | 63 |

| | |
|---|----|
| Figure 2.5: Principle of the Griess assay..... | 68 |
| Figure 2.6: Griess assay standard curve to determine the concentration of nitrite using the absorbance 540 nm..... | 68 |
| Figure 3.1: Colorimetric assay to detect TNT in soil samples from Belgium. | 75 |
| Figure 3.2: Overlay HPLC chromatograms from the RDX and TNT extraction of Ukraine and Moldova soil samples..... | 76 |
| Figure 3.3: Overlay chromatograms from RDX and TNT extraction of Czech Republic soil samples..... | 76 |
| Figure 3.4: Overlay HPLC chromatograms of the selective enrichment for the Ukraine soil sample..... | 77 |
| Figure 3.5: RDX-removal from the enrichment culture using different soil inocula from the UK soil sample..... | 78 |
| Figure 3.6: Growth of <i>R. rhodochrous</i> 11Y in medium containing 450 μ M KNO ₃ or 150 μ M RDX in the absence or presence of TNT. | 79 |
| Figure 3.7: An RDX dispersion plate inoculated with single colonies isolated from soil samples..... | 81 |
| Figure 3.8: Unrooted phylogenetic tree for the RDX-degrading bacteria isolated in this study..... | 83 |
| Figure 3.9: RDX uptake by isolated bacteria during the resting cell assay..... | 84 |
| Figure 3.10: PCR products from amplification of the <i>xplA</i> region in newly isolated RDX-degrading bacteria..... | 85 |
| Figure 3.11: Percentage of RDX removal by RDX-degrading isolates in the presence of 2 μ M of TNT over 9 h..... | 86 |
| Figure 3.12: Effect of increasing concentrations of TNT on growth of <i>R. rhodochrous</i> 11Y in minimal medium containing RDX or KNO ₂ as the sole source of nitrogen..... | 87 |
| Figure 3.13: Effect of 2-ADNT and 4-ADNT on XplA activity..... | 88 |

| | |
|--|-----|
| Figure 3.14: Effect of 2,4- and 2,6-DNT on XplA activity..... | 89 |
| Figure 4.1: Sequence comparison of the 7.5 kbp region flanking <i>xplA/xplB</i> in <i>R. rhodochrous</i> 11Y with the partial 52.2 kbp flanking <i>xplA</i> region of <i>Microbacterium</i> sp. MA1..... | 96 |
| Figure 4.2: The regions flanking <i>xplA</i> in <i>Gordonia</i> sp. KTR9..... | 96 |
| Figure 4.3: Schematic representation of the primer pair locations used to amplify the <i>xplA</i> flanking regions in <i>Rhodococcus</i> spp. and <i>Williamsia</i> sp. EG1..... | 98 |
| Figure 4.4: Rooted phylogenetic tree analysis of the RDX-degrading isolates used to characterise RDX-degrading genomic island..... | 100 |
| Figure 4.5: Growth and RDX-removal activity between eight <i>Rhodococcus</i> spp isolated from six distinct geographical locations | 102 |
| Figure 4.6: Growth and RDX-removal activity by <i>R. rhodochrous</i> 11Y, <i>Williamsia</i> sp. EG1, <i>Microbacterium</i> sp. MA1, and <i>Gordonia</i> sp. KTR9..... | 103 |
| Figure 4.7: Comparison of the genes flanking <i>xplA</i> between <i>R. rhodochrous</i> 11Y and <i>Microbacterium</i> sp. MA1..... | 104 |
| Figure 4.8: PCR products from amplifying the regions between <i>marR</i> to the end of <i>xplA</i> within the genome of <i>Williamsia</i> sp. EG1..... | 106 |
| Figure 4.9: PCR products from amplifying upstream of <i>xplB</i> and downstream of <i>xplA</i> in <i>Williamsia</i> sp. EG1 | 107 |
| Figure 4.10: PCR products from the amplification of the <i>xplB</i> region in <i>Williamsia</i> sp. EG1 | 108 |
| Figure 4.11: PCR products of amplify the genes upstream of <i>marR</i> region in <i>Williamsia</i> sp. EG1 | 109 |
| Figure 4.12: PCR products amplifying the region between <i>marR</i> and <i>xplB</i> gene in <i>Williamsia</i> sp. EG1..... | 110 |

| | |
|---|-----|
| Figure 4.13: Comparison of the published contigs of <i>Williamsia</i> sp. EG1 to partial sequence of <i>Microbacterium</i> sp. MA1..... | 111 |
| Figure 4.14: Comparison of the <i>xplA</i> flanking region among <i>Microbacterium</i> sp. MA1, <i>R. rhodochrous</i> 11Y and <i>Williamsia</i> sp. EG1..... | 112 |
| Figure 4.15: Comparison of the nucleotide sequence of the <i>xplA</i> and <i>xplB</i> genes amongst the RDX degrading bacteria..... | 112 |
| Figure 4.16: Genome analysis of <i>R. rhodochrous</i> 11Y and <i>Williamsia</i> sp. EG1 using an Agilent TapeStation 2200..... | 113 |
| Figure 4.17: Schematic representation of the partial 53,711 bp plasmid sequence flanking <i>xplA</i> and <i>xplB</i> in <i>R. rhodochrous</i> 11Y..... | 116 |
| Figure 4.18: Schematic representation of the RDX-degrading genomic island in four genera of aerobic RDX-degrading bacteria..... | 119 |
| Figure 5.1: RDX removal by <i>R. rhodochrous</i> 11Y wild type and knock-out strains during the resting cell assay..... | 127 |
| Figure 5.2: The <i>xplA</i> gene cluster arrangement in <i>Gordonia</i> sp. KTR9..... | 128 |
| Figure 5.3: Cloning of <i>xplB-glnA</i> into pET-28(a)+ vector..... | 132 |
| Figure 5.4: SDS-PAGE of expression trials of <i>xplB-glnA</i> as N-terminally His-tagged protein in <i>E. coli</i> BL-21 (ED3) and <i>E. coli</i> Rossetta 2 (DE3)..... | 133 |
| Figure 5.5: SDS-PAGE and western blot analysis for the expression trials of <i>xplB-glnA</i> as N-terminally His-tagged protein in <i>E. coli</i> BL-21 (DE3)..... | 134 |
| Figure 5.6: Cloning of <i>xplB-glnA</i> into pGEX2T vector..... | 135 |
| Figure 5.7: SDS-PAGE analysis for the expression trials of GST-tagged <i>xplB-glnA</i> in <i>E. coli</i> ArticExpress and <i>E. coli</i> BL-21(DE3)..... | 135 |
| Figure 5.8: SDS-PAGE analysis for the purification of GST-tagged XplB-GS using glutathione sepharose 4B batch purification..... | 136 |
| Figure 5.9: SDS-PAGE and western analysis of purified GST-tagged XplB-GS..... | 136 |

| | |
|---|-----|
| Figure 5.10: SDS-PAGE analysis of XplA and XplB from <i>R. rhodochrous</i> 11Y..... | 137 |
| Figure 5.11: Photo of the total lysate expressing XplB-GS from <i>Gordonia</i> sp. KTR9 and XplB from <i>R. rhodochrous</i> 11Y, as well as well as overlaid chromatograms of FAD peaks from purified XplB-GS and XplB-GS. | 138 |
| Figure 5.12: SDS-PAGE for the <i>E. coli</i> BL-21cell lysate expressing pGEX2T, pGEX2T- <i>xplB-glnA</i> and pGEX2T- <i>xplB</i> | 139 |
| Figure 5.13: RDX removal by XplA with XplB and XplB-GS. | 140 |
| Figure 5.14: Sequence alignment of the XplB region of the XplB-GS fusion protein from <i>Gordonia</i> sp. KTR9 and XplB from <i>R. rhodochrous</i> 11Y..... | 141 |
| Figure 5.15: Unrooted phylogentic tree between several FAD-containing proteins which has conserved Trp with XplB portion of XplB-GS..... | 142 |
| Figure 5.16: Photo of the total lysate expressing XplB and XplB(W386S) mutant from <i>R. rhodochrous</i> 11Y, as well as well as overlaid chromatograms of FAD peaks from purified XplB and XplB(W386S).. | 143 |
| Figure 5.17: A model of the structure of XplB | 144 |
| Figure 5.18: SDS-PAGE gel from purification of XplB (S385W)-GS..... | 145 |
| Figure 5.19: Multiple sequence alignment of three GS proteins close homologues to GS-XplB.. | 147 |
| Figure 5.20: Model structure of GS from from XplB-GS of <i>Gordonia</i> sp. KTR9. | 148 |
| Figure 5.21: Glutamine synthetase activity assay of purified GS-XplB..... | 150 |
| Figure 6.1: Biodegradation pathway of RDX catalysed by XplA from <i>R. rhodochrous</i> 11Y..... | 155 |
| Figure 6.2: Topology of the XplA-heme | 156 |
| Figure 6.3: The XplA-heme active site..... | 157 |
| Figure 6.4: The putative ligand transport channels in the XplA-heme protein..... | 158 |

| | |
|---|-----|
| Figure 6.5: The sequence region flanking <i>gt-xplA</i> in <i>G. terrae</i> strain NBRC 100016 and <i>cypB</i> in <i>G. polyisoprenivorans</i> NBRC 16320..... | 165 |
| Figure 6.6: Model structure comparison of the putative active site of CYPA to the crystal structure of XplA-heme active site..... | 167 |
| Figure 6.7: Cloning of the <i>gt-xplA</i> gene into pET-28(a)+ vector..... | 169 |
| Figure 6.8: Example of a typical chromatogram of GT-XplA purification on Ni-affinity column using an AKTA-purifier and SDS-PAGE of the purification fractions of the GT-XplA..... | 170 |
| Figure 6.9: Cloning of <i>cypA</i> and <i>cypB</i> genes into pET-16b vector..... | 170 |
| Figure 6.10: SDS-PAGE of the fractions from purification steps of the CYPA and CYPB..... | 171 |
| Figure 6.11: Western blot analysis of the fractions from purification steps of CYPA and CYPB using monoclonal His-antibody..... | 172 |
| Figure 6.12: SDS-PAGE and western blotanalysis of the expression trials of CYPA. | 172 |
| Figure 6.13: Cloning of the <i>cypA</i> gene into pET-28(+).a..... | 173 |
| Figure 6.14: SDS-PAGE analysis for the expression trials of CYPA as a C-terminally His-tagged protein..... | 174 |
| Figure 6.15: SDS-PAGE analysis of expression trials for CYPA in <i>E. coli</i> Rossetta 2 (DE3) and ArticExpress..... | 174 |
| Figure 6.16: Prediction of the transmembrane region in the CYPA protein using DAS-Transmembrane prediction..... | 175 |
| Figure 6.17: Sequence alignments of the CYPA and XplA heme domain..... | 176 |
| Figure 6.18: Cloning steps of the truncated <i>cypA</i> gene into previously digested pET-16b..... | 176 |
| Figure 6.19: Expression of CYPA as a truncated protein in pET-16b..... | 177 |

| | |
|--|-----|
| Figure 6.20: SDS-PAGE and western blot analysis for the expression trial of truncated-CYPA in pET-16b..... | 178 |
| Figure 6.21: SDS-PAGE and western blot analysis for the purification steps of truncated CYPA..... | 178 |
| Figure 6.22: UV-visible spectra of the purified GT-XplA, Truncated-CYPA and CYPB proteins..... | 180 |
| Figure 6.23: UV-visible spectra for RDX-binding of GT-XplA, truncated-CYPA, CYPB and purified XplA.. | 181 |
| Figure 6.24: Example of an agarose gel from the mutagenesis experiment of the cytochromes P450..... | 182 |
| Figure 6.25: SDS-PAGE of the expression trials for single and double mutants of the truncated-CYPA..... | 184 |
| Figure 6.26: The residues located in the heme binding site of XplA..... | 189 |

List of Tables

| | |
|---|-----|
| Table 2.1: List of the primers used in this study | 52 |
| Table 2.2: List of RDX degrading bacteria used to study the RDX degrading genomic island | 55 |
| Table 3.1: Effect of TNT on RDX-removal activity by <i>R. rhodochrous</i> 11Y | 80 |
| Table 3.2: List of RDX-degrading bacteria isolated from different geographical locations | 82 |
| Table 5.1: Multiple sequence anligment of XplB-GS, XplB from <i>R. rhodochrous</i> 11Y with several FAD-containing protein..... | 142 |
| Table 5.2: Classification of the GS fused with XplB in <i>Gordonia</i> sp. KTR9 based on multiple sequence alignment..... | 146 |
| Table 5.3: Sequence and the position of the residues located in active site loops of the model structure GS fused with XplB. | 149 |
| Table 6.1: The composition of the auto induction medium | 163 |
| Table 6.2: The corresponding residues of XplA-heme active site in CYP A, CYP B and GT-XplA. | 168 |
| Table 6.3: Mutant constructs generated from truncated <i>cypA</i> and <i>gt-xplA</i> | 183 |
| Table 6.4: Preliminary results from the whole cell assay of the XplA-homologues and mutants toward RDX by Griess assay..... | 185 |

Acknowledgements

During my years of study in York, I have met and worked with many helpful, great scientists in the Centre of Novel Agricultural Products (CNAP), and their work has been both inspiring and educational for me.

Here, I would like to thank the following people who have helped and supported me in producing the work for this thesis:

To Professor Neil Bruce for giving me the opportunity to do a PhD in his group, and for his advice, support, and courage throughout my studies here.

To my Thesis Advisory Panel (TAP) members, Professor Peter Young and Dr. James Chong, for the supportive discussion, feedback and advice given during meetings.

To Dr. Astrid Lorenz for patiently introducing me the project. To Dr. Elizabeth Rylott, thank you so much for helpful comments and discussion on my project and thesis.

To Dr. Joe Bennett (Ironman) for proof reading several parts of my thesis. To Dr Federico Sabbadin for showing interest in my work and helpful discussions on cytochromes P450. To Luisa Elias, for her kindness helping me with the AKTA-purifier and her technical advice on protein expression and purification.

To Dr. Deborah Rathbone in the Biorenewables Development Centre for help with the genome sequencing of *R. rhodochrous* 11Y and *Williamsia* sp. EG1. To Dr. Yi Li for help with sequence assembly.

To Emily Johnston for being such a nice friend, for helping me with English, introducing me to the English culture (mainly Geordie culture).

To David and Louise for the support in the lab, with thanks to Dave for the interest shown in the politics of my area: I know it is very hard to understand.

To the previous and current member of M2/ CNAP for being great friends: Chong, Andy, Will, Shaza, Mariya, Anna, Sue, Kyriakos, Maria, Nicola, Zakuan (Squash partner), Laziana, Shikin, Rachael, and Dan.

To HCDP program of the Kurdistan Regional Government/IRAQ for providing me with the scholarship that enabled me to study my P.hD in York.

And last but not the least, for my lovely family: mum, dad, brothers and sisters for their support, love and care of me during this degree. Your love is enough to challenge anything in life and continue in dreaming bigger.

Author's Declaration

I declare that I am the sole author of the work in this dissertation and that it is original except where indicated by special reference in the text. No part of the dissertation has been submitted for any other degree to any other institution.

Publications arising from this work

CHONG, C. S., **SABIR, D. K.**, LORENZ, A., BONTEMPS, C., ANDEER, P., STAHL, D. A., STRAND, S. E., RYLOTT, E. L. & BRUCE, N. C. 2014. Analysis of the xplAB-Containing Gene Cluster Involved in the Bacterial Degradation of the Explosive Hexahydro-1,3,5-Trinitro-1,3,5-Triazine. *Applied and Environmental Microbiology*, 80, 6601-6610.

Chapter 1: Introduction

1.1 Microbial adaptation to xenobiotic compounds

Since the industrial revolution, massive amounts of “xenobiotic” organic compounds have been chemically synthesised and released into the biosphere. These compounds often have structures or properties that do not exist in nature [1], and many are toxic, such as explosives, antibiotics, disinfectants, fungicides, herbicides or insecticides [1, 2]. It is estimated that 150×10^6 tonnes of xenobiotics are released annually into the environment [3], producing considerable pollution in the biosphere and effecting the wildlife and human health [2, 4, 5].

Bacteria have been on our planet for more than 3.8 billion years [6], and are renowned for their extraordinary variation in metabolic properties, cellular structure and lifestyle; for instance *Escherichia coli*, *Shigella flexneri*, *Salmonella enterica*, *Klebsiella pneumoniae*, *Serratia marcescens* and *Yersinia pestis* are all belong to a small taxonomic group of enteric bacteria, however their morphology, cellular metabolism and life style are remarkably diverse, depending on the ecological niche, as is shown in Figure 1.1 [7].

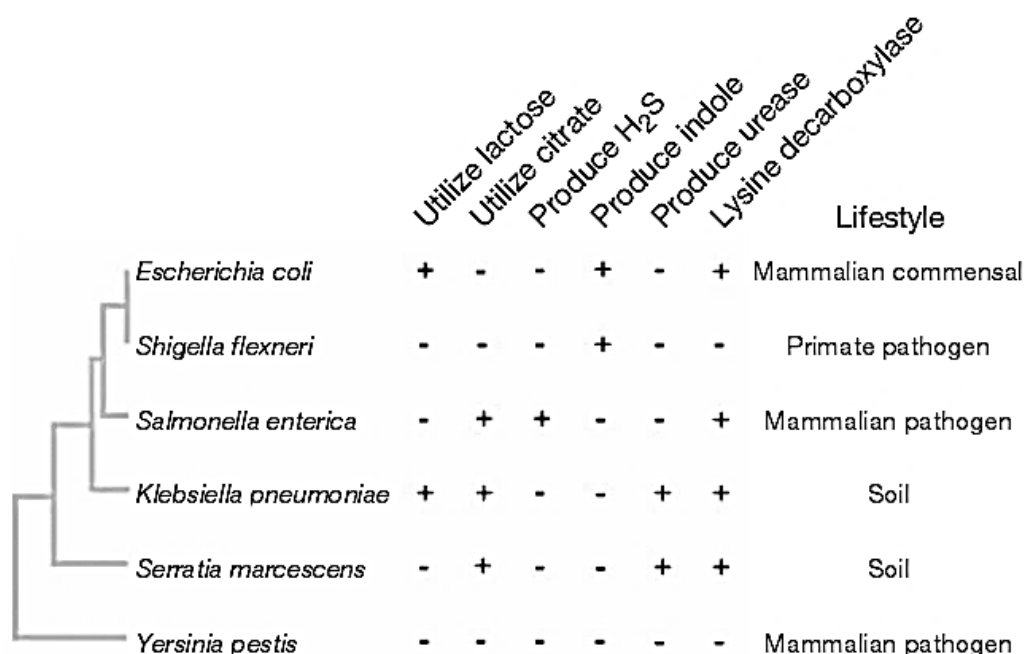


Figure 1.1: Physiological and lifestyle diversity of number of enteric bacteria. Reproduced from Ochman *et al.* (2000) [7].

Such metabolic diversity amongst bacteria reflects the genomic plasticity of these organisms, in which the “flexible” gene pool, carrying additional beneficial traits for the host under special environmental circumstance, can be rapidly manipulated through the processes of evolution and adaptation [8]. This feature has made it possible for bacteria to survive in almost every environment on the planet, from extremely high to extremely low temperatures, in various acidic or alkaline environments, and even in the dark, cold abyssal zone at the bottom of oceans, under extreme hydrostatic pressure and nutrient limitation [9].

Given that most xenobiotic compounds are rich in carbon and/or nitrogen, it is perhaps no surprise that bacteria have evolved catabolism pathways for many of these toxic compounds, including those which have been relatively recently introduced (within the last 50 years) to the environment [10]. Humans have taken advantage of this bacterial “evolutionary greenhouse” to detoxify and recycle xenobiotic pollutants in the biosphere [1] by using bacteria themselves, or the enzyme(s) responsible for metabolism of the xenobiotic [2].

1.2 Molecular mechanisms of microbial evolution

Three factors contribute towards the diversity of bacterial genomes; firstly, the ability to produce small changes in the existing sequence through substitution, inserting or deleting a few nucleotides. Secondly through DNA rearrangement and intragenomic reshuffling of the genomic content, and thirdly, via the acquisition of foreign DNA from another organism through horizontal gene transfer [6, 11].

1.2.1 Microbial evolution through small scale mutation in existing DNA

The concept of molecular evolution as a result of small genetic mutations was developed by Motoo Kimura and Tomoko Ohta (Figure 1.2). With “Neutral Theory of Molecular Evolution”, Kimura [12] developed a mathematical calculation to estimate nucleotide substitution rates, and proposed that most mutations are neutral or nearly neutral and these spread through genetic drift. Ohta [13] expanded the concept and proposed a relationship between random genetic drift and selection in the so called “nearly neutral theory of molecular evolution”. Ohta suggested slight deleterious mutations play an important role in molecular evolution.



Figure 1.2: Photos of the pioneer scientists of modern molecular evolution - Motoo Kimura (left) and Tomoko Ohta (Right). The photos are reproduced from History of Recent Science and Technology (<http://authors.library.caltech.edu/5456/1/hrst.mit.edu/index.html>).

Overall, mutations can be silent or neutral, not affecting the fitness of the organism, have a deleterious or lethal effect, or be advantageous and improve the fitness of the organism within an environmental niche. In most cases, mutations have either a deleterious or lethal effect on the fitness of the organism [6, 7, 14, 15], however the gene which carries the deleterious mutation can disappear after a few generations through natural selection [15]. *In silico* sequence analysis of the 3,595 groups of homologous sequences in public databases, identified 17 groups of genes in different organisms which have potentially evolved through adaptation mutations, mainly through nonsynonymous mutations [15]. The melamine-degrading enzyme (melamine deaminase, TriA) was proposed to have been evolved from atrazine chlorohydrolase (AtzA). TriA was identified in melamine-degrading *Pseudomonas* sp. strain NRRL B-12227 and has 98 % sequence identity to AtzA from the atrazine-degrading *Pseudomonas* sp. strain ADP. Each enzyme is 475 amino acids long differing by only nine amino acids. Both atrazine and melamine are xenobiotics; as melamine has existed in the environment for a longer period, it may have potentially contributed to the rapid evolution of AtzA from TriA [16]. Resistance to penicillin in *Streptococcus*

pneumoniae was proposed to originally evolve via point mutations in the *pbp* genes in the commensal penicillin-sensitive strain *S. mitis*. The mutated *pbp* genes then transformed in *S. pneumoniae*, by homologous recombination, to form a mosaic of *pbp* blocks. These mutations are responsible for the alteration of penicillin-binding proteins (PBP), target proteins of penicillin. The modified PBPs have less affinity for the drug and thus enhance the fitness of the bacteria in the presence of the drug [17]. Moreover, spontaneous mutations in the N-terminal cap domain of haloalkane dehalogenase (*dhlA*) were shown to play an important role in the modification of enzyme specificity, and subsequently contribute to the evolution of *Xanthobacter autotrophicus* to degrade the xenobiotic 1,2-dichloroethane [18].

1.1.2 Large scale cellular DNA manipulation

Bacterial genomes frequently undergo processes of reduction, re-arrangement, duplication and inversion, as mechanisms to adapt to their ecological niche [19]. Several enzymes including transposases and integrases, which are usually related to mobile DNA elements, mediate these processes in the cell. Sequence rearrangement is also regarded as an important step in the acquisition of foreign genetic material through horizontal gene transfer [5, 20].

For instance, the small genome size found in members of the genus *Mycoplasma* is not indicative of primitivity of the organisms, but is rather due to the shrinkage of the bacterial genome and loss of non-essential genes through bacterial adaptation [21]. In 2002 Moran proposed that a reduction in bacterial genome size, a particularly common phenomenon in parasite bacteria, can have adaptive advantages for the organism in terms of accelerating growth rate and maintenance within the host, although examples of several remaining non-functional or pseudogenes in the small genomes of *Rickettsia* and *Buchnera* could argue against the hypothesis [21].

Plasmid reduction has had an important role in increasing the pathogenicity of *Shigella* sp. and another enteroinvasive *Escherichia coli*, changing the lifestyle of these strains; a region including the *cadA* gene (identified on a plasmid of an ancestral commensal *E. coli*) is deleted in these strains. The gene encodes a lysine decarboxylase (LDC), the product of which, cadaverine, was found to greatly inhibit *Shigella* enterotoxin activity [22].

In bacteria, DNA rearrangement is another mechanism in the process of evolution [7]. For example large chromosomal inversions in the genome of pathogenic *Pseudomonas aeruginosa* has boosted bacterial speciation and colonisation in the lungs of cystic fibrosis patients [23]. Conversely, an experimental attempt to investigate the effects of artificial large chromosomal inversion in *Lactococcus lactis* found varied impact on bacterial cell fitness, but mainly disadvantageous effects [24].

Bacterial genome reduction and re-arrangement can also occur through transposable elements; discrete DNA segments that are able to move, without need of sequence homology, between donor and target sites. These mobile elements themselves also play an important role in microbial adaptation, and there are several xenobiotic-degrading activities which have been traced to products of transposable elements [10, 25].

There are three classes of transposable element based on a genetic element and transposition mechanism [10, 25, 26]: Class-I, Class-II, and conjugative transposons.

Class-I type transposons include simple insertion elements (ISs), in which short DNA sequences carry the genetic materials for transpositional recombination only [26, 27], and composite transposons, in which genes for the various beneficial traits including xenobiotic degradation are located between two nearly identical copies of ISs, in direct or invert orientations. The majority of ISs contain a short, ten to 40 bp terminal inverted-repeat sequence, flanked by direct-repeated sequences (DRs) [10, 25, 27]. In *Pseudomonas* sp. strain P51, genes involved in chlorobenzene degradation, *tcbA* and *tcbB*, are located on a 12 kbp composite transposon, Tn5280, flanked by two insertion elements IS1066 and IS1067 on the p51 plasmid [28]. Additionally, the benzene catabolic genes on plasmid pHMT112 from *Pseudomonas putida* ML2 are located on the Class I composite transposon Tn522, flanked by two directed repeated ISs IS1489v1 and IS1489v2 [29].

Class II transposons, are also known as Tn3 family type transposons. These elements usually carry two genes involved in their transposition: *tpnA* encoding a transposase, and *tpnR* encoding a resolvase. Transposition in this class occurs through two steps in a replicative pathway: in the first step the entire donor replicon is integrated into a target site by the action of transposase to produce both cointegrate and direct-repeat sequence of two transposons (Figure 1.3). In the second step, the cointegrate is broken down by

the action of resolvase, through site-specific recombination, to produce a target sequence carrying transposon and regenerated donor replicon (Figure 1.3) [10, 25, 26, 30].

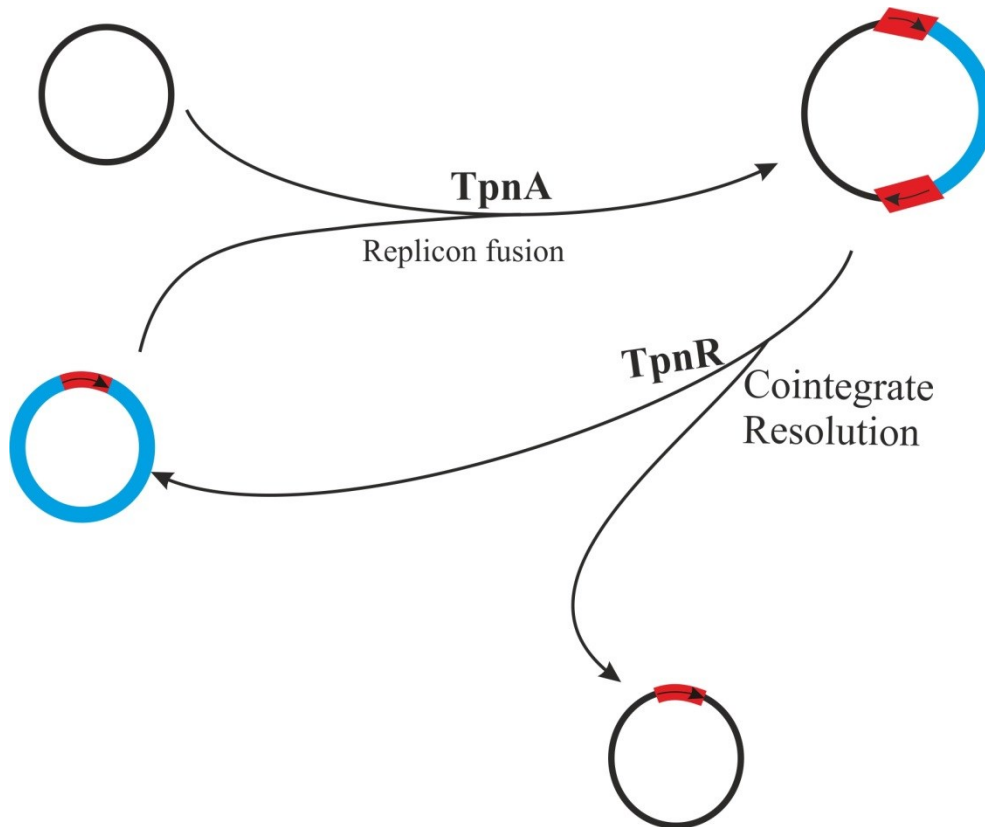


Figure 1.3: Two step replicative process of Class II (Tn3) transposition. Entire donor replicon is inserted into a target site to form a cointegrate by the action of transposase enzyme encoded by *tpnA*. This cointegrates then breaks down to the target sequence with the transposon and regenerated donor. Reproduced from Grindley (1983) [30].

The third class of transposons are called Conjugative Transposons or Integrative Conjugative Elements (ICEs), and historically called Genomic Islands and Integrative Plasmids [1, 10, 31]. The ICEs are self-transmissible blocks of DNA elements, usually located on chromosomes, and frequently near to a gene encoding tRNA. These elements carry genes which give beneficial traits to the host, as well as genes for their transmission, regulation and maintenance [32]. They can be found in both gram positive and gram negative bacteria, and differ from Class I and II transposons in that they are able to transfer horizontally between unrelated microorganisms through conjugation [8, 31, 33]. Generally, ICEs are larger than both Class-I and Class-II transposons, sometimes reaching up to 200 kbp [8, 34]. Although it has been proposed that the GC

composition of ICEs differs compared with the rest of the genome [8, 11], computation analysis for the 95 characterised ICEs revealed that this is not usually the case, with < 30 % of the tested ICEs differing (higher or lower) in GC content when compared with the rest of the genome. However, dinucleotide bias is found to be a key feature of ICEs, with 62 % exhibiting dinucleotide bias. Importantly, most novel genes are predicted to be associated with ICEs [34].

These elements are excised from the chromosome through the site-specific recombination and take circular form, replicated from the host chromosome and can be transferred to recipients by conjugation. The transferred DNA can then be integrated into the bacterial chromosome through recombination between a specific site of the circular form and a site in the genome of their host, whereas the remaining ICE in the host cells is then integrated back to the chromosome (Figure 1.4) [1, 8, 10, 31-33]. Thus transposition of these elements has phage and plasmid life cycle, in which they integrate into, and excise from, the chromosome as phage, and transfer by conjugation as a plasmid [31-33].

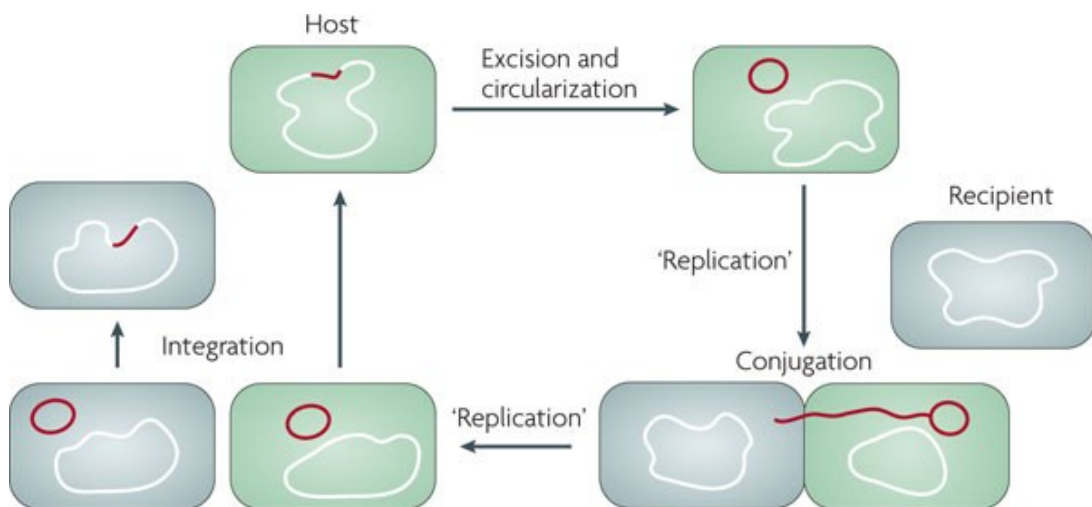


Figure 1.4: Transposition of the ICEs. The ICE is excised from the host genome and circularises, then can be transferred to recipient cells by conjugation and lastly integrate into the host genome. Reproduced from Wozniak and Waldor (2010) [33].

Considering that unique transposition features of this class of transposons, Burrus *et al.* (2002) [31] suggested the term “Integrative and Conjugative Elements, ICEs” for this group of mobile elements, rather than “Genomic Islands”. The authors argued that the term “genomic island” for these mobile elements, which was initially used to coin

pathogenicity islands, would be rather a generalised name and functional classification of these elements. Additionally, genomic islands could also refer to wider groups of mobile elements with very different structures, and they could belong to either class of transposons or even statllite phage-like elements [31]. Despite these facts, different names are still in use for this group of mobile elements.

Dobrindt *at al.* (2004) [11] proposed that ICEs might have originally derived from integrating plasmids or phages, that can go through successive evolution over time. The ICEs can became immobile through reduction evolution and lose the genes required for this process, or other mobile elements such as insertion elements and transposons, can be added before excision to the new host (Figure 1.5).

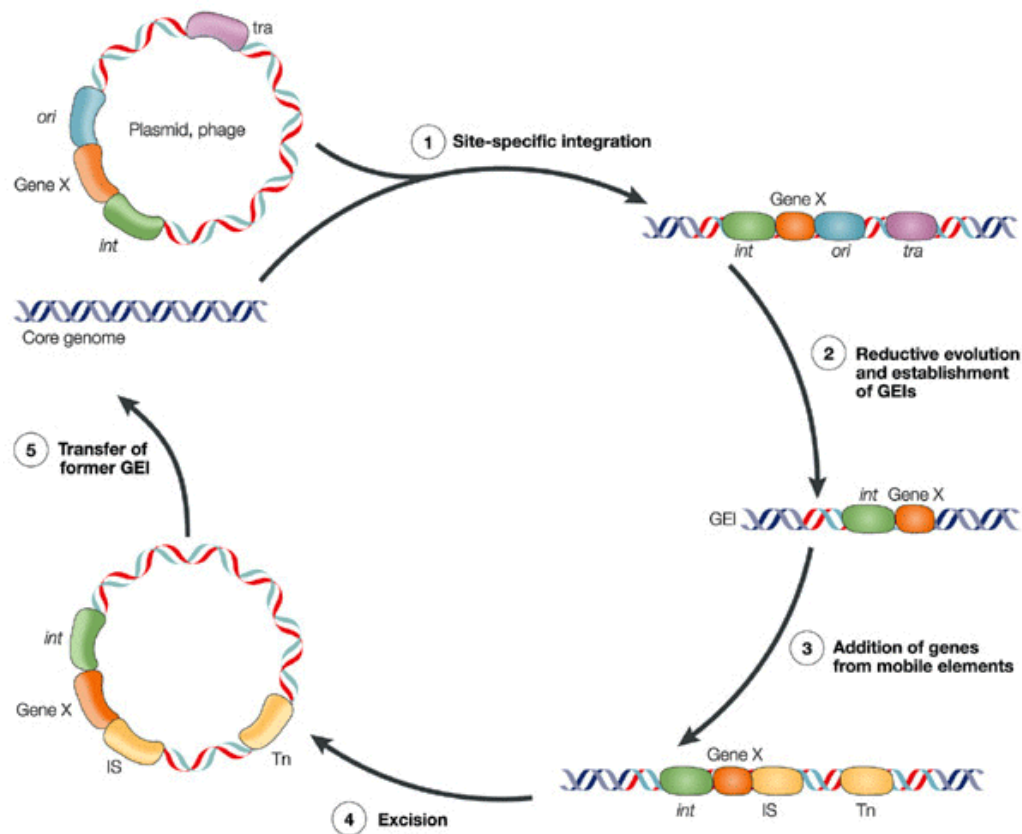


Figure 1.5: Hypothetical Integrative and Conjugative Elements (ICEs) lifecycle. ICEs carry genes with beneficial traits for the host (*Gene x*), as well as genes for autonomous replication (*ori*), transfer (*tra*), and intergration (*int*). These mobile elements integrate into a host's chromosome through site-specific integration (1), which then can either immobile by losing the gene(s) involve in their mobility (2), or other mobile elements like insertion elements (IS) or transposable elements (Tn) can be added (3). To be transferred into a new host, genomic islands need to excise from chromosome and transfer to another bacterial cell chromosome. Reproduced from Dobrindt *at al.* (2004) [11].

The best-characterised xenobiotic degrading ICE is the 105 kbp self-transmissible *clc* element involved in chlorobenzene degradation in *Pseudomonas* sp. strain B13 [35, 36]. Other examples include the 55 kbp *Tnbph* element involved in biphenyl and 4-chlorobiphenyl degradation on the transposable element Tn4371 [37] and the 90 kbp *bph-sal* element involved in biphenyl and salicylate degradation in *Pseudomonas putida* KF715 [38]. More recently a 232 kbp *phn* island in the phenanthrene-degrading bacterium *Delftia* sp. Cs1-4 [39] has also been reported.

1.1.3 DNA acquisition through horizontal gene transfer

Acquisition of the DNA sequences from a close, or distantly related, organism through horizontal gene transfer is considered be a main strategy in bacterial evolution and adaptation [5, 7, 8, 20]. The systematic examination of 116 prokaryotic total genome sequences showed that 14 % of the 324,563 genes in these organisms were acquired through recent horizontal gene transfer. The number of the acquired genes was found to vary between bacterial species, for instance 21 % of *E. coli* genes are thought to be acquired by horizontal gene transfer, compared with only 2 % in the total genome of *Mycoplasma genitalium* G-37 (Figure 1.6) [40].

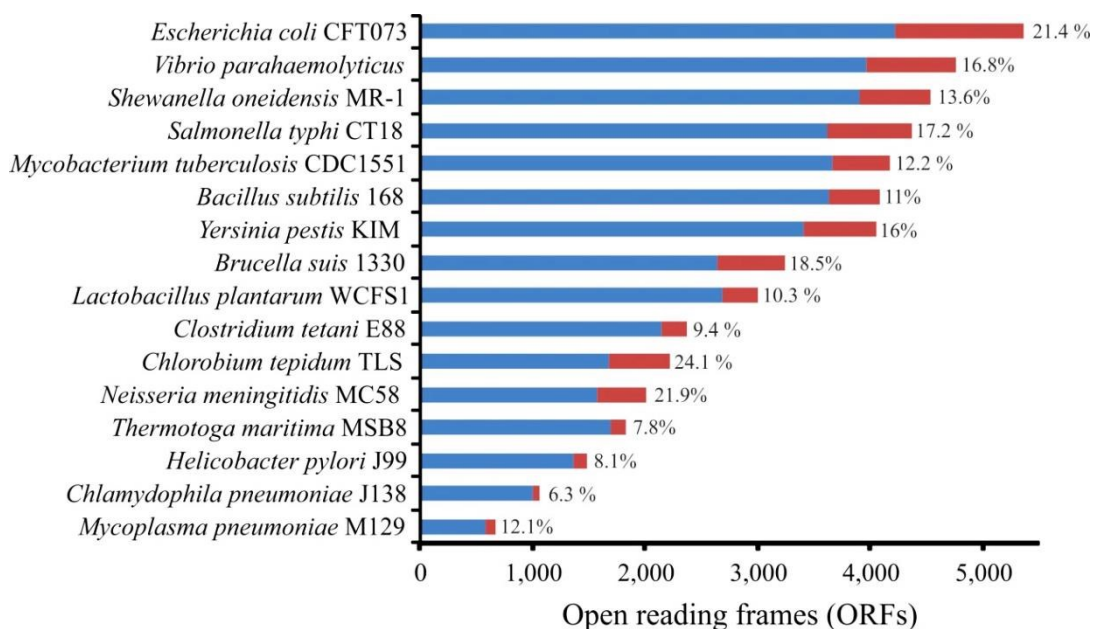


Figure 1.6: Example of distribution of the horizontally acquired genes amongst the genome of various bacteria. Each bar represents the number of genes in the corresponding bacterium; the red part of the bar represents the ratio of horizontally acquired genes in the genome. Graph produced using data published by Nakamura *et al.* (2004) [40].

Successful horizontal gene transfer has three requirements; firstly, a method to deliver DNA sequence from the donor to the recipient genome. Secondly, the acquired sequence must integrate in the recipient genome. Thirdly, expression of the new DNA segment must in some way result in beneficial traits in the cell [7]. The first two steps occur through three possible mechanisms: transformation, transduction or conjugation [7, 32].

Natural transformation is the process of the active uptake and inheritable integration of the naked exogenous DNA fragment from the environment into the bacterial genome [7, 41]. Given the difference in the cell wall structure of gram negative and gram positive bacteria, mechanisms of DNA uptake from extra cellular milieu into the cytoplasm is also different between these two groups of bacteria. In gram negative bacteria, a DNA fragment should pass through the outer membrane then the cell wall and finally, cytoplasmic membrane, whereas in gram positive bacteria, the outer membrane barrier does not exist [41, 42]. In addition to this, the natural competence, a physiological state allowing bacteria to naturally uptake DNA from the environment, is also different amongst bacteria. At least 40 bacterial species have been identified as naturally competent and able to uptake DNA from the environment [43], while other bacteria become competent to take up DNA only under certain physiological conditions [42, 43]. In both gram positive and gram negative bacteria, only one of the two DNA strands is transformed into the cytoplasm in order to integrate into host genome, the other strand is degraded into nucleotides then released either outside of the cell (in gram positive bacteria) or into the periplasmic space (in gram negative bacteria) [41]. The advantage of the natural transformation in terms of bacterial adaptation is not well understood. Two hypotheses have been proposed to explain the natural competency in bacteria; firstly, that transformation of DNA occurs mainly to provide DNA as a nutrient by the transformed cells, or the imported DNA is used by the cell to repair damaged DNA [44]. The second hypothesis is that transformation provides the genetic diversity and increased fitness of the bacteria in the so-called “sex hypothesis” [44]. Johnborg *at al.* (2007) assessed both models in a review paper based on many experimental data [44]. The authors argued that natural genetic transformation occurs to enable DNA to be used as a nutrient by bacteria, particularly in *Streptococcus pneumoniae*. In this bacterium only the sense-strand of imported DNA is transferred into the cytoplasm, whereas the complementary strand is degraded outside the cell; a rather wasteful way of gathering

food [44]. Natural competencies of streptococcal species have been shown to increase the fitness of the bacterium, the best example is acquiring resistance to the beta-lactam antibiotic penicillin by *S. pneumonia* from the evolved commensal *S. mitis* [17, 44]. Moreover, use of DNA as a nutrient can also be considered to contribute towards the fitness of naturally competent bacterial enabling their survival in ecological niches when compared to non-competent bacteria.

Bacteria can acquire new genetic materials from bacteriophage in the process of transduction [7]. In general, infection of the bacterium cell with the phage can be either multiplication of phage particles and then release to the environment after lysis of the host cell, or integration of the phage genome into the host chromosome as a prophage in the process of lysogenization. Transduction has also been shown to play an important role in the genome diversity of bacteria and several prophages have been identified in the genome sequence of bacteria [45]. In addition to introducing the bacteriophage DNA into the bacterial genome as a “generalised transduction”, bacteriophage can also work as a vehicle to transfer DNA material from previously infected hosts into the new bacterial chromosome in a process called “specialised transduction” [7, 45]. The latter type of transduction mainly occurs when the prophage imprecisely excises from bacterial chromosome, resulting in the package of a small fragment of the bacterial genome within the DNA phage [46]. The evolutionary advantage of lysogenic bacteria has been described for some strains of bacteria. In one of the earliest examples, Edlin *et al.* (1977) [47] reported that P1, P2 and Mu prophages provided a reproductive fitness for the host *E. coli* strains; the growth rates of lysogens strains of *E. coli* were much faster than nonlysogen strains in glucose limited conditions, however both lysogen and non-lysogen strains had the same growth rate in non-nutrient limitation conditions [47]. Moreover, phages are also important in the dissemination of genomic islands. The gene encoding toxic shock toxin (*tst*) in *Staphylococcus aureus* is carried by a 15 kbp pathogenicity island, SaPII, which is located on the chromosome and flanked by 17 bp direct repeats. It has been shown that, upon infection of the bacterium cell with the *S. aureus* phage 80 α , SaPII is excised from the chromosome; it replicates autonomously, and is encapsulated into its own DNA into phage particles. Upon transfer into a new host, the SaPII integrates into the recipient cell using integrase encoded by the gene on SaPII [48].

Conjugation is the direct transfer of the single stranded DNA from a donor to recipient cells through a multi-protein apparatus called conjugation or mating apparatus [33, 41, 49]. Conjugation has been shown to play an important role in the quick adaptation of microorganisms to the new environment through acquiring genetic material from evolved strains. Several genes involved in xenobiotic degradation are found in self-transmissible catabolic plasmids, which usually have several insertion and transposon elements [10]. Naphthalene catabolism genes, *nahAC*, have shown to be located on the self-transmissible plasmid and can be transferred from the naphthalene-degrading bacteria to their cured progeny via filter mating [50]. Moreover, genes involved in the mineralisation of the xenobiotic melamine in *Rhodococcus* sp. strain Mel [51] and mercury resistance genes [52] have also been shown to be located on self-transmissible plasmids.

1.3 Explosives as xenobiotic compounds

1.3.1 Overview of explosives

Explosives are a group of organic compounds that under thermal, chemical or physical effect decompose extremely rapidly, creating a large amount energy in the form of heat and gas.

Blackpowder (gunpowder) was the first formulated explosive which was accidentally discovered by Chinese alchemists during the process of separating gold from silver in low temperature reactions in 220 BC. The composition of blackpowder was made up by mixing charcoal and sulphur, with potassium nitrate as an oxidiser. Blackpowder was only discovered in Europe in the 13th century by the English monk Robert Bacon [53].

Nitroglycerine (Glyceroltrinitrate, GTN) a nitrate ester, was discovered by an Italian Professor Asanio Sobrero in 1846, and a few years later manufactured by a Swedish inventor, Immanuel Nobel, by mixing glycerol with a cooled mixture of nitric and sulphuric acids [53]. Although GTN was a more powerful explosive than blackpowder, the liquid physical state and chemical instability made the process of production extremely hazardous. Currently explosive compounds can be grouped into three main categories: nitrate esters, nitroaromatics, and nitramines [53].

Nitrate esters are a group of explosives which are characterised by nitro groups linked to carbon atoms via ester bonds, with examples such as GTN and pentaerythritoltetranitrate (PETN). Both GTN and PETN are also medically important compounds; the release of nitric oxide as a result of enzymatic action have made these compounds useful as vasodilators during some medical condition, coronary angina being one example [54].

Nitroaromatic explosives are characterised by several nitro groups ($-\text{NO}_2$) on an aromatic structure, examples for this group include 2,4,6-trinitrotoluene (TNT), and the propellant 2,4-dinitrotoluene (2,4-DNT). Nitroamines contain one or more *N*-nitro groups on aromatic rings, examples for this group of explosives are hexahydro-1,3,5-trinitro-1,3,5-triazine (RDX, Research Department eXplosive or Royal Demolition eXplosive) and octahydro-1,3,5,7-tetranitro-1,3,5,7-tetrazocine (HMX; High Melting Point eXplosive or Her Majesty's eXplosive) (Figure 1.7) [54, 55].

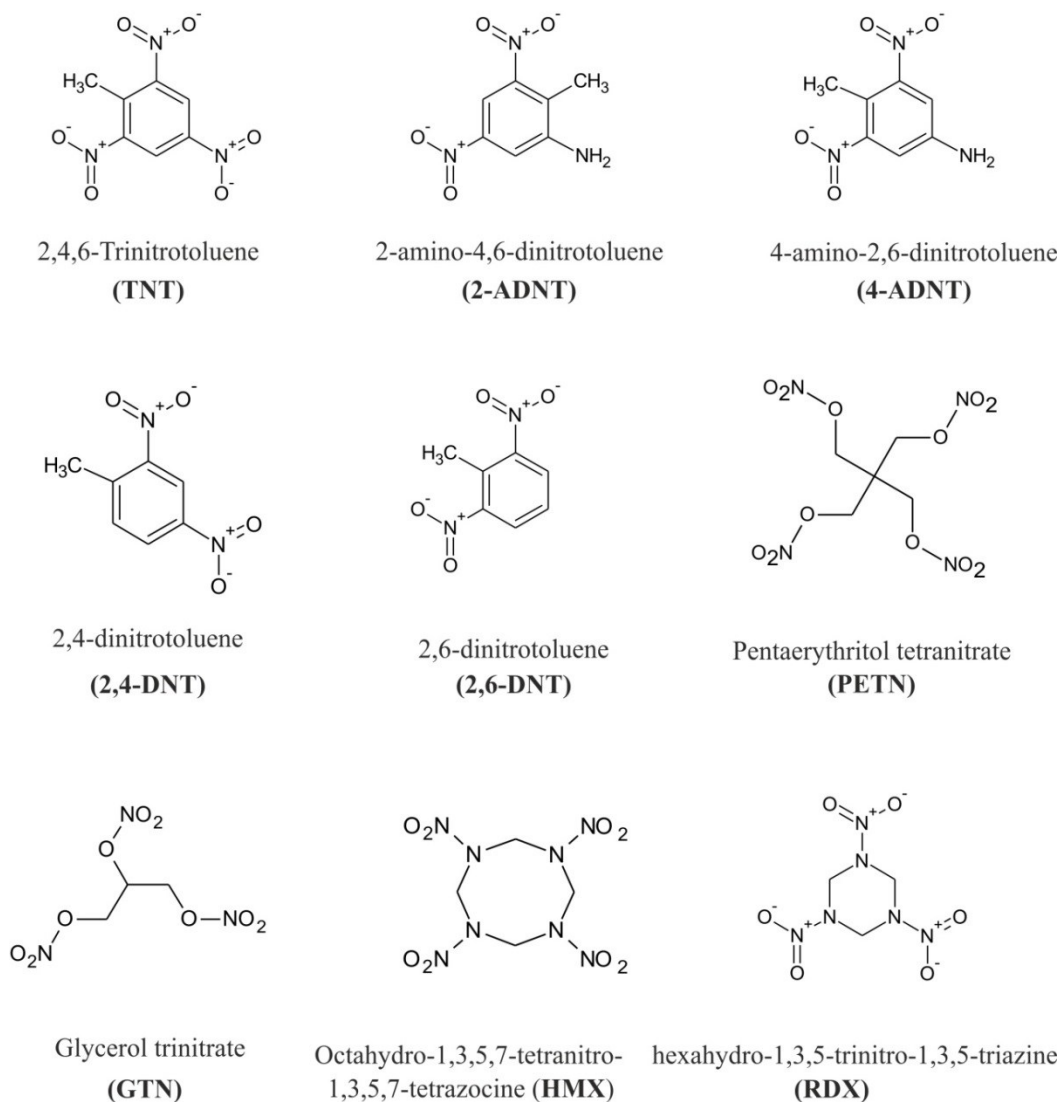


Figure 1.7: Examples of explosives and explosives transformation products of the explosives which usually find in explosive contaminated sites. The structures are drawing using ChemSketch version 12.0 [56] by Chong (2011) [57].

Both TNT and RDX are amongst the most commonly used explosives around the world and their toxicity has raised serious environmental concerns. The rest of this chapter will focus on these two compounds as explosive xenobiotic compounds.

TNT was first discovered by German scientist Julius Wilbrand in 1863 [53] and it was the main explosive used during the first World War [53, 58] and is still considered to be the most widely used and important military compound [54, 58, 59]. Several factors contribute in the wide usage of TNT around the world including cheap raw materials, easy manufacturing processes, moderate stability for physical impact, relatively high

explosive power, and good compatibility with other explosives. Moreover, TNT has thermal stability, low volatility and low hygroscopicity; providing stability in moist conditions and detonation in water (Table 1.1) [53].

RDX was first prepared by a German scientist Georg Friedrich Henning in 1899 for medicinal purposes (Table 1.1). It was first used as an explosive by Herz in 1920 and has extensively been used since the Second World War for both military and industrial purposes [53]. It has a high explosive power, nearly 40 % higher than TNT. This feature has made RDX an important high explosive compound currently in use [54] and it is mainly used as a mixture with either TNT or HMX [60, 61].

Table 1.1: Properties of TNT and RDX [53, 61]

| Characteristics | TNT | RDX |
|---|-------------------------|----------------|
| CAS Number | 3808-89-2 | 00121-82-4 |
| Chemical formula | $C_7H_5N_3O_6$ | $C_3H_6N_6O_6$ |
| Molecular weight | 227.1 | 222.1 |
| Colour | Pale yellow crystalline | White crystal |
| Melting temperature/ °C | 80.8 | 204 |
| Thermal ignition temperature/ °C | 300 | 260 |
| Crystal density at 20 °C/g cm ⁻³ | 1.654 | 1.82 |
| Energy of formation/ kJ kg ⁻¹ | -184.4 | + 417 |
| Enthalpy of formation/ kJ kg ⁻¹ | -261.5 | + 318 |

1.3.2 Environmental contamination by explosives

Production, use, storage and decomposition of explosives have resulted in large scale contamination worldwide. The precise scale of contamination is not clear, however in United States alone it is estimated that 24.6 million acres has been contaminated with munitions and the cost of the cleaning is estimated to be \$16- \$165 billions [62].

Distribution of explosive compounds in contaminated sites is highly heterogeneous and it depends on the type of training range and munition used [55, 60, 63]. In a study to investigate the distribution of energetic compounds in 23 military training ranges in United States and Canada, the concentrations of RDX and TNT were found in hand grenades ranges to span between <0.01 to 51 mg/kg and <0.01 to 36 mg/kg for RDX and TNT, respectively. HMX was mainly found in anti-tank rocket range impact areas with concentrations ranged between < 23 to 987 mg/kg [63], whereas the primary residue at the artillery and mortar firing points are the 2,4- and 2,6-dinitrotoluene (DNT) isomers [64]. The most extensive contaminated site in the training ranges was found near low-ordered, partial detonations artillery ranges with grams of pure soil explosive [63]. Similarly, the concentration of RDX, HMX, TNT, 2-amino-4,6-dinitrotoluence (2-ADNT), and 4-amino-2,6-dinitrotoluence (4-ADNT) were found to be vary at the Camp Edwards Impact Area in United States, including detection of RDX in the ground water in the area [60].

TNT is recalcitrant to degradation in the environment; the three nitro groups of TNT withdraw electrons from the benzene moiety and make it difficult for electrophilic attack by microbial oxygenases [55]. In the case of RDX, in addition to the structure, which is also recalcitrant to degradation, RDX is also highly mobile in soil, so contamination of ground water from leaching is higher than for other explosives [60, 64, 65].

Both TNT and RDX are toxic and potential carcinogenic compounds [66]. TNT has been shown to be mutagenic in *Vibrio fischeri* [67, 68], *Salmonella typhimurium* (strains TA 98 and TA 100), mammalian cell line of hamster lung (V79 cells) [69], and to cause chlorosis in plants [70]. Humans exposed to TNT have suffered liver damage, toxic hepatitis and blood cell abnormality such as anaemia and jaundice [71].

The toxicity of RDX is mainly due to its effect on the central nervous system as well as renal and gastrointestinal systems. The toxicity of this compounds has been demonstrated in humans [72], mice, rats, dogs [73] and plants [74]. Accidental ingestion of RDX by humans showed several symptoms including several seizure, nausea, vomiting, postictal coma and abdominal tenderness [72].

1.3.3 Microbial transformation of TNT

There are a number of mono-nitroaromatic compounds like chloramphenicol, aureothin, phidolopin, nitropyolutorin, oxypyrrrolnitrin and 3-nitropropionic acid that exist in nature [54, 58]. However most nitroaromatics are substituted with multiple nitro groups and these are novel in the environment. These xenobiotic compounds have been intensively produced in the last century as explosives, pesticides, dyes, and polyurethane foams [58]. Microorganisms have evolved to tolerate the toxicity of these xenobiotic compounds and in some cases metabolise them.

Mineralisation of mono- or di-nitro group compounds can occur in nature, though microbial degradation of the tri-nitro substituted compound TNT is particularly challenging and has not yet been clearly reported [55, 75]. However, several species of bacteria have been isolated and identified for their ability to transform TNT under aerobic and anaerobic condition using one of the two pathways shown in Figure 1.8 [76-80].

Type I oxygen-insensitive nitroreductases reduce nitro group of TNT through (pathway A, Figure 1.8). These are soluble flavoproteins found in many enteric bacteria and can reduce nitro groups on many different nitroaromatic compounds, including TNT, accompanied by oxidation of either NADP or NADPH. The TNT reduction by type-I oxygen-insensitive nitroreductase is followed by the production of hydroxylaminodinitrotoluene (HADNT), aminodinitrotoluene (ADNT) and diammonitrotoluene (DANT) and then diarlymine (only in bacteria) [81]. Examples of Type I nitroreductases with activity toward TNT are PnrA from *Pseudomonas putida* JLR11 [79] and nitroreductase (NR) from *Enterobacter cloacae* strain 96-3[82]

Some members of the Old Yellow Enzyme family of flavoproteins can transform TNT by pathway B (Figure 1.8). These enzymes can also transform TNT via direct ring reduction and hydride addition to form monohydride-Meisenheimer or dihydride-

Meisenheimer complexes [81]. Examples of this family of enzymes are Pentaerythritol tetranitrate reductase (PETNr) reductase and XenB from *Enterobacter cloacae* PB2 [77] and *Pseudomonas fluorescens* I-C [78], respectively.

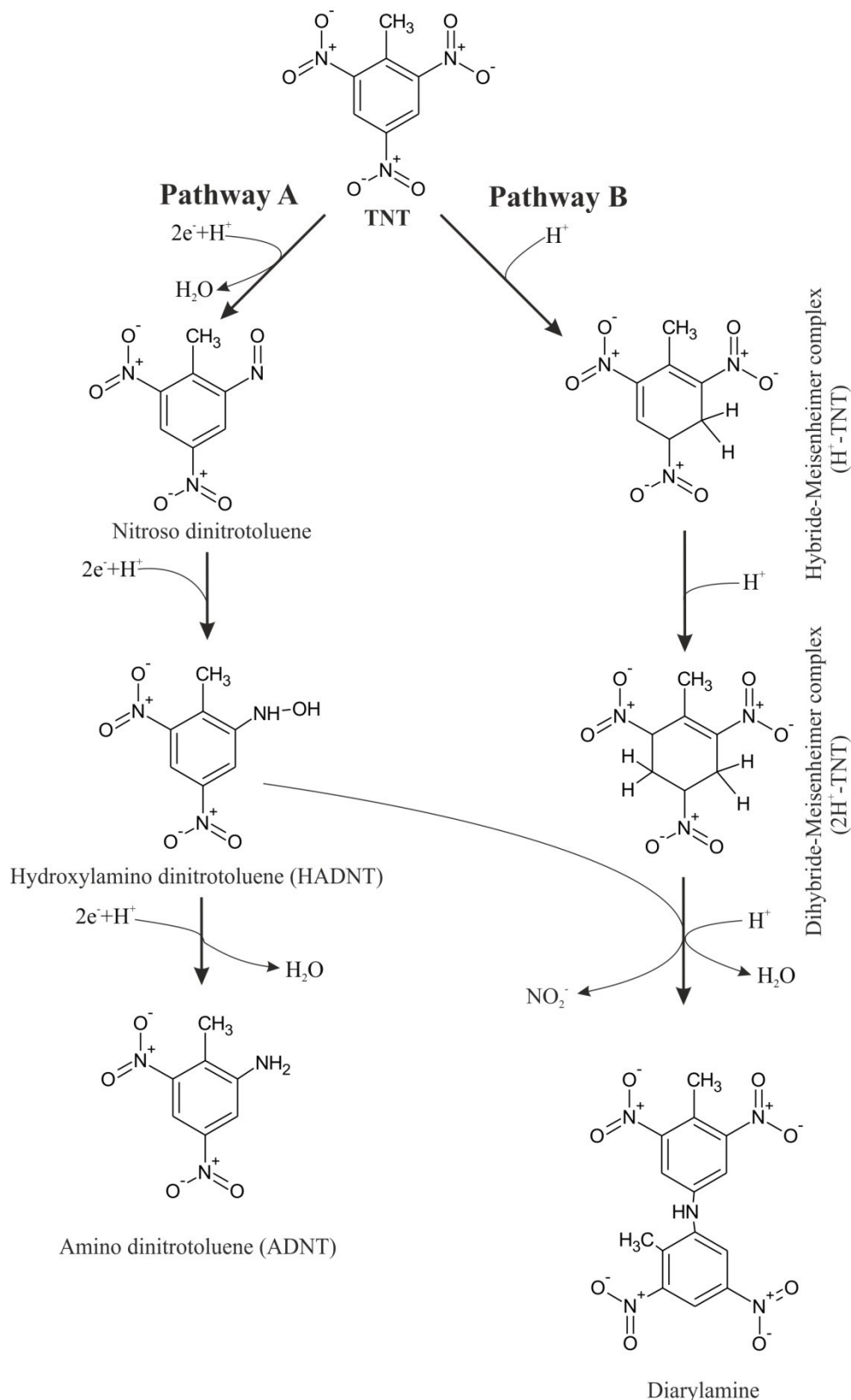


Figure 1.8: Biotransformation pathways of TNT. In Pathway A, transformation of TNT occurs via reduction of a nitro group to form HADNT and ADNT. In Pathway B, TNT is transformed by hydrogenation of the aromatic ring structure to produce a Meisenheimer complex, which goes on to produce nitrite and diarylamine [75, 81, 83, 84]. The structures are drawing using ChemSketch version 12.0 [56] by Chong (2011) [57].

1.3.4 Microbial degradation of RDX

The explosive compound RDX is considered to be strictly xenobiotic in the biosphere, as unlike the nitro aromatic TNT, natural nitramine compounds have not been identified in nature [54]. Structurally, RDX is not as stable as TNT and enzymatic attack to one of the three nitro groups or the -CH₂- group is enough to destabilise the ring structure and initiate spontaneous decomposition [85].

Reports of microbial degradation of RDX started in the 1980s [86], and three pathways have since been described for RDX biodegradation: anaerobic RDX-degradation through successive reduction [86], anaerobic denitration of RDX through the formation of methylenedinitramine [87], and aerobic denitration of RDX [88, 89].

The biodegradation of RDX via successive reduction was proposed by McCormick *et al.* (1981) [86]. In this pathway, RDX is sequentially reduced to form hexahydro-1-nitroso-3,5-dinitro-1,3,5-triazine (MNX), hexahydro-1-3-dinitroso-5-nitro-1,3,5-triazine (DNX), hexahydro-1,3,5-trinitroso-1,3,5-triazine (TNX), and then produce formaldehyde (HCHO) and methanol (CH₄O) (pathway A, Figure 1.9) [86]. Hawari *et al.* (2000) [87] suggested this pathway occurs via a two-electron reduction of RDX by type I oxygen-insensitive nitroreductase. Indeed, purified type I nitroreductase from *Enterobacter cloacae* strain 96-3 was shown to reduce RDX, however the metabolite products of RDX reduction were not identified in that study [90]. RDX-degradation through a two-electron reduction was also reported for a nitrate reductase (EC 1.6.6.2) from *Aspergillus niger* [91]. This enzyme reduced RDX anaerobically to MNX and then, differing from the previous pathway, the ring structure of MNX is broken down to produce an intermediate metabolite methylenedinitramine (similar to pathway B, Figure 1.9), which then produced nitrous oxide (N₂O), formaldehyde (HCHO), and an ammonium ion (NH₄⁺) [91]. Several anaerobic bacterial species have also been identified as being able to degrade RDX by this pathway [86, 92, 93].

A second RDX-degradation pathway was proposed by Hawari *et al.* (2000) [87] after identifying two novel metabolite products, methylenedinitramine [(O₂NNH)₂CH₂] and bis(hydroxymethyl)nitramine [(HOCH₂)₂NNO₂], from anaerobic RDX-degradation by municipal anaerobic sludge in a phosphate-buffered (pH 7) mineral salt medium using glucose as a carbon source [87]. The authors suggested that RDX degradation occurs via an initial ring structure cleavage of RDX to produce the above mentioned intermediate

products, which are then converted to nitrous oxide, formaldehyde, formic acid and methane by the action of different indigenous organisms in the sludge (pathway B, Figure 1.9). The enzyme responsible for the initial N-C-N bond cleavage of the RDX ring was not identified [87], however later it was proposed that the ring cleavage of RDX could be occurring via a single electron reduction by oxygen sensitive type-II nitroreductase. This enzyme converts RDX to an unstable radical anion, and subsequent denitration cleaves the intermediate product to form methylenedinitramine [89]. *Klebsiella pneumoniae* strain SCZ-1, a gram negative facultative anaerobic bacterium, was also found to degrade RDX mainly through the (pathway B, Figure 1.9). Additionally, the aerobic RDX- transformation by XenA and XenB mainly occurs through this pathway [94].

Biodegradation of RDX can also occur via denitration. In this pathway, the denitration of RDX results in the cleavage of the ring structure and produces 4-nitro-2,4-diazabutanal (NDAB, $\text{NO}_2\text{NHCH}_2\text{NHCHO}$), methylenedinitramine (MEDINA, $\text{NO}_2\text{NHCH}_2\text{NHNO}_2$), and formamide. NDAB is the dead end product, which is mainly produced from di-denitration and di-hydration of RDX. MEDINA is an intermediate product of mono-denitration and mono-hydration of RDX which, with formamide, are further transformed abiotically to N_2O , NH_3 , and CO_2 (Figure 1.10)[88]. Interestingly, although this pathway was described in aerobic bacteria, oxygen is not involved in microbial degradation of RDX [89].

Three enzymes have been identified that denitrate RDX via this pathway; an eukaryotic cytochrome P450 2B4 (EC 1.14.14.1) from rabbit liver [85], a cytochrome P450 from *Rhodococcus rhodochrous* 11Y called XplA [95, 96] and a flavoprotein diaphorase (EC 1.8.1.4) from *Clostridium kluyveri* [97].

Bhushan *et al.* (2003) [85] has shown that the cytochrome P450 2B4 can degrade RDX in the same pathway (Figure 1.10) with the production of nitrite, formaldehyde and NDAB. Interestingly, the activity of cytochrome P450 2B4 toward RDX was three fold faster than the activity of the enzyme towards its reported standard substrate pentoxyresorufin in pH 7.2 at 37 °C. Additionally, enzyme activity was strongly inhibited by oxygen which reduced reaction rates three fold. Moreover, for the first time, it was proposed that a cytochrome P450 might be involved in RDX-degradation

by *Rhodococcus* sp. DN22 before the identification of XplA in *R. rhodochrous* 11Y [85].

The XplA protein is an unusual cytochrome P450 as it has a flavodoxin domain N-terminally fused with to a heme domain [96]. RDX degradation pathway by XplA from *R. rhodochrous* 11Y was described by Jackson *et al.* (2007) [95]; interestingly, denitration of RDX by XplA is not oxygen-dependent but the presence of oxygen determines the nature of the end products. Under aerobic condition, RDX is double denitrated and double hydrated to produce NDAB, two molecules of nitrite and one molecule of formaldehyde. Under anaerobic conditions, RDX is single denitrated and hydrated to produce MEDINA, one molecule of nitrite and one molecule of formaldehyde [95]. The denitration activity of XplA towards RDX was also reduced by two folds in aerobic conditions compared to anaerobic conditions (Figure 1.10) [98].

Diaphorase (EC 1.8.1.4) from *Clostridium kluyveri* transforms RDX anaerobically via the mono denitration pathway. Similar to the anoxic denitration of RDX by XplA, the RDX ring structure is cleaved after the first denitration and hydration to produce MEDINA, which is then converted to nitrite, formaldehyde, ammonium, and nitrous oxide (Figure 1.10). Likewise XplA and cytochrome P450 2B4, the activity of this enzyme was inhibited by oxygen and reduced activity by 92 % under aerobic condition [97].

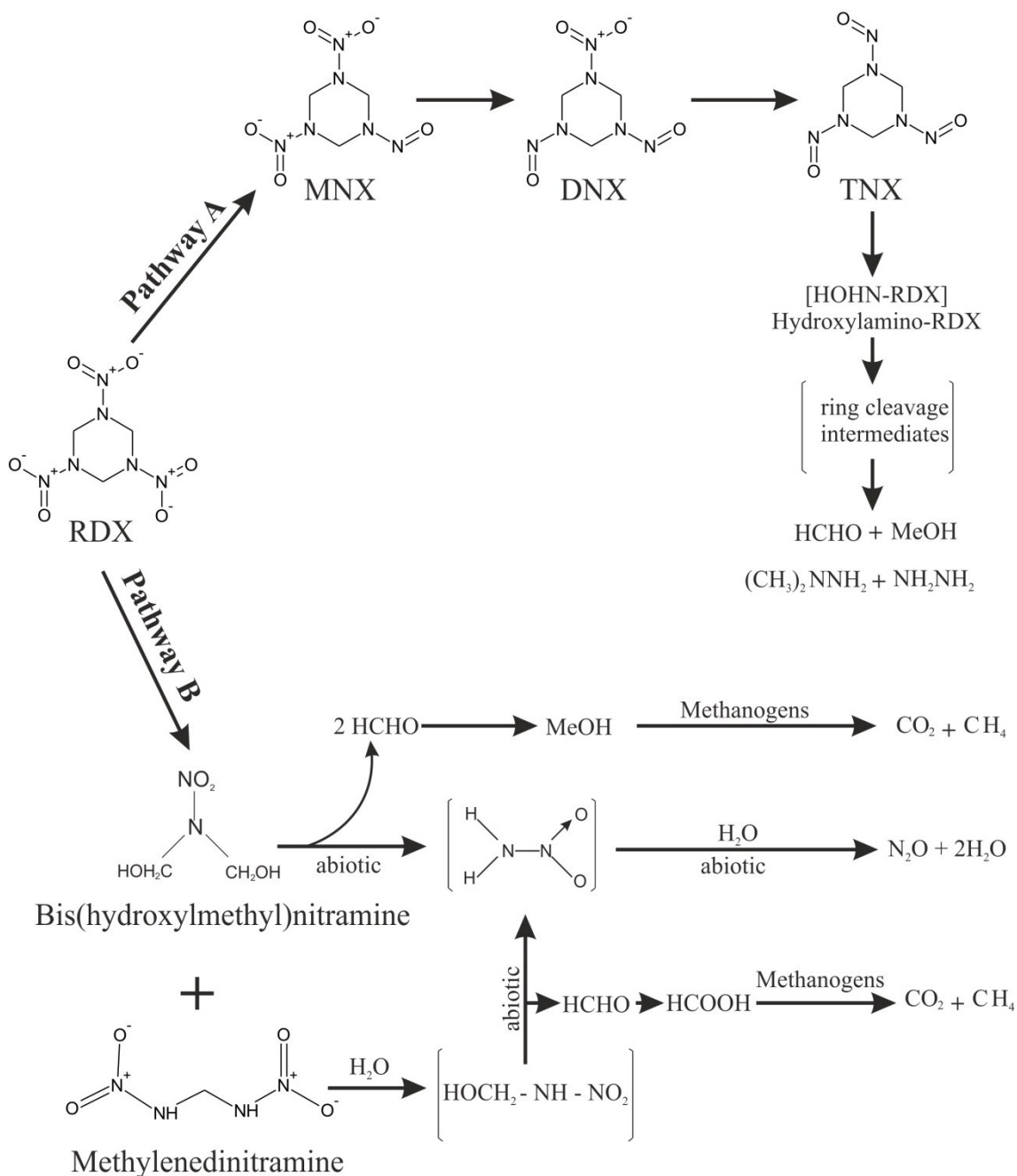


Figure 1.9: Biodegradation of RDX under anaerobic conditions. In Pathway A, RDX is degraded via a two electron reduction to form MNX, DNX and TNX [86]. In Pathway B, the ring structure of RDX is cleaved via a single electron reduction by Type I reductase to produce methylenedinitramine and bis(hydroxymethyl) nitramine, which is then converted to nitrous oxide, carbon dioxide, and methane [87]. The structures are drawing using ChemSketch version 12.0 [56] by Chong (2011) [57].

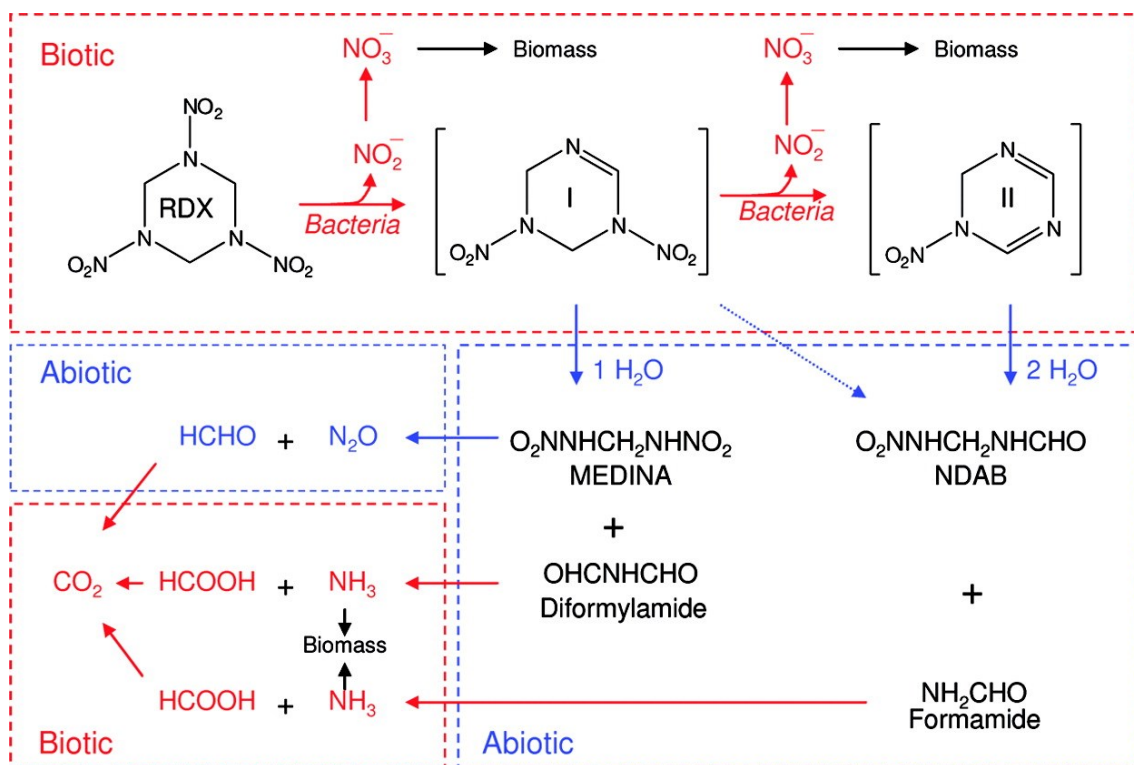


Figure 1.10: Aerobic denitration pathway of RDX in *Rhodococcus* sp. DN22. The intermediate products I and II are the result of single and double denitration processes, respectively. Reproduced from Annamaria *et al.* (2010) [88].

1.3.5 RDX denitration by cytochrome P450 XplA

Although diaphorase (EC 1.8.1.4) [97], cytochrome P450 2B4 (EC 1.14.14.1) [85], XenA, XenB [94], Type I nitroreductase [90] and nitrate reductase (EC 1.6.6.2) [91] can all transform RDX, research has mainly focused on XplA as a potential enzyme to clean up RDX-contaminated sites as it degrades RDX in both aerobic and anaerobic conditions and the rate of the RDX-removal is faster than by other reported enzymes.

The gene *xplA* encoding XplA was first identified by Seth-Smith *et al.* (2002) in the 7.5 kbp pHSX1 genomic library of *R. rhodochrous* 11Y, an RDX-degrading bacterium isolated from explosive contaminated soil of the UK. When the pHSX1 fragment of 11Y was transferred into non-RDX-degrading bacterium *R. rhodochrous* CW25, the transformed CW25 acquired RDX-degradation capacity. Sequencing of pHSX1 showed that the region encodes a flavodoxin reductase, a flavodoxin domain fused to cytochrome P450 and an acetyl CoA synthase (Figure 1.11) [96]. To identify the key enzyme responsible of RDX-degradation capacity in the pHSX1 region, the pHSX1 region was sub-cloned into 3.5 kbp pHSX1a and 2.3 kbp pHSX1b (Figure 1.11). Each sub-clone was transferred into *R. rhodochrous* CW25, and transformed CW25 with either sub-clone acquired the ability to degrade RDX. It was therefore concluded that XplA is an essential enzyme for RDX degradation and indigenous reductase from the host cell can supply electrons to XplA when the reductase partner is missing [96].

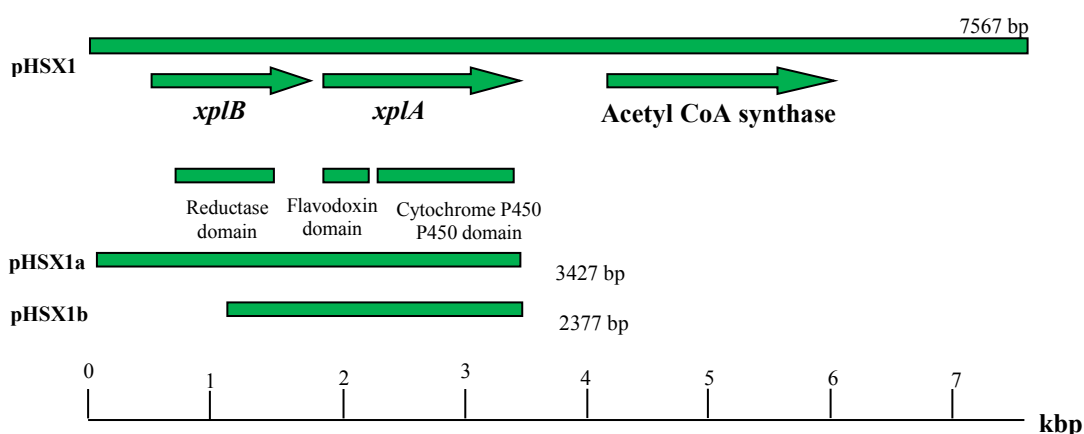


Figure 1.11: The 7.5 kbp fragment flanking the *xplA/xplB* region from *R. rhodochrous* 11Y responsible for conferring the ability to degrade RDX in *R. rhodochrous* CW25. The region was found to encode three proteins; ferredoxin reductase (XplB), a flavodoxin domain fused N-terminally to the cytochrome P450, and acetyl CoA synthase. Reproduced from Seth-Smith *et al.* (2002) [96].

The XplA from *R. rhodochrous* 11Y was recombinantly expressed and characterised. Spectrophotometric analysis of purified XplA showed the peak of the protein at 420 nm, and this peak shifted to 408 nm upon reduction with sodium dithionite, and then shifted back to 448 nm, a characteristic Soret peak of cytochrome P450, when the reduced XplA was bubbled with carbon monoxide (Figure 1.12) [98].

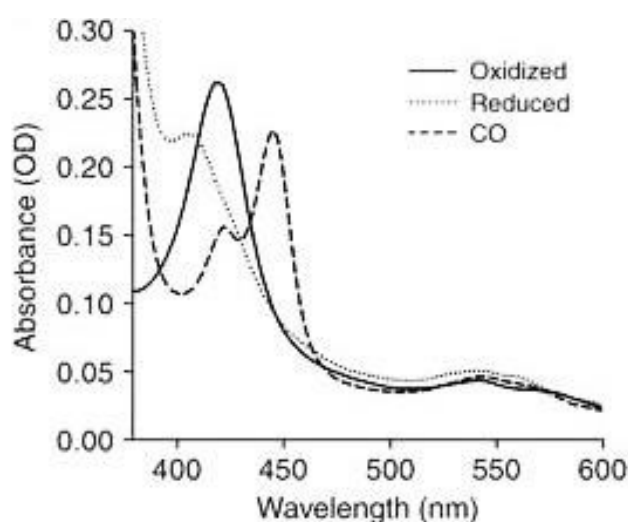


Figure 1.12: Spectrophotometric analysis of the purified XplA protein in oxidised form, reduced form with sodium dithionite, and reduced with CO. Reproduce from Rylott *et al.* (2006) [98].

Digestion of the purified protein with trypsin and mass spectrometry (MS/MS) identification of the peptides revealed that the P450 domain of XplA is fused to a flavodoxin protein; a unique arrangement which was not previously known for cytochrome P450 proteins. Moreover, it was shown that the flavodoxin domain of XplA is active and has an FMN cofactor [98]. Interestingly, RDX denitritation by XplA is not an oxygen-dependant reaction, different from most other cytochromes P450 which usually have oxygenase activity [95]. The crystal structure of the XplA-heme revealed the oxygen-independent activity of this protein is due to the replacement of highly conserved residues Glu/Asp-Thr/Ser in other P450s, required for oxygenase activity, with Met-394 and Ala-395 in the active site of XplA. The importance of Ala-395 for denitritation activity of the enzyme was shown by mutating the residue to threonine: this dramatically reduced the k_{cat}/K_M of the enzyme by approximately 200-fold (More details on crystal structure of XplA-heme is on Chapter 6) [99].

Intriguingly, since the identification of *xplA* in *R. rhodochrous* 11Y, the gene has been identified in a number of RDX-degrading bacteria around the world with > 99 % sequence identity. Homologues of *xplA* were found in 18 RDX-degrading *Rhodococcus* spp isolates from the UK [100]; *Rhodococcus* sp. DN22 isolated from Australia [100]; *Rhodococcus* sp. YH1 [100], *Rhodococcus* sp. T7, and *Rhodococcus* sp. T9N isolated from Israel [101] *Gordonia* sp. KTR9, *Williamsia* sp. EG1 [102], and *Microbacterium* sp. MA1 isolated from United States [103].

The presence of nearly identical *xplA* in RDX-degrading bacteria isolated from distinct geographical locations suggests the recent evolution of the gene. Interestingly, sequence comparison of the 52.2 kbp partial sequence of the plasmid carrying *xplA* in *Microbacterium* sp. MA1 with the 7.5 kbp sequence of the pHSX1 library of *R. rhodochrous* 11Y revealed that in addition to *xplA/xplB*, there is a ~4 kbp flanking region that is also nearly identical (> 99%) between these two phylogenetically distant related bacteria [103]. Therefore, it was suggested that the gene was acquired by horizontal gene transfer prior to its global distribution. Furthermore, the conjugal transfer of plasmid pGKT2, which carries *xplA* and *xplB*, from *Gordonia* sp. KTR9 to *Gordonia polyisoprenivorans*, *Rhodococcus jostii* RHA1 and *Nocardia* sp. TW2 has been reported, which further supports this proposal [104].

Similar to XplA, its partnering reductase XplB from *R. rhodochrous* 11Y has been recombinantly expressed and characterised [95]. XplB is a flavoprotein, containing one molecule of FAD as a co-factor. The protein was expressed recombinantly fused with a GST tag. Cleavage of the GST-tag from XplB resulted in precipitation of the protein. Soluble XplB was shown to actively transfer electrons from NADPH to the heme centre of XplA to degrade RDX; suggestion XplB is a reductive partner to XplA. Additionally, *xplB* has been also found alongside *xplA* in all aerobic RDX-degrading bacteria that have been tested to date. However, in *Gordonia* sp. KTR9, *xplB* is naturally fused to *glnA* which encodes glutamine synthetase [105].

1.3.6 Application of XplA and XplB for environmental remediation

Pollution by explosives has risen in recent years as a major environmental concern. Methods like incineration and composting have been applied to de-contaminate polluted areas, however these methods can be expensive and some in some cases produce additional environmental problems.

The XplA and XplB enzymes have also been intensively studied for their potential ability to remediate RDX. For this purpose, transgenic lines of *Arabidopsis thaliana* expressing *xplA*, were initially created and tested for RDX-removal capacity in axenic liquid cultures. The transgenic lines rapidly removed all the RDX whereas untransformed plant lines had no significant uptake of RDX during the same time course [98].

The plant line with the highest rate of RDX removal (35S::*XPLA*-10) was selected for further studies using soil contaminated with 50, 250, 500 and 2,000 mg/kg of RDX. In addition to the fact the transgenic plants did not show any sign of suffering from the phytotoxic effect of RDX, the shoot and root biomasses of these plants were nearly three times bigger than the wild-type. Moreover, three times less RDX was detected in the transgenic line compared to wild-type. Thus, *xplA* in *A. thaliana* confers resistance to RDX toxicity. That the transgenic line produced greater shoot and root biomasses in the presence of RDX compare to plants grown on pristine soil suggests that *xplA* also confers the ability to use RDX as a source of nitrogen [98] (Figure 1.13).

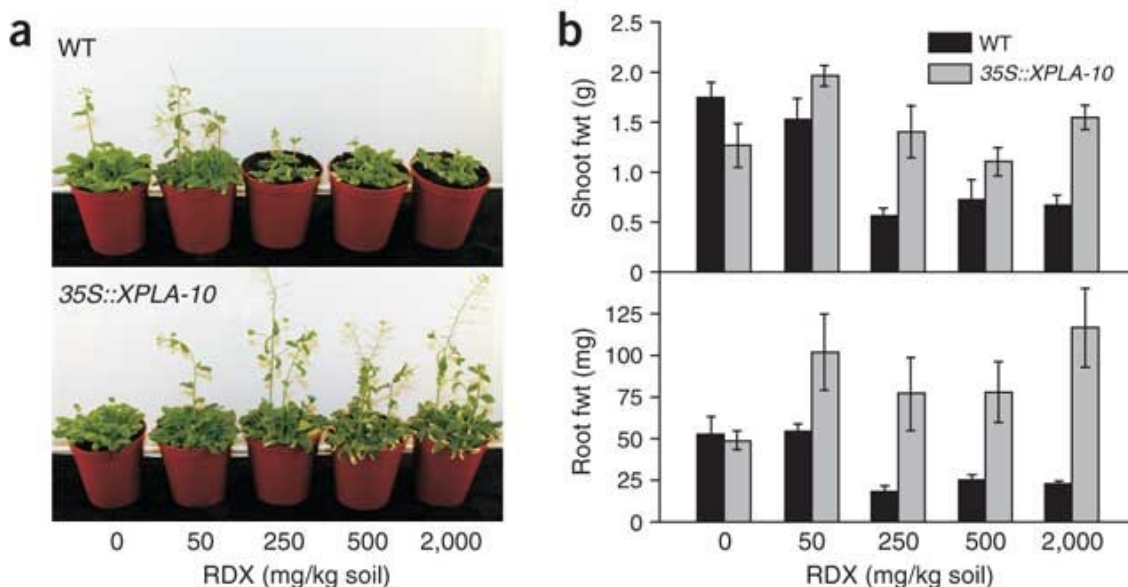


Figure 1.13: (A) Growth of eight week old transgenic (*XPLA-10*) line and wild-type plants in uncontaminated and soil contaminated with 50, 250, 500 and 2000 mg/ kg RDX. (B) Shoot and root biomass of wild-type and transgenic plants. Fwt– fresh weight. Reproduced from Rylott *et al.* (2006) [98].

Homozygous *XPLAB* transgenic lines was created by transforming *35S::XPLA-10* with *xplB* gene. Transferring *xplB* to *XplA*-expressing lines remarkably improved the RDX-removal capacity by the *xplA* transgenic line. RDX-removal by the eight-week old *XplAB-2* and *XplAB-27* lines in a soil leachate was four times higher than *35S::XPLA-10* transgenic plant; all RDX (180 μ M) was disappeared from by *XplA/XplB* expressing lines, whereas just 25% of RDX removed by *35S::XPLA-10* transgenic line, and no RDX removal were detected with wild-type [95].

Although these transgenic plants were shown to actively remove RDX in soil contaminated with RDX, one obstacle to the application of transgenic plants in the real world would be the inhibitory effect of the co-contaminant explosive TNT towards *XplA* in the contaminated site. It has been shown that TNT strongly inhibits the RDX-denitration activity of *XplA* [95], as well as RDX-degradation activity by *Rhodococcus* sp. YH1 [106].

To overcome this barrier, the *XplAB-2* transgenic line was re-transformed with the *nfsI* gene from *Enterobacter cloacae*, encoding a TNT-transforming enzyme. The transgenic plants could not only degrade RDX, but could also withstand the phytotoxicity and

inhibitory effects of TNT. Currently, Professor Neil Bruce's group, and collaborators, are studying switchgrass (*Panicum virgatum*) transgenic lines expressing *xplA/xplB* and *nfsI*, and field trials of RDX phytoremediation by transgenic plants are underway at an explosive-contaminated site in the U.S.

1.3.7 Aims of the project

The explosive RDX is a strictly xenobiotic compound and has been in the environment for a relatively short period of time. To date XplA has only been identified in bacteria from explosive contaminated sites, and no close homologues or natural substrates have been identified for XplA. These findings lead to intriguing questions about the origin of XplA, thus, the aims of this study are to:

- 1- Isolate new bacteria harbouring similar XplA or different enzymes with activity towards RDX allowing the construction of an evolutionary map for *xplA*, as well as an attempt to discover a new RDX-degrading enzyme not affected by TNT.
- 2- Investigate the mechanism by which *xplA*-carrying bacteria survive in explosive contaminated sites, in which TNT is a co-contaminant.
- 3- Compare *xplA*-flanking regions in RDX-degrading bacteria isolates that have originated from distinct geographical locations in order to characterise the mobile element carrying the gene.
- 4- Investigate the potential evolutionary advantage of the natural fusion of XplB to glutamine synthetase (XplB-GS) protein in RDX-degrading bacterium *Gordonia* sp. KTR9.
- 5- Shed light on the evolutionary origin of the *xplA* gene by characterising three putative cytochromes P450 whose sequences have been recently released and share sequence similarity to XplA.

Chapter 2: Materials and Methods

2.1 Chemicals and reagents

All chemicals, reagents and DNA modification enzymes used in this study, unless specified, were purchased from Bio-Rad Laboratories Ltd., Invitrogen, New England Biolabs, Promega, Sigma-Aldrich and Thermo Fisher Scientific.

The explosives RDX and TNT (both > 95% purity) were kindly provided by the Defence Science and Technology Laboratory, Fort Halstead, U.K.

Oligonucleotide primers for routine PCR were designed using an online service (<http://primer3.ut.ee/>) [107, 108]. Primers for cloning were designed based on the In-Fusion® HD cloning (Clontech Laboratories) website (<http://bioinfo.clontech.com/infusion/convertPcrPrimersInit.do>). For site directed mutagenesis studies, primers with substituted nucleotides were designed manually following the criteria detailed by the QuickChangeII Site-Directed Mutagenesis method. All primers were synthesised either by Sigma-Aldrich or Integrated DNA Technologies. A list of the primers used in this study, unless otherwise specified, can be found in Table 2.1.

2.2 Bacterial strains

The aerobic RDX-degrading bacteria used to characterise the RDX-genomic island belonged to four different genera and originated from different geographical locations (Table 2.2). *Gordonia terrae* strain NBRC 100016 and *Gordonia polyisoprenivorans* NBRC 16320 were supplied by The Biological Resource Centre (NBRC), National Institute of Technology and Evaluation (NITE) in Japan.

Escherichia coli DH5 α (Invitrogen) was supplied from NCB group socks. *E. coli* BL21 (DE3) was supplied by Invitrogen, *E. coli* Rosetta 2 (DE3) by Novagen-Merck and *E. coli* ArtricExpress by Agilent Technologies.

2.3 Plasmids

The gene expression vectors used in this study were pET-16b (Novagen-Merck), pET-28a (+) (Novagen-Merck) and pGEX2T (GE Healthcare Life Sciences).

The pET-16b vector has an ampicillin/carbenicillin selective marker and is used to express genes as N-terminally His-tagged proteins (Figure 2.1). pET-28a(+) has a kanamycin selective marker and is used to express genes as either N-terminally or C-

terminally His-tagged proteins (Figure 2.2). pGEX2T also has a carbenicillin/ampicillin selective marker and is used to increase the solubility of the protein tagging the coding region N-terminally with a glutathione S-transferase (GST) peptide (Figure 2.3).

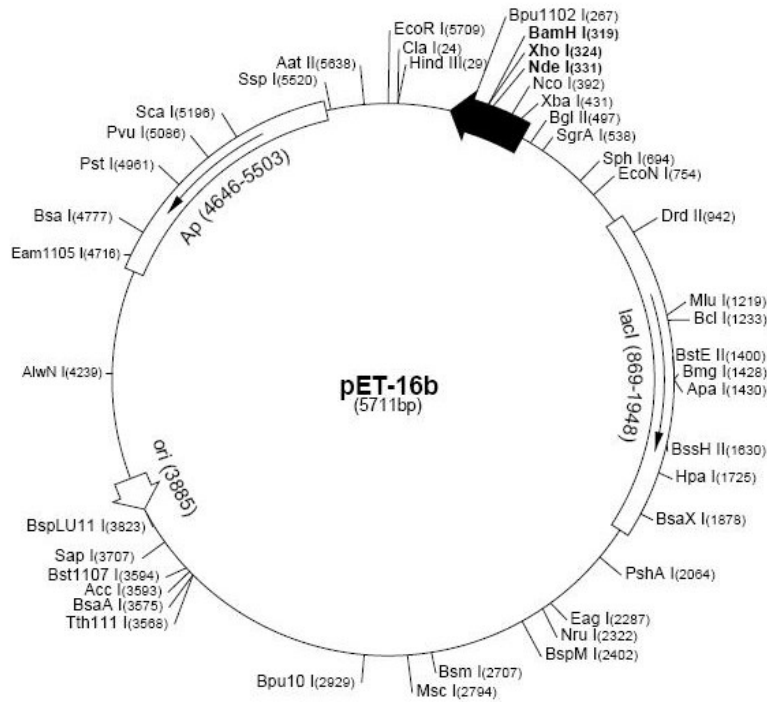


Figure 2.14: Vector map of pET-16b. The vector has an ampicillin (shown as Ap in the figure) resistance gene and is designed to express heterologous genes as His-tag proteins using a T7 promoter. Multiple cloning sites in the vector are shown as a black arrow.

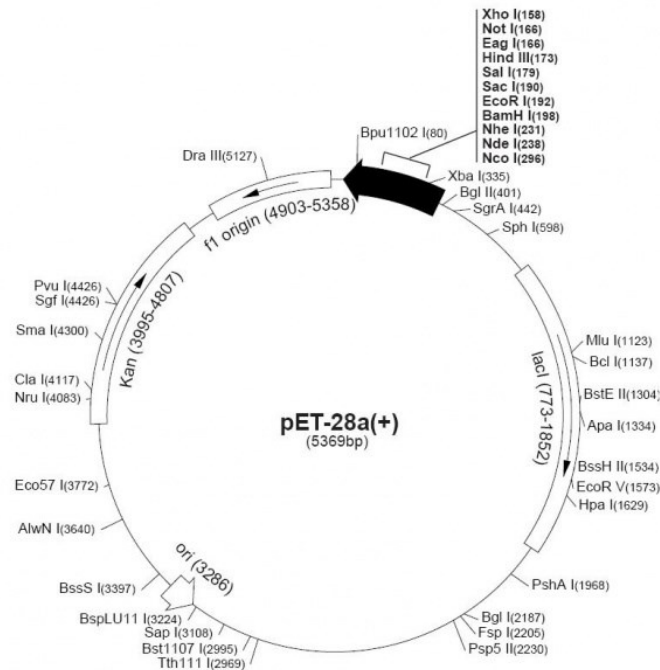


Figure 2.15: Vector map of pET-28a(+). The vector has a kanamycin (shown as Kan) resistance gene and is designed to express heterologous genes as N-terminal or C-terminal His-tag proteins using a T7 promoter. Multiple cloning sites in the vector are shown as a black arrow.

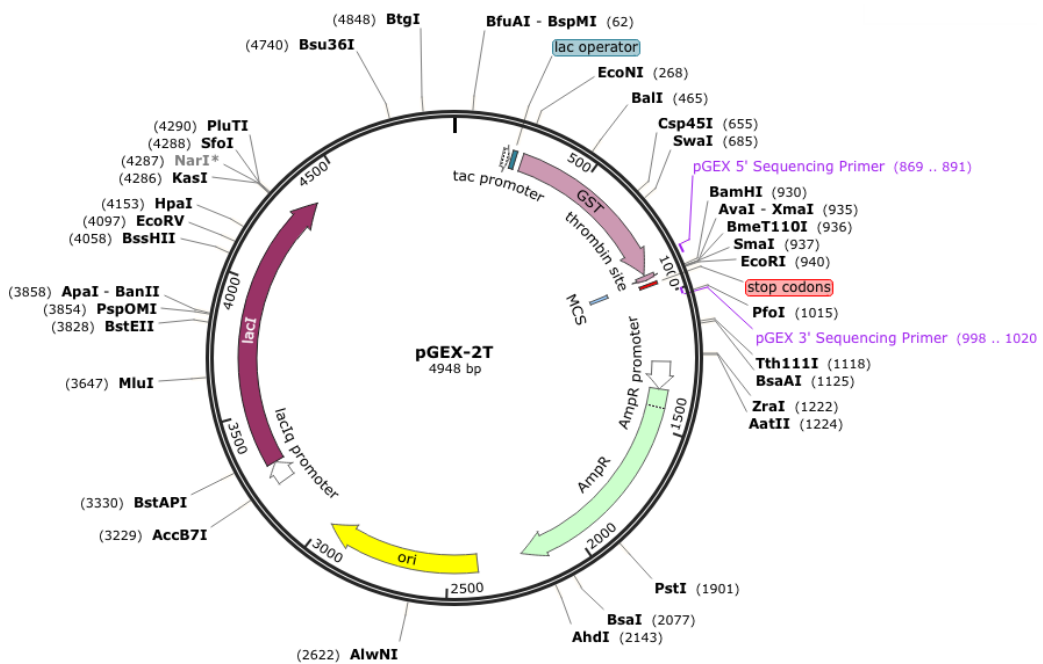


Figure 2.16: Vector map of pGEX-2T. The vector has ampicillin/carbenicillin resistance gene and is designed to express heterologous genes with an N-terminally fused glutathione S-transferase (GST) peptide using the *tac* promoter.

Table 2.1: List of the primers used in this study:

Primer used to amplify RDX-degrading genomic island amongst RDX-degrading bacteria (Chapter 4)

| Name | Primer binding sequence | Sequence 5'-3' | Product size (bp) |
|------|-------------------------|--------------------------------|-------------------|
| A-F | GAF-F | CGATTCCGTATCCGACCTC | 1,426 |
| A-R | TranscRp-504R | GATGTTCTCCGTTGATCG | |
| B-F | RegulatoryPrt-89F | GGTTCACATGGCTTTTCACC | 886 |
| B-R | SensorK-935R | CTATCGCATCGCTCAGGAGT | |
| C-F | SensorK-1078F | CATTCCGTCTATTCCGGTTC | 958 |
| C-R | SensorK-123R | CGTGGTCGTGACAGTCATCT | |
| D-F | Sensork-337F | CGTCATCAGTACGAGCTGGA | 1,295 |
| D-R | Carbesterase-167R | AGAGTCGGGCACATGACAC | |
| E-F | HypoPrt-453F | GGTCTCGCAACACACTGAAC | 1,274 |
| E-R | MarR-194R | GCACTGTTGAGTCCGAGATG | |
| F-F | HypoPrt-453F | ACGTCGGAATTCAGTGTCCGGCCGGACC | 1,351 |
| F-R | Permease-6R | GAGTCGAAGAGGGCACTCAG | |
| G-F | Permease-7F | CTGTGTGGTGTGGTGATGGT | 1,038 |
| G-R | Permease-7R | CTACTCCCCGGTCTTCTTCGGAAT | |
| H-F | Permease-8F | ACTACATCGTGCTGCTGTCC | 1,078 |
| H-R | Dihydro-8R | GTCGAGCATATGCACGTCGGGGATACG | |
| I-F | Dihydro-9F | GATGTCAACGAATGGACGAT | 1,049 |
| I-R | xplB-9R | GTCGATCCGAAGTGGAACAC | |
| J-F | xplB-10F | CGGTGATGATGCGTGAAC | 900 |
| J-R | XplA-192R | CAGTTCACCCTCTCCGTAGGTGGAGGTGAC | |
| K-F | xplB-11F | ACCCGAACACCCGAGATGGAGTGTGGAGA | 1,065 |
| K-R | xplA-11R | TCAGATAGCCGAAAGCGACT | |
| L-F | xplA-12F | CACGCGTCCTACAACACTACC | 1,073 |
| L-R | SSD12R | AACAGCTCCTCACGGTAAGC | |
| M-F | xplA13F | ATCGTCCTGTCCTGAAAACC | 977 |
| M-R | AMP13R | GTTGTGGCAGGTGTTGAGTT | |
| N-F | AMP14F | ATCAGCGATGGGACGATAC | 1,143 |
| N-R | AMP14R | ATGCCAGGTGAACGTGT | |
| O-F | AMP15F | GTGATGTACGAGGGCAAGC | 981 |
| O-R | AMP486dwnR | GACGGCATACAAGACGAACA | |

Primers to amplify the internal region of the *xplA* (Chapter 3)

| Name | Sequence 5'-3' |
|------------|----------------------|
| XplA-513F | AGAGTTTGATYMTGGCTCAG |
| XplA-1033R | TCAGATAGCCGAAAGGGACT |

Primers to amplify 16S rRNA [109] (Chapter 3 and 4)

| Name | Sequence 5'-3' |
|-------|-----------------------|
| 7F | AGAGTTTGATYMTGGCTCAG |
| 1510R | ACGGYTACCTTGTTACGACTT |

Primers to sequence inserts in expression vectors (Chapter 4, 5 and 6)

| Name | Sequence 5'-3' |
|---------------|-------------------------|
| T7 Promoter | TAATACGACTCACTATAGGG |
| T7 Terminator | GCTAGTTATTGCTCAGCGG |
| pGEX 3' | GGGCTGGCAAGCCACGTTTGGTG |
| pGEX 5' | CCGGGAGCTGCATGTGTCAGAGG |

Primers to clone *xplB-glnA* into pET-28a(+) and pGEX2T (Chapter 5)

| Name | Sequence 5'-3' |
|-----------------------------|--|
| pET-28- <i>xplB-glnA</i> -F | TCGCGGATCCGAATTCATGAGTACATCCGCGCTCG |
| pET-28- <i>xplB-glnA</i> -R | GGTGGTGGTGTCTCGAGTCAGCAGACCGATTTCGGCCG |
| pGEX- <i>xplB-glnA</i> -F | GGTCCGCGTGGATCCATGAGTACATCCGCGCTCG |
| pGEX- <i>xplB-glnA</i> -R | GTCGACCCGGGAATTCCTCAGCAGACCGATTTCGGCCG |

Primers to mutate Trp-386 to Ser in XplB from *R. rhodochrous* 11Y, and mutate Ser-385 to Trp in XplB-GS (Chapter 5)

| Name | Sequence 5'-3' |
|------------------|-------------------------------|
| XplB(W386S)-F | GTCGATTTTCGACGGCTCGATGCGGATCG |
| XplB(W386S)-R | CGTCGATCCGCATCGAGCCGTCGAAA |
| XplB(S385W)-GS-F | GTCGATTTTCGACGGCTGGATGCGGATCG |
| XplB(S385W)-GS-R | CGTCGATCCGCATCCAGCCGTCGAAA |

Primers used to clone cytochromes P450 into expression vectors (Chapter 6)

| Name | Sequence 5'-3' |
|--------------------|---|
| pET-28GtP450-F | TCGCGGATCCGAATTCATGACCCTGATCCATGTCTGGTA |
| pET-28GtP450-R | GGTGGTGGTGCTCGAGTCAGCTCAAGGAGATGGGCAT |
| PET-16bCYPA-F | TCGAAGGTCGTCATATGATGAGCGACATACAAGCTGC |
| pET-16bCYPA-R | GTTAGCAGCCGGATCCTCAGGGAATCAGGCGTAGAG |
| pET-16bCYPB-F | TCGAAGGTCGTCATATGATGACAACCACTGACACACTGT |
| pET-16bCYPB-R | GTTAGCAGCCGGATCCTCATGACAGGCGGACAGTA |
| pET-28-CYPA-F | AGGAGATATACCATGGCAATGAGCGACATACAAGCTC |
| pET28-CYPA-R | CCGCAAGCTTGTGACGGGAATCAGGCGTAGAGG |
| pET-16b-turnCYPA-F | TCGAAGGTCGTCATATGGCAACGTCAACCAGTCCC |
| pET-16b-turnCYPA-R | TCGAAGGTCGTCATATGACGTCAACCAGTCCCGCA |

Primers used for site directed mutagenesis in the cytochrome P450 (CYPA) in *Gordonia polyisoprenivorans* NBRC 16320 (Chapter 6)

| Name | Sequence 5'-3' |
|--------------|--------------------------------------|
| CYPA-D256A-F | GGGCACATGGCCGTCGGGTACCTGATCGCAGC |
| CYPA-D256A-R | ATCAGGTACCCGACGGCCATGTGCCCGAGGC |
| CYPA-E299Q-F | CGATCCACCACAACTGTGTTTCTACCGGT |
| CYPA-E299Q-R | GTTAGCAGCCGGATCCTCAGGGAATCAGGCGTAGAG |
| CYPA-P184L-F | GAGACCATGCTGATGCTGGCCG |
| CYPA-P184L-R | GCCAGCATCAGCATGGTCTCGAA |
| CYPA-L252V-F | GATGCTTTACAGCGTCCGGGCACATG |
| CYPA-L252V-R | GCCATGTGCCCGACGCTGTAAAG |
| CYPA-M248V-F | CGTGCGACAGCGCTGGTGCTTTACAG |
| CYPA-M248V-R | CGACGCTGTAAAGCACCAGCGCTGTC |
| CYPA-I100L-F | GTGCGAGACACGGTCCTCGGCAAGGA |
| CYPA-I100L-R | GCAGGTCCTTGCCGAGGACCGTGTCTC |

Primers used for site directed mutagenesis in the cytochrome P450 from *Gordonia terrae* NBRC 100016 (Chapter 6)

| Name | Sequence 5'-3' |
|----------------|---------------------------|
| GtP450-N396A-F | GGTGCACCCGCCCCCGCCTA |
| GtP450-N396A-R | GGTAGGCGGGGGCGGGTGCA |
| GtP450-P395M-F | GTCCGGTGCAATGGCCCCCGCCTAC |
| GtP450-P395M-R | GAGGTAGGCGGGGGCCATTGCACCG |

Table 2.2: List of RDX degrading bacteria used to study the RDX degrading genomic island (Chapter 4)

| Bacterial strains | 16s rRNA Accession number | Country of isolation | Source |
|-------------------------------|---------------------------|----------------------|------------------------------------|
| <i>R. rhodochrous</i> 11Y | AF439261.1 | UK | [110] |
| <i>Rhodococcus</i> sp. B1-1 | KF700363 | Belgium | Isolated by Dr. Astrid Lorenz |
| <i>Rhodococcus</i> sp. DS1 | KF933858 | Belgium | In this study |
| <i>Rhodococcus</i> sp. 9UK | KJ566615 | UK | Isolated by Dr. Cyril Bontemps |
| <i>Rhodococcus</i> sp. 5U | KJ566616 | Ukraine | In this study |
| <i>Rhodococcus</i> sp. YH1 | AF103733.1 | Israel | Provided by Prof Zeev Ronen [111] |
| <i>Rhodococcus</i> sp. DN22 | X89240.1 | Australia | [112] |
| <i>Rhodococcus</i> sp. EG2 | KF571869.1 | US | Provided by Dr. Peter Andeer [113] |
| <i>Williamsia</i> sp EG1 | KF571870.1 | US | Provided by Dr. Peter Andeer [113] |
| <i>Microbacterium</i> sp. MA1 | FJ357539 | US | Provided by Dr. Peter Andeer [103] |
| <i>Gordonia</i> sp. KTR9 | DQ068383 | US | Provided by Dr. Karl Indest [114] |

2.4 Media

2.4.1 Minimal medium

Minimal medium was made up of 50 mM potassium phosphate buffer (pH 7.2) containing glycerol (10 mM), glucose (5 mM), and succinate (5 mM) as a carbon source, trace elements [115], and 100 μ M RDX from a 1 M stock of RDX dissolved in DMSO, unless otherwise specified, as a sole source of nitrogen.

2.4.2 Luria Bertani Broth (LB) medium

Luria Bertani Broth (LB) medium was prepared by dissolving tryptone (10 g/L), yeast extract (5 g/L) and NaCl (10 g/L) in distilled water. Luria-Bertani Agar (LA) was made by adding 15 gram of agar into 1 L of LB prior of autoclaving.

2.4.3 MacConkey Broth

MacConkey broth was prepared by dissolving 40 g/L of MacConkey powder (Oxoid) in water.

2.4.4 SOC media

SOC (Super Optimal broth with Catabolite repression) was prepared by dissolving of NaCl (0.5 g/L), tryptone (20 g/L) and yeast extract (5 g/L) in water. The medium was autoclaved and then 20 mM of sterile filtrated glucose was added.

2.4.5 RDX dispersion agar plates

The RDX dispersion agar plates were made by dissolving 15 g of agarose in 1 L minimal medium (section 2.4.1) containing 2 mM RDX as a sole source of nitrogen. The plates have an opaque appearance due to insoluble crystals of RDX (the solubility limit of RDX is $< 180 \mu\text{M}$ at $30 \text{ }^\circ\text{C}$ [116]). Bacteria able to degrade RDX create a zone of clearance which is produced by the removal of precipitated RDX.

2.4.6 *Gordonia terrae* strain NBRC 100016 growth medium

Both broth and agar plates for culturing *G. terrae* strain NBRC 100016 were prepared according to the supplier's protocol as follows: Broth (pH 7.0) was prepared by dissolving of peptone (5 g/L), yeast extract (3 g/L), and $\text{MgSO}_4 \cdot 7\text{H}_2\text{O}$ (1 g/L) in distilled water. Yeast-Krainsky's Agar (pH 7.3) used for plating bacteria was made by dissolving glucose (10 g/L), L-asparagine (1 g/L), K_2HPO_4 (0.5 g/L), yeast extract (2 g/L) and agar (17 g/L) in water.

2.4.7 *Gordonia polyisoprenivorans* NBRC 16320 growth medium

The broth medium (pH 7.0) was made of polypeptone (10 g/L), yeast extract (2 g/L) and $\text{MgSO}_4 \cdot 7\text{H}_2\text{O}$ (1 g/L) in distilled water. Plates were made by adding 15 g/L of agar to the broth medium.

2.4.8 Y medium

The Y medium (pH 7.6) was made up of yeast extract (5 g/L), tryptone (20 g/L) and MgSO₄·7H₂O (5 g/L) in distilled water. The pH was adjusted to 8 with 20 mM Tris-HCl.

2.5 Microbiological techniques

2.5.1 Bacterial growth on RDX medium

Growth and RDX removal of RDX-degrading bacteria were compared by inoculating 50 µl of 0.1 g/ml bacterial cells into 50 ml minimal medium in 250 ml flasks containing 100 µM RDX as the sole source of nitrogen, at 30 °C with shaking at 180 rpm. The growth of the bacteria was monitored by measuring the OD₆₀₀ using a UV-160A recording spectrophotometer (Shimadzu Corp., Kyoto, Japan). The RDX depletion was measured by taking 200 µl samples from the culture, centrifuging at 13,000 rpm for 10 minutes and analysing the supernatant by HPLC (Section 2.8.1).

2.5.2 Resting cell experiments

The RDX-degrading bacteria (50 µl) from 0.1 g /L cells in 50 mM potassium phosphate buffer pH 7.2 were inoculated into 50 ml minimal medium in 250 ml flask containing 100 µM of RDX. Bacteria were grown at 30 °C with shaking (180 rpm) to OD₆₀₀ ~0.4-0.6. Cells were harvested by centrifuging the culture in 50 ml Falcon tubes at 4,500 rpm for 10 minutes. The cells were washed twice with 50 mM potassium phosphate buffer (pH 7.2) to remove any RDX absorbed to the cells. Cell suspensions (100 µl), made from 0.1 g wet cell biomass in 1 ml of potassium phosphate buffer pH 7.2, was added to 900 µl of potassium phosphate buffer (pH 7.2) containing 100 µM of RDX as a final concentration. Resting cell assays were carried out at room temperature with shaking at 3,000 rpm. RDX removal by the bacteria was monitored by taking 100 µl aliquots at different time points followed by a quick stop of the reaction with 10 µl of 10 % TCA. The RDX concentration was measured by injecting 50 µl of the reaction into the HPLC (Section 2.8.1).

2.5.3 Effect of TNT on RDX degradation by bacteria

The inhibitory effect of TNT on RDX degradation by bacteria was investigated by comparing the RDX removal capacity of the bacteria in the presence and absence of 2 μ M TNT. Cell suspensions (100 μ l), made up of 0.1 g/ml of cells, were used to inoculate 50 ml of minimal medium in 250 ml flasks containing 100 μ M RDX, with or without 2 μ M TNT. Cultures were grown with shaking (180 rpm) at 30 °C degree. RDX removal from both cultures were compared by taking an aliquot (200 μ l) from the cultures after 9 hours incubation.

2.6 Molecular biology techniques

2.6.1 Bacterial total genome extraction

Bacterial total genomic DNA was extracted by lysing the bacterial cells using TE buffer containing 10 mg/ml lysosyme, 10 % SDS and 20 mg/ml proteinase K. Cell debris was pelleted by centrifugation at 8000 rpm and proteins were removed using phenol-chloroform. Nucleic acids were precipitated using 3M sodium acetate and isopropanol, washed in 70 % ethanol and resuspended in nuclease free water.

2.6.2 Total genome sequencing

The total bacterial genome was extracted (section 2.6.1) and sequenced on the Next Generation Sequencing platform Ion Torrent (Life Technologies) at the Biorenewables Development Centre (University of York). The Ion Torrent sequencing platform was used because it was readily available at the University of York. Additionally, Ion Torrent is currently a fast, relatively cheap technique, which produces longer sequence reads than the other major sequencing platform available (Illumina). However, Ion Torrent has a lower read accuracy than Illumina (Miseq, GAIIx, HiSeq) [117]. The raw sequence reads were assembled using the software package Newbler (version 2.7).

2.6.3 Polymerase chain reaction

Polymerase chain reactions were performed in a PCR thermocycler (ThermoElectron Corp). GoTaq DNA polymerase (promega) was used for routine screening purposes and Phusion DNA polymerase (New England Biolabs) for 16S rRNA amplification, cloning and site directed mutagenesis.

GoTaq DNA polymerase reactions (50 μ l) contained 1.2 U GoTaq DNA polymerase, 2.5 mM MgCl₂ solution, 1x Green GoTaq Flexi buffer, 0.2 mM dNTPs, 0.5 μ M of primer, and 10-200 ng of DNA template. Thermocycler conditions consisted of one cycle of 95 °C for 2 minutes, and then 35 cycles of denaturation at 95 °C for 30 seconds, annealing at an optimised temperature for 30 seconds, and then extension at 72 °C for 1 minute/ 1 kbp amplicon. This was followed by a final extension phase at 72 °C for 10 minutes. Annealing temperatures varied according to each primer pair. In general, the annealing temperature of the reaction was the melting temperature of the primers minus 5 °C.

Phusion polymerase reactions (50 μ l) were made of 1.0 U Phusion DNA polymerase, 1x Phusion HF buffer, 3 % DMSO, 10 pmol of dNTPs, 0.5 μ M of each primer, and (50-250 ng) of DNA template. The following thermocycler conditions were used unless otherwise stated; one cycle of DNA denaturation at 98 °C for 30 seconds, followed by 25 cycles of denaturation at 98 °C for 10 seconds, annealing at 50-70 °C for 30 seconds and extension temperature at 72 °C (30 seconds/1 kbp of amplicon). This was followed by a final extension phase at 72 °C for 10 minutes.

2.6.4 Agarose gel electrophoresis

The DNA fragments and plasmids were separated using a 1 % (w/v) agarose gel made up from 1 gram of agarose dissolved in 100 ml of Tris-acetate-EDTA (TAE) buffer (4.84 g/L of Tris-HCl, 1 mmol of EDTA and 1.142 ml glacial acetic acid). Ethidium bromide (100 μ M) was added to the agarose before pouring the gel into the tray. The DNA samples (5- 10 μ l) were mixed with loading dye, consisted of 0.25 % (w/v) bromophenol blue, 0.25 % (v/v) xylene cyanol, and 30 % (v/v) glycerol, before loading into agarose gel wells. The DNA was visualized under UV light at 312 nm. The size of the DNA product was determined based on 1 kb DNA ladder (NEB).

2.6.5 Purification of DNA fragments for sequencing

The DNA fragments from PCR reactions or digested plasmids were cleaned up using Wizard[®] SV Gel and PCR Clean-Up System (Promega) according to the manufacturer's protocol. The DNA concentration was determined using a nanodrop spectrophotometer (Thermo Scientific).

2.6.6 Short fragment of DNA sequencing and analysis

The sequencing of short fragment DNA (PCR products or plasmids) was carried out at the Genomics Laboratory, Technology Facility (University of York) or at GATC-BIOTECH (UK). The ABI Sequence Scanner Software v1.0 (Applied Biosystems) was used to check the profile of the sequence.

2.2.7 Phylogenetic analysis

Taxonomic characterization of the isolates was performed by amplifying the 16S rRNA sequence using the 16S rRNA primers (Table 2.1) and Phusion High-Fidelity DNA Polymerase (NEB) (Chapter 2.6.3). The PCR products were cleaned-up (Chapter 2.6.5) and directly submitted for sequencing (Chapter 2.6.6). The phylogenetic trees were generated by first aligning the 16S rRNA sequences using ClustalX2, and then using MEGA software (version 6.0) [118], and Neighbour-joining method. The GenBank accession number for each sequence was obtained through submitting the sequence to the NCBI database from BankIt (<http://www.ncbi.nlm.nih.gov/WebSub/?tool=genbank>).

2.6.8 Generating competent *E. coli* cells

A single colony was used to inoculate 5 ml of pre-warmed Y medium for 2 hours with shaking at 37 °C. This starter culture was used to inoculate 250 ml LB medium in 2 L flask. Cells were grown at 18 °C with shaking to OD₆₀₀ 0.4-0.6. The culture was harvested by centrifugation at 4 °C for 15 minutes (13,000 x g). Cell pellets were resuspended in 100 ml filter sterilized ice-cold TfbI solution (potassium acetate (3 g/L), rubidium chloride (12 g/L), calcium chloride dehydrate (1.5 g/L), manganese (II) chloride tetrahydrate (9.9 g/L), glycerol (15%), pH 5.8 by adjusted it with 10% (v/v) acetic acid. The culture was incubated on ice for 5 minutes. Cells were harvested again at 4 °C with 3,000 rpm centrifugation for 15 minutes. Cells were resuspended in 10 ml filter sterilized TfbII (MOPS (10 mM), calcium chloride dehydrate (75 mm), rubidium chloride (10 mm) and glycerol (15%), pH 6.5 by adjusted it with KOH) and incubated on ice for 5 minutes. Aliquots (100 µl) of the cell solution were transferred to Eppendorf tubes, snap frozen in liquid nitrogen and stored in -80 °C freezer.

2.6.9 Plasmid transformation by heat shock method

The *E. coli* competent cells were transformed by adding 50-100 ng of the plasmid to the cells and incubating on ice for 30 minutes (1:50 of 10 fold diluted β -mercaptoethanol in water was added to ArcticExpress cells prior of transformation by 10 minutes). The heat shock was performed at 42 °C for 90 seconds (or 20 seconds for ArcticExpress). Cells were then incubated on ice for 10 minutes. SOC or LB medium (500 μ l) was added into the competent cells for incubation with shaking at 37 °C for 1 hour. An aliquot of the cells (50-150 μ l) was then spread on LB plates containing (50-100 μ g/ml) of plasmid selective antibiotic. In the case of *E. coli* Rossetta 2 (DE3) cells, additional 34 μ g/ml of chloramphenicol was added to the plate.

2.6.10 Plasmid extraction

Plasmid extraction was performed for cloning and sequencing purposes. The extraction was carried out using the QIAprep Spin Miniprep Kit (Qiagen) following manufacturer's protocol.

2.6.11 Restriction endonuclease digestion of DNA

Restriction endonuclease digestion of plasmids was carried out at 37 °C using the ratio of 10 U of enzyme to 1 μ g of plasmid DNA. The compatible buffer for restriction endonuclease digestion was chosen based on manufacturers recommendations.

2.6.12 DNA Cloning

All the cloning mentioned in this study was performed using the In-Fusion® HD cloning system (Clontech Laboratories). The method is fast and simple, allowing precise cloning of the DNA fragment into the linearized vector by adding 15 bp extensions (5') sequence at the ends of the primer, which are complementary to the linearized vector at the restriction site. The method allows cloning of any insert, into any location, within any vector. Furthermore, it does not require phosphatase treatment, or enzymatic ligation.

For the In-Fusion® HD cloning, primers for the gene of interest were designed based on the cloning vector and cloning site using the on-line software provided by manufacture (section 2.1). The gene of interest was amplified using PCR with high fidelity Phusion

DNA polymerase enzyme (New England Biolabs) (Section 2.6.3). The plasmid was linearized at the desired restriction sites using specific restriction enzymes (Section 2.6.11). Both linearized plasmid and the PCR products were cleaned up using Wizard[®] SV Gel and PCR Clean-Up System (Promega) (Section 2.6.5). Concentration of insert and plasmid were measured using a nanodrop spectrophotometer (Thermo Scientific). The cloning reaction (10 µl) was prepared by mixing 10-200 ng of PCR product (depending on the size of the gene of interest) with 50-200 ng of linearized vector, and 2 µl of 5x In-Fusion HD Enzyme Premix. The mixture was incubated at 50 °C for 15 minutes. An aliquot of the reaction (2 µl) was used to transform *E. coli* Dh5α competent cells (section 2.6.9). The successful clone was identified by colony PCR (Section 2.2.14). The correct sequence of the insert was confirmed by sequencing the plasmid using plasmid specific primers (Section 2.6.6).

2.6.13 Site directed mutagenesis

Site directed mutagenesis was carried out according to the QuickChangeII Site-Directed Mutagenesis protocol (<http://www.chem.agilent.com/library/usermanuals/Public/200523.pdf>). The mutant plasmid was created by PCR (Section 2.6.3).

PCR reaction (50 µl) was made with 1x Phusion HF buffer, primers (500 nM), plasmid (30-50 ng), dNTPs (200 µM), 1 U of Phusion DNA polymerase. The PCR programme was as follows; 98 °C for 5 minutes, 16 cycles of 98 °C for seconds and 72 °C for 6:30 minutes. Negative controls were prepared in which polymerase was not added. Successful mutations were primarily checked by running an aliquot of the reaction on agarose gel. The parental stand (methylated) was digested with *DpnI* (NEB) (20 U) at 37 °C for 1 hour. An aliquot (2 µl) of the reaction was transformed into *E. coli* DH5α competent cells. Plasmids of a few colonies were extracted (Section 2.6.10), and successful mutants were confirmed by sequencing the insert (Section 2.6.6).

2.6.14 Colony PCR

Colony PCR was performed for routine screening purposes. Single colonies were selected from the plate using a sterile pipette tip and stirred in a PCR tubes containing 25 µl of GoTaq polymerase reaction (Section 2.6.3). The reaction was performed in PCR thermocycler (Section 2.6.3).

2.7 Protein Techniques

2.7.1 Protein quantification

Protein concentrations were determined according to the Coomassie (Bradford) Protein Assay Reagent Kit (Pierce) (Figure 2.4). A standard curve was created by serial dilution of the provided albumin standard (BSA). Sample (10 μ l) was mixed with 300 μ l of the reagent. Reaction was carried out in 96 well plates. The absorbance of the samples was read at 595 nm. Protein concentration (μ g/ml) is calculated from the absorbance using the following equation: $C = A/0.009$

Where

C: is a protein concentration by (μ g/ml)

A: is the absorbance at 595 nm

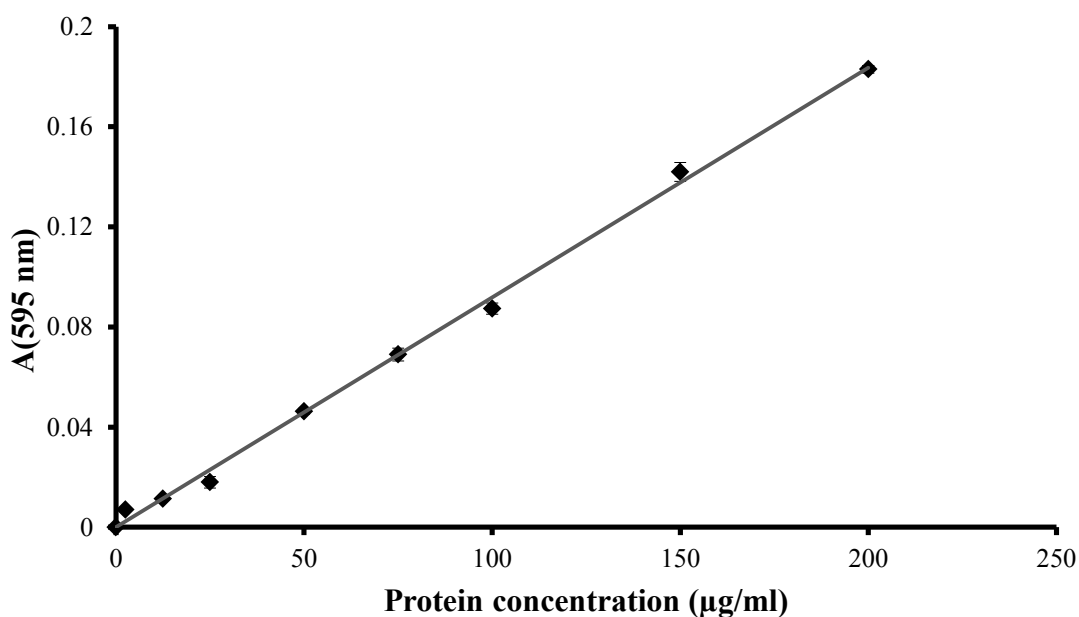


Figure 2.17: Standard curve of the protein concentration versus absorbance at 595 nm.

2.7.2 Cell lysis by sonication

Cell pellets were resuspended in appropriate buffer (His-binding buffer was used for His-tagged proteins and PBS (phosphate-buffered saline) buffer for GST-tagged proteins) containing 0.1 M phenylmethane sulfonylfluoride (PMSF) (protease inhibitor). Sonication was carried out using a Misonix S-4000 sonicator at 70 kHz for 4 minutes, as 3 seconds off followed by 7 seconds on. Samples were kept on ice during the process of sonication.

2.7.3 Expression and purification of XplA and XplB from *R. rhodochrous* 11Y

The XplA protein was produced as an N-terminally His-tagged protein from a previously prepared pET-16b-*xplA* construct [98]. The expression and purification of the protein was performed as described by Rylott *et al.* (2006) [98]. The XplB protein was expressed from a previously generated *xplB*-pGEX2T construct and purified as described by Jackson *et al.* (2007) [95].

2.7.4 Sodium Dodecyl Sulphate – PolyAcrylamide Gel Electrophoresis (SDS-PAGE) with the Bio-Rad system

SDS-PAGE was made following the standard procedure [119] and described as follows: Gels were polymerised with 12 % (w/v) acrylamide in the separating gel and 4 % (w/v) acrylamide in the stacking gel. The protein loading dye (2X) was made up as 2 ml of 625 mM Tris-HCL pH 6.8, 4 ml of 10 % (w/v) SDS, 2 ml of glycerol, 1 ml of β -mercaptoethanol, 30 mg of bromphenol blue and 1 ml of H₂O. Samples were prepared for SDS-PAGE by mixing with loading dye to 1x concentration and heating at 100 °C for 5 minutes. Samples were centrifuged briefly before loading them in the gel. Gels were run at 200 V until the dye front ran off of the end of the gel. The gels were either stained with InstantBlue, a coomassie-based staining solution (Expedeon, UK), or transferred to nitrocellulose for western blot analysis.

2.7.5 Protein identification by MALDI-MS analysis

The desired protein band was cut from the SDS-PAGE gel and protein identification was carried out at the proteomics laboratory, Technology Facility (University of York)

using Bruker autoflex III MALDI-TOF/TOF. Data was analysed by Mascot (Matrix Science)

2.7.6 Western blot analysis

Following the SDS-PAGE, the non-stained separating layer of the gel was used for western blot analysis. Gel was equilibrated in pre-chilled Towbin buffer (25 mM Tris, 192 mM glycine, 20 % v/v methanol, pH 8.3) for 5 minutes. A gel-membrane sandwich complex was then made by placing the gel onto the nitrocellulose membrane, with three layers of pre-soaked filter paper in Towbin buffer on the top of the gel and bottom of membrane. Protein was transferred onto the membrane by applying 25 Voltage on Trans-Blot SD Semi-Dry Transfer Cell (Bio-Rad) for 20 minutes. Ponceau S stain (0.1 % w/v Ponceau S, 5 % v/v acetic acid) was used to ensure the successful transfer of the protein onto the membrane by immersing the membrane into Ponceau S solution for 5 minutes. Transferred protein was visualised by partially destaining the membrane with water. The blot was completely destained by washing with PBS buffer (NaCl (7.2 g/L), Na₂HPO₄ (1.48 g/L), NaH₂PO₂ (0.45 g/L), pH 7.2) before the blocking step.

2.7.6.1 His-tagged protein detection

Membrane was blocked with PBS buffer containing 3 % (w/v) non-fat milk powder at 4 °C with shaking overnight, followed by washing three times with washing buffer (PBS buffer containing 0.05 % Tween 20) with 5 minute incubations. The blot was incubated with PBS buffer containing 3 % (w/v) BSA (Bovine serum albumin) and Monoclonal Anti-polyHistidine Peroxidase Conjugate (Sigma-Aldrich) for 2 hours, and followed by another three washing steps with PBS containing 0.05 % Tween 20. The devolvement step was done by incubating the membrane in a solution consisting of 2 ml of 4-chloro-1-naphthol (Sigma-Aldrich, made by dissolving one tablet in 10 ml methanol), 10 ml of triethanolamine buffer saline (137 mM NaCl, 27 mM KCl, 12 mM triethanolamine, pH 7.5), and 5 µl of freshly added H₂O₂. The reaction was stopped by washing the membrane in water.

2.7.6.2 XplB detection

The membrane was blocked in 25 ml PBS buffer containing 3 % (w/v) non-fat milk powder (Sigma-Aldrich) at 4 °C room overnight with gentle shaking. The blot was

incubated with XplB polyclonal antibody diluted by (1/5000-1/20000) in 20 ml (PBS buffer with 3 % (w/v) of BSA) for 1 hour. Washing of the membrane was carried out as follow, twice with PBS containing 0.1 % Tween 20 for 5 minutes; twice with PBS containing 0.5 % Tween 20 and 1M NaCl for 5 minutes; and then a brief rinse of the membrane in PBS and PBS containing 3 % (w/v) of BSA. The membrane was then incubated with secondary goat anti-rabbit conjugated to alkaline phosphatase antibody, diluted by 1/20000 in 20 ml of PBS buffer containing 3 % (w/v) BSA, for 1 hour at room temperature. The membrane was washed again as follows, twice with PBS containing 0.1% Tween 20 for 5 minutes, twice with PBS containing 0.5 % Tween 20 and 1M NaCl for 5 minutes, and then with brief rinse in 10 mM Tris pH 9.6. The signal was developed using Sigma tablets containing of active compound of nitroblue tetrazolium (NBT) and 5-bromo-4-chloro-3-indolyl phosphate dipotassium (BCIP). The tablet was dissolved in 10 ml of water and the membrane was immersed until the signal appeared. The reaction was stopped by washing the membrane with PBS 0.1 % Tween 20, then PBS and water.

2.7.7 Homology modelling

The model structure of the protein of interest was created by searching for the template in <http://swissmodel.expasy.org/>. A superimposed model structure on the template was generated and visualised using Chimera UCSF software [120]. Structure alignment was evaluated through Root Mean Square Deviations (RMSDs) value using Reply log command.

2.8 Analytical Techniques

2.8.1 High-performance liquid chromatography (HPLC)

The HPLC analytical system (Waters) (Milford, USA) used in this study contained a 510 pump, a Waters Alliance 2695 separation module and a Waters 2996 Photodiode Array. For RDX and TNT detection, sample (50 µl) was injected at a flow of 1 ml/minute into the system. The HPLC isocratic condition was used, in which mobile solvent consisted of either 60:40 or 50:50 methanol: water.

For the FAD (Flavin Adenine Dinucleotide) detection (Chapter 5), the sample was injected at a flow rate of 0.75 ml/minute. Five mM ammonium acetate buffer, pH=6.5

(solvent A) and methanol (solvent B) was used at 30 °C. The HPLC gradient condition consisted of: 5 minutes solvent A 85 %: solvent B 15 %; 20 minutes solvent A 25 %: solvent B 75 %; 5 minute solvent A 0 %: solvent B 100 %; 5 minutes solvent A 85 %: solvent B 15 %. A Sunfire C18 5 μ M column (Waters, Wexford, Ireland) was used to separate the compound.

The absorbance peak of each compound was identified by comparing the retention time and the spectra generated from the Waters photodiode array detector with the retention times and spectra of standard. Chromatograms were generated using Empower-Pro Analysis Software at the absorbance at 230 nm for RDX and TNT or at 265 nm for the FAD detection. Concentration of the compound was measured by comparing the retention area of the sample with the retention area of the known concentration of the standard.

2.8.2 Griess (nitrite) assay

The Griess assay was used to determine the amount of nitrite (NO_2^-) in samples. The method relies on the colour (pink) produced as the result of the reaction of nitrite with the Griess reagent, which is measured at A_{540} nm (Figure 2.5).

Sample (200 μ l) was mixed with 50 μ L of sulfanilamide and incubated for 5 minutes (10 mg/mL sulfanilamide in 0.68 M hydrochloric acid). Then 20 μ L of *N*-(1-naphthyl)-ethylenediamine dihydrochloride (NED) (10 mg/mL NED in water) was mixed into the reaction. Absorbance at 540 nm (blanked against Griess reagent) was measured. The concentration of nitrite is calculated as $N = (A + 0.001) / 0.0229$ (Figure 2.6).

N = Nitrite concentration in (μ M), A = Absorbance at 540 nm.

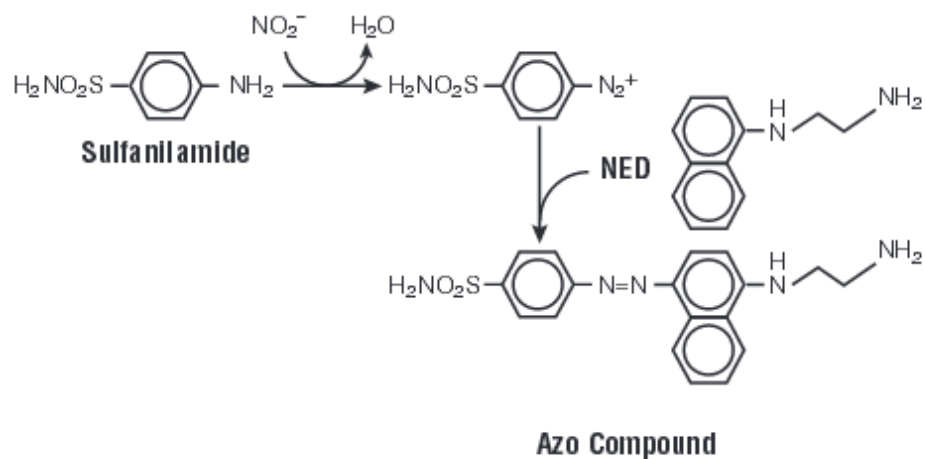


Figure 2.18: Principle of the Griess assay. Reproduced from Griess Reagent system handbook by Promega (<https://www.promega.co.uk/~media/files/resources/protocols/technical%20bulletins/0/griess%20reagent%20system%20protocol.pdf>).

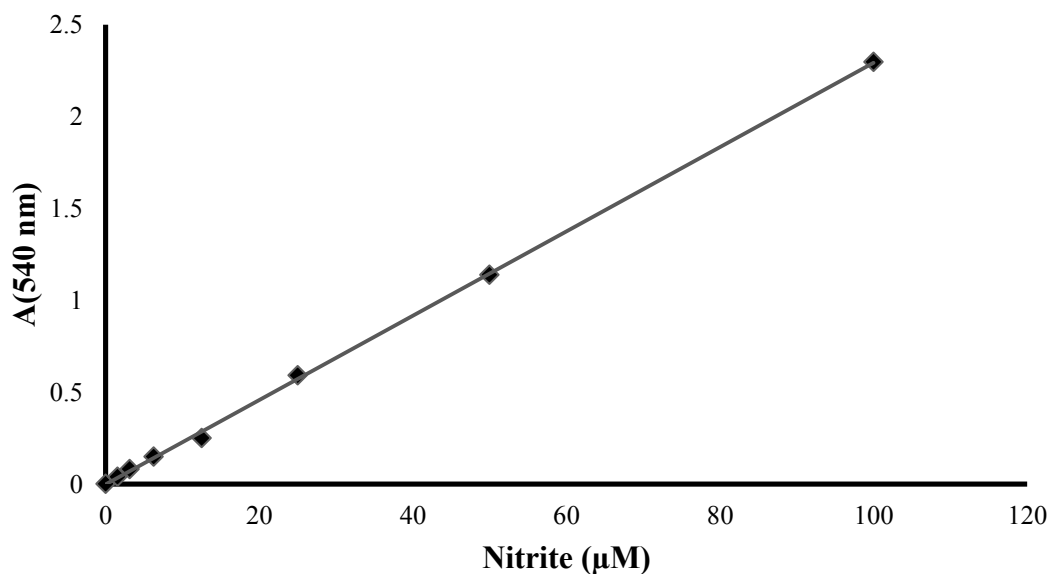


Figure 2.19: Griess assay standard curve to determine the concentration of nitrite using the absorbance 540 nm.

Chapter 3: Isolation of RDX-degrading bacteria from different geographical locations

3.1 Introduction

RDX is a toxic potential carcinogenic compound [121]; pollution with RDX is of concern and it is classified by the U.S. Environmental Protection Agency (EPA) as a priority pollutant [66]. Although the XplA/XplB system has been shown to actively degrade RDX at the lab scale, RDX persists at contaminated sites. One possible explanation for the continued pollution is the inhibitory effect of the co-contaminant explosive TNT toward XplA activity [95]. The nitroaromatic compound TNT has been shown to inhibit RDX degradation by indigenous microorganisms in explosive-contaminated soil under anaerobic conditions [122]; and by *Rhodococcus* sp. YH1 under aerobic condition [106]. Additionally, TNT strongly inhibits XplA activity *in vitro* [95]. Therefore, identification of an RDX-degrading enzyme unaffected by TNT would be advantageous for the decontamination of RDX polluted sites. Moreover, despite the fact that TNT strongly inhibits XplA activity, all RDX-degrading bacteria that have been reported so far have been isolated from soil contaminated not just with RDX but TNT also. It is therefore possible that these organisms have also evolved a mechanism to detoxify TNT alongside metabolism of RDX. Nejidat *et al* (2008)[106] reported that when *Rhodococcus* sp. YH1 had been previously grown in minimal medium containing ammonium as a sole source of nitrogen source, it is subsequently able to transform TNT to 2-amino-2,6-dinitrotoluene (2-ADNT) and 4-amino-2,6-dinitrotoluene (4-ADNT) before finally degrading RDX. However, the bacterium did not transform TNT if it had been previously grown on RDX medium [106].

This chapter focuses on the isolation of new RDX-degrading bacteria in different geographical locations, with the aim of discovering new enzymes and increasing understanding about the diversity of the *xplA* gene. Furthermore, the physiological mechanism by which *xplA*-harbouring microorganisms are able to thrive in sites contaminated by both TNT and RDX is also investigated.

3.2 Materials and Methods

3.2.1 Sample collections

In order to isolate new RDX-degrading bacteria, explosive-contaminated soil samples were collected from six different geographical locations: Belgium, Germany, Ukraine, Moldova, the Czech Republic, and the UK. The Belgium soil samples were collected by Dr. Astrid Lorenz from an old TNT munition manufacturing site, whereas samples from Germany were sent us from a training range at Senne. Furthermore, soil samples were also collected from the explosive contaminated sites of Ukraine, Moldova and the Czech Republic. In the UK, samples were collected by Professor Neil Bruce and Dr. Elizabeth Rylott from the BAE Systems Glascoed site, located in the south east of Wales, near Newport, Gwent. The UK site was particularly interesting in terms of history of contamination with explosives; it was first opened in 1940 and still manufactures munitions. The duration of explosives contamination at the remaining sites is not known.

3.2.2 RDX and TNT extraction from the soil

The levels of RDX and TNT were determined in soil samples based on EPA (Method 8330 (<http://www.epa.gov/epawaste/hazard/testmethods/sw846/pdfs/8330a.pdf>)). Two grams of soil were dried at room temperature and ground using 10 mm diameter steel balls in a “tumbler” rotator overnight. Acetonitrile (or methanol) (10 ml) was added, sample shaken for 1 hour and pelleted by centrifugation. Five ml of the supernatant was mixed with 5 ml CaCl₂ (5 g/L) and shaken again for 1 hour in the tumbler rotator. The samples were filtered through acetonitrile-resistant filters (0.2 µm) and 50 µl of it was injected on HPLC to determine the amount of RDX and TNT (Chapter 2.8.1). The total amounts of RDX and TNT were calculated from the HPLC results. Spiked control samples indicated that the recovery rates for RDX and TNT were 53 % ± 8, and 77% ±7, respectively.

3.2.3 Enrichment cultures

Selective enrichments were carried out to isolate RDX-degrading bacteria by inoculating soil samples into 50 ml minimal medium (Chapter 2.4.1) containing RDX as the sole source of nitrogen. A 50-fold dilution of the medium was sub-cultured into

fresh medium weekly. Unless specified otherwise, all cultures were grown at 30 °C, in an incubator with shaking at 180 rpm. In all enrichments, RDX-degrading bacteria were first identified by spreading aliquots from the enrichment medium on to RDX-dispersion plates and checking for a zone of clearance around the colony (Chapter 2.4.5). Single colonies were isolated by streaking bacteria from colonies on dispersion plates onto LB plates. The purity of single colonies was confirmed by analysing the 16S rRNA sequence of each isolate. To increase the chances of isolating RDX-degrading bacteria some alterations were made as explained below:

Enrichment Method 1

Approximately one gram of soil sample was diluted into minimal medium containing 1 mM RDX. Cultures were grown for one week and then sub-cultured by inoculating fresh minimal medium with 1 mM RDX. Sub-culturing was performed three times in total and different dilutions of culture were spread on agar dispersion plates (Chapter 2.4.5).

Enrichment Method 2

MacConkey broth was used as a selective medium for gram negative bacteria. The medium was chosen because all *xplA* carrying bacteria reported to date are Gram positive, and a Gram negative species might have evolved a different mechanism for RDX-metabolism. In this method, 5 ml of soil slurry, made up by resuspending 1 g of soil in 5 ml potassium phosphate pH 7.2, was used to inoculate 45 ml of MacConkey broth, which was then grown at 30 °C overnight. An aliquot (1 ml) was then used to inoculate 50 ml minimal medium containing 1 mM RDX as the sole source of nitrogen. Cultures were grown for one week, followed by sub-culturing of 50-fold dilutions into fresh minimal medium with RDX for one month in total.

Enrichment Method 3

Different carbon sources enrich for different bacterial communities, and using leucine as a carbon source has been shown to select the most diverse bacterial community [123]. The soil sample enrichment was performed as described in method 1, except 2 mM and 6 mM leucine was used as a carbon source.

Enrichment Method 4

TNT is known to strongly inhibit XplA activity [95], so in order to increase the chances of discovering a new non-XplA-like enzyme, that is able to metabolise RDX in the presence of TNT, the isolation for RDX-degrading bacteria was performed by doing the enrichment studies in the presence of TNT. Prior to performing the enrichment, the optimal TNT concentration was determined. A TNT concentration which inhibits the RDX-degrading activity by XplA-carrying bacteria but is not lethal to bacteria was determined as follows: Fifty microliters of (0.1 g/ml) *R. rhodochrous* 11Y cells were inoculated into 50 ml of minimal medium (Chapter 2.4.1) containing 150 μ M RDX and 450 μ M of KNO_3 in 250 ml flasks. Alongside, 250 ml flasks containing 50 ml of minimal medium, 150 μ M RDX, 450 μ M of KNO_3 , and a range of TNT concentrations (5, 10, 15, 20, 25, 30, 40, 45, 50 μ M) were also inoculated with *R. rhodochrous* 11Y cells. Bacterial growth was monitored by measuring the turbidity at OD_{600} at day 7, and the RDX remaining in the medium was measured by HPLC (Chapter 2.8.1).

Enrichment Method 5

This was carried out as enrichment method 1, except 100 μ M of KNO_3 and NH_4Cl was added as additional nitrogen sources. The RDX content in the medium was checked a week after incubation by HPLC (Chapter 2.8.1).

Enrichment Method 6

Five grams of soil was used to inoculate 50 ml minimal medium containing 100 μ M of RDX as the sole source of nitrogen. An aliquot (200 μ l) was taken from the culture at different time points to measure RDX content in the medium by using HPLC (Chapter 2.8.1). RDX-degrading bacteria were isolated as described in the enrichment method 3.2.3.

3.2.4 Identification and characterisation of RDX-degrading bacteria

Identification of the isolates was carried out by amplification then sequencing of the 16S rRNA gene and phylogenetic analysis (Chapter 2.6.3). RDX degradation by the isolates was compared by performing resting cell assays (Chapter 2.5.2). The effect of

TNT on RDX degradation capacity by the isolates was further investigated by comparing the RDX-removal rate with and without 2 μM of TNT (Chapter 2.5.3).

3.2.5 Effect of TNT on the growth of *R. rhodochrous* 11Y

To investigate the long term effect of TNT on the ability of *R. rhodochrous* 11Y to degrade RDX, a cell suspension (100 μl), made up of 0.1 g/ml of wet weight cells, was used to inoculated 50 ml of minimal medium in 250 flasks containing 100 μM RDX, or 300 μM KNO_2 , with 0, 1, 5, 10 and 50 μM of TNT. The growth of the bacteria was monitored by measuring the OD_{600} .

3.2.6 Effect of dinitrotoluenes on the activity of purified XplA

A stock solution containing 250 μM NADPH, 100 μM RDX and XplB (830 $\mu\text{g}/\text{ml}$) was prepared in a total volume of 9 ml 50 mM potassium phosphate buffer pH 7.2. Aliquots (180 μl) were transferred into Eppendorf tubes, TNT (2,4,6-trinitrotoluene), 2,4-DNT (2,4-dinitrotoluene), and 2,6-DNT (2,6-dinitrotoluene) were added to give 2 and 10 μM of each compound in 200 μl mixture. The reaction volume was made up to 200 μl and the reaction was started upon the addition of purified XplA (4 $\mu\text{g}/\text{ml}$) and stopped after 30 minutes by the addition of 10 % of 1.5 M of trichloroacetic acid. The RDX remaining in each reaction was measured by HPLC.

The effect of 2-ADNT (2-amino-4,6-dinitrotoluene) and 4-ADNT (4-amino-2,6-dinitrotoluene) on RDX-denitration activity by purified XplA was also assessed by measuring nitrite release from RDX-denitration activity of XplA by the Griess assay. To do this, a stock solution was prepared as described above. Aliquots were transferred into 96 well plates, and 2-ADNT or 4-ADNT was added to give a final concentration of 2.5 μM and 10 μM in 200 μl reaction. The reaction was started upon the addition of XplA and the reaction measured by nitrite release using the Griess assay (Chapter 2.8.2).

3.3 Results

3.3.1 RDX and TNT extraction from soil samples

Extraction of RDX and TNT was carried out on the soil samples from Belgium, Ukraine and Moldavia. TNT was detected in the Belgium soil samples by our collaborators using colorimetric assay to detect TNT. The photo presented in Figure 3.1 was taken by Dr. Astrid Lorenz showing appearance of the pink colouration indicative of TNT present in the samples that were collected. However, neither TNT nor RDX was found in these samples by HPLC or mass spectrometry, carried out by Miss Valeria Gazda in Centre for Novel Agricultural Products - University of York.



Figure 3.20: Colorimetric assay to detect TNT in soil samples from Belgium. The darker red indicates a higher concentration of TNT.

In the Ukraine soil sample, approximately 36 mg/kg of TNT was found, with no RDX (Figure 3.2), whereas no TNT or RDX was detected in the Moldova (Figure 3.2) or Czech Republic soil samples (Figure 3.3).

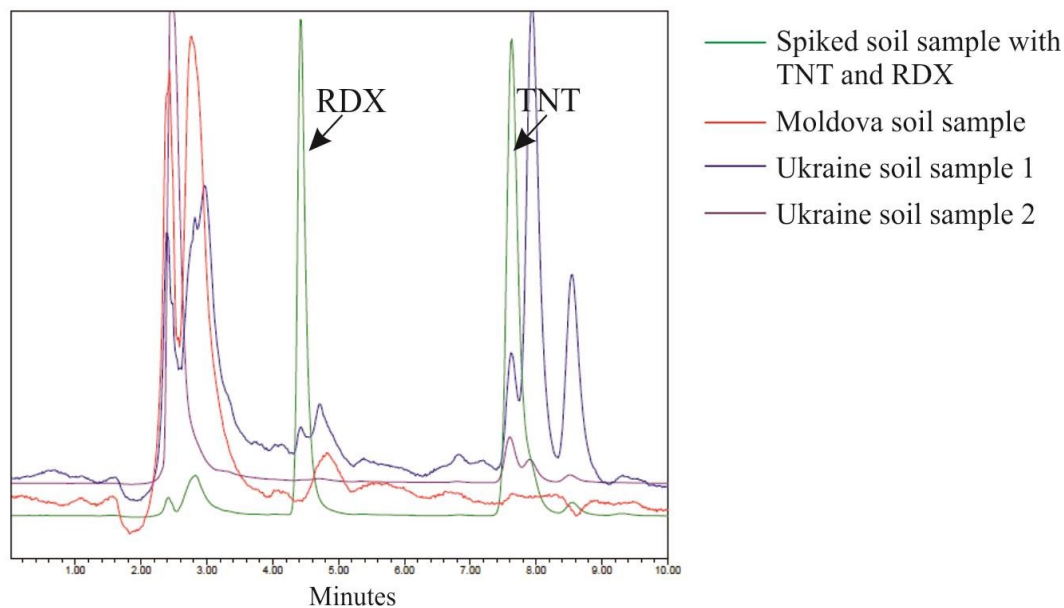


Figure 3.21: Overlay HPLC chromatograms from the RDX and TNT extraction of Ukraine and Moldova soil samples. HPLC mobile phase Methanol 50:50 H₂O.

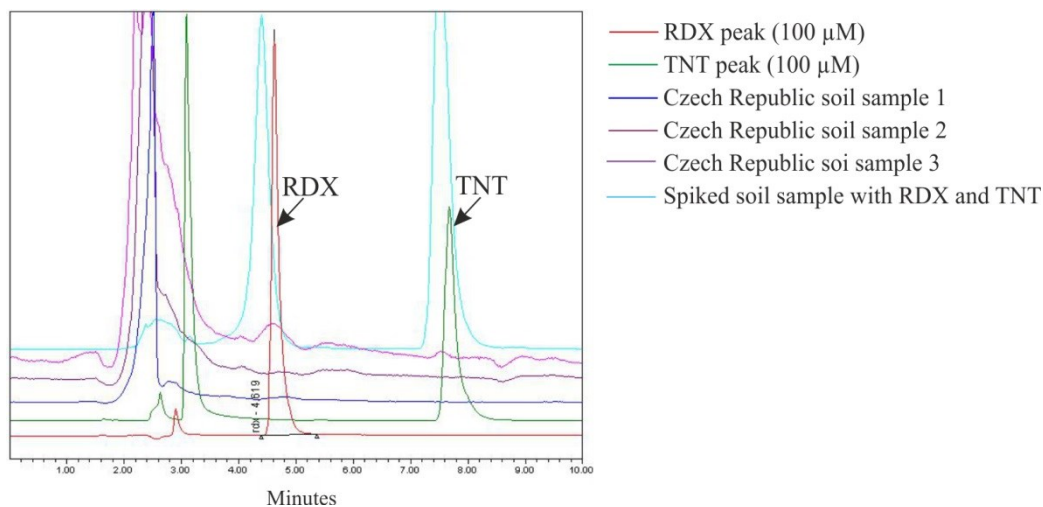


Figure 3.22: Overlay chromatograms from RDX and TNT extraction of Czech Republic soil samples. HPLC mobile phase Methanol 50:50 H₂O.

As neither RDX or TNT were detected in the soil samples from Czech Republic, it was assumed that the chances of RDX-degrading bacteria being present in the samples was reduced compared to the samples containing explosives; therefore, enrichment studies were not carried out with these samples. Selective enrichment methods 1, 2 and 3 were carried out for the Belgium samples, bacteria able to grow using RDX as a sole source

of nitrogen were only isolated using enrichment method 1.

Selective enrichment was also carried out on the German, Ukraine, and Moldovian soil samples, using methods 5 to investigate if RDX removal activity could be detected in the minimal medium with 100 μM RDX when the samples use as inoculum after 7 days of incubation. All RDX was removed from the medium when the soil sample from Ukraine was used as inoculum (Figure 3.4) but no RDX removal was detected when the soil sample from Germany were used as inoculum. No further sub-culturing was carried out on the German soil samples. Only a few isolates were found in the Ukrainian soil samples, which were further characterised as described in the next section.

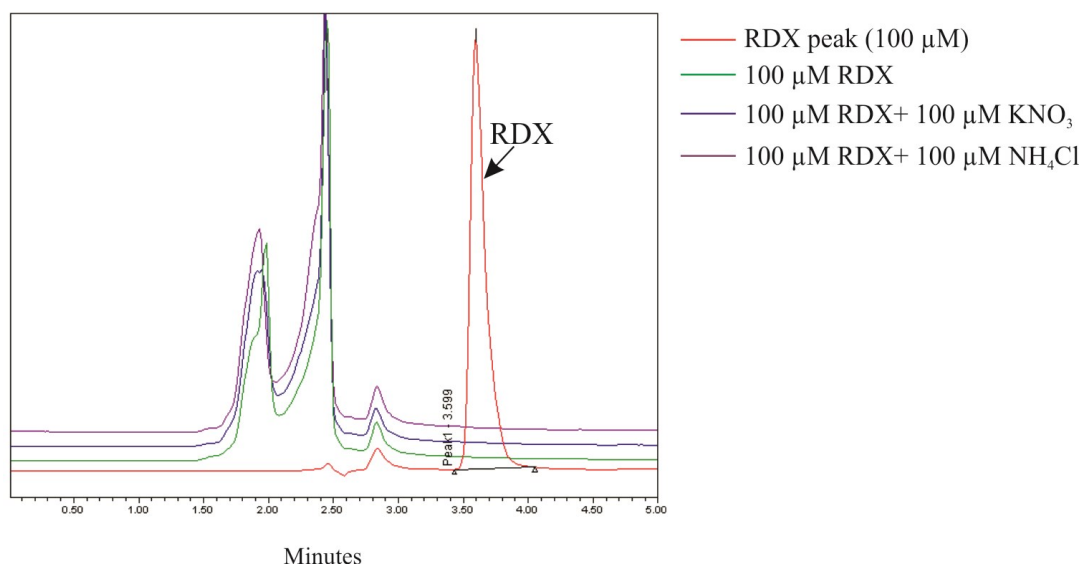


Figure 3.23: Overlay HPLC chromatograms of the selective enrichment for the Ukraine soil sample inoculated in the minimal medium after 7 days incubation. Mobile phase Methanol 60:40 H_2O .

Selective enrichment methods 4 and 6 were performed for the United Kingdom soil samples collected from 15 distinct locations on the BAE Systems Glascoed site. The results using enrichment method 6, which monitored the decrease in RDX over time are presented in Figure 3.5. In the samples from stations 8, 10 and 12, clear RDX removal from the medium was observed. The aberrant result from station 15 shows an apparent increase in RDX concentration over time, and may be due to the RDX concentration in the soil sample exceeding the solubility limit, or another, unidentified technical error; it

was recorded that this sample was collected from heavily explosives-contaminated site. Further sub-culturing of the enrichment medium resulted in the isolation of a number of RDX degrading bacteria.

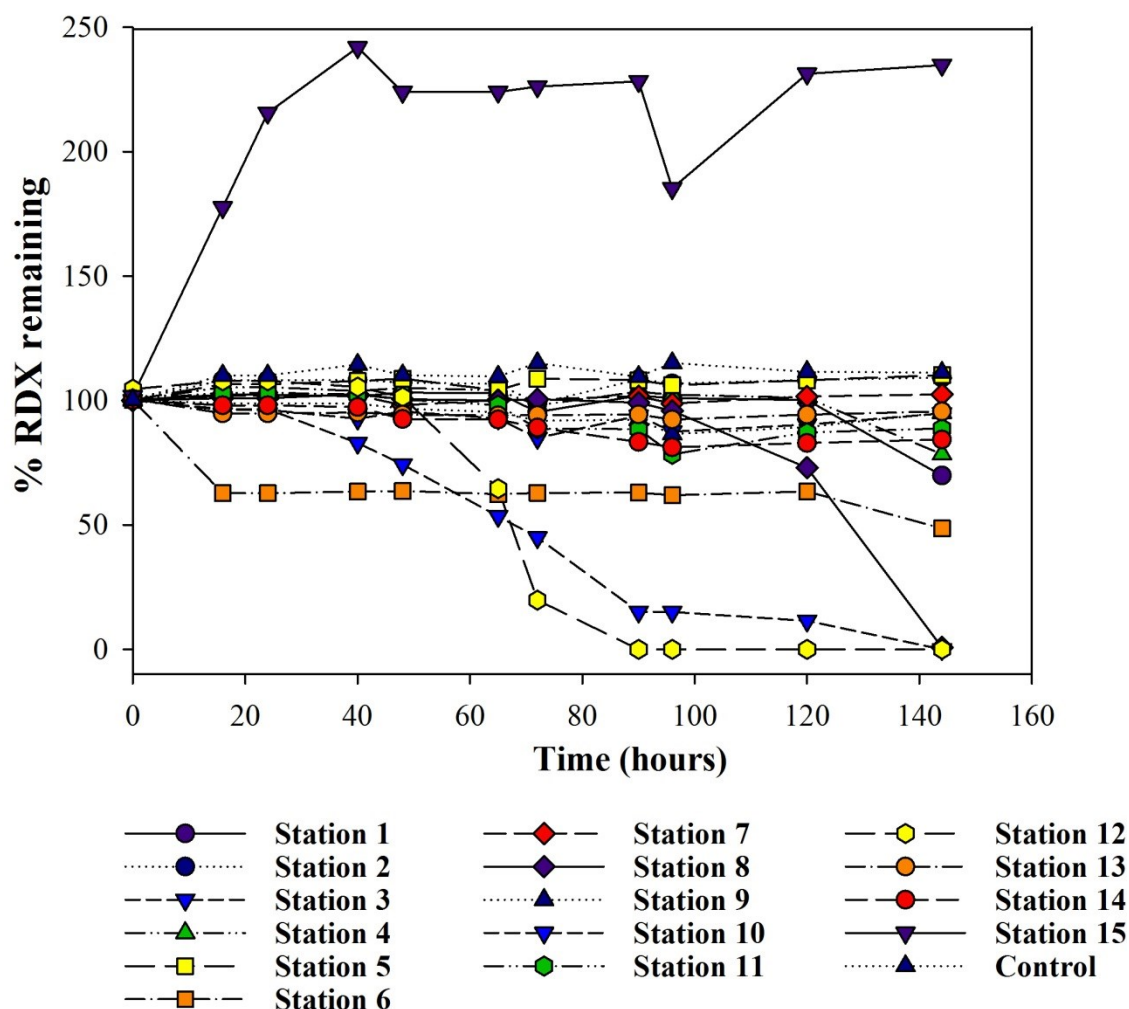


Figure 3.24: Percentage of RDX-removal from the enrichment culture using different soil inocula from the UK soil sample (BAE Systems). The RDX remaining in the medium was measured by HPLC (Mobile phase, Methanol 60: 40 Water).

Prior to performing enrichment method 4 for the UK soil samples, whereby RDX-degrading species would be isolated in the presence of TNT to favour the isolation of non-*xplA* carrying bacteria, the concentration of TNT was optimised. The optimisation was performed to find a concentration of TNT which strongly inhibited *XplA* yet had the least toxicity towards the bacterial cells. To do this, *R. rhodochrous* 11Y was grown in minimal medium containing either 150 μM RDX or 450 μM KNO_3 , and with

different concentrations of TNT (5, 10, 15, 20, 25, 30, 40, 45, 50 μM). Bacterial growth was measured after 7 days and compared to the growth in the absence of TNT (Figure 3.6).

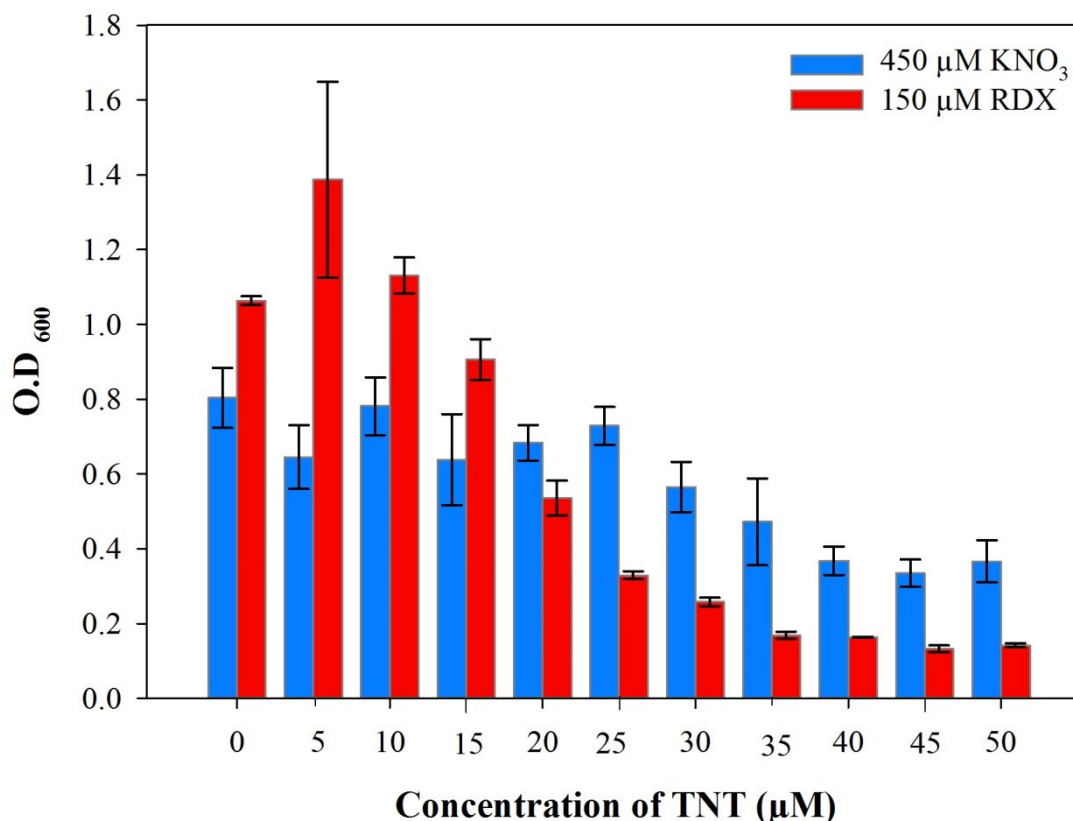


Figure 3.25: Growth of *R. rhodochrous* 11Y after 7 days in medium containing 450 μM KNO₃ (blue bar) or 150 μM RDX (red bar) in the absence or presence of TNT. Data are the average of three biological replicates \pm SD.

As shown in Figure 3.6, in the absence of TNT *R. rhodochrous* 11Y grew equally well using either KNO₃ or RDX as sole nitrogen source. Additionally, at the lowest concentrations of TNT (5, 10 and 15 μM), growth using RDX as sole nitrogen source was not affected after 7 days; the higher growth in RDX medium after 7 days may be due to TNT transformation capability of the bacterium at low concentration and less to the inhibitory effect of TNT transformation products on the activity of XplA. However, when the TNT concentration was increased above 15 μM , the inhibitory effect of TNT on RDX-metabolising XplA activity, and subsequent growth was observed. Where KNO₃ was supplied as the nitrogen source, the inhibitory effect of TNT was less

marked in concentrations lower than 30 μM . The strong effect of TNT on the growth of the bacterium in the KNO_3 *versus* RDX medium was observed with TNT concentrations from 25 μM , where the growth was suppressed by approximately 2-fold more in the presence of RDX compared to KNO_3 .

Analysis of the RDX content in the media after 7 days showed that with increasing TNT concentration, more RDX remained in the medium, indicating that TNT was inhibiting the activity of XplA (Table 3.1).

Table 3.3: RDX remaining (μM) in the medium after growth of *R. rhodochrous* 11Y in the presence of 25- 50 μM of TNT.

| Concentration of TNT (μM) | Remaining RDX (μM) |
|--|---|
| 25 | 86 |
| 30 | 114 |
| 35 | 119 |
| 40 | 137 |
| 45 | 138 |
| 50 | 133 |

Following this optimisation procedure, a concentration of 25 μM of TNT was added for the enrichment cultures on the UK soil samples; however, no RDX-degrading bacteria were subsequently isolated.

3.3.2 Identification and characterisation of the RDX-degrading bacteria

Following selective enrichment procedures, many morphologically distinct, RDX-degrading bacteria were isolated from the Belgium, Ukraine and UK soil samples (Figure 3.7).

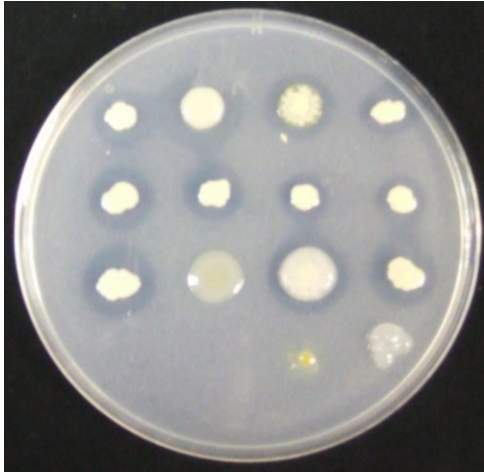


Figure 3.26: An RDX dispersion plate inoculated with single colonies isolated from soil samples. A zone of clearance is apparent around the colonies which are able to degrade RDX.

Characterisation of the isolates were performed on the basis of colony morphology on LB plates and 16s RNA sequencing. Isolates differing by one or more nucleotide in the 16S rRNA were considered as separate isolates. Overall, 13 colonies were isolated, with 16s rRNA sequencing showing they were all *Rhodococcus* spp. The given names for the isolates are shown in Table 3.2.

Table 3.4: List of RDX-degrading bacteria isolated from different geographical locations

| Name of isolate | Country of origin |
|-----------------------------|-------------------|
| <i>Rhodococcus</i> sp. DS1 | Belgium |
| <i>Rhodococcus</i> sp. DS2 | United Kingdom |
| <i>Rhodococcus</i> sp. DS3 | United Kingdom |
| <i>Rhodococcus</i> sp. DS4 | United Kingdom |
| <i>Rhodococcus</i> sp. DS5 | United Kingdom |
| <i>Rhodococcus</i> sp. DS6 | United Kingdom |
| <i>Rhodococcus</i> sp. DS7 | United Kingdom |
| <i>Rhodococcus</i> sp. DS8 | United Kingdom |
| <i>Rhodococcus</i> sp. DS9 | United Kingdom |
| <i>Rhodococcus</i> sp. DS10 | United Kingdom |
| <i>Rhodococcus</i> sp. DS11 | United Kingdom |
| <i>Rhodococcus</i> sp. DS12 | United Kingdom |
| <i>Rhodococcus</i> sp. 5U | Ukraine |

The phylogenetic tree of the isolates is shown in Figure 3.8, *Rhodococcus* sp. DS2 -12 and *Rhodococcus* sp. 5U were most closely related to the RDX-degrading bacterium *Rhodococcus* sp. DN22 isolated from Australia [112] and the non-RDX degrading bacterium *R. qingshengii* strain BGQ-1 (GenBank accession number: KF704112.1) isolated from the Qinghai-Tibet Plateau for crude oil degrading bacteria by Wang, Y (unpublished data). *Rhodococcus* sp. DS1 was more distantly related to the other isolates, and more closely related to a dibenzo-p-dioxin-degrading bacterium *R. opacus* SAO101 (GenBank accession number: AB032565) isolated from a Japanese soil sample [124] and a nitrophenolic-compound-degrading bacterium *R. wratislaviensis* strain J7 (GenBank accession number: AY940038).

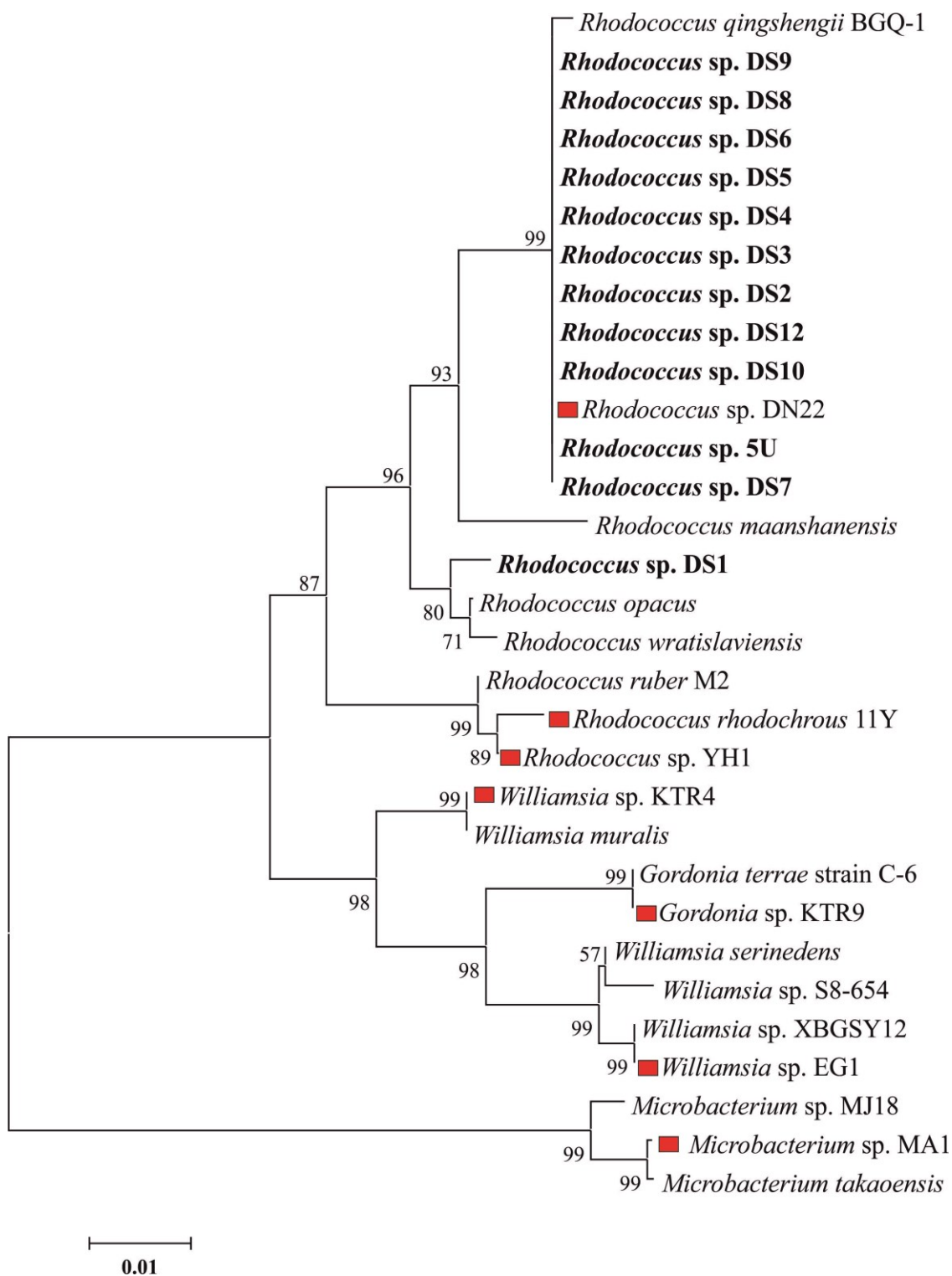


Figure 3.27: Unrooted phylogenetic tree for the 16S ribosomal RNA gene sequence of the RDX-degrading bacteria isolated in this study (shown in bold) and closely related bacteria in the databases. Previously reported RDX-degrading bacteria have a red square next to the branch.

In order to characterise the isolates further, resting cell assays were carried out (Figure 3.9). The rates at which RDX was removed from the media by the isolates appeared to split into two groups: *Rhodococcus* sp. DS1, DS4, 5U and DS9 all removed RDX more slowly than *R. rhodochrous* 11Y and the other isolates. The second group *Rhodococcus* sp. DS8, *Rhodococcus* sp. DS2, *Rhodococcus* sp. DS3 and *Rhodococcus* sp. DS11 all removed RDX at faster rates than *R. rhodochrous* 11Y.

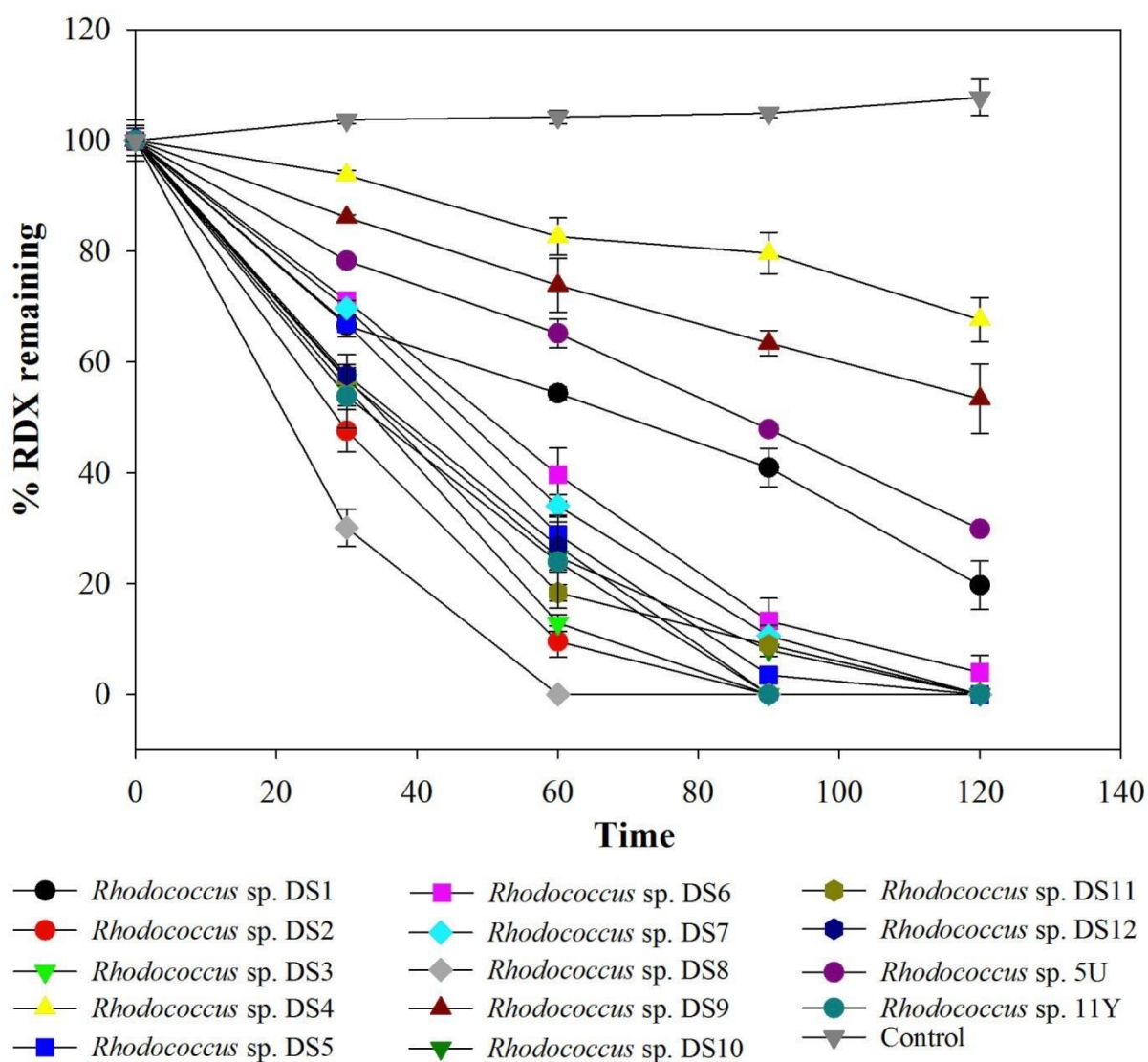


Figure 3.28: RDX uptake by isolated bacteria during the resting cell assay. Data is the average of two or three biological replicates \pm SD.

In order to identify if the enzyme conferring the ability to grow on RDX as a sole nitrogen source is *xplA*, PCR analysis was conducted. The *xplA* gene was amplified in all the isolates regardless of the geographical locations from which they had been isolated (Figure 3.10).

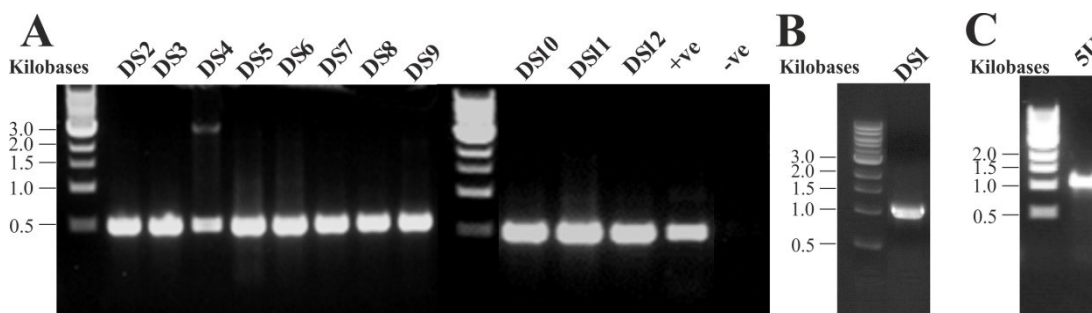


Figure 3.29: PCR products from amplification of the *xplA* region in newly isolated RDX-degrading bacteria. A shows the 520 bp region of the *xplA*-heme domain in the UK isolates, +ve is the positive control using the same primers with *R. rhodochrous* 11Y genome, -ve is the PCR product of the same reaction using nuclease-free distilled water instead of genomic DNA. B and C show the amplification of the 1,073 bp of *xplA* in the Belgian and Ukrainian isolates, respectively.

In order to compare RDX uptake by the isolates in the presence of TNT, RDX removal was measured in the presence and absence of 2 μ M of TNT (Chapter 2.5.3). As shown in Figure 3.11, as little as 2 μ M TNT inhibits RDX removal. RDX uptake by *R. rhodochrous* 11Y and *Rhododoccus* sp. DS1 was most affected by the presence of TNT, whereas *Rhodococcus* sp. DS7 was least affected (Figure 3.11).

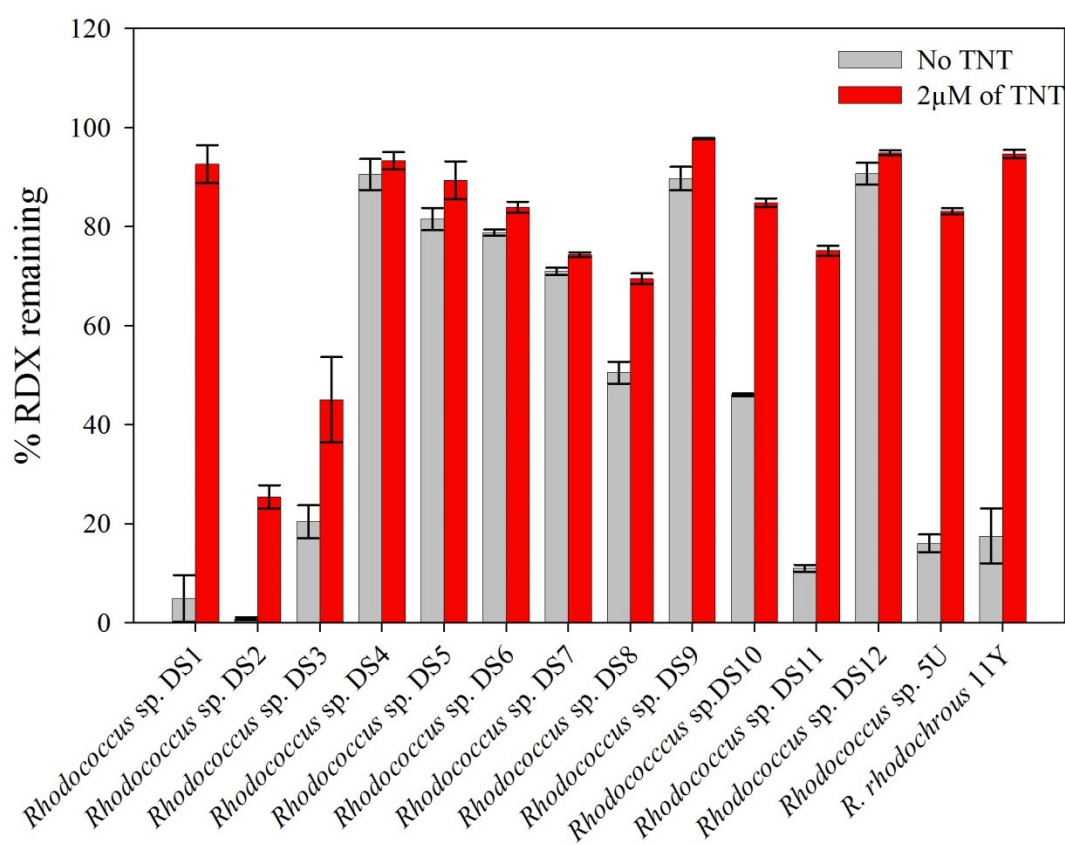


Figure 3.30: Percentage of RDX removal by RDX-degrading isolates in the presence of 2 μM of TNT over 9 h. Data is the average of two or three biological replicates ± SD.

The result from Figure 3.11 support the inhibitory effect of TNT on RDX removal activity reported for *Rhodococcus* sp. YH1 [106] and poses the question: How do XplA-expressing bacteria degrade RDX in a military site co-contaminated with TNT? To tease apart the effects of TNT on XplA activity from the more general cellular toxicity of TNT, *R. rhodochrous* 11Y was grown in flasks where RDX was the sole nitrogen source (Figure 3.12A) and separately, where KNO_2 was the sole nitrogen source (Figure 3.12B). As shown in Figure 12A, as little as 1 μM of TNT has a significant inhibitory effect at the 1 day incubation on the bacterial growth, whereas the growth of *R. rhodochrous* 11Y with KNO_2 was unaffected by the same concentration of TNT. Although TNT concentration was not measured over time, several bacteria, including many *Rhodococcus* spp, are known for having nitroreductase enzymes which can convert TNT to 4-ADNT 2-ADNT. Transformation of TNT to ADNT was reported for the *Rhodococcus* sp. YH1 [106], therefore, recovery of growth by the bacteria over the

time course was thought to be most likely due to less or non-inhibitory effect of the TNT transformation products toward XplA.

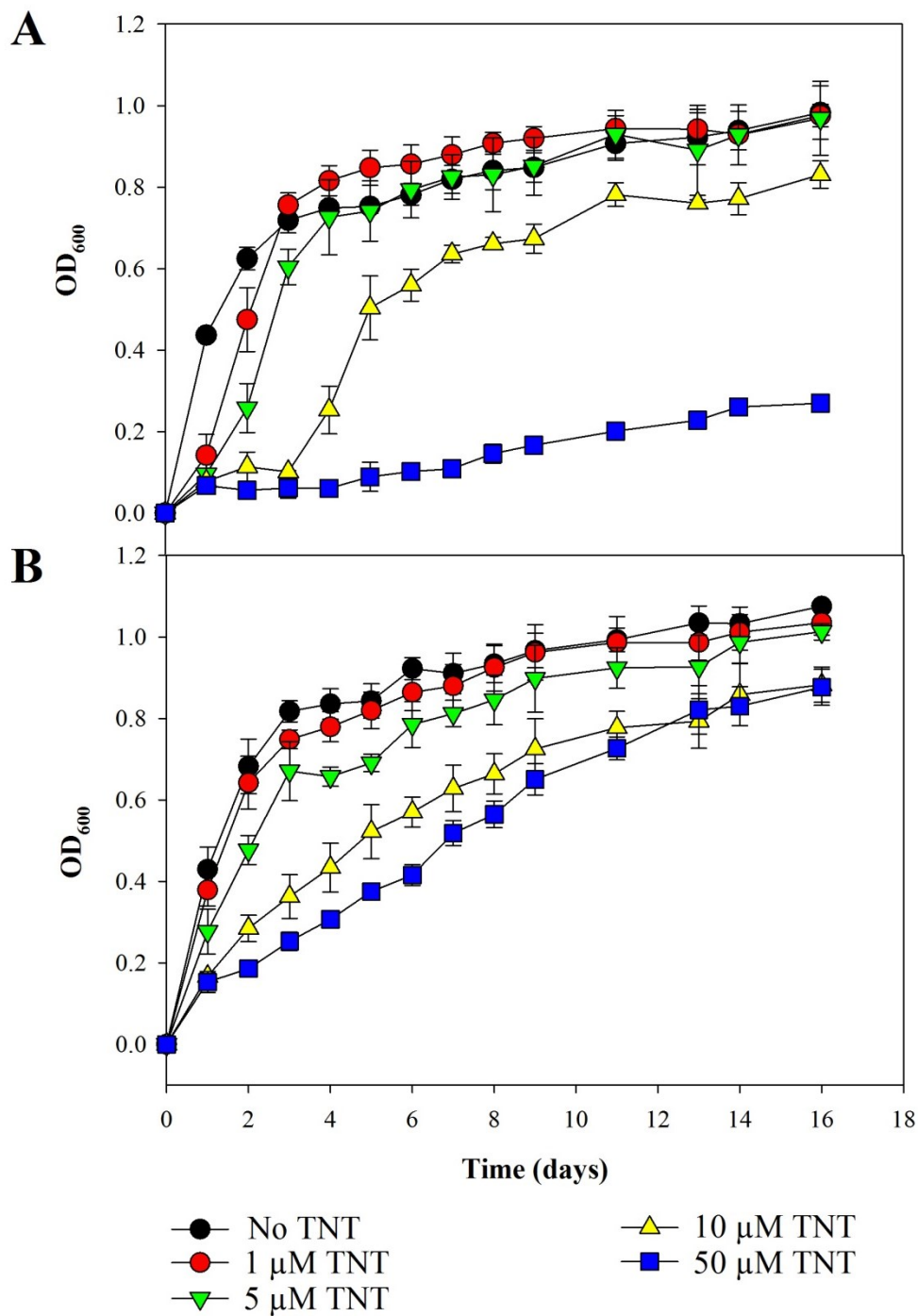


Figure 3.31: Effect of increasing concentrations of TNT on growth of *R. rhodochrous* 11Y in minimal medium containing RDX (A) or KNO₂ (B) as the sole source of nitrogen. Results are the mean of three biological replicates \pm SD.

To test the hypothesis if the gradual decreasing effect of TNT on the growth of 11Y is due to less or non-inhibitory effect of the TNT derivatives on XplA activity, the effect of 2 and 4-ADNT on XplA activity was tested by measuring the nitrite release from RDX-denitration by XplA using the Greiss assay. As shown in Figure 3.13, at concentrations at which TNT is inhibitory to XplA, neither 2 or 4-ADNT had any significant effect on XplA-dependent nitrite release.

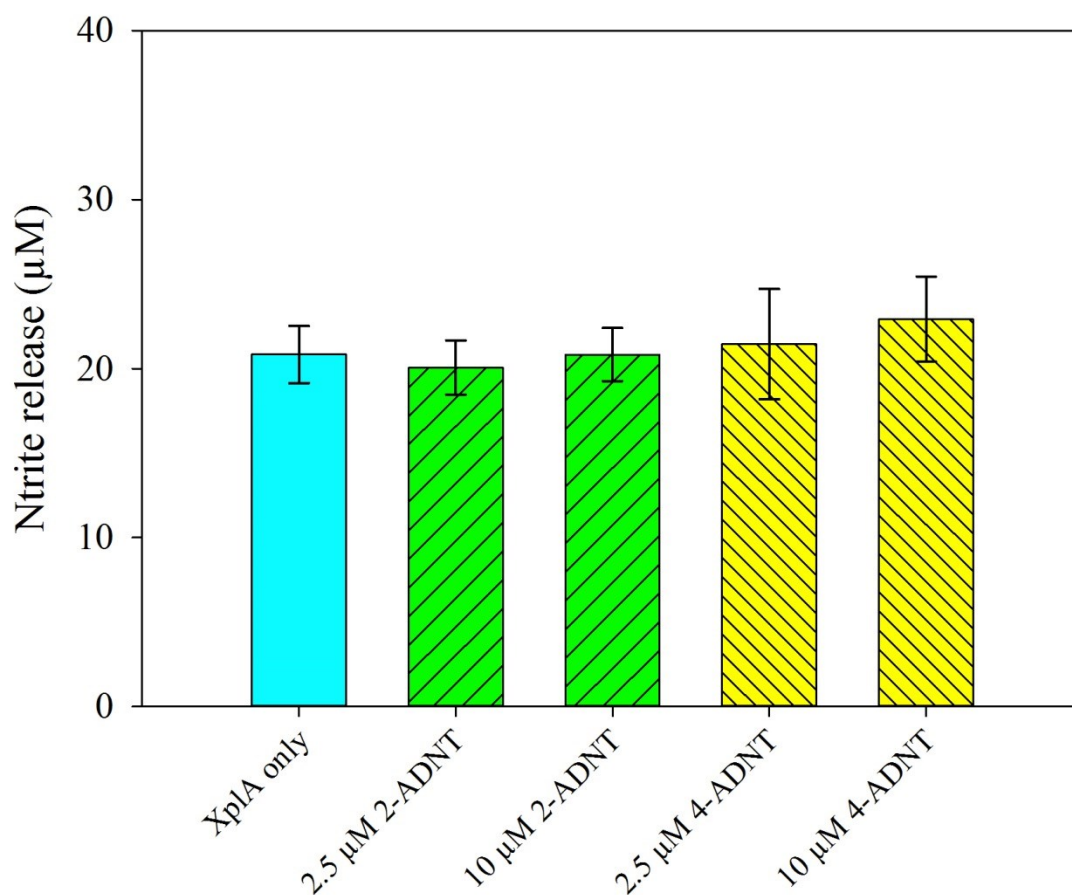


Figure 3.32: Nitrite release from RDX-denitration by XplA in the presence of 2-ADNT and 4-ADNT. Data is the average of four biological replicates \pm SD.

These data suggest that reducing one of the three nitro groups of TNT to an amino group is enough to prevent inhibition of XplA, at least in the concentrations tested. To confirm this observation, it was decided to investigate the effect of 2,4-DNT and 2,6-DNT on RDX degradation. As shown in Figure 3.14, no significant difference in the

rate of RDX-denitration was observed in the present of 2 or 10 μM of 2,4-DNT or 2,6-DNT, whereas, 2 μM and 4 μM of TNT reduced XplA activity by 64% and 87%, respectively.

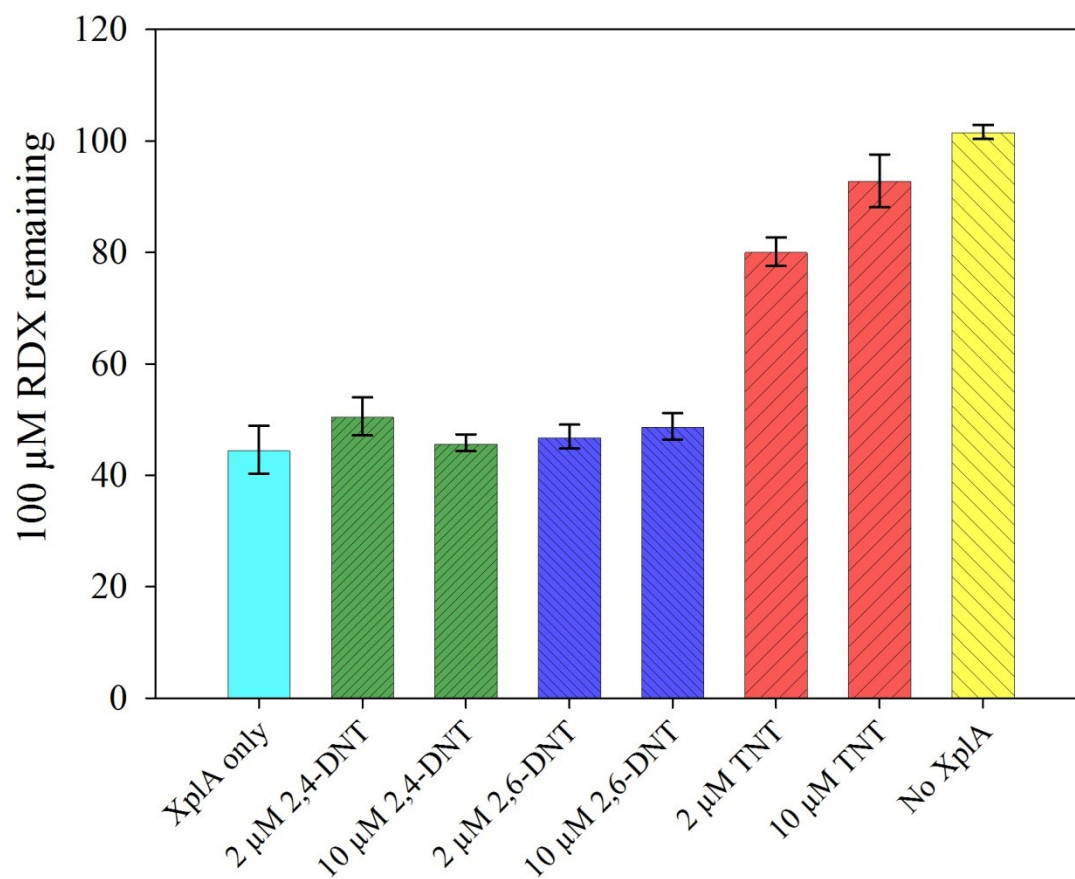


Figure 3.33: RDX-removal activity of the XplA with and without 2,4- and 2,6-DNT in comparison with TNT. Data is the average of five biological replicates \pm SE.

3.4 Discussion

In this study, soil samples from different geographical locations that were military sites or industrial sites where munitions are processed were used to isolate RDX-degrading bacteria. The locations were all historically contaminated with explosives; however, following collection, analysis to detect RDX and TNT in the Belgium, Ukraine and Moldovan soil samples, showed that TNT was only found in the soil samples from Ukraine. The inability to detect RDX in the Ukrainian soil could be due to the different adsorption properties of the two compounds; TNT is known to bind strongly to the soil, whereas RDX is highly mobile in soil [65].

Selective enrichment from these soil samples resulted in the isolation of in total, thirteen RDX-degrading bacterial species from the soil samples from Belgium, Ukraine and the United Kingdom. Based on 16S rRNA sequences, the isolates were found to belong to the genus *Rhodococcus*. In addition to *Rhodococcus* spp., Gram positive *Microbacterium* sp. MA1 [103], *Gordonia* sp. KTR9, *Williamsia* sp. KTR4 [114] *Williamsia* sp. EG1 [113] and Gram negative *Stenotrophomonas maltophilia* PB1 [125], *Pseudomonas* sp. HK-6 [126], *Pseudomonas putida* II-B and *Pseudomonas fluorescens* I-C [94] have all been reported to have the ability to degrade RDX. However, the evidence, based on the Biolog analysis system and the fatty acid profile [126], is insufficient to conclude that HK-6 is in the *Pseudomonas* genus.

To maximise the chances of isolating new RDX-degrading species, some alterations were made to the enrichment methods; the additional nitrogen sources KNO_3 and NH_4Cl were added during the enrichment because it has been reported that adding ammonium to RDX-containing medium enhanced RDX-degradation by Gram negative *Pseudomonas putida* II-B, and *Pseudomonas fluorescens* I-C [94]. Leucine was used as a carbon source because it was reported to support the most diverse bacterial communities [127]. MacConkey broth was used in the first step of the soil enrichment as Gram positive bacteria are reported to predominate in the explosive contaminated sites [96, 100, 101, 103, 106, 112-114, 128], and MacConkey broth is known to inhibit the growth of Gram positive bacteria [129]. Additionally TNT is known to inhibit RDX denitration by XplA [95], TNT was used to increase the chance of discovering new isolates with novel, non-XplA-based mechanisms for RDX metabolism. However, despite these modifications, no novel RDX-degrading spp. were identified.

Rhodococcus spp. is the most frequently reported genus with the ability to degrade RDX in aerobic conditions; RDX-degrading species include *R. rhodochrous* 11Y and 19 other *Rhodococcus* spp. from the UK [100], *Rhodococcus* sp. YH1 [111], *Rhodococcus* sp. T7 and *Rhodococcus* sp. T9N from Israel [101], *Rhodococcus* sp. DN22 from Australia [112], *Rhodococcus* spp from Belgium (unpublished data as cited in [128]) and *Rhodococcus* sp. EG2A and EG2B from the United states [113]. Additionally, from a taxonomical viewpoint, both *Williamsia* and *Gordonia* are closely related to *Rhodococcus* spp. This is suggestive that *Rhodococcus* spp is the most abundant RDX degrading genus on explosive contaminated sites. In support of this observation, *Rhodococcus* spp. was found to be the predominant genus in a study by Andeer *et al.* (2013) [113], where fully labelled ¹⁵N-RDX was used to analyse bacterial communities able to degrade RDX [113]. The dominance of *Rhodococcus* spp. at explosive-contaminated sites is probably due to the genome flexibility and adaptive capacity of these bacteria to metabolise xenobiotic compounds. *Rhodococcus* species are generally known for having a versatile metabolic activity, and several *Rhodococcus* spp. have been isolated and characterised for their ability to degrade many other anthropogenic compounds for example *Rhodococcus erythropolis* strain PR4 [130] and *Rhodococcus opacus* R7 [131] were isolated for their abilities to degrade several different chain lengths of alkanes as a carbon or energy source, and *Rhodococcus globerulus* P6 [132] and *Rhodococcus corallinus* B-276 [133] were isolated for their ability to degrade polychlorobiphenyl and trichloroethene, respectively.

The RDX-degrading capacity of the isolates was found to be mediated XplA. Although, XenA, XenB [94] and Type I oxygen insensitive nitroreductases [90] have been reported to have the ability to degrade RDX this is not their primary role in metabolism. XplA has been found in all RDX-degrading Gram positive bacteria tested to date [96, 100-103, 128], with sole exception of *Rhodococcus* sp. HS4 [100]. Although the enzyme responsible for RDX-degradation in *Rhodococcus* sp. HS4 was not identified, it is considered that the RDX-degrading capacity of the bacterium is due to a *xplA*-related cytochrome P450 enzyme, as the activity is inhibited by the P450 inhibitor metyrapone [100]. The conservation, and dominance, of *xplA* across a diverse geographical range of RDX-contaminated sites [100-103, 128] is intriguing considering the relatively recent introduction of the novel compound RDX in the environment. In a metagenomic study, *xplA* was even identified in the extreme anaerobic condition of the ovine rumen, in

which RDX was efficiently degraded [134]. The wide dispersion of the highly conserved *xplA* gene in nature has led to questioning of the mechanism by which the gene has dispersed around the world, and the evolutionary origin of *xplA* is investigated further in Chapters 4 and 6.

The comparison of RDX-degradation in the presence and absence of TNT suggests that TNT affects RDX-degradation in all of the isolates. It has been reported that TNT strongly inhibits RDX-degradation by *Rhodococcus* sp. YH1 [106] and by indigenous microbial soil in anaerobic conditions [122]. Growth of *R. rhodochrous* 11Y in RDX versus KNO₂-supplemented media with TNT suggests that TNT is affecting the growth of RDX-degrading bacteria in two ways; first by inhibiting XplA, and second through the toxicity of TNT and possibly its transformation products towards the bacteria. The detoxification pathway of TNT in bacteria that are resistant to TNT, such as *Enterobacter cloacae*, has been well-characterised [77]. As described in Chapter 1, many bacteria have the capability of transforming TNT to HADNTs predominantly 2,4-HADNT in the case of *E. cloacae*, by a nitroreductase *nfsI*. The HADNT products are further reduced to ADNTs. Subsequent transformation events can follow, and triaminotoluene (TAT) has been identified in some bacteria under anaerobic conditions [135]. An alternative pathway catalysed by members of the Old Yellow Enzyme family of flavoproteins transforms TNT via hydride and dihydride Meissenheimer complexes [75, 81, 83].

The inhibitory effect of TNT on XplA activity in *R. rhodococcus* 11Y in liquid cultures decreases over time, suggesting that these bacteria have some, albeit limited, ability to detoxify TNT. In agreement with this, the transformation of TNT to ADNTs has been reported in *Rhodococcus* sp. YH1 [106]. Moreover, a gene encoding for a nitroreductase was found from the total genome sequence of *R. rhodochrous* 11Y (Contig00054) which has 100 % sequence identity to the nitroreductase family protein in *Rhodococcus* sp. EsD8 (Accession number: WP_006940961) and *Rhodococcus rhodochrous* ATCC 21198 (Accession number: CCW13257) (Methodology and study on the *R. rhodochrous* 11Y genome is in Chapter 4). Interestingly, 2-ADNT, 4-ADNT, 2,4-DANT and 2,6-DANT were not found to significantly inhibit the activity of XplA. The results presented here show that TNT inhibits RDX-degradation by *xplA* expressing bacteria, supporting the inhibitory effect reported in *Rhodococcus* sp. YH1 by Nejjidat *et al.* (2008) [106], and inhibitory effect of TNT on XplA protein reported by Jackson *et al.*

(2007) [95]. Considering the fact that many bacteria and fungi are able to detoxify TNT under aerobic conditions [76, 77, 136-141], survival of the *xplA*-carrying bacteria at the explosive-contaminated sites could be hypothesised through detoxification of TNT by TNT-transforming organisms. Gram positive bacteria are generally found to be more sensitive to TNT, and TNT products, than Gram negative bacteria [141]. This study has indicated that both TNT and reduction products slow the growth of RDX-degrading *Rhodococcus* spp., highlighting the presence of recalcitrant TNT as a hindrance to RDX-degradation in the environment.

Chapter 4: Characterisation of the RDX-degrading Genomic Island

4.1 Introduction

Microorganisms are known for their ability to quickly adapt to environmental changes, including exposure to xenobiotics [10]. There are many xenobiotic degrading bacteria that have been reported, and characterised, for their potential application in biotechnology [1].

Microorganisms have also evolved to degrade the explosive RDX, a toxic synthetic compound which has been in the environment for less than a century [128]. The biodegradation of RDX was initially reported only under anaerobic conditions [86, 92, 142, 143]; however, in the late 1990s, three aerobic RDX-degrading *Rhodococcus* spp, with the ability to utilise RDX as a sole source of nitrogen, were isolated from Israel, Australia and the United Kingdom [96, 111, 112].

The enzymes involved in the aerobic biodegradation of RDX were first isolated from *R. rhodochrous* 11Y and identified as an unusual cytochrome P450, XplA, and accompanying flavodoxin reductase partner, XplB [96]. Subsequently, a number of aerobic RDX-degrading bacteria have been reported, from different geographical locations [100, 101, 103, 113, 114, 128], but all belonging to the *Actinomycetales* and *xplA* with > 99 % identity has been identified in those tested [100-103, 128]. The highly conserved nature of *xplA* suggests its rapid distribution by horizontal gene transfer [100, 103, 128].

Genes involved in xenobiotic catabolism are often located in a mobile genetic element, accompanied by insertion elements and are integrated into the bacterial chromosomal or plasmid [10]. Both *xplA* and *xplB* are plasmid encoded in *Microbacterium* sp. MA1, *R. rhodochrous* 11Y [103] and *Gordonia* sp. KTR9 [105]. Partial sequence analysis of the plasmid carrying the *xplA* and *xplB* genes in *Microbacterium* sp. MA1 revealed that the genes are also associated with transposable elements in this bacterium [103]. Furthermore, a 6.7 kbp region flanking *xplA* and *xplB* is nearly identical (> 99 %) between *Microbacterium* sp. MA1 and *R. rhodochrous* 11Y (Figure 4.1) [103].

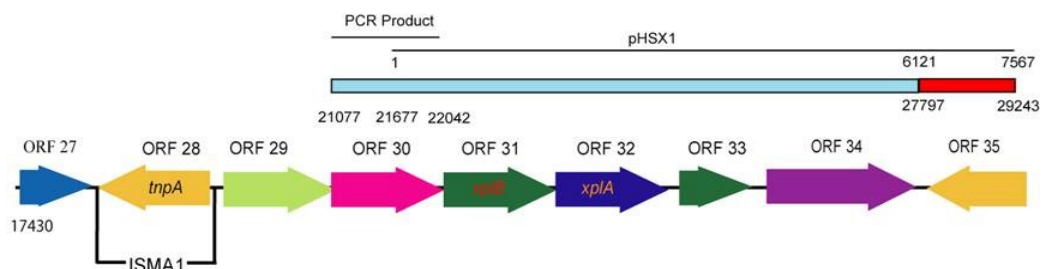




Figure 4.34: Sequence comparison of the 7.5 kbp region flanking *xplA* and *xplB* in *R. rhodochrous* 11Y (top) with the partial sequence of the pMA1 plasmid from *Microbacterium* sp. MA1. Reproduced from Andeer *et al.* (2009) [103].

 pHSX1 and PCR amplified *R. rhodochrous* 11Y sequence with > 99 % nucleotide identity to ORF30 to ORF 34 in *Microbacterium* sp. MA1 fosmid library; pHSX1 is the 7,567 bp sequence of the *xplA/xplB* region in *R. rhodochrous* 11Y [96].

 pHSX1 sequence with no similarity to *Microbacterium* sp. MA1 fosmid sequences.

In *Gordonia* sp. KTR9, an RDX-degrading bacterium isolated from North America [114], *xplA* is located on a 182 Kbp plasmid (pGKT2) (GenBank accession number: CP002112) [105]. The *xplA* gene in *Gordonia* sp. KTR9 has high sequence identity to other known RDX-degrading bacteria (> 99 %), while the 5' end of *xplB* is fused with a glutamine synthetase-encoding gene, *glnA* [105]. Upstream of *xplB-glnA*, are *cyp15C* and *xplR*, which encode cytochrome P450 and transcriptional regulatory protein, while downstream of *xplA* are four genes encoding for hypothetical proteins (Figure 4.2).

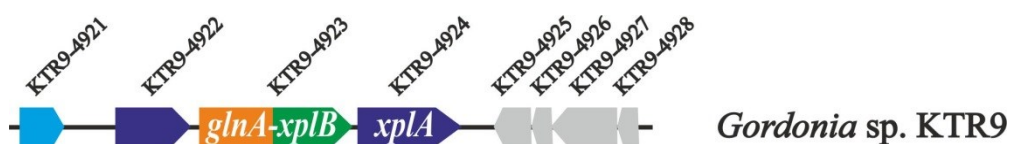


Figure 4.35: The regions flanking *xplA* in *Gordonia* sp. KTR9. The gene locus KTR9_4921, KTR9_4922, KTR9_4923 and KTR9_4924 are encoded for transcriptional regulators, cytochrome P450, XplB-GS and XplA proteins, respectively. The gene loci KTR9_4925 to KTR9_4928 are encoding hypothetical proteins.

In this chapter, the mobile element carrying *xplA* and *xplB* will be characterised by comparing the sequence in the vicinity of *xplA* between several RDX-degrading bacteria isolated from distinct geographical locations. In addition, the *xplA/xplB* was compared between these isolates to construct the evolutionary origin of *xplA* gene.

4.2 Materials and Methods

The *xplA* and *xplB* containing region was studied in eleven RDX-degrading bacterial species (Table 2.2, Chapter 2). The species originated from different geographical locations and belong to four genera of aerobic RDX-degrading bacteria.

The isolates were characterised based on phylogenetic trees using 16S rRNA sequences as described in Chapter 2.2.7. Further characterisation of the isolates was carried out by investigating the growth and RDX-removal rates of the isolates in minimal medium containing 100 μ M RDX as a sole source of nitrogen (Chapter 2.5.1).

Initially, the RDX-genomic islands were studied by identifying the boundary of the sequence similarity in the *xplA* region between *R. rhodochrous* 11Y and *Microbacterium* sp. MA1. A cosmid library, which had been previously prepared from *R. rhodochrous* 11Y genomic DNA by Dr. Cyril Bontemps, was used, in combination with sequence data from pHSX.1, a plasmid library containing 7,567 bp sequence of the *xplA* and *xplB* region from *R. rhodochrous* 11Y [96]. A cosmid library was sequenced using primer walking to obtain more sequence in the region of *xplA* and then compared with online data of a 52.2 kbp sequence from *Microbacterium* sp. MA1 (GenBank accession number: FJ577793).

Subsequently, PCR analysis, using overlap primers designed from *R. rhodochrous* 11Y sequence, was used to amplify the same region in the other *Rhodococcus* spp. and *Williamsia* sp. EG1. A list of the primers used to amplify the *xplA* and *xplB* region can be found in Table 2.1, Chapter 2. The location of each primer binding site in the gene cluster is shown in Figure 4.3. The diversity of the *xplA* and *xplB* genes was investigated by studying single nucleotide polymorphisms (SNP) in the *xplA/B* region between the isolates. The *xplA* and *xplB* genes were sequenced from the PCR products as shown in Figure 4.3.

Lastly, the full genomes of *R. rhodochrous* 11Y and *Williamsia* sp. EG1 were sequenced to identify the genes in common on the *xplA*-carrying plasmids between those bacteria. The genome sequencing methodology is described in Materials and Methods, Chapter 2.6.2.

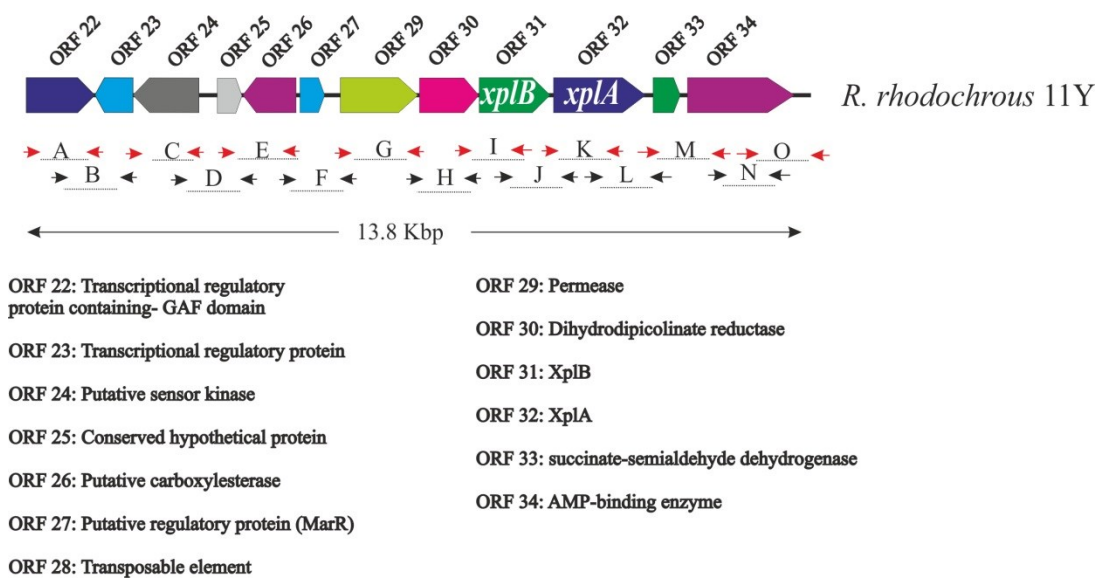


Figure 4.36: Schematic representation of the primer pair locations used to amplify the *xplA* flanking regions in *Rhodococcus* spp. and *Williamsia* sp. EG1. The sequence of each primer can be found in Table 2.1, Chapter 2.

4.3 Results

4.3.1 Characterisation of RDX-degrading isolates

Further characterisation of the RDX-degrading bacteria was performed by generating a phylogenetic tree, using 16S rRNA sequences, and monitoring the growth and RDX removal capacity of the bacteria in minimal medium containing 100 μ M RDX as a sole source of nitrogen.

The RDX-degrading bacteria belong to *Actinomycetales*, and a phylogenetic tree of the isolates is shown in Figure 4.4. *Rhodococcus* sp. EG2 (U.S.A.), *Rhodococcus* sp. 5U (Ukraine), *Rhodococcus* sp. 9UK (United Kingdom), *Rhodococcus* sp. BL-1 (Belgium), and *Rhodococcus* sp. DN22 (Australia), were found to be closely related to each other and more distantly related to *R. rhodochrous* 11Y (United Kingdom) and *Rhodococcus* sp. YH1 (Israel).

Microbacterium sp. MA1 appears distantly related to all *Rhodococcus* spp., whereas *Williamsia* sp. EG1 and *Gordonia* sp. KTR9 are more closely related to the *Rhodococcus* spp (Figure 4.4).

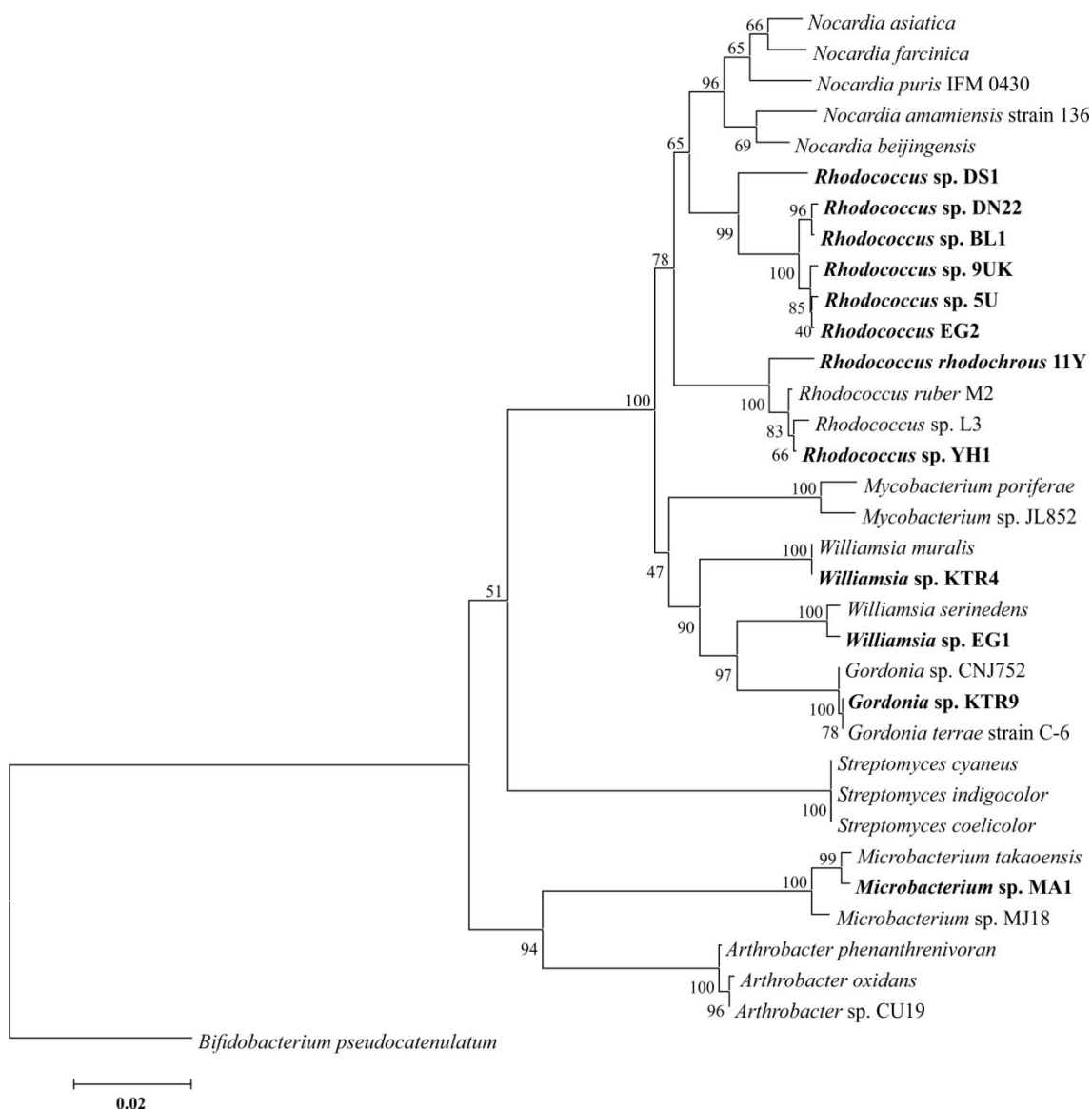


Figure 4.37: Rooted phylogenetic tree analysis of the RDX-degrading isolates. The 16S rRNA sequences were analysed using the neighbour joining method and bootstrapped with 1000 replicate runs using the MEGA 6 tree building program. The RDX-degrading species used in this study are shown in bold. The scale bar indicates substitutions per nucleotide, and the tree was rooted using 16S rRNA sequence of *Bifidobacterium pseudocatenulatum*.

To compare the ability of all the RDX-degrading species listed in Table 2.2 (Chapter 2) to grow and take up RDX in liquid culture, they were grown in minimal medium with 100 μ M RDX as the sole source of nitrogen. All the cultures of *Rhodococcus* spp. removed RDX at faster rates than *Microbacterium* sp. MA1, *Gordonia* sp. KTR9 and *Williamsia* sp. EG1. The amount of RDX removed by the *Rhodococcus* spp. after 16 hours was 100 %, 79 %, 98 %, 93 %, 64 %, 65 % and 100 % by *R. rhodochrous* 11Y,

Rhodococcus sp. YH1, *Rhodococcus* sp. 9UK, *Rhodococcus* sp. DN22, *Rhodococcus* sp. 5U, *Rhodococcus* sp. BL-1 and *Rhodococcus* sp. DS1, respectively (Figure 4.5A).

Amongst the four different genera, *Williamsia* sp. EG1 had the lowest rate of RDX removal from the medium with just 4 % removed after 16 hours, whereas *Gordonia* sp. KTR9 and *Microbacterium* sp. MA1 had removed 20 and 25 % of the RDX, respectively (Figure 4.6A).

In terms of growth, *Rhodococcus* spp were shown to grow at faster rates than those in other genera. Amongst the *Rhodococcus* spp., *Rhodochrous* sp. DS1 was the slowest growing bacterium, achieving an OD₆₀₀ of 0.43 after 44 hours of incubation (Figure 4.5B). *Gordonia* sp. KTR9 was the slowest growing of the non *Rhodococcus* spp., with an OD₆₀₀ of just 0.22 after 44 hours (Figure 4.6B); half the growth of the slowest *Rhodococcus* spp.

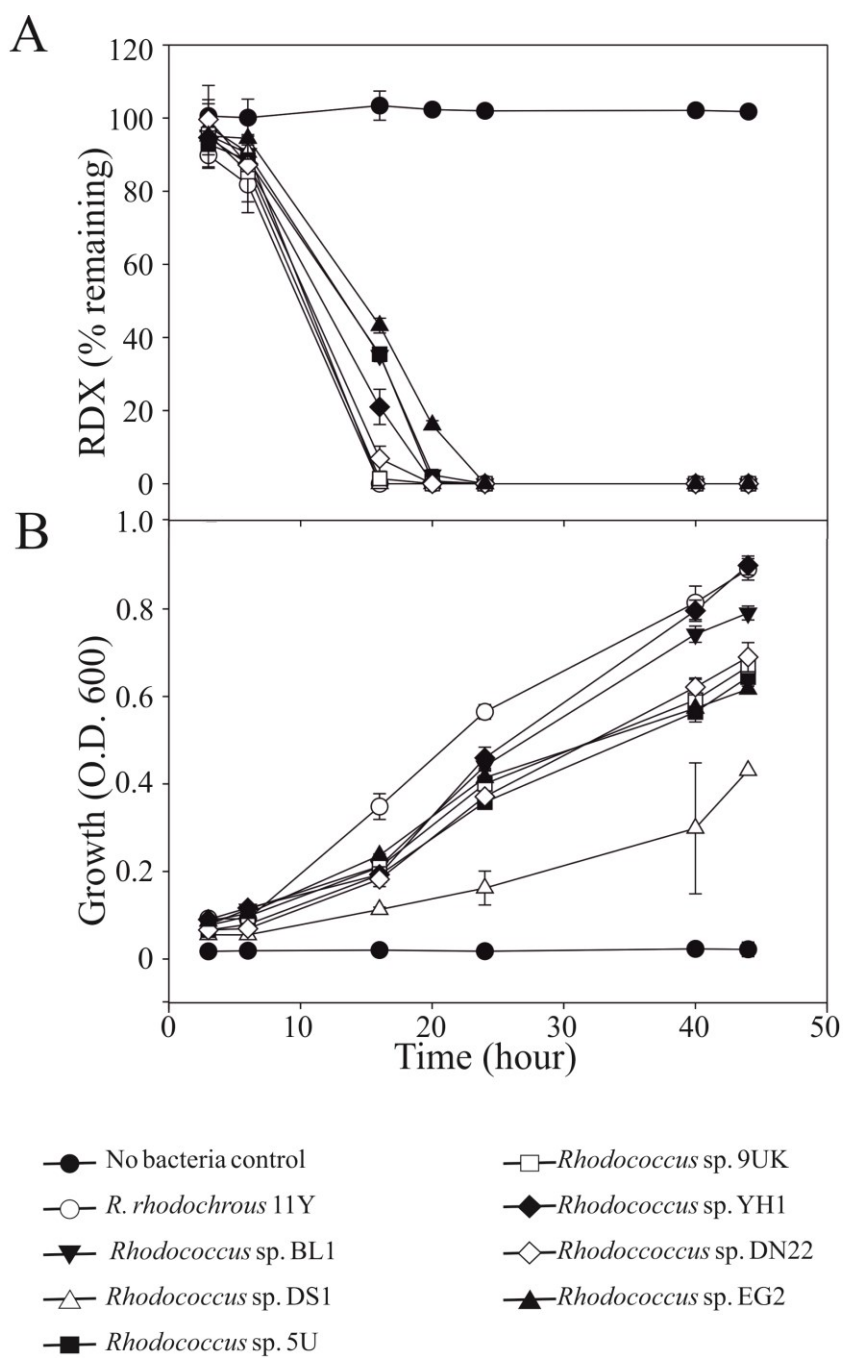


Figure 4.38: RDX removal (A) and growth (B) of eight *Rhodococcus* spp. Data shown are mean of three biological replicates \pm SD. Reproduced from Chong *et al.* (2014) [144].

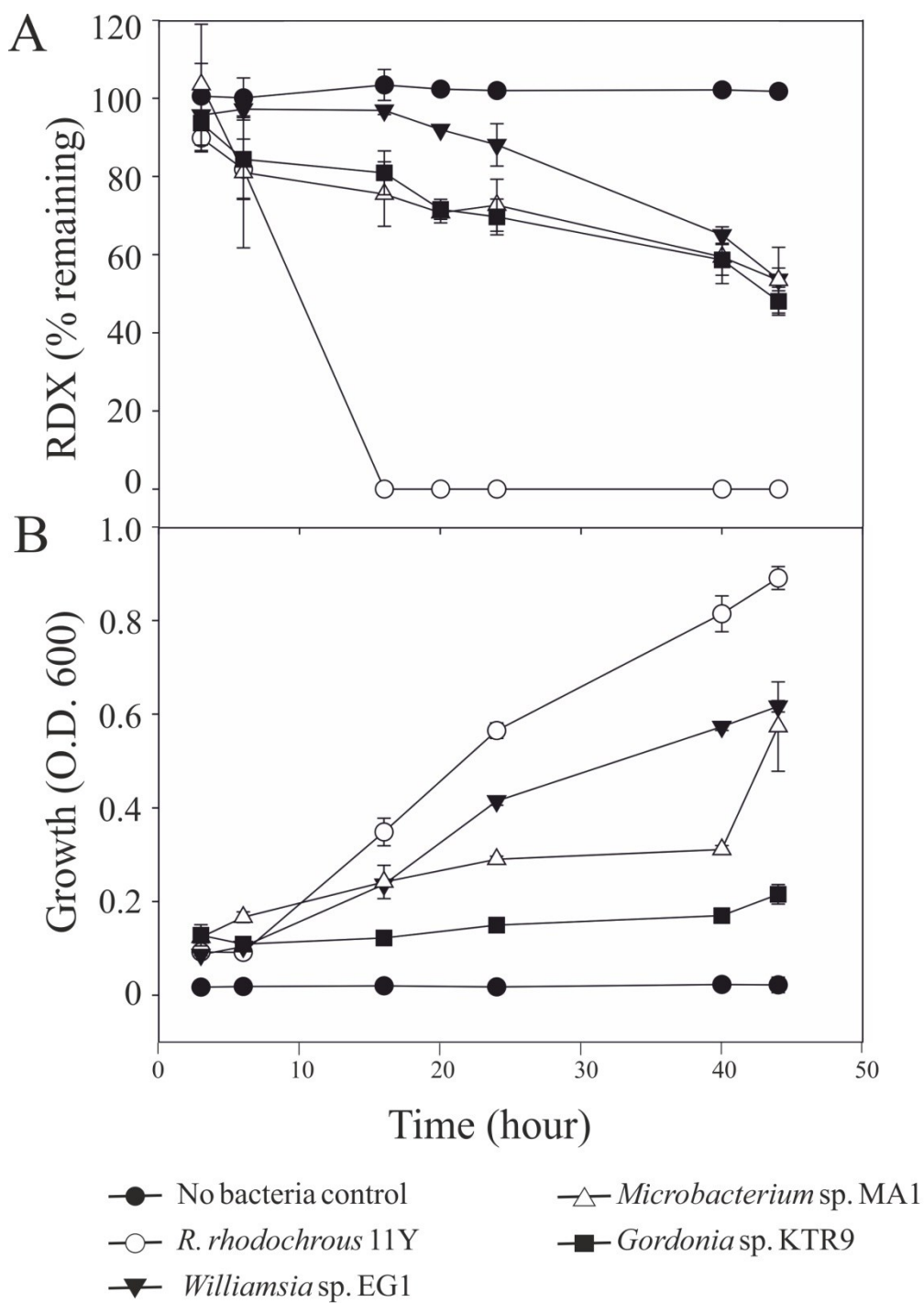


Figure 4.39: RDX removal (A) and growth (B) of *R. rhodochrous* 11Y, *Williamsia* sp. EG1, *Microbacterium* sp. MA1, and *Gordonia* sp. KTR9. Data shown are mean of three biological replicates \pm SD. Reproduced from Chong *et al.* (2014) [144].

4.3.2 Analysis of the sequence flanking *xplA* in the RDX-degraders

Approximately 15 kbp of the region flanking *xplA* was sequenced in *R. rhodochrous* 11Y using the primer walking method. The sequence from each primer walk (~1 kbp) was verified by designing complementary primers and using PCR to analyse the region.

A sequence comparison showed that there is a 13.8 kbp region of the *R. rhodochrous* 11Y sequence, encoding twelve ORFs, that shares > 99 % sequence identity to the 14.3 kbp region in *Microbacterium* sp. MA1. There were only three differences in the whole region between these two phylogenetically-distant related species: Firstly, the gene encoded for the transposable element (pMA1.028) and 148 nucleotide sequences downstream of the gene is present in *Microbacterium* sp. MA1, but missing in *R. rhodochrous* 11Y. Secondly, the gene encoding a transcriptional regulatory protein containing a GAF-domain (pMA1.022) is truncated in *Microbacterium* sp. MA1, while the full length gene is present in *R. rhodochrous* 11Y. Lastly, there are six SNPs within the whole 14.3 kbp region, with one of the SNP located upstream of the *xplB* gene (pMA1.030), four are located in the *xplB/xplA* region, and the last one is located in the gene downstream of *xplA* (pMA1.033) (Figure 4.7).

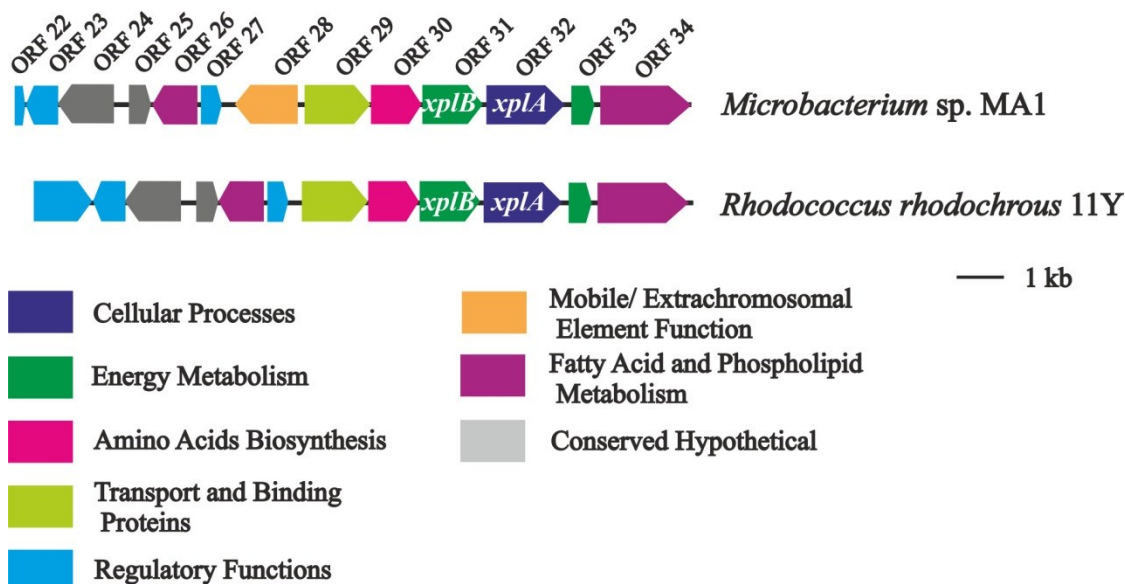


Figure 4.40: Comparison of the genes flanking *xplA* between *R. rhodochrous* 11Y and *Microbacterium* sp. MA1. The 14.3 kbp region (ORF 22 to ORF 34) in *Microbacterium* sp. MA1 is highly conserved in *R. rhodochrous* 11Y. The ORF 28, which encoded for the transposable element, is the only gene which is missing in *R. rhodochrous* 11Y. The colour code for each gene is described in the figure.

Sequence comparison of the 13.8 kbp region spanning ORFs 22-34 from *R. rhodochrous* 11Y with the, *xplA* carrying plasmid (pGKT2) from *Gordonia* sp. KTR9 showed that there is only a 3,099 bp region that is nearly identical (> 99 %) between these two bacteria. The 3,099 bp region starts at the 4th nucleotide from the ATG start site of the *xplB* gene and extends to the 103 nucleotides downstream of *xplA*. Additionally, there were just three SNPs within that region, one located in *xlpA* and the other two in the *xlpB* region.

Further analysis using PCR (Chapter 2.6.3) with the primers listed in Table 2.1 confirmed that the 13.8 kbp region in *R. rhodochrous* 11Y could be amplified in the other seven *Rhodococcus* spp. using the overlapping primer pairs (Data not shown).

In *Williamsia* sp. EG1, the gene cluster appeared to be different from the other three genera of RDX-degrading bacteria: while the *xplA* and *xplB* region was amplified, the region between *marR* and *xplB* could not be amplified in the bacterium using the F, G, H and I primer pairs at either 50 or 55 °C annealing temperature (Figure 4.8) .

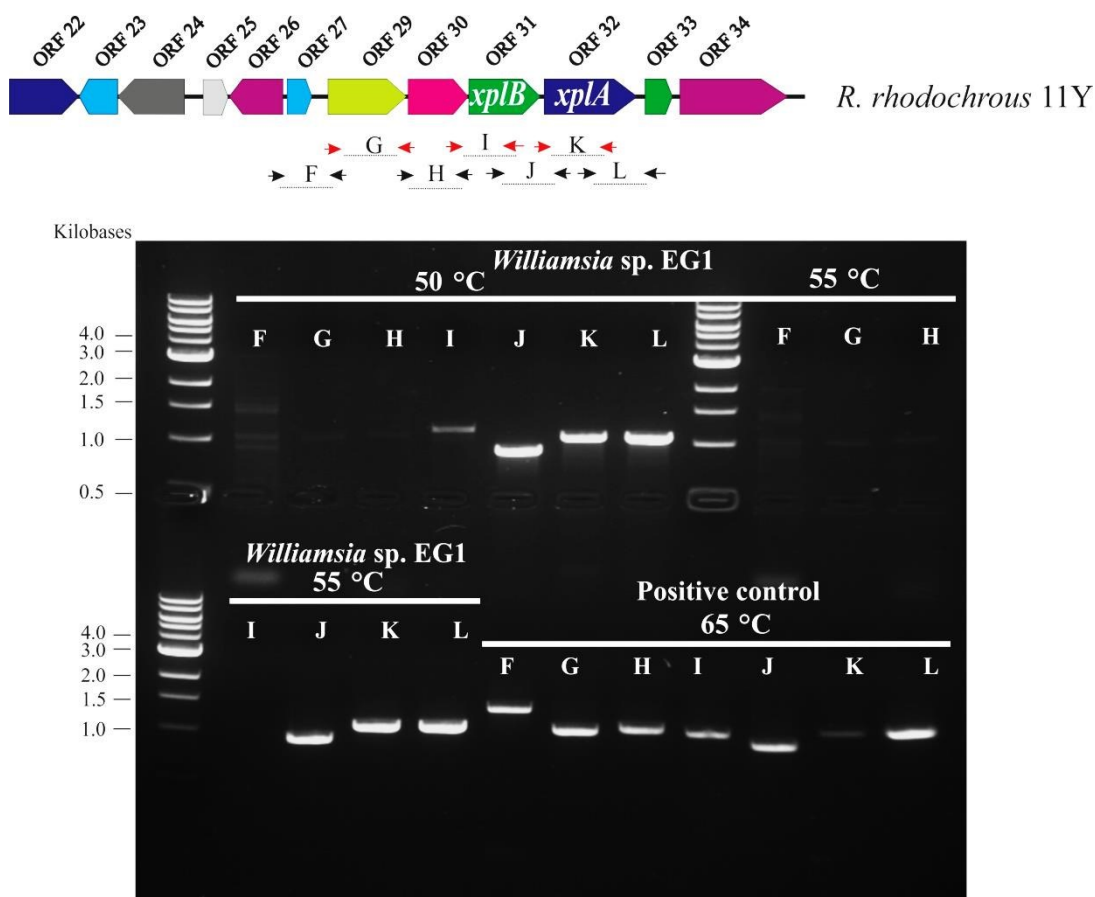


Figure 4.41: PCR products from amplifying the regions between *marR* to the end of *xplA* within the genome of *Williamsia* sp. EG1. The PCR was carried out using two different annealing temperatures (50 °C and 55 °C). *R. rhodochrous* 11Y genome was used as a positive control. The product sizes are: 1,351 bp, 1,038 bp, 1,078 bp, 1,049 bp, 900 bp, 1,065 bp, 1,073 bp from F to L region, respectively.

Further attempts to amplify the *marR* to *xplB* region in *Williamsia* sp. EG1 were made using PCR and a wider range of annealing temperatures (45 °C, 50 °C and 55 °C). Simultaneously, PCR was also carried out to amplify the two genes downstream of *xplA* in *Williamsia* sp. EG1 using three primer pairs (M, N and O) (Figure 4.9). The expected PCR products were found for the two genes downstream of *xplA*, while again, the expected bands were not found for the region between *marR* and *xplB* in the *Williamsia* sp. EG1 genome (Figure 4.9).

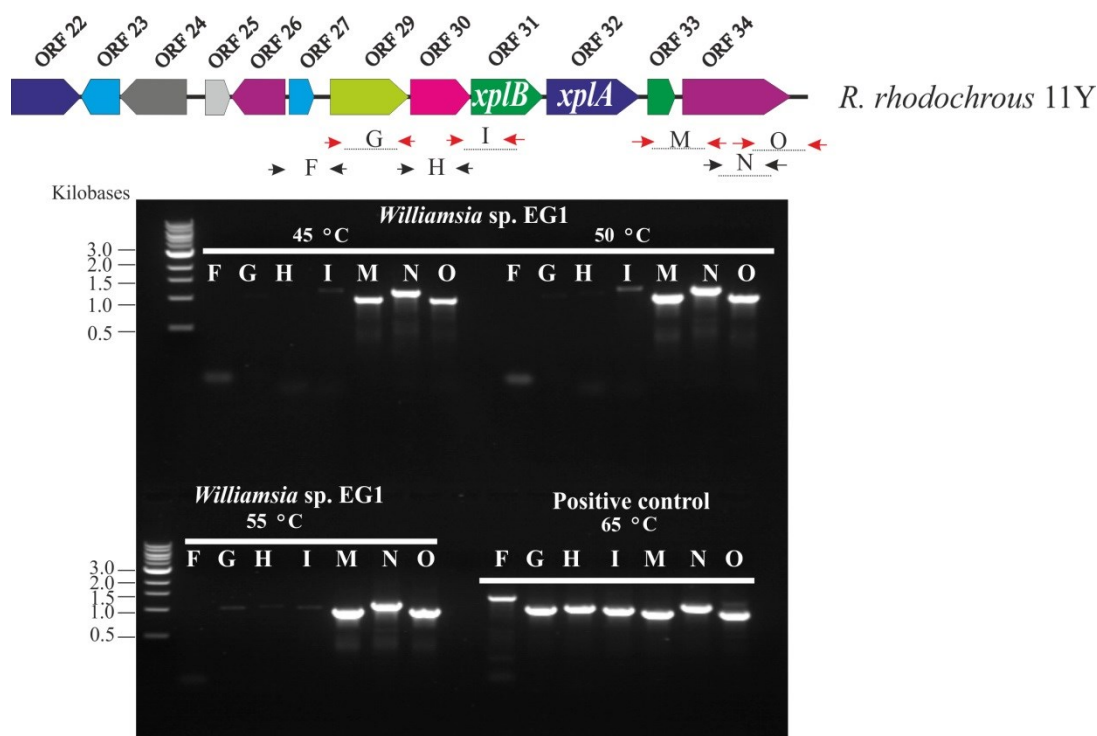


Figure 4.42: PCR products from amplifying upstream of *xplB* and downstream of *xplA* in *Williamsia sp. EG1*. The annealing temperatures of the reaction were 45 °C, 50 °C, 55 °C. The expected size of the products of F, G, H, I, M, N, and O are 1,351 bp, 1,038 bp, 1,078, 1,049 bp, 977, 1,143, 981, respectively. Genomic DNA from *R. rhodochrous* 11Y was used as a positive control.

In order to investigate whether *Williamsia sp. EG1* has a full length *xplB* or if *xplB* is fused to *glnA* in a similar manner to that seen in *Gordonia sp. KTR9*, a forward primer was designed to anneal to the first nucleotide of *xplB* (5'-ATGGACATCATGAGTGAAGTGG-3') and was used with the reverse internal *xplB* primer (I-R) as well as an internal reverse primer of *xplA* (J-R) (Figure 4.10). Additionally, primers designed to amplify the full length of *xplB-glnA* were also used. The results revealed that *Williamsia sp. EG1* has a full-length *xplB* gene which is not fused to *glnA*.

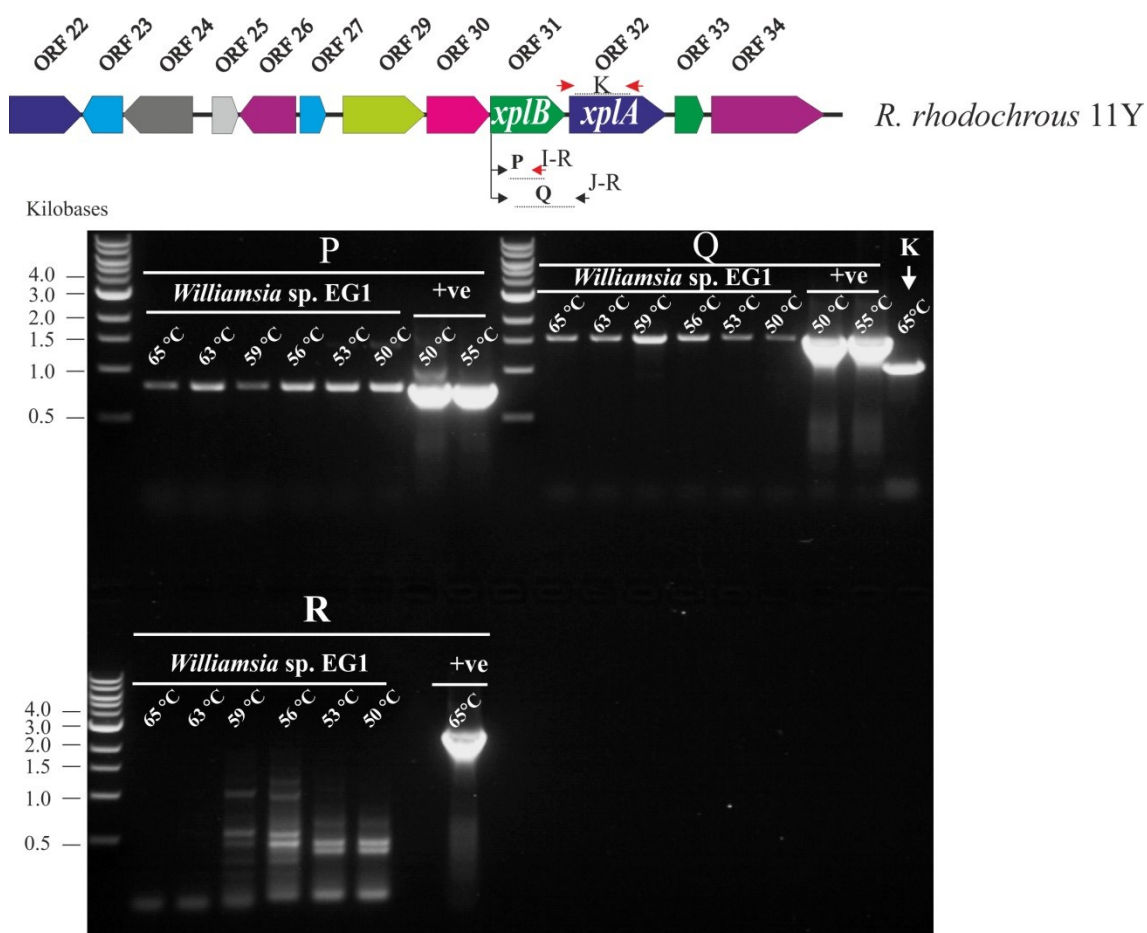


Figure 4.43: PCR products from the amplification of the *xplB* region in *Williamsia* sp. EG1. P refers to the PCR products using the primers designed to amplify *xplB* from the start codon with an internal *xplB* reverse primer; the expected band is 797 bp. Q refers to the product of the same forward primer with the internal reverse primer from *xplA* gene (J-R); the expected product size is 1,532 bp. R refers to the PCR product of the primers which amplify full length *glnA-xplB*; expected product size is 2,445 bp. The annealing temperature of each product is written above each band. Positive controls for both P and Q were made by using the same primers but with *R. rhodochrous* 11Y DNA. The same primers were used for the positive control (+) of R, but with the *Gordonia* sp. KTR9 DNA. K is the PCR product from the *xplA* region in *Williamsia* sp. EG1 genome, expected size = 1,065 bp.

Although the region from *marR* to *xplB* could not be amplified from *Williamsia* sp. EG1 by PCR, the upstream region of *marR* was amplified by PCR as shown in Figure 4.11.

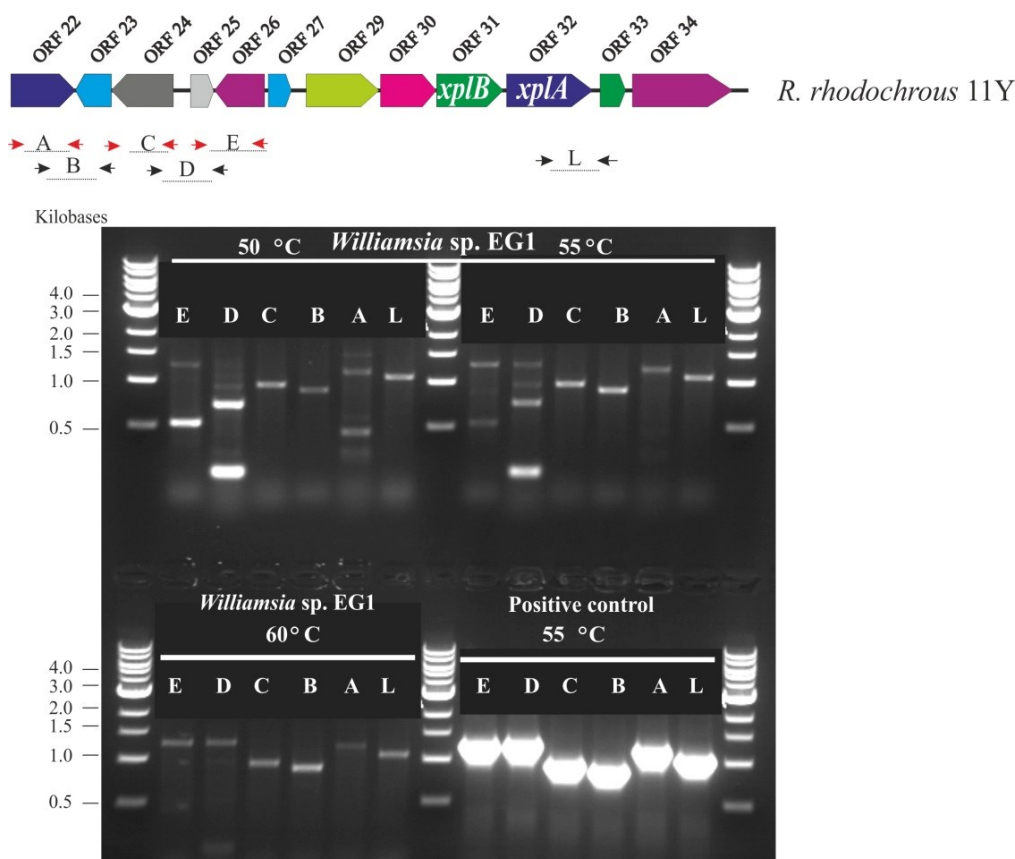


Figure 4.44: PCR products of the five primer pairs which were designed to amplify the genes upstream of *marR* in *Williamsia* sp. EG1 genome. The E, D, C, B and A letters represent the PCR products for the region of the upstream of the *marR* gene; L is the PCR product for *xplA* region. The annealing temperature for each reaction is written above the bands. *R. rhodochrous* 11Y was used as a positive control. The product size for E, D, C and B are 1,246, 886, 958, 1,130 and 1,274 respectively. The PCR product for L is 1,073 bp.

The data presented in Figure 4.11 demonstrate that *Williamsia* sp. EG1 has all five ORFs (ORF27 to ORF 22), in the same order as in *Microbacterium* sp. MA1 and *R. rhodochrous* 11Y, but unlike *Microbacterium* sp. MA1, the *Williamsia* sp. EG1 has a full length *gaf* gene. The *gaf* to *marR* region was also confirmed by sequencing the PCR products A to E.

To investigate the proximity of *marR* to *xplB* and sequence upstream region of *xplB*, an attempted was made to amplify the region using primers designed to anneal to nucleotide number 97 upstream of the *marR* region (5'- ACGTCGAGTGTCGGGCGG ACC-3') with the reverse primer annealing to base number 86 downstream of *xplB* (5'- AGTTGCTGTGCGGTGAAAC-3'). No PCR product was detected in the *Williamsia* sp. EG1 genome using a gradient of annealing temperatures (56-70 °C), while the expected PCR product was found in the positive control (Figure 4.12).

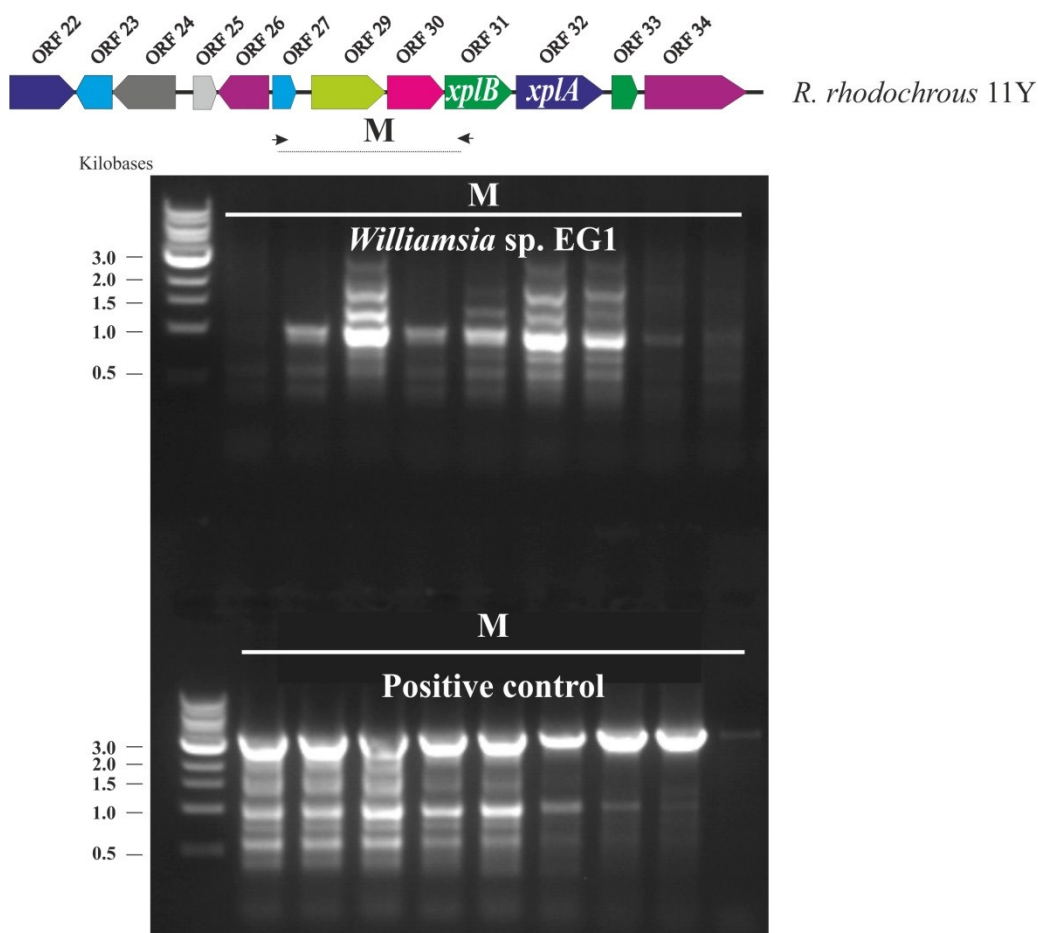


Figure 4.45: PCR products amplifying the region between *marR* and *xplB* gene in *Williamsia* sp. EG1. The PCR was carried out using a gradient annealing temperature from 56 °C to 70 °C with the primers anneal to upstream of *marR* and downstream of *xplB*. Positive control is the PCR products of the same primers using *R. rhodochrous* 11Y genome. Expected product size is 3,388 bp.

Recently, three short contigs in the *xplA*-region were published from the fosmid library sequence of the *Williamsia* sp. EG1 [113]. The first contig, which has the GenBank accession number KF571922, is 2,141 bp and is identical to *xplA* starting at the nucleotide position number 60 to the nucleotide number 393 of the 450 bp long gene encoding succinate-semialdehyde dehydrogenase (termed A in Figure 4.13).

The second contig, (GenBank accession number: KF571923), is 952 bp and is identical to the minus strand of the 1,071 bp length gene encoding a dihydrodipicolinate reductase from the nucleotide position number 1,007 to 56 (terms as B in Figure 4.13).

The third contig of *Williamsia* sp. EG1 (GenBank accession number: KF571924), is 909 bp and is identical to the sequence encoding the transposable element (ORF28) at the position 895 to the nucleotide number 321 of the 1,395 bp length gene encoding for the

permease (ORF 29) (terms as C in Figure 4.13). A summary of the published sequence data for *Williamsia* sp. EG1 can be seen in Figure 4.13.

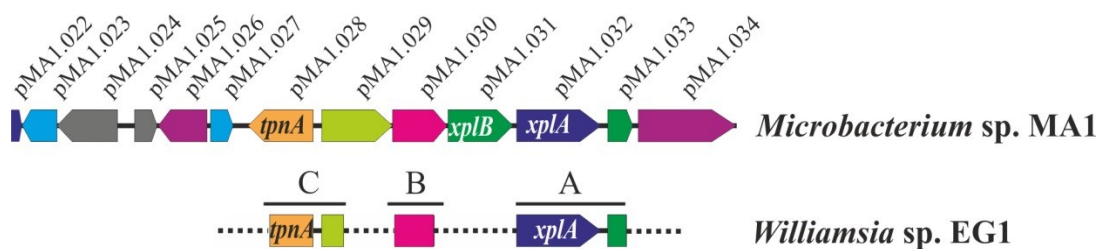


Figure 4.46: Comparison of the published contigs of *Williamsia* sp. EG1 to partial sequence of *Microbacterium* sp. MA1. A, B and C represent the region from contig sequence which has accession number KF571922, KF571923, and KF571924, respectively. Dotted line is unconfirmed sequence area between genes. Straight line is continuous region.

Overall, a 5,645 bp region, starting from nucleotide 32 of *xplB* to the gene encoding the AMP-binding enzyme (pMA1.034), was sequenced in *Williamsia* sp. EG1. The region between the *gaf* to *marR* was also confirmed by PCR and sequencing. The region upstream of *xplB* could not be amplified by PCR using the primers designed from *R. rhodochrous* 11Y genes, nor by using primers designed for *xplB-glnA* from *Gordonia* sp. KTR9. The results presented here suggest that the region upstream of *xplB* is different from other known RDX-degrading bacteria. A summary of the *xplA*–flanking regions in *Williamsia* sp. EG1, *R. rhodochrous* and *Microbacterium* sp. MA1 is shown in Figure 4.14.

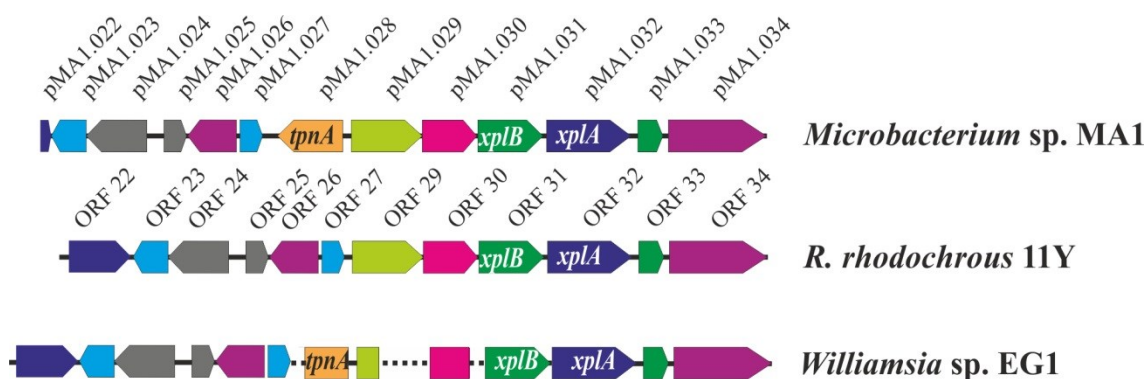


Figure 4.47: Comparison of the *xplA* flanking region in three different genera of aerobic RDX-degrading bacteria, *Microbacterium* sp. MA1, *R. rhodochrous* 11Y and *Williamsia* sp. EG1. The dotted line represents unconfirmed gene sequence. Straight line is continuous genes.

Despite the fact that several of the genes flanking *xplA* and *xplB* are highly conserved in all the RDX-degrading bacteria studied here, only *xplA* and *xplB* appear to be directly involved in RDX degradation [95, 96, 144]. To understand the evolutionary relationship between these isolates, a SNPs study was carried. Sequence analysis revealed that the bacteria all contained nearly identical copies of the *xplA* and *xplB* genes, as shown in Figure 4.15. There are only six SNPs, Three of the SNPs are located in the heme-domain of the *xplA* gene, occurring at positions 757, 877 and 1621, which affect residues 253, 293 and 541, respectively.

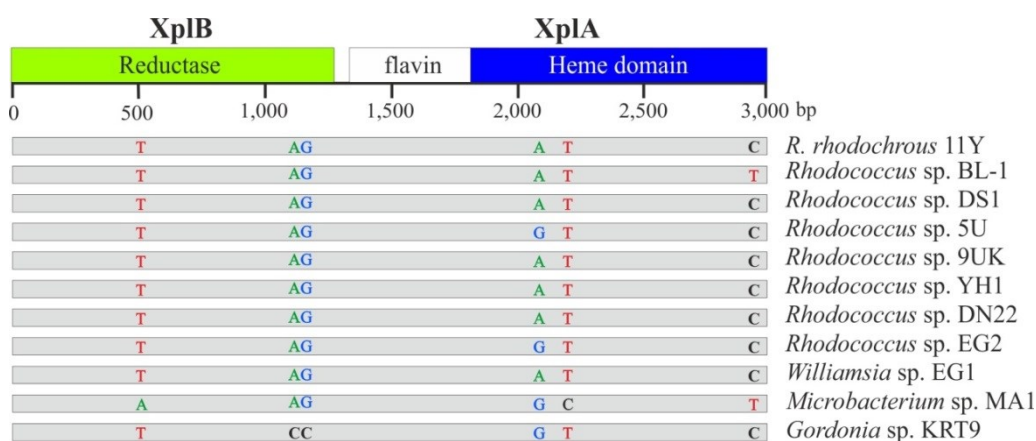


Figure 4.48: Comparison of the nucleotide sequence of the *xplA* and *xplB* genes amongst the RDX degrading bacteria. Only the SNP variation is shown in all the isolates.

4.3.3 Total genome sequencing

To identify the sequence upstream of *xplB* in *Williamsia* sp. EG1 and sequence the plasmid carrying the *xplA* and *xplB* genes in *R. rhodochrous* 11Y, both bacteria were submitted for total genome sequencing. The methodology for total genome sequencing is described in Chapter 2.6.2. Prior to sequencing, the 16S rRNA regions were sequenced to ensure that the DNA samples were from the correct species (data not shown). Additionally, the *xplA* gene was amplified from the DNA samples to make sure that the plasmids had not been cured from the bacterial genomes during the extraction process. The quality and quantity of the genomic DNA samples was analysed using an Agilent TapeStation 2200, and the results are shown in Figure 4.16.

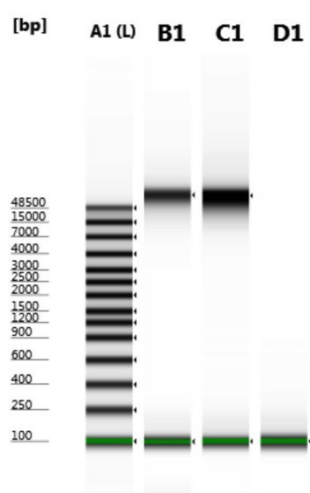


Figure 4.49: Genome analysis of *R. rhodochrous* 11Y and *Williamsia* sp. EG1 using an Agilent TapeStation 2200. A1 is a ladder (93.8 ng/ μ l). B1 is the 5-fold dilution of *R. rhodochrous* 11Y genome (concentration= 12.9 ng/ μ l). C1 is the 5-fold dilution of *Williamsia* sp. EG1 genome. D1 is the blank.

The genome sequencing was performed by Dr. Deborah Rathbone in the Biorenewables Development Centre at the University of York using Ion Torrent (Life Technologies) next generation sequencing.

The raw data from the genome sequencing was assembled by Dr. Yi Li in the Centre for Novel Agricultural Products at the University of York using Newbler (version 2.7), the results of the sequence assembly are shown in Table 4.1.

Table 1: Sequence assembly results of the total genome sequence of *R. rhodochrous* 11Y and *Williamsia* sp. EG1

| | <i>R. rhodochrous</i> 11Y | <i>Williamsia</i> sp. EG1 |
|------------------------|---------------------------|---------------------------|
| Peak depth | 87.0 | 212.0 |
| Number of all contigs | 2,362 | 155 |
| Number of bases | 8,794,871 | 4,428,181 |
| Average of contig size | 4,514 | 37,150 |
| N50 of contig size | 8,725 | 66,310 |
| Largest contig size | 153,643 | 252,087 |
| Estimated genome size | 8.9 MB | 4.4 MB |

4.3.3.1 Analysis of the total genome sequence of *R. rhodochrous* 11Y

Scanning for *xplA* in the contigs of the *R. rhodochrous* 11Y genome sequencing, revealed that the gene appeared in the 50,923 bp contig00008 in *R. rhodochrous* 11Y. The contig could not be assembled to any other contig using Newbler software, nor by PHRAP (<http://www.phrap.org/>) software having the total genome sequence of *R. erythropolis* PR4 (= NBRC 100887), plasmid (pGKT2) of *Gordonia* sp. KTR9 or *Gordonia bronchialis* DSM 43247 as a reference sequence.

Manual sequence analysis showed that the 5' end of the contig00008 overlaps with the reverse complementary sequence of the 2,578 bp length contig000853 as both contigs contained a portion of the sequence encoding a helicase-associated protein (gene locus: KTR9_4946) within plasmid (pGKT2) in *Gordonia* sp. KTR9. Subsequent PCR confirmed that the contigs 00008 and 000853 can be assembled together (Data not shown). As no other contigs aligned in this region, further contig assembly was not possible.

Sequence annotation of the 53,711 bp region spanned by contigs 00008 and 000853 was carried out using a Bacterial Annotation System (BASys) [145] and NCBI Prokaryotic Genome Annotation Pipeline (PGAP), then further checked manually using the BLAST search engine in NCBI. The annotation revealed that the region encodes 58 ORFs, 21 of which are hypothetical proteins, and three genes encode for transposable elements

(Gene loci: 11Y.043, 11Y.044 and 11Y.057), which are located downstream of *xplA* (Figure 4.17). The first two transposable elements encoded by (Gene loci: 11Y.043 and 11Y.044) belong to the Class II transposable elements, and are identical to a multispecies transposase in *Corynebacterineae* (GenBank accession number: WP_011331220). The third transposable element (Gene locus: 11Y.058) is identical to a putative site-specific recombinase (gene locus: RER_pREC1-00620) of the linear plasmid 1 pREC1 in *Rhodococcus erythropolis* PR4.

The 15 kbp region downstream of the gene loci: 11Y.043, encodes for first transposable element to the end of the sequence was found to be nearly identical (15913/15915; 99 %) to the linear plasmid1 (pREL1, length= 271,577 bp) of the alkane-degrading bacterium *R. erythropolis* PR4 [130] at the region (Gene loci: RER_pREC1-00610 to RER_pREC1-00750).

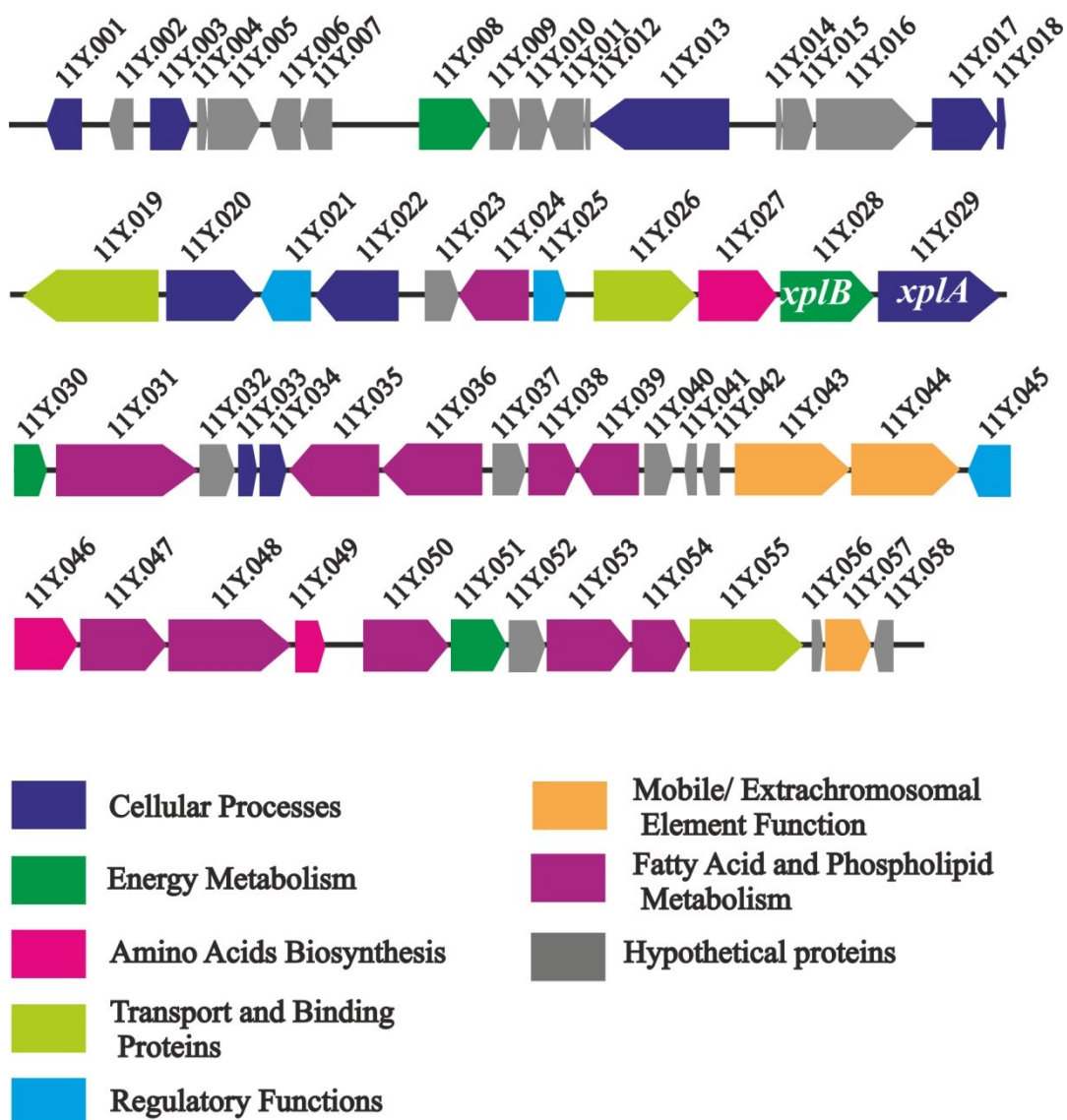


Figure 4.50: Schematic representation of the partial 53,711 bp plasmid sequence flanking *xplA* and *xplB* in *R. rhodochrous* 11Y. The colour code for each gene is explained in the figure.

Interestingly, there was an 11.8 kbp region found to be nearly identical (> 99 %) between the partial plasmid sequence of the *R. rhodochrous* 11Y and the plasmid carrying *xplA* (pGEKT2) from *Gordonia* sp. KTR9. The region starts at the nucleotide position number 364 upstream of Gene locus 11Y.02 to the end of the gene locus 11Y.017 in *R. rhodochrous* 11Y, which is identical to the sequence region from gene loci KTR9_4945 to KTR9_4801 in *Gordonia* sp. KTR9. There were three differences in the 11.8 kbp region between these two bacteria: First, the transposable element encoded by gene locus KTR9_4947 is missing in the partial sequence of *R. rhodochrous* 11Y.

Second, the gene encodes for replicative DNA helicase in *Gordonia* sp. KTR9 (Gene locus: KTR9_4801) which is truncated and fused with truncated 23s rRNA sequence in *R. rhodochrous* 11Y (Gene locus: 11Y.017). Lastly, there were six nucleotides (CCGAGC) in a noncoding region between the gene loci 11Y.010 and 11Y.011, which are missing in the corresponding region in *Gordonia* sp. KTR9.

4.3.3.2 Analysis of the total genome sequence of *Williamsia* sp. EG1

The whole genome sequence of *Williamsia* sp. EG1 was first scanned for *xplA* and *xplB*. Surprisingly, the sequences for *xplA* nor *xplB* could not be found in the assembled contigs. Further sequence analysing was carried out by comparing all the contigs to a partial 53 kbp region from *R. rhodochrous* 11Y and full plasmid (pGKT2) sequence, carry *xplA/xplB*, from *Gordonia* sp. KTR9. Again there was no significant sequence similarity between the *Williamsia* sp. EG1 contigs and either the *R. rhodochrous* 11Y gene cluster or plasmid (pGKT2) of *Gordonia* sp. KTR9.

To investigate the possibility of whether the wrong sample had been sequenced, 16S rRNA of *Williamsia* sp. EG1 (GenBank accession number: KF571870.1) was aligned against the assembled contigs, and the entire length of the sequence found to align to contig00109 with 99 % sequence identity (1359/1366). Further analysis of the raw sequence data identified a single fragment (~ 300 bp) with > 99 % sequence identity to the *xplA* of *R. rhodochrous* 11Y. As there were no contigs containing the *xplA* region from the whole genome sequencing of *Williamsia* sp. EG1, no further analysis on the *xplA* region using these data could be done.

Overall, a 13.8 kbp gene cluster (termed the A region in Figure 4.18) flanking *xplA* and *xplB* which is conserved amongst *Rhodococcus* spp. regardless of the geographical location from where each species had been isolated. The A region is also conserved in *Microbacterium* sp. MA1, with the exception of a transposable element (Gene locus: pMA1.028), which is missing in the *Rhodococcus* spp gene cluster, and a *gaf* gene (Gene locus: pMA1.022), which is truncated in *Microbacterium* sp. MA1. Several genes within the A region of *Williamsia* sp. EG1 were also amplified by PCR and sequenced. *Williamsia* differs from *Rhodococcus* spp. by having a gene encoding a transposable element next to the *aroP* gene, whereas *Williamsia* sp. EG1 is different from *Microbacterium* sp, MA1 by having a full length of the *gaf* gene. There is only 3.1 kbp of the A region in *Gordonia* sp. KTR9, which encodes to *xplA* and *xplB* genes. The *xplB*

gene in *Gordonia* sp. KTR9 is fused at the 5' end to *glnA*; different from all the other bacteria studied here.

Partial sequencing of the 53 kbp region flanking *xplA* in *R. rhodochrous* 11Y revealed a 11.8 kbp sequence (termed the B region in Figure 4.18) upstream of the A region and a 570 bp sequence upstream of a transposable element (gene loci=11Y.043) (termed the C region in Figure 4.18) sharing sequence homology (> 99 %) with a 13.6 kbp region and 932 bp region of the plasmid (pGKT2) in *Gordonia* sp. KTR9. There are two main differences in the B region between *Gordonia* sp. KTR9 and *R. rhodochrous* 11Y. In *Gordonia* sp. KTR9 there is a transposable element (Gene locus: KTR9-4947) in the B region which is missing from the corresponding region in *R. rhodochrous* 11Y. Furthermore the gene locus: KTR9-4801, which encodes a replicative DNA helicase, is truncated and fused with truncated 23s rRNA in *R. rhodochrous* 11Y (Gene locus: 11Y.017). In the C region of *Gordonia* sp. KTR9, the Gene locus KTR9_4944 encoding for the hypothetical protein, is truncated in *R. rhodochrous* 11Y (Gene locus: 11.042).

In addition to the sequence homology between *R. rhodochrous* 11Y and *Gordonia* sp. KTR9, there are two regions (termed the D1 and D2 regions in Figure 4.18) which are nearly identical between the 52 kbp sequence of *Microbacterium* sp. MA1 and the plasmid (pGKT2) of *Gordonia* sp. KTR9. The D1 region is 2185 bp upstream of a transposable element (Gene locus: pMA1.015) in *Microbacterium* sp. MA1 which is identical to the 2188 kb region (Gene loci: KTR9_4933 to KTR9_4937) located at 5.2 kbp downstream of the *xplA* in *Gordonia* sp. KTR9. The D2 region is 1260 bp located downstream of the same transposable element (Gene locus: pMA1.015) in *Microbacterium* sp. MA1, and it is identical to the 1273 kb region (Gene loci: KTR9_4802 to KTR9_4806) located nearly 150 kb upstream region of the *xplA/xplB* in *Gordonia* sp. KTR9. A summary of the sequence analysis can be seen in Figure 4.18.

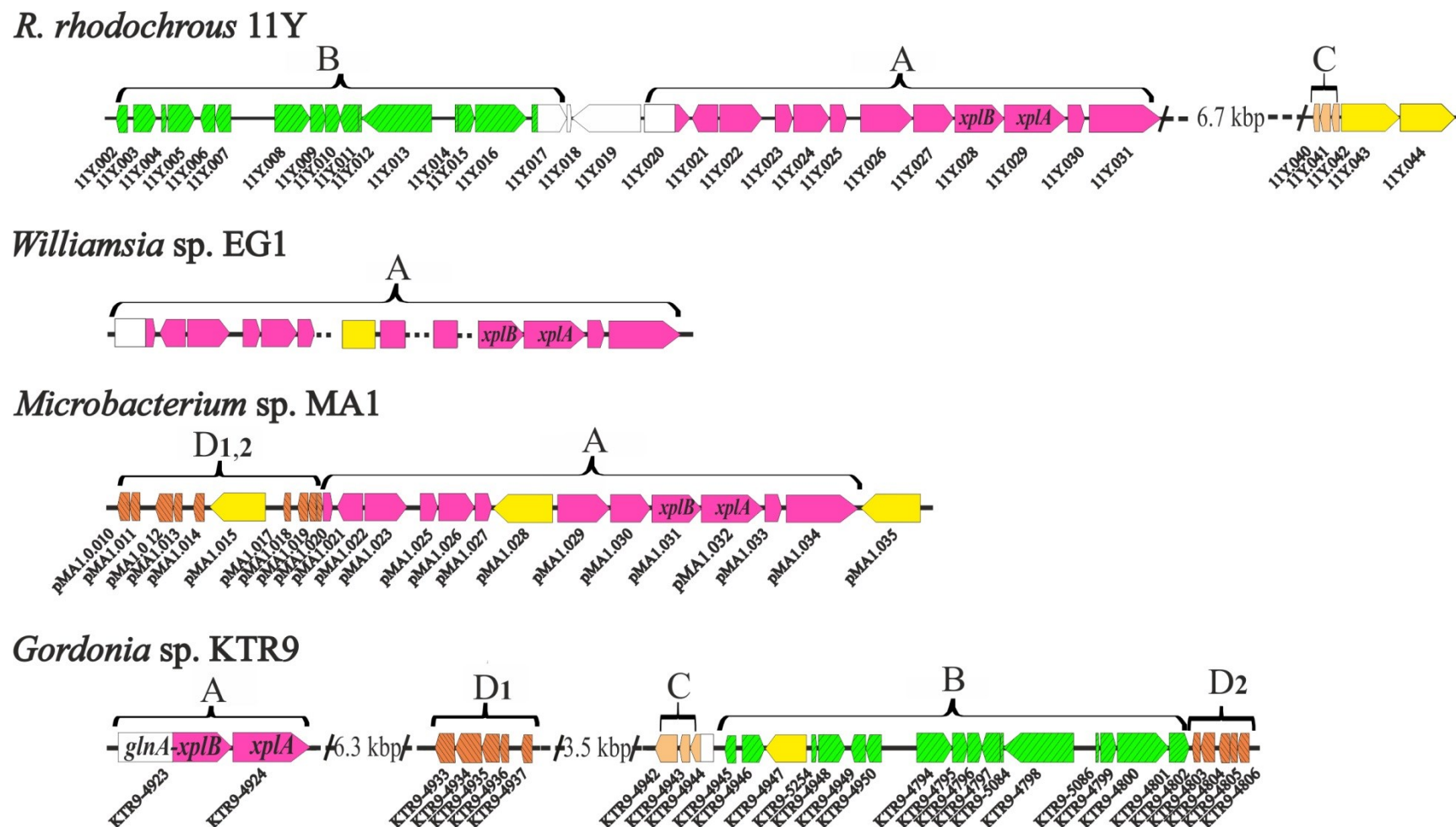


Figure 4.51: Schematic representation of the RDX-degrading genomic island in four genera of aerobic RDX-degrading bacteria. A is region containing *xplA* and is 13,865 bp in *R. rhodochrous* 11Y, 14,312 bp in *Microbacterium* sp. MA1 and 3,099 bp in *Gordonia* sp. KTR9. In this region *Microbacterium* sp. MA1, contains a transposable element which is absent in both *R. rhodochrous* 11Y and *Gordonia* sp. KTR9. Additionally, in *Gordonia* sp. KTR9 the *xplB* gene is fused with *glnA*. B refers to a 11,846 bp region in *R. rhodochrous* 11Y, which shares sequence homology with a 13,687 region in

Gordonia sp. KTR9. In this region, the transposable element *tnpA* of *Gordonia* sp. KTR9 (Gene locus: KTR9_4947) is missing in *R. rhodochrous* 11Y. C is the 570 bp region located next to two transposable elements in *R. rhodochrous* 11Y (Gene loci: 11Y.041 and 11Y.042), and it shares sequence similarity to the 932 bp sequence in *Gordonia* sp. KTR9. The D1,2 region in *Microbacterium* sp. MA1 is composed of 4,873 bp, and is similar to the 3,461 bp region in *Gordonia* sp. KTR9 in two separate regions D1 and D2. D1 which is 2,188 bp and D2 is 1,270 bp; the transposable element *tnpA* is located in the D1,2 region in *Microbacterium* sp. MA1 (Gene locus: pMA.015) is missing in *Gordonia* sp.KTR9. White coloured regions have no sequence homology in corresponding bacteria. Dotted line is unconfirmed sequence region. The gene encoded for transposable elements are shown in yellow colour.

4.4 Discussion

Comparison of the RDX removal rates between RDX-degrading isolates showed that all *Rhodococcus* spp. had faster RDX removal rates than *Microbacterium* sp. MA1, *Gordonia* sp. KTR9 and *Williamsia* sp. EG1.

Considering that XplA alone is enough to denitrate the RDX structure in the organism [98, 105] and XplB enhances this activity [95, 144], the differences in the RDX-removal rate is either due to the impairment of XplA/XplB proteins, or differences in the physiology between the strains and species. The sequence analysis presented in this chapter showed that both *xplA* and *xplB* are highly conserved between the RDX-degrading bacteria with only six SNPs in the entire length of the two genes.

The *xplA* gene in *Williamsia* sp. EG1, the species with the slowest rate of RDX-removal, is 100 % identical to the *xplA* gene of *R. rhodochrous* 11Y, the fastest RDX-removal bacterium. Thus, differences in RDX-removal rates are not due to the impairment in the XplA functionality, and are more likely due to differences in the physiology between the strains and species presented here.

Studies whereby the *xplA* and *xplB*-carrying plasmid (pGKT2) from *Gordonia* sp. KTR9 was transferred into *Gordonia polyisoprenivorans*, *Rhodococcus jostii* RHA1 and *Nocardia* sp. TW2 via transconjugation, demonstrated that pGKT2 conferred the ability to grow using RDX as sole nitrogen source, with the faster rate of RDX-removal by *Rhodococcus jostii* RHA1 [104]. Additionally, *R. jostii* RHA1 transformed with *xplA* from *Gordonia* sp. KTR9 through pTip type II shuttle vector resulted in a 14 times faster rate of RDX-removal by the transformed *R. jostii* [105].

It is known that there are differences between the rates of xenobiotic catabolism by the same enzyme within different species. For example, *Ancylobacter aquaticus* AD20, *Ancylobacter aquaticus* AD25 and *Xanthobacter autotrophicus* GJ10 all carry identical copies of the *dhlA* gene for haloalkane dehalogenase and they degrade 1,2-dichloroethane (DCE), and other halogenated aliphatic compounds, at significantly different rates on the genus level but are less different at the strain level [146]. Thus, it is not surprising that *R. rhodochrous* CW25 transformed with the 7.5 kbp region (pHSX1) from *R. rhodochrous* 11Y, which encodes both XplA, XplB, showed slower RDX removal rate compared to the *R. rhodochrous* 11Y [96].

Another factor that could influence differences in the RDX-degradation rates between the species is XplB activity. The *xplB* knock-out in *R. rhodochrous* 11Y decreased the RDX-degradation rate by 70 % [144] and transgenic plant lines expressing both *xplA* and *xplB* removed RDX faster than plants expressing *xplA* alone [95]. Both of these observations demonstrate that XplB is important for RDX degradation. *Gordonia* sp. KTR9 has the second slowest RDX-removal rate of all the bacteria tested here and is likely to be the result of a single mutation (3rd substitution) in XplB which encodes serine-385 in the place of a highly conserved aromatic tryptophan residue. Moreover, the fusion of *xplB* to *glnA* is likely to further inhibit the reductase activity of XplB. The XplB-GS fusion is studied and discussed in more detail in Chapter 5.

XplB in *Microbacterium* sp. MA1 has isoleucine-172 in the place of conserved phenylalanine-172 in the XplB of RDX-degrading bacteria. Although, the homology modelling of the XplB protein was revealed that the Phe residue is not located in the FAD moiety of the XplB protein (data not shown), replacing an aromatic residue (phenylalanine) by isoleucine might affect the activity of the protein, similar to XplB in *Gordonia* sp. KTR9.

Williamsia sp. EG1 exhibited the slowest rate of RDX removal of all the isolates, slower even than *Gordonia* sp. KTR9 which contains a XplB-GS fusion with reduced XplB activity. While the partial *xplB* sequence from *Williamsia* sp. EG1 was identical to *xplB* from *R. rhodochrous* 11Y, sequence directly upstream of *xplB* in *Williamsia* sp. EG1 could not be obtained. It is possible that *xplB* in the *Williamsia* sp. EG1 is fused to an unknown protein, resulting in decreased reductase activity, in a manner similar to the XplB-GS fusion in *Gordonia* sp. KTR9 or the levels of *xplB* expression are impaired.

A particularly curious observation during the analysis of the *xplA/B*-containing region in *Williamsia* sp. EG1 was the inability to obtain DNA sequence, either by PCR or total genome sequencing techniques, directly upstream from *xplB*. This could be due to a high GC content of the region or repetitive DNA sequences. Such a case is not without precedence: sequence assembly of the contig carrying a gene for chlorate reduction was also reported to fail due to the presence of several repeat sequences in the region [147]. [105]. Additionally, although a portion of the *xplA* gene was found in the raw sequence data of *Williamsia* sp. EG1, the *xplA/xplB* genes could not be located in the genome sequence of this bacterium. Loss of the plasmid by the majority of the bacterial cells

after growth in non-selective LB medium prior to DNA extraction could be one possible explanation for the absence of *xplA/xplB* in the genome sequence of the bacterium. With few plasmids present, coverage may have been too low in the *xplA* region for the sequence to be adequately assembled. If the *xplA/xplB*-containing plasmid has been lost during growth in LB, this perhaps suggests the plasmid is not stable, and can be cured when the selective pressure is not present. A previous attempt to create independent *xplA* and *xplR* knock-out strains of *Gordonia* sp. KTR9 resulted in the strains being cured of the plasmid [105]. Moreover, a study to identify the gene responsible for RDX-degradation in *Rhodococcus* sp. HS4 suggested that long term storage in non-selective medium in freezing conditions might have caused a loss of the RDX-degradation capacity in the bacterium [57].

The *xplA* and *xplB* genes are highly conserved amongst different genera of aerobic RDX-degrading bacteria isolated from distinct geographical location, which further supports the theory of the recent evolution of these genes, and dissemination around the world through the horizontal gene transfer [100, 103, 104]. In a similar manner, naphthalene degrading genes (*nahAc*) [148], N-heterocycle morpholine degrading genes (*morABC*) [149], atrazine degrading genes (*atzABC*) [150] and haloalkane dehalogenase (*dhaA*) [151], (chloro)biphenyl-degrading (*bph*)genes [152], as well as *dhlA*, the gene involved in 1,2-dichloroethane in *Xanthobacter* and *Ancylobacter aquaticus*, [146, 153] were all found to be highly conserved to the level of identical copies of the same gene found amongst different bacteria isolated from diverse geographical locations.

In addition to *xplA* and *xplB*, there are several neighbouring genes which are nearly identical between bacteria from four different genera. This fact is surprising, considering that *xplA* alone is sufficient for the catabolism of RDX [98, 105].

Considering that *xplA* is located on a plasmid, rather than within the chromosomal genome in both *R. rhodochrous* 11Y, *Microbacterium* sp. MA1 [103] and *Gordonia* sp. KTR9 [105], that there are transposable elements in neighbouring regions (Figure 4.18), it is possible that the *xplA* and *xplB* genes are part of a larger mobile element such as an Integrative and Conjugative Element (ICE) or genomic island in the conjugative plasmid. Similarly, the genes for the degradation of xenobiotics such as chlorobenzene by *Pseudomonas* sp. strain B13 [35, 36] and biphenyl degradation by *Ralstonia eutropha* A5 are also found part of the on the larger mobile element [152]. ICEs are

known to excise and integrate into the genome through conjugation [1, 31], and sequence analysis of the *R. rhodochrous* 11Y genome has shown that there is a gene encoding an phage related intergrase (Gene locus: 11Y.057) belonging to the tyrosine recombinase family, which shares 100 % sequence identity with a site-specific recombinase in *R. erythropolis* PR4. Moreover, the RDX-degradation capacity of *Gordonia* sp. KTR9 was successfully transferred into *Gordonia polyisoprenivorans*, *Rhodococcus jostii* RHA1 and *Nocardia* sp. TW2 through conjugation[104], demonstrating that this is a possible transfer mechanism.

The genomic island in *R. rhodochrous* 11Y is 36,032 bp in length and encodes 42 ORFs, starting from 11Y.002 to 11Y.043 (Figure 4.18). The first transposable element (gene locus= 11Y.043) is likely to be the end of the genomic island as the 15 kb downstream of this gene is nearly identical (> 99 %) to the plasmid1 (pREL1) from the alkane-degrading *R. erythropolis* PR4. Interestingly, pREL1 has been shown to share sequence homology with the downstream region of the pathogenicity island in the plasmid pRFWT701 of *R. equi* [130].

In *Gordonia* sp. KTR9, several genes within RDX-degrading genomic islands are missing or rearranged on the plasmid carrying *xplA* and *xplB*, which suggest that the genes have been acquired by horizontal gene transfer through recombination events. Interestingly, the sequence analysis of plasmid (pGKT2) in *Gordonia* sp. KTR9 suggests that *xplA* and *xplB* are integrated into an operon involved in the degradation of N-heterocyclic alkaline, as the genes upstream of *xplB/xplA* (*xplR*, *cyp151C* and *glnA*) share high sequence similarity and arrangement to the *mor* and *pipe* gene clusters involved in the degradation of morpholine, piperidine and related compounds in mycobacterium and rhodococci [105]. The lack of several genes within the *xplA* and *xplB* containing genomic island in *Gordonia* sp. KTR9 that are present in *R. rhodochrous* 11Y and *Microbacterium* sp. MA1, indicates that the encoded gene products are not required for RDX degradation. This is referred to as the common evolutionary prospect “use it or lose it”, in which microorganisms lose the gene(s) which are not essential for catabolic activity [21]. The deletion of *aroP* and *marR*, the two genes upstream of the *xplA* and *xplB* gene in *R. rhodochrous* 11Y, previously thought to be involved in RDX degradation [144], did not affect RDX degradation in the bacterium. The large reduction of the plasmid from the pathogenic *Shigella* spp. and enteroinvasive *Escherichia coli*, which was acquired from the ancestral commensal *E.*

coli, was reported to enhance virulence in both bacteria [22]. However, there is no direct evidence of the advantage of the genome reduction of *Gordonia* sp. KTR9.

Chapter 5: Expression, Purification and Characterisation of the XplB- Glutamine Synthetase Fusion Protein

5.1 Introduction

The partnering reductase XplB is an NADPH-dependent flavodoxin protein which contains one mole of FAD as a cofactor and shares sequence homology with the bovine adrenodoxin reductase partner to the mitochondrial P450 (GenBank: P08165.3)[96]. XplB is involved in the activation of the catalytic centre of XplA via the transfer of an electron from NADPH to a flavodoxin domain fused to the N-terminal of the P450 domain of XplA [95].

The role of XplB in RDX degradation has been shown in both *R. rhodochrous* 11Y and a transgenic plant line expressing the *xplA/B* genes. Knock-out experiments on the *xplA*, *xplB*, *aroP* and *marR* genes in *R. rhodochrous* 11Y revealed that *xplB* is directly involved in the RDX-degradation and knock-out of the gene in *R. rhodochrous* 11Y reduced the RDX-degradation capacity by ~70 % compare to wild-type [144] (Figure 5.1).

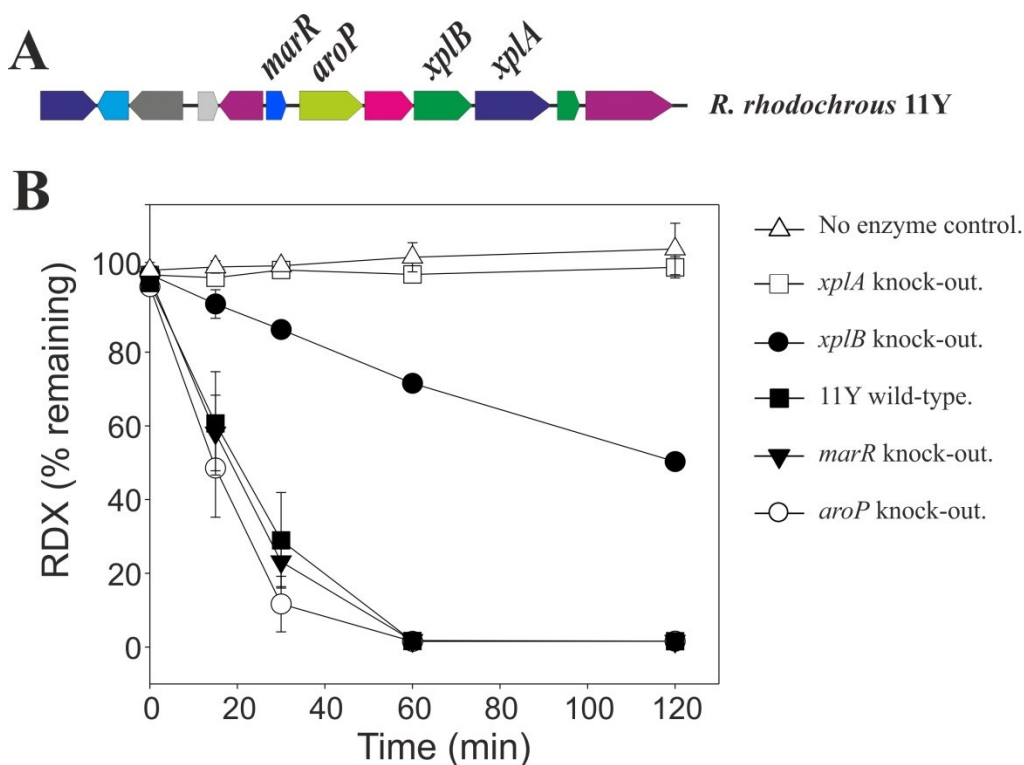


Figure 5.52: RDX removal by *R. rhodochrous* 11Y wild type and knock-out strains during the resting cell assays. (A) The 13.8 kbp region in the vicinity of *xplA* in the bacterium. (B) The RDX-removal capacity by each *xplA*, *xplB*, *aroP* and *marR* knock-out strains in *R. rhodochrous* 11Y in comparison to the wild-type. Reproduced from Chong *et al.* (2014) [144].

Similarly, plants expressing *xplA* and *xplB* genes removed RDX significantly faster than transgenic plants expressing *xplA* alone [95].

In *Gordonia* sp. KTR9, the gene encoding XplB is naturally fused with a glutamine synthetase encoded by the *glnA* [105], an arrangement which has not yet been found in other RDX degrading bacteria (Chapter 4). A transcriptomic study of *Gordonia* sp. KTR9 revealed that the *xplB-glnA* fusion is part of an operon along with two surrounding genes: *xplA* downstream and *cyp151C* upstream. Furthermore, the transcription start site for these three genes is located 12 nucleotides upstream from the *cyp151C* gene (Figure 5.2) [29].



Figure 5.53: The *xplA* gene cluster arrangement in *Gordonia* sp. KTR9. The arrow represents the transcription start site, which is located 12 nucleotides upstream of *cyp151C*. Reproduced from Chen *et al.* (2012) [154].

Glutamine synthetase (GS; EC 6.3.1.2) is an essential enzyme in nitrogen metabolism, catalysing the ATP-dependant production of glutamine from glutamate and ammonia.

There are three different classes of GSs: GSI, GSII and GSIII [155-157]. The GSIs are dodecamer enzymes, made up of 12 identical subunits, and are mainly found in bacteria and archaea. The GSIIs are decamer enzymes, comprising of two pentamer subunits and are located in eukaryotic and soil-borne bacteria. The GSIIIs, like the GSI class, are also dodecamer enzymes and are found in a few anaerobic and cyanobacteria [155, 156].

The GSI enzymes are further subdivided into two subclasses, GSI- α and GSI- β . In the GSI- α class, the activity of the enzymes is regulated by glutamine feedback inhibition, while GSI- β activity is regulated by adenylation of a tyrosine residue located in the active site of the protein. The GSI- β enzymes also differ from GSI- α enzymes by having a short insertion of an amino acid sequence which is not found in GSI- α [155-158].

In addition to glutamine production, the GSI- α enzyme in *Bacillus subtilis* is known for its important role in regulating nitrogen metabolism in the cell by controlling the expression of GlnR and TnrA [158, 159]. Mutation of the *B. subtilis* GSI- α enzyme

resulted in constitutive expression of both nitrogen regulatory genes *glnR* and *tnrA* [160]

This chapter will focus on characterisation of the naturally fused XplB-GS protein in *Gordonia* sp. KTR9. The functionality of the XplB part of XplB-GS was compared with XplB from *R. rhodochrous* 11Y. Additionally, the GS component part of XplB-GS was characterised, and the potential role of the protein within the cell was investigated.

5.2 Materials and Methods

5.2.1 Cloning *xplB-glnA*

The *xplB-glnA* gene was cloned into the pET-28(a)+ vector at the *EcoRI* and *XhoI* restriction sites to allow for expression of a N-terminally His-tagged protein. As expression was low and there was not enough soluble protein, the gene was subsequently cloned into pGEX2T, at the *BamHI* and *EcoRI* sites, in order to express the gene as an N-terminally GST-tagged protein.

The primers used to amplify the full-length gene, with complementary overhang sequences to each plasmid, were designed based on In-Fusion HD cloning software (Clontech Laboratories) (Chapter 2, Table 2.1). The *xplB-glnA* gene was amplified from the *Gordonia* sp. KTR9 genome using PCR (Chapter 2.6.3).

Cloning was performed as described in Chapter 2.6.12 using 20 ng of PCR product with 100 ng of linearized vector. An aliquot of the reaction (2 μ l) was used to transform *E. coli* DH5 α competent cells (Chapter 2.2.9). Transformed cells were then plated on LA plates containing 100 μ g/ml of kanamycin and 100 μ g/ml carbenicillin for pET-28(+a) and pGEX2T vectors, respectively.

The successful cloning was confirmed by performing colony PCR (Chapter 2.6.3) using plasmid specific primers and GoTaq polymerase (Chapter 2, Table 1). Plasmids from a few positive colonies were extracted and sent for sequencing (Chapter 2.6.6).

5.2.2 Expression of *xplB-glnA*

The *xplB-glnA* gene was initially expressed as an N-terminally His-tagged protein by using pET-28(a)+. The expression trials were performed using *E. coli* BL-21 (DE3) and

E. coli Rossetta 2 (DE3) cells. The cells were grown to OD₆₀₀ ~0.6-0.8 at 37 °C and then the gene expression was induced with 1 mM IPTG at 20 °C with shaking. An aliquot (50 ml) was collected from the culture in a 50 ml falcon tube before induction as well as 1, 3 and 18 hours after induction. The aliquots were spun down, pellets were snap frozen and kept at -80 °C for subsequent analysis on SDS-PAGE.

The *xplB-glnA* gene was also expressed as N-terminally GST-tagged protein using pGEX2T vector. The expression of pGEX2T-*xplB-glnA* was carried out in *E. coli* BL-21(DE3) and *E. coli* ArticExpress cells. The cells were grown at 37 °C to OD₆₀₀ ~0.6 and then the *xplB-glnA* expression was induced using varying concentrations of IPTG (0.1, 0.25 and 1 mM IPTG). The cells were kept shaking at 15 °C for 14 hours. Cultures were harvested prior to and 14 hours post-induction. Expression levels were compared on SDS-PAGE with an empty vector, pGEX2T, as a control.

After several trials, maximal expression of *glnA-xplB* was achieved by expressing the gene in *E. coli* BL-21(DE3), induction was most efficient with 0.5 mM IPTG supplemented with 50 µg/ml riboflavin at 20 °C for 14 hours.

5.2.3 Reductase assay for XplB and XplB-GS

Purified XplB-GS was tested for reductase activity with purified XplA protein. Commercial spinach ferredoxin reductase (0.1 Unit) (Sigma-Aldrich), which has been reported to work as a reductase partner to XplA [95], was used as a positive control. The reaction mixture was in 1 ml of 50 mM potassium phosphate buffer (pH 6.8), contained 300 µM NADPH, purified XplA and XplB or spinach ferredoxin reductase. The reaction was initiated by the addition of 100 µM of RDX at room temperature and stopped intermittently with 10 % TCA. RDX removal was monitored by HPLC and nitrite release, from degraded RDX by XplA, was measured by Griess assay (Chapter 2.8.2). The amount of reductase and XplA used in each experiment is mentioned in each corresponding results section.

5.2.4 Determination of the amount of FAD in XplB

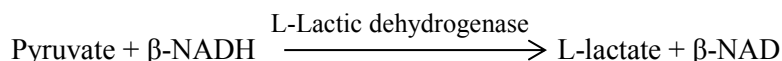
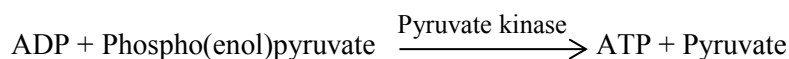
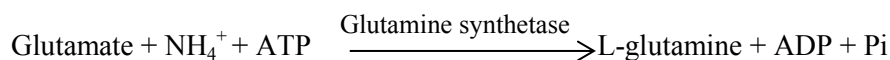
The amount of FAD cofactor bound to XplB and XplB-GS proteins was measured following the method described by Aliverti *et al.* (1999) [161]. The protein was boiled at 100 °C, in the dark, for 20 minutes and the precipitated protein removed by

centrifugation at 13,000 rpm for 10 minutes. FAD in the supernatant was analysed by spectrophotometry and HPLC, using commercially available FAD as a reference. For the spectrophotometric analysis, the UV-visible spectrum of the protein was recorded (200 to 600 nm) in 1 ml UV cuvettes.

5.2.5 Activity assay for glutamine synthetase

The activity of XplB-GS was measured based on the protocol described by Kingdon HS *et al.* [162] as cited by Sigma-Aldrich.

A 3 ml reaction mixture contained the following components: 34.1 mM imidazole, 8.5 mM ATP, 1.1 mM phosphoenolpyruvate, 60 mM MgCl₂, 18.9 mM KCl, 45 mM NH₄Cl, 0.25 mM NADH, 28 units pyruvate kinase, and 40 units L-lactic dehydrogenase and 0.6 unit of *E. coli* glutamine synthetase K12 (as a positive control), or 1 ml of purified XplB-GS. The components were mixed by inversion of the cuvette and the A₃₄₀ was monitored until constant at 37 °C. The reaction was initiated upon the addition of the substrate sodium glutamate (102 mM). The activity of glutamine synthetase was calculated based on the oxidation rate of β-NADH to β-NAD on the spectrometer at A₃₄₀ during the conversion of L-glutamate to L-glutamine. The principle of the assay is shown below (Reproduced from Sigma-Aldrich Company https://www.sigmaaldrich.com/content/dam/sigma-aldrich/docs/Sigma/Enzyme_Assay/glutaminesynthetase.pdf).



5.3 Results

5.3.1 Cloning and expression of *xplB-glnA*

xplB-glnA was initially cloned, using an In-Fusion® HD cloning system, into pET-28(a)+ to be expressed as a N-terminal His-tagged protein (Figure 5.3).

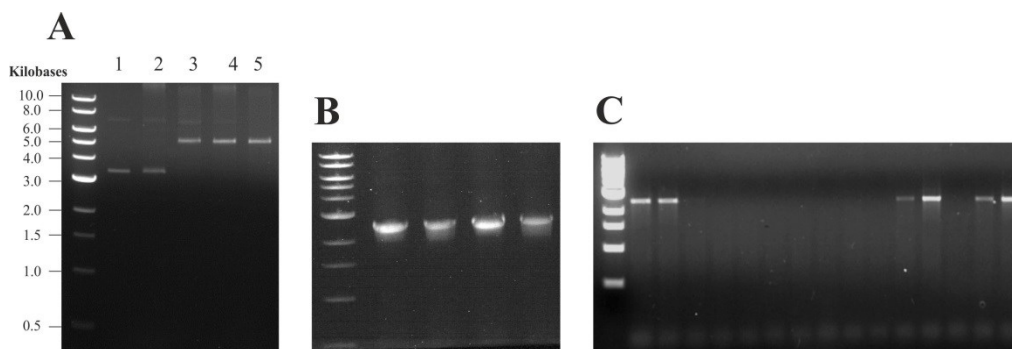


Figure 5.54: Cloning of *xplB-glnA* into pET-28(a)+ vector. (A) pET-28(a)+ digestion: 1 and 2 are undigested plasmid; 3 and 4 are single digested plasmid with *EcoRI* and *XhoI*, respectively; 5 is the double digested plasmid with both restriction enzymes. (B) Amplification of the *xplB-glnA* gene by PCR, product size = ~2.5 kbp. (C) Colony PCR of the different transformed colonies.

During preliminary expression trials using *E. coli* BL-21 and *E. coli* Rossetta 2 (DE3), soluble XplB-GS was not detected and even as early as three hours after induction, significant amounts of the protein were detected in the insoluble fraction (Figure 5.4).

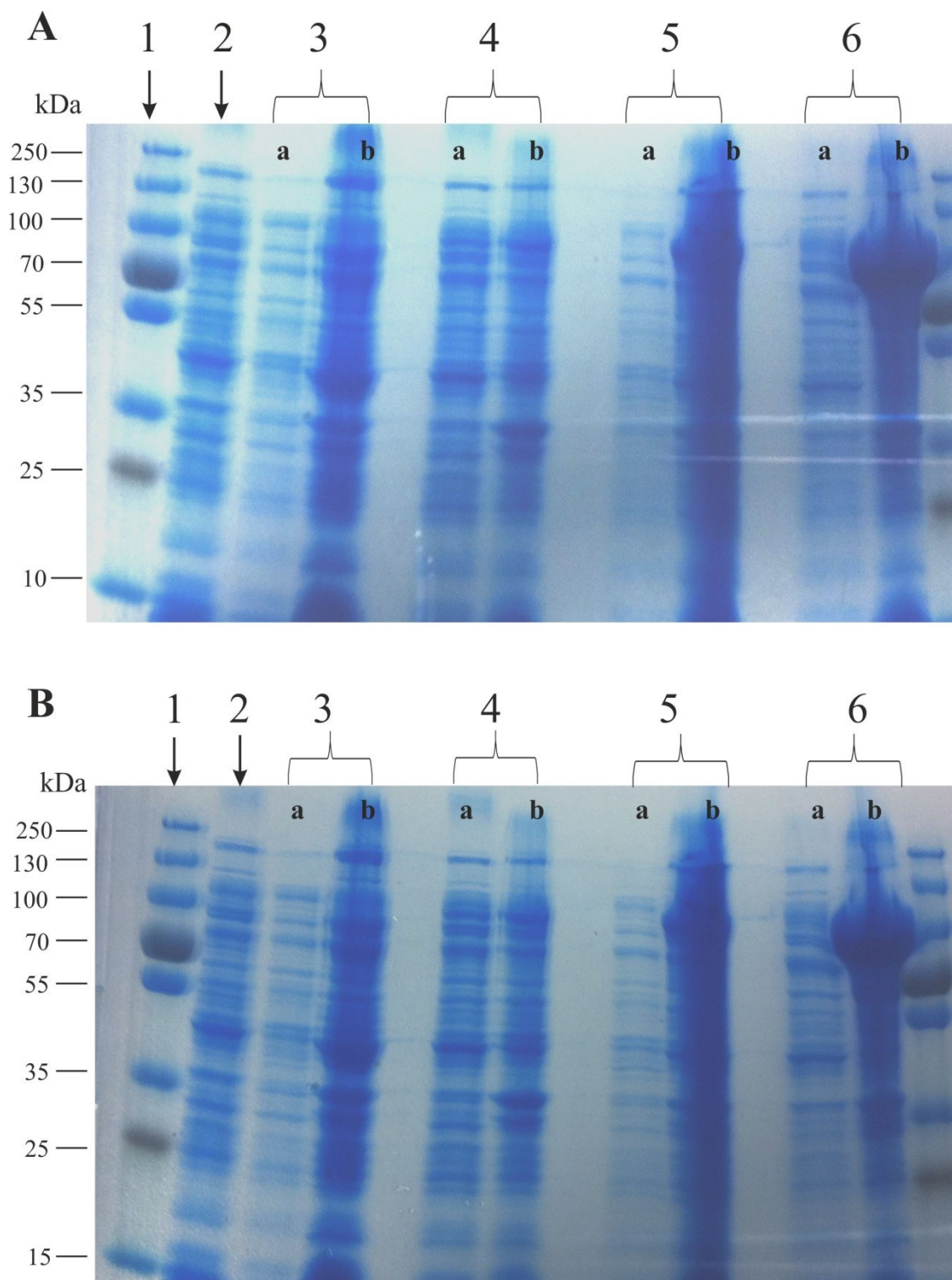


Figure 5.55: Expression trials of *xplB-glnA* as N-terminally His-tagged protein. (A) and (B) are 12 % (w/v) SDS-PAGE gels of *E. coli* BL-21 (DE3) and *E. coli* Rossetta 2 (DE3) expressing XplB-GS, respectively. In both A and B panels, the gels show from left to right; molecular markers (1); lysate from cells containing the empty vector (2), *E. coli* cell lysate before induction (3), and the *E. coli* cells induced after one hour (4), three hours (5) and 18 hours (6). The letter (a) refers to the soluble fraction of the cell lysate, (b) to the insoluble fraction. Expected protein size ~92 kDa.

From the results of the SDS-PAGE presented in Figure 5.5, it appeared that only low levels of soluble XplB-GS were achieved with pET-28a-*xplB-glnA* in *E. coli* BL-21 (DE3) using 0.1 mM IPTG at 20 °C shaking for 18 hour. However, soluble protein was just detectable by western blot analysis using anti-XplB polyclonal antibody.

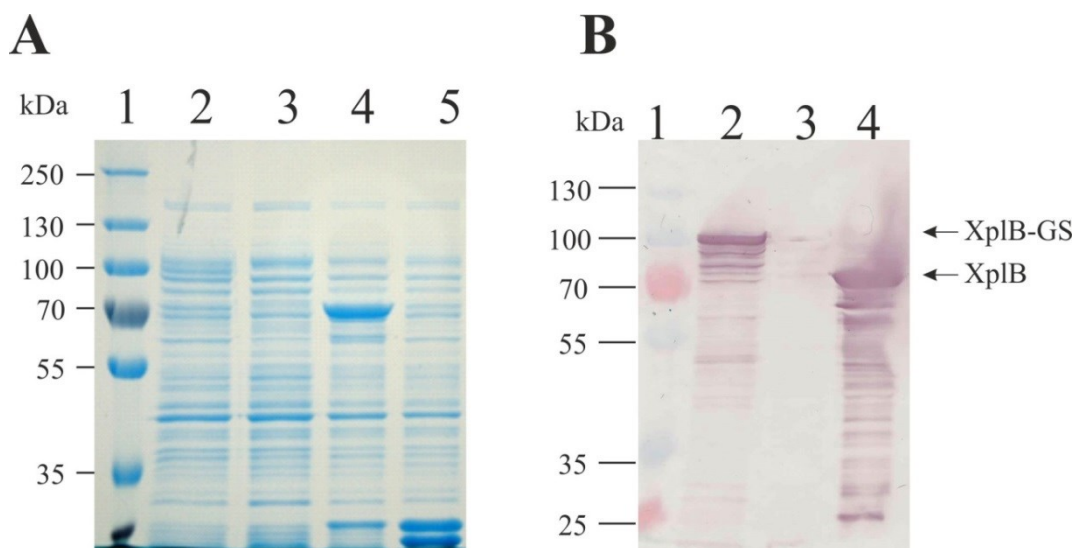


Figure 5.56: SDS-PAGE (A) and western blot (B) analysis for the expression trials of *xplB-glnA* as N-terminally His-tagged protein in *E. coli* BL-21 (DE3). In both A and B, (1) is protein markers; (2), (3), (4) and (5) refer to the *E. coli* cell lysate expressing pET-28a-*xplB-glnA*, pET-28a, pGEX2T-*xplB*, and pGEX2T, respectively. Molecular weight of XpB-GS is 92 kDa and XplB is 72 kDa.

XplB from *R. rhodochrous* 11Y was also reported to be insoluble and the characterisation of the protein was carried out by recombinantly expressing the protein fused with a 26 kDa GST-tag using pGEX2T vector [95]. As the pET-28a system failed to yield soluble protein, it was decided to clone the *xplB-glnA* sequence into pGEX2T (Figure 5.6).

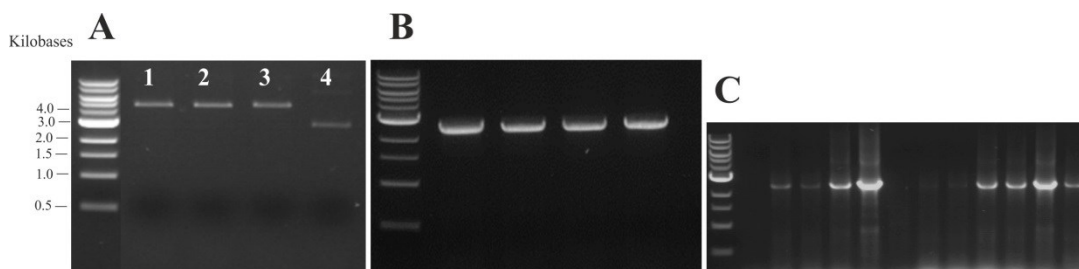


Figure 5.57: Cloning of *xplB-glnA* into pGEX2T vector. (A) The pGEX2T digestion vector at *Bam*HI and *Eco*RI restriction sites; (1) is the double digested plasmid with both restriction enzymes; (2) and (3) are single digestion of the plasmid with *Bam*HI and *Eco*RI, respectively; (4) is the undigested plasmid control. (B) 1 % (w/v) agarose gel of the PCR product of the insert (*xplB-glnA*) gene (four replicates), product size= ~2.5 kb. (C) 1 % (w/v) agarose gel of the colony PCR for several transformed *E. coli* cells.

The expression trials of the pGEX2T-*xplB-glnA* construct were conducted using *E. coli* ArticExpress and BL-21 expression strains. The expression of *xplB-glnA* was induced with 0.1, 0.25 and 0.25 mM of IPTG, at 15 °C for 14 hours. The amount of the soluble protein achieved with the N-terminally GST-tagged protein was significantly higher when compared to the N-terminally His-tagged XplB-GS (Figure 5.7).

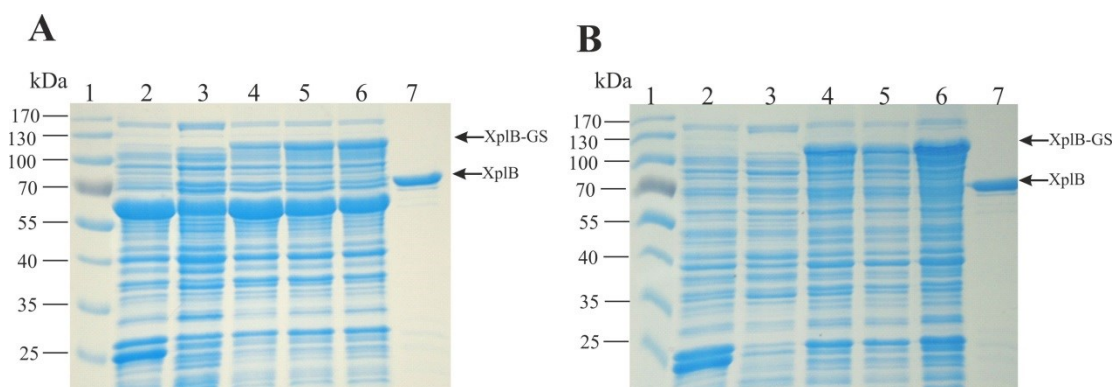


Figure 5.58: SDS-PAGE analysis for the expression trials of GST-tagged *xplB-glnA* in *E. coli* ArticExpress (A) and *E. coli* BL-21(DE3) (B). In (A) and (B), the gels show from left to right, molecular markers (1), lysate of the *E. coli* strain expressing an empty vector (2), lysate of the *E. coli* strain expressing *xplB-glnA* before induction (3), and the cells lysate induced with 0.1 mM IPTG (4), 0.25 mM IPTG (5) and 0.5 mM IPTG (6) after 14 hours, and purified XplB (7); expected protein size ~114 kDa.

The production of over-expressed XplB-GS in *E. coli* BL-21 was subsequently scaled up into 6 x 500 ml culture in 2L flasks and purified using glutathione sepharose 4B batch purification as described Jackson *et al.* (2007) (Figure 5.8) [95].

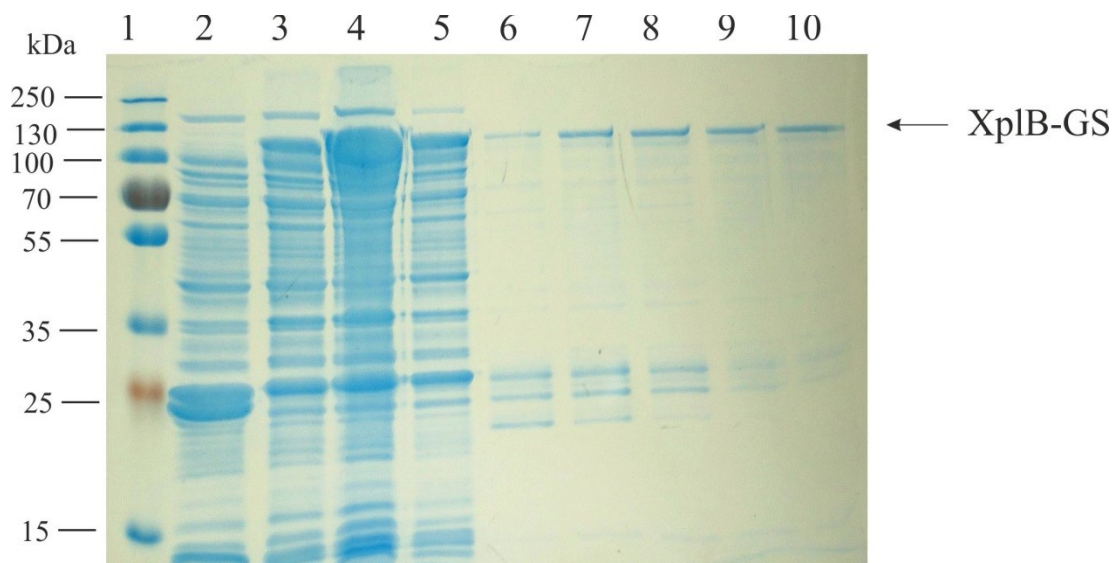


Figure 5.59: SDS-PAGE analysis for the purification of GST-tagged XplB-GS using glutathione sepharose 4B batch purification. From left to right; molecular markers (1), lysate of the *E. coli* expressing an empty vector (2), lysate of the *E. coli* expressing *xplB-glnA* gene (3), flow-through (4), washed proteins (5), and eluted protein (6-10). Size of the protein is ~114 kDa.

The identity of purified XplB-GS was confirmed by western analysis using XplB polyclonal antibody (Figure 5.9) and MALDI-MS analysis.

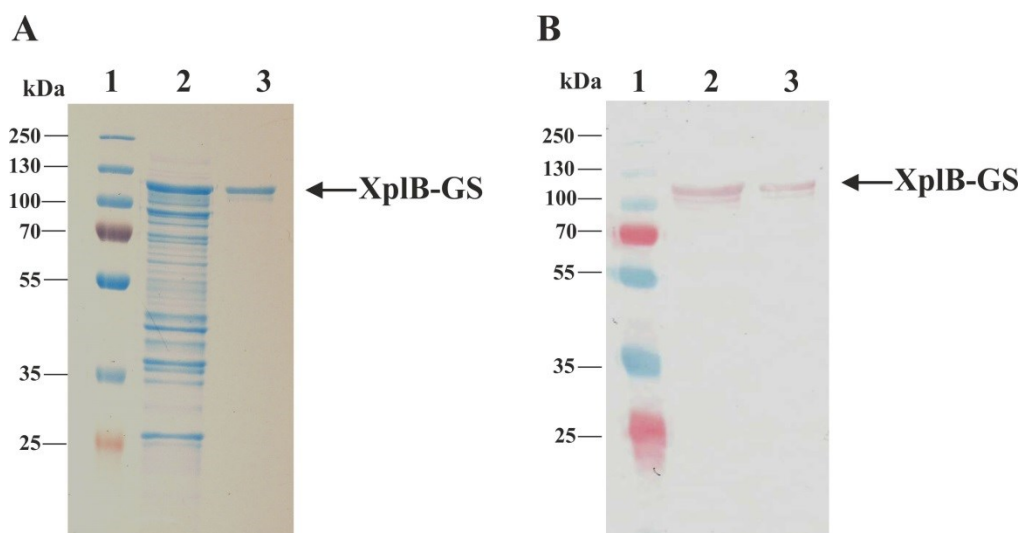


Figure 5.60: SDS-PAGE (A) and western analysis (B) of purified GST-tagged XplB-GS. In both (A) and (B), (1) refers to the protein marker, (2) is the *E. coli* lysate expressing *xplB-glnA*, and (3) is the purified XplB-GS. Expected size of the protein ~114 kDa.

It was noticed when performing SDS-PAGE and western blots analysis (Figure 5.9), that there was a band below that of purified XplB-GS suggesting that some protein was degraded after purification.

5.3.2 Characterisation of XplB-GS

Prior to testing the reductase activity of XplB-GS, XplB and XplA from *R. rhodochrous* 11Y were purified as described in Chapter 2.7.3 (Figure 5.10).

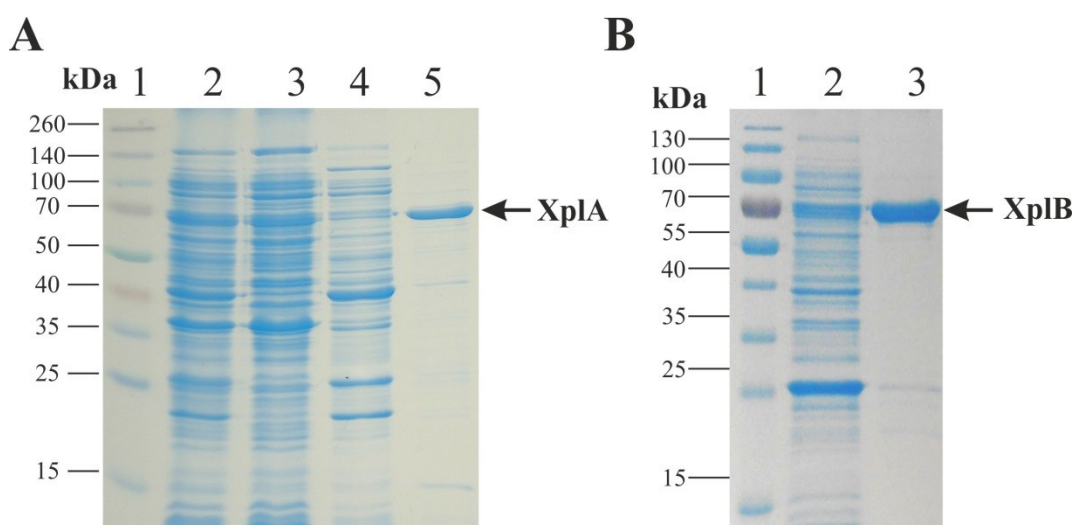


Figure 5.61: SDS-PAGE analysis of XplA (A) and XplB (B) from *R. rhodochrous* 11Y. (A) SDS-PAGE analysis for *E. coli* Rossetta 2 (DE3) expression of *xplA* as N-terminally His-tagged protein in pET-16b, the gel shows from left to right, protein markers (1), lysate (2), flow-through (3), washed proteins (4), purified XplA (5); expected XplA size= 66 kDa. (B) SDS-PAGE analysis for the *E. coli* BI-21 (DE3) expression of *xplB* as N-terminally GST-tagged protein in pGEX2T, the gel shows from left to right, protein markers (1), *E. coli* lysate (2), purified XplB (3); expected XplB size= 72 kDa.

The activity of the purified proteins was assessed before conducting the reductase assay for XplB-GS. XplA (0.08 mg) was assayed for RDX degrading activity using commercial spinach ferredoxin reductase (Sigma-Aldrich). The XplA was found active, as reported by Rylott *et al.* (2006) [98], and nitrite released from the RDX degradation was detected and measured by Griess assay (Chapter 2.8.2). No RDX was observed in the absence of XplA or reductase (Data not shown).

Purified XplB (0.22 mg) was also assayed for reductase activity with XplA. XplB from *R. rhodococcus* 11Y was also found to be active as described by Jackson *et al.* (2007) [95].

When XplB was replaced with XplB-GS in the reaction mixture, there was no nitrite released after 3 hours incubation. Further analysis, using HPLC confirmed that RDX had not been depleted (Data not shown).

During purification of recombinant XplB-GS from *E. coli*, it was noticed that the total lysate was colourless, while the lysate of *E. coli* expressing *xplB* was yellow (Figure 5.11A). This was also observed for the purified proteins; XplB was a yellow colour, whereas XplB-GS colourless.

It has been reported that FAD is only loosely bound in XplB [95], as XplB-GS was colourless, it appeared likely that no FAD was bound to the purified protein. The amount of FAD in 3.5 μ M of XplB and XplB fused GS was measured using both HPLC and spectrophotometric methods. No FAD was not detected in XplB-GS, while nearly 25 % FAD was found in XplB (Figure 5.11B).

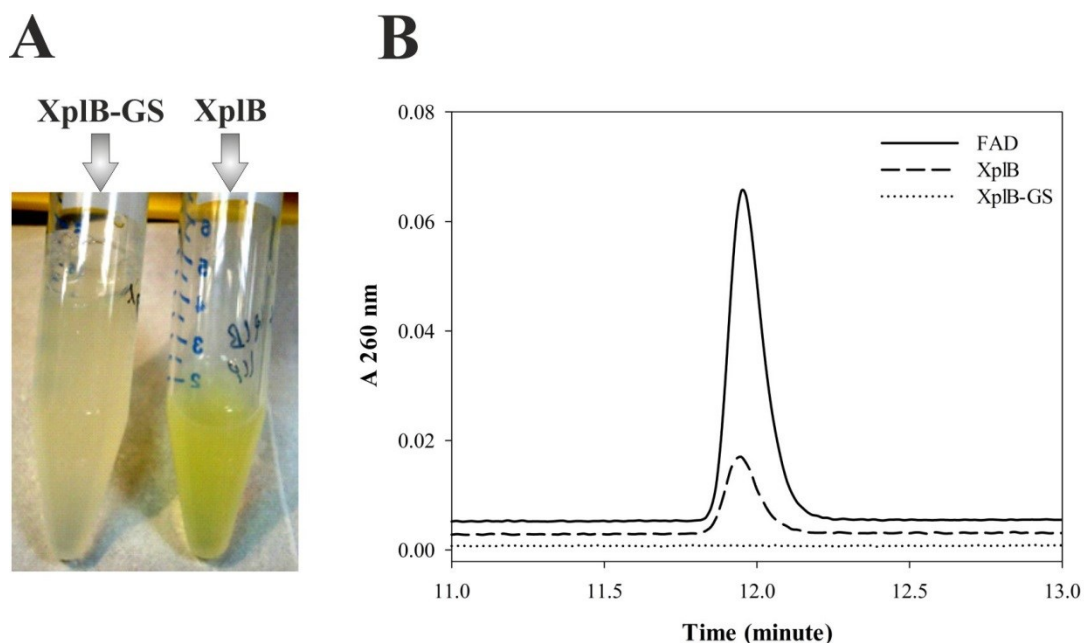


Figure 5.62: (A) *E. coli* BL21 (DE3) lysate expressing XplB-GS (right) and XplB (left). (B) Overlaid chromatograms of FAD peaks from purified XplB and XplB-GS by HPLC with commercial FAD as a reference.

In order to investigate whether the encoded XplB portion of the XplB-GS fusion was inactive or had lost activity during protein purification, the lysate from cultures of *E. coli* BL-21 cells expressing pGEX2T-*xplB-glnA* were tested with XplA for RDX-degrading activity.

Equal amounts of cell lysate (3.7 mg) expressing pGEX2T, pGEX2T-*xplB-glnA* and pGEX2T-*xplB* were used instead of purified protein as a reductase in assays containing purified 1.25 mg of XplA. The reaction was initiated by the addition of 100 μ M RDX, and stopped after 10, 60 and 120 minutes. The expression of the *glnA-xplB* and *xplB* in the lysates was also confirmed by SDS-PAGE (Figure 5.12).

Figure 5.14 shows that when lysate from cells expressing pGEX2T-*xplB* was used as the reductase, all the RDX was removed within 10 minutes. However, when the lysate from cells expressing pGEX2T-*xplB-glnA* was used, although reductase activity was detected, this was much lower than activity in lysate from cells expressing just the empty vector (pGEX2T) (Figure 5.13). Thus, this data is confirming that XplB fused with GS is inactive as a reductase partner to XplA.

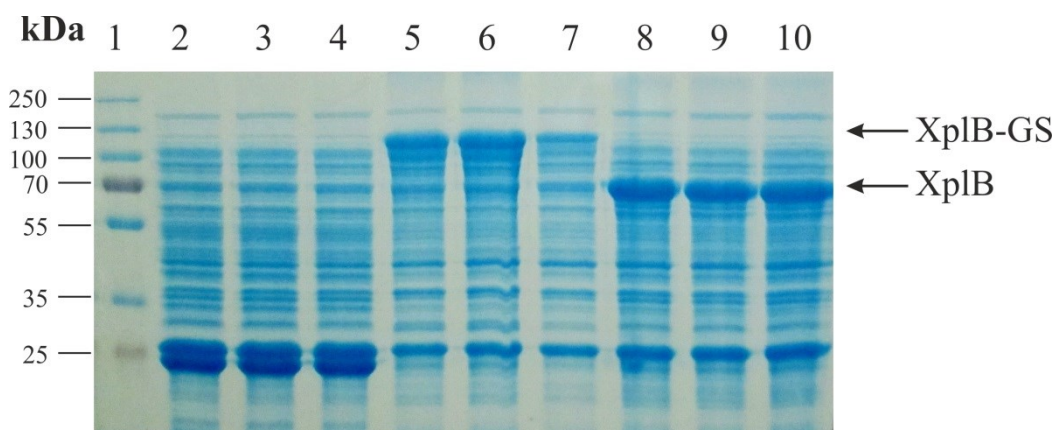


Figure 5.63: SDS-PAGE for the *E. coli* BL-21(DE3) cell lysate expressing pGEX2T, pGEX2T-*xplB-glnA* and pGEX2T-*xplB*. The gel shows from left to right, protein markers (1), the lysate of the cells expressing an empty vector (2-4), XplB-GS (5-7), and XplB (8-10).

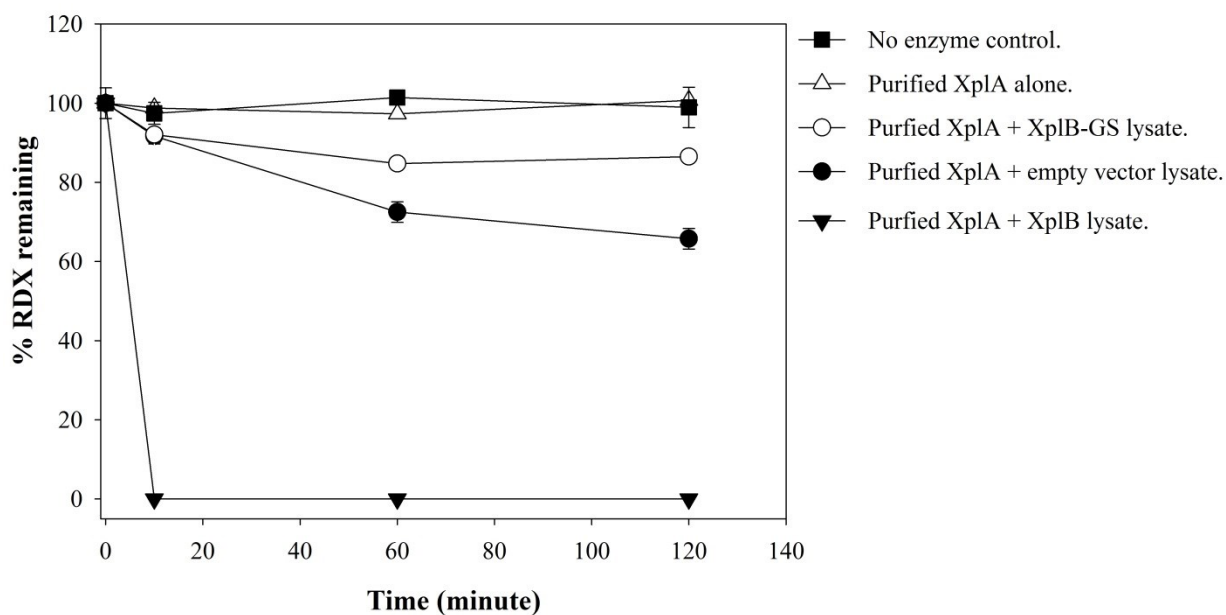


Figure 5.64: RDX removal by XplA with XplB and XplB-GS. The assays all contained 50 mM potassium phosphate buffer, pH 6.8, 300 μ M NADPH. Data shown are mean of three biological replicates \pm SD.

The sequence alignments of the XplB portion of the XplB-GS were shown > 99% sequence identity with full length XplB from *R. rhodochrous* 11Y (Figure 5.14). There are just two amino acids differences: first is the Met-1 which is missing in XplB-GS as a result of the fusion to GS. Second is Ser-385 in the XplB of *Gordonia* sp. KTR9 which is Trp-386 in XplB from *R. rhodochrous* 11Y. The Ser/Trp-386 was found to be the result of a single base difference, TCG encoding tryptophan and TGG encoding serine.

```

Xp1B_KTR9      -DIMSEVDVAPRVAVVGAGPSGCFTAQQLRKQWPEVEVTVFDRLLPTPFGLRLRYGVAPDHQ 59
Xp1B_11Y      MDIMSEVDVAPRVAVVGAGPSGCFTAQQLRKQWPEVEVTVFDRLLPTPFGLRLRYGVAPDHQ 60
                *****

Xp1B_KTR9      GTKNVIRQLSRVFDDRTRFVGNIELGRNLSIEDLRAAFDVVVLATGLSGDRRLGIPGDDL 119
Xp1B_11Y      GTKNVIRQLSRVFDDRTRFVGNIELGRNLSIEDLRAAFDVVVLATGLSGDRRLGIPGDDL 120
                *****

Xp1B_KTR9      PGIVGSGRFTRCVNDHFAAGDLPTVGRVVLVGGGNVAMDIIIRLLSKQPDEFTGSDLHPD 179
Xp1B_11Y      PGIVGSGRFTRCVNDHFAAGDLPTVGRVVLVGGGNVAMDIIIRLLSKQPDEFTGSDLHPD 180
                *****

Xp1B_KTR9      TLGRLRSEGPRRIDVVVRSTPTDAKFDPMRELAHLASTEFLADAGVLATAESSDPRS 239
Xp1B_11Y      TLGRLRSEGPRRIDVVVRSTPTDAKFDPMRELAHLASTEFLADAGVLATAESSDPRS 240
                *****

Xp1B_KTR9      AALAHVVERESPAAPATTVVFHFGSTPVEVIGTDRAEAVKVRTGVHTTTLACDVTITAIG 299
Xp1B_11Y      AALAHVVERESPAAPATTVVFHFGSTPVEVIGTDRAEAVKVRTGVHTTTLACDVTITAIG 300
                *****

Xp1B_KTR9      FESAVNDDLDLTLYRDADPGEDFLAPGLYRTGWLHSSTGALPEMRARARALAARIRRDHA 359
Xp1B_11Y      FESAVNDDLDLTLYRDADPGEDFLAPGLYRTGWLHSSTGALPEMRARARALAARIRRDHA 360
                *****

Xp1B_KTR9      GHHPARPGLVAIPYEVIDRTVDFDGSMRIDEAEVASASPGRIRQKVREVDAMLALARTVP 419
Xp1B_11Y      GHHPARPGLVAIPYEVIDRTVDFDGSMRIDEAEVASASPGRIRQKVREVDAMLALARTVP 420
                *****

Xp1B_KTR9      AESVC 424
Xp1B_11Y      AESVC 425
                *****

```

Figure 5.65: Sequence alignment of the XplB region of the XplB-GS fusion protein from *Gordonia* sp. KTR9 (XplB-KTR9) and XplB from *R. rhodochrous* 11Y (XplB_11Y). The residue Ser-385 and Trp-386 are highlighted with yellow and are red in colour.

Trp-386 was thought to be important for the functionality of XplB protein as the multiple sequence alignment was revealed that the residue is highly conserved amongst several FAD-containing proteins in database which share as low as 26 % sequence identity to XplB. The sequence alignment of the proteins, their sequence identity to XplB-GS and the accession number of each protein is shown in Table 5.1. Additionally, the phylogenetic trees of the FAD-containing proteins, which were used in the Table 5.1, are shown in Figure 5.15.

Table 5.5: Shows the conserved tryptophan residue, corresponding to ser-385 in XplB-GS, amongst several FAD containing proteins in database using ClustalW2 website at the EMBL European Bioinformatics Institute (<http://www.ebi.ac.uk/>). Name of the organisms are written in the left hand side, ID is the sequence identity of the protein to XplB-GS. UniProt AC is the accession number of the protein in UniProt database. The conserved Trp residues are highlighted in yellow; Ser-385 in *Gordonia* sp. KTR9 is also red in colour.

| Organism | ID | UniProt AC | Sequence (N-terminal to C-terminal) |
|--|------|------------|---|
| <i>Sphingomonas</i> sp. Lh128 | 34% | J8SFQ3 | WQKIDAEVAA-ARDGAPREKFVELEKMIATGRA----- 434 |
| <i>Sphingobium herbicidovorans</i> | 34% | A0A031KFT7 | WQKIDAEVAA-ARDGAPREKFVELEKMIATGRA----- 434 |
| <i>Novosphingobium pentaromativorans</i> | 33% | G6E792 | WQKIDAEVAN-ARDGSPREKFVAVEKMLAAASKP----- 436 |
| <i>Novosphingobium</i> sp. PP1Y | 33% | F6INK1 | WQKIDAEVAN-ARDGSPREKFVAVEKMLAAASKP----- 436 |
| <i>Sphingopyxis</i> sp. Me1 | 32% | N9WDZ9 | WRKIDAEVAA-ALEGNPREKFVVRVEAMIEAIGR----- 430 |
| <i>Caenispirillum salinarum</i> Ak4 | 32% | K9H0D3 | WKRIDAAEVAR-AAQGRPREKFVVRVEMLAALDG----- 450 |
| <i>Sulfuritalea hydrogenivorans</i> | 35% | W0SE92 | WQKIDAEVAA-AGQGRQREKLTRIGELLAAQDN----- 440 |
| Mine drainage metagenome | 33% | E6PE74 | WKRIDAAEVAR-AAQGRPREKFVVRVEMLAALDG----- 439 |
| <i>Selaginella moellendorffii</i> | 29% | D8TIF6 | WERLNTEMEKGAVKGKPREKIVGIDEALAIGLAKEKE----- 462 |
| <i>Arthrobacter aurescens</i> | 26% | A1RCG9 | WRIDQAEALGRQARRPRQKFI SVDQLLEASRAAN----- 531 |
| <i>Rhodococcus opacus</i> Pd630 | 26% | W8GTV2 | WQRIDKTERAGGKAAGRTRTKLITIE SMLAARADT----- 556 |
| <i>Corynebacterium glutamicum</i> | 30% | R9T2J9 | WHLDDAERALGEPGGRERKKIVVWDMVRHARPEYDI----- 455 |
| <i>Gordonia</i> sp. KTR9 | 100% | E1R0R9 | SMRIDAEVAA-ASPGRIRQKRVREVDAMLALARTVPAESVC----- 814 |
| <i>Rhodococcus rhodochrous</i> 11Y | 99% | Q8GPH8 | WMRIDAEVAA-ASPGRIRQKRVREVDAMLALARTVPAESVC----- 425 |
| <i>Pseudomonas resinovorans</i> | 45% | S6AWF9 | WKRIDAEELRS-APDGRVRRKVRNRSDMLSI AHENFPGVQQ----- 431 |
| <i>Nitratireductor pacificus</i> | 43% | K2MCG5 | WKRIDAAEIAA-APENRCRVKINSRDAMLALAFQEEECPR----- 425 |
| <i>Citrobacter braakii</i> | 36% | Q8VQF5 | WQRIDAEASR-TEHGRCRTKLPDIATMLDFARNRTHERTTDDTYRKQITDTVGHKEKR----- 451 |
| <i>Mycobacterium cosmeticum</i> | 32% | W9AIQ9 | WQRIDAEVAA-ARDGAPREKFVELEKMIATGRA----- 434 |

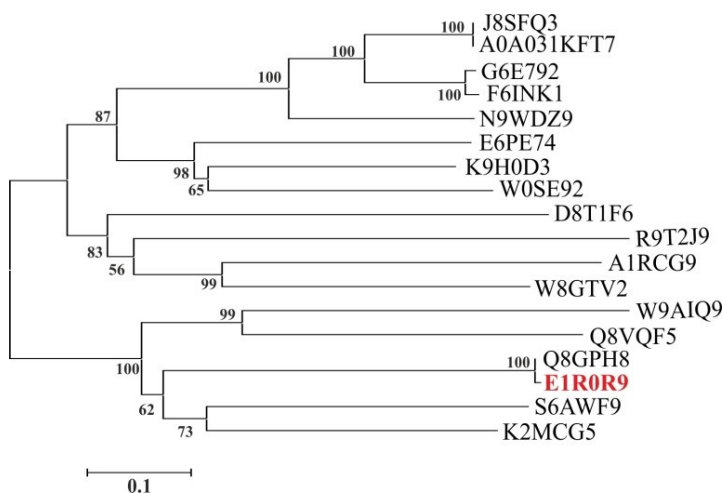


Figure 5.66: Unrooted phylogenetic tree between several FAD-containing proteins which has conserved Trp with XplB portion of XplB-GS using MEGA 6 tree building program and neighbour joining method, bootstrapped with 1000 replicates. The accession number of XplB-GS from *Gordonia* sp. KTR9 is red and bold. The organisms which have the FAD-protein were identified are in Table 5.1 above.

5.3.2.1 An investigation into the role of Trp-386 in the catalytic activity of XplB

To investigate whether Ser-385 is the reason for the lack of activity and reduced flavin binding in XplB-GS, the equivalent residue in XplB (Trp-386) was mutated to serine.

The XplB (W386S) mutant was created through a single mutation (C instead of G) as described in (Chapter 2.6.13), by using primers shown in (Chapter 2, Table 2.1).

The *xplB* and *xplB(w386s)* were expressed as described Jackson *et al.* (2007) (Chapter 2.7.3) [95]. On purification, it was observed that the lysate of the XplB(W386S) mutant was much paler in colour, whereas the wild type XplB expressing culture was yellowish (Figure 5.16A). Both proteins were purified and the level of FAD measured by HPLC analysis. FAD was found in XplB but not in the XplB(W386S) mutant (Figure 5.16B). Furthermore, when XplB and XplB(W386) were used as reductases for XplA, activity was only observed when XplB protein was supplied as the reductase; no RDX was removed in assays using XplB-W386 as reductase (Data not shown).

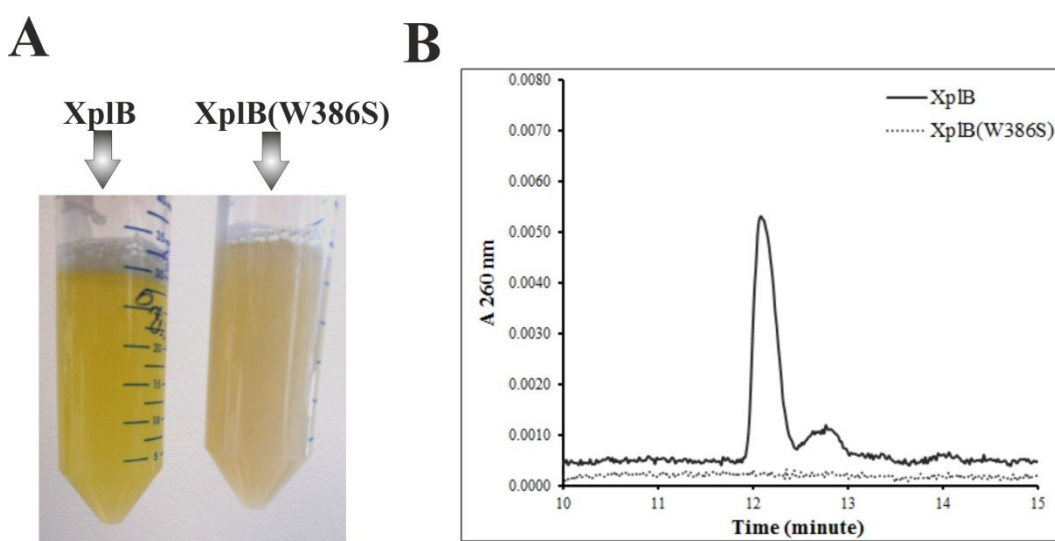


Figure 5.67: (A) Total lysate of *E. coli* BL-21 expressing XplB and XplB(W386S). (B) Overlaid chromatograms of FAD peaks from purified XplB and XplB(W386S) by HPLC.

As Trp-386 appears to play a crucial role in retaining FAD in XplB, homology modelling was used to predict the location of this residue in the structure of the protein.

Using automated homology modelling software (<http://swissmodel.expasy.org/>), the structure of XplB was created based on the template structure of NADPH: adrenodoxin oxidoreductase (AR) from the steroid hydroxylating system of adrenal cortex mitochondria of bovine (*Bos taurus*) (PDB: 1E6E subunit A) (Access date: 15/9/2014) [163]. This adrenodoxin oxidoreductase is the closest structure solved for protein that shares sequence identity (29.73 %) with XplB. The structure of XplB was superimposed onto the template structure (RMSD value: 0.767 Å) and visualized using the Chimera UCSF software [120]. Surprisingly, the Trp-385 was found not located on the FAD moiety of the protein, but instead on the last α -helix towards the C-terminus of XplB (Figure 5.17).

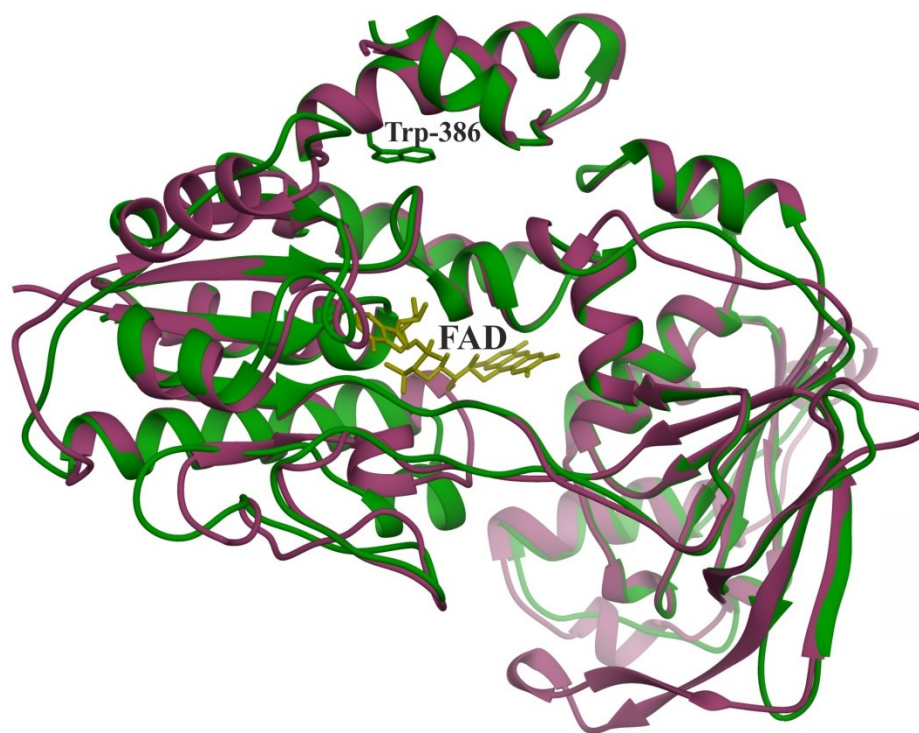


Figure 5.68: A model of the structure of XplB (green) superimposed on chain C of adrenodoxin oxidoreductase (pink). FAD is yellow. Predicted position of Trp386 is labelled in the XplB structure. Root mean square deviation (RMSD 0.767 Å).

To investigate the influence, and more specifically the FAD retaining capacity, Ser-385 in XplB-GS was mutated to Trp-385. XplB(S385W)-GS was expressed in *E.coli* B1-21. During the purification step, it was noticed that the cell lysate from the XplB(S385W)-GS mutant was yellow. However, following purification, as shown in Figure 5.18, the XplB(S385W)-GS mutant protein was colourless.

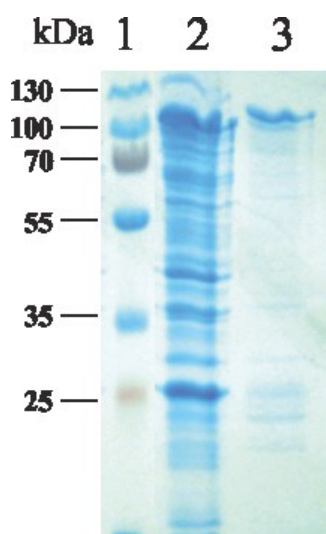


Figure 5.69: SDS-PAGE gel from purification of XplB (S385W)-GS. From left to right, protein markers (1), cell lysate (2) and purified protein (3).

Using HPLC analysis, purified XplB(S385W)-GS was found to lack any detectable FAD. Further studies using XplB(S385W) (0.9 mg) as a reductase partner to purified XplA in Greiss assays confirmed that XplB(S385W)-GS was inactive.

E. coli lysate expressing empty vector, *xplB-glnA* and *xplB(S385W)-glnA* were assayed for the RDX-removal activity on HPLC using equal amount of purified XplA. The results showed that XplB(S385W) is active as there was a faster rate of RDX removal by XplA (42 ± 11 %) when the lysate expressing XplB(S385W)-GS used as a reductase, whereas just 16 ± 0.5 % of RDX was removed by XplA when an empty vector was as a reductase.

5.3.3 Characterization of GS portion of XplB-GS

In *Gordonia* sp. KTR9, XplB is fused with a key enzyme in nitrogen metabolism, GS [105]. Whether this fusion affects GS activity and subsequent nitrogen metabolism is not known. Here, the GS portion of the fusion is investigated by both sequence analysis and the activity assay for GS.

5.3.2.1 Sequence analysis of the GS protein fused to XplB

The class of GS from XplB-GS was identified using multiple sequence alignments (MSA) with several characterised GSI protein sequences [155-157]. The MSAs revealed that the GS in XplB-GS belongs to GSI- α , lacking the insertion signature sequence found in class GSI- β [155] (Table 5.2).

Table 5.6: Classification of the GS fused with XplB in *Gordonia* sp. KTR9 based on multiple sequence alignment. GS proteins from *Streptomyces coelicolor*, *Synechococcus* sp., *Anabaena* sp., *Salmonella typhimurium*, *Pyrococcus furiosus*, *Haloferax volcanii*, and *Methanococcus voltae* are classified by Brown *et al.* (1994) [155]. The GS proteins from *Mycobacterium tuberculosis*, and *Bacillus subtilis* are characterised by Hayward *et al.* (2009) [157] and Murray *et al.* (2013) [156], respectively. Name of the organism, GS class, UniProt accession number, and a portion of the sequence alignment in the insertion region is shown below. The insertion sequence is yellow highlighted in the alignment.

| Organism | Class | UniProt AC | Sequence (N-terminal to C-terminal) |
|-----------------------------------|---------------|------------|---|
| <i>Mycobacterium tuberculosis</i> | GSI- β | P9WN39 | STGIADTAYFGAEAEFYIFDVSFDSRANGSFYEVD A I SGWNTGAATEA 170 |
| <i>Streptomyces coelicolor</i> | GSI- β | P15106 | STGIADTAFFGPEAEFFVFDVSRFATRENESFYHIDSEAGAWNTGALED- 165 |
| <i>Synechococcus</i> sp. | GSI- β | P28605 | ASGIGDTAYFGPEAEFFVFDVRFDTENKGFYYVDSVEGRWNSGRKEP- 168 |
| <i>Anabaena</i> sp. | GSI- β | K7W630 | STGLGDTAFFGPEAEFFIFDDVRYDQTTNSGYYYVDSVEGRWNTGREE-- 166 |
| <i>Salmonella typhimurium</i> | GSI- β | P0A1P6 | ATGIADTVLFGPEPEFFLFDDIRFGASISGSHVAIDDI EGAWNSSTKYE- 166 |
| <i>Pyrococcus furiosus</i> | GSI- α | Q05907 | KE--GYKAYIGPEPEFYLFK-----KNGTWELEIPDV- 141 |
| <i>Haloferax volcanii</i> | GSI- α | P43386 | ELGY-DVNVA-PEPEFFLFEE-----DEDGRATVTVNTDA- 164 |
| <i>Bacillus subtilis</i> | GSI- α | P12425 | DLGFSDFNLG-PEPEFFLFKL-----DEKGEPTLELNDK- 153 |
| <i>Methanococcus voltae</i> | GSI- α | P21154 | EEFKGEYFVG-PEPEFFILK-----NENK--WVPGDD- 156 |
| <i>Gordonia</i> sp. KTR9 | ----- | E1R0R9 | ERTGLEMRTG-TEPEMTWEG-----EGFETFRPDS- 176 |

The MSA of GS from *Gordonia* sp. KTR9 with the three closest homologues from the ExPASy database (<http://www.expasy.org/>), shares >78 % sequence identity with the protein, reveals that the GS in XplB-GS is truncated. The missing region consists of 71 amino acids at the C-terminal, comprising 15 % of the total protein size (Figure 5.19).

| | | |
|---|---|-----|
| <i>Mycobacterium vulneris</i> (X5LA15) | RLEYKLPDAACNPYLTHAAMLVSIDDGLKNQISPGAPTVGSSYESTDAEL | 400 |
| <i>Mycobacterium farci</i> (A0A024LZ23) | RLEYKLPDAACNPYLTHAAMLVSIDDGLKNQINPGAPTVGSSYESTEPPEL | 400 |
| <i>Mycobacterium fortuitum</i> (K0VLG7) | RLEYKLPDAACNPYLTHAAMLVSIDDGLKNQISPGAPTVGSSYESTEPPEL | 400 |
| <i>Gordonia</i> sp.KTR9 (E1R0R9) | RLEYKLPDASCNPFLTHAVLLAAIDGGLKNQTDPGAPTVG----- | 390 |
| | *****:***:***.:*.:*****.***** | |
| <i>Mycobacterium vulneris</i> (X5LA15) | FGELPLTLGDALAAFKADDYLINALGAPLGNLLLEYKTDEWARFNSSITD | 450 |
| <i>Mycobacterium farci</i> (A0A024LZ23) | FGELPLTLGDALAAFKADDYLINALGARLGNLLLEYKTDEWARFNSSITD | 450 |
| <i>Mycobacterium fortuitum</i> (K0VLG7) | FGELPLTLGDALAAFKADDYLINALGAPLGNLLLEYKTDEWARFNSSITD | 450 |
| <i>Gordonia</i> sp.KTR9 (E1R0R9) | ----- | |
| <i>Mycobacterium vulneris</i> (X5LA15) | WERTMYWEDTP | 461 |
| <i>Mycobacterium farci</i> (A0A024LZ23) | WERNMYWEDTP | 461 |
| <i>Mycobacterium fortuitum</i> (K0VLG7) | WERTMYWEDTP | 461 |
| <i>Gordonia</i> sp.KTR9 (E1R0R9) | ----- | |

Figure 5.70: Part of the multiple sequence alignment of three GS proteins close homologues to GS-XplB. The name of the organism and the UniProt accession number of each protein is written next to its corresponding sequence. The yellow highlighted sequence is the region which is missing in the GS of *Gordonia* sp. KTR9.

It is known that most of the active site residues in the glutamine synthetase are located in the C-terminal of the protein [156]. To investigate whether the missing residues form part of the active site, the model structure of the GS was created based on the closest homologue in the protein database bank for which structural data is available: GS from *Bacillus subtilis* (pdb: 4lnn.1.I) (Access date: 18/09/2014).

GS from *B. subtilis* shares 29.06 % sequence identity with GS from XplB-GS. Superimposing the model structure of the GS from XplB-GS on the GS from *B. subtilis* (RMSD: 1.141 °A) revealed the structure and position of the missing active sites and amino acids (Figure 5.20).

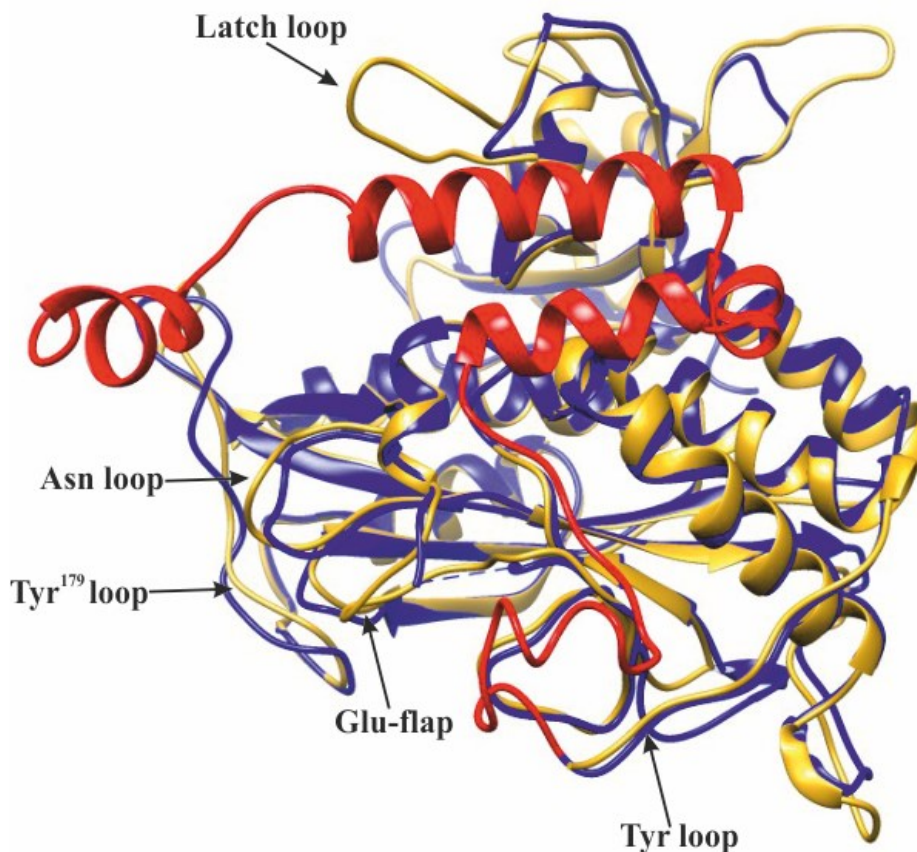


Figure 5.71: Superimposed model structure of the GS from XplB-GS of *Gordonia* sp. KTR9 (blue colour) on the GS structure of *B. subtilis* (golden colour). The location of each active site loop is labelled. The red coloured region is the sequence which is found in the GS structure of the template and is missing in the GS from *Gordonia* sp. KTR9. Root mean square deviation (RMSD 1.14 °Å).

Based on the homology modelling shown in Figure 5.20 and knowledge from the structure of the GSI- α of *B. subtilis* [156], it was found that the missing residues in the GS fusion include two residues which are involved in the formation of the active site Tyr loop. The other residues located on the other loops, mediating the catalysis activity of the enzyme, present in GS from *B. subtilis* are also found in GS from *Gordonia* sp. KTR9. This is including Asn loop which found remarkably similar between GS of GS-XplB and GS from *B. subtilis*, while the Asp⁵⁰, (Latch loop) is found to be extended in the fused GS compared to the GS from *B. subtilis*. The position and the sequence of the residues located on each loop are shown in Table 5.3.

Table 5.7: Sequence and the position of the residues located in active site loops of the model structure GS fused with XplB.

| Site | Position | Sequence |
|--------------------------------|----------|---------------------------|
| Asp ⁵⁰ (latch loop) | 65-89 | QHRTAMANLQAGRDGVLMAGGVGAS |
| Tyr ¹⁷⁹ loop | 172-181 | TFRPDSSPAYH |
| Asn loop | 253-264 | FMPKPGVGGYMGN |
| Glu flap | 324-330 | DAGQFAP |
| Tyr loop | 384-390 | PGAPTVG |

5.3.2.2 Measuring glutamine synthetase activity in the GS-XplB fusion

Purified XplB-GS (0.283 mg/ml) was assayed for the glutamine synthetase activity. As the GS from *Gordonia* sp. KTR9 is a fusion protein, XplB from *R. rhodochrous* 11Y was tested to see if it interfered with the assay. The result shows that GS fused to XplB is active and able to convert 55.9 ± 3.7 $\mu\text{mol. min}$ of L-glutamate to L-glutamine at pH 7.1 at 37 °C (Figure 5.21).

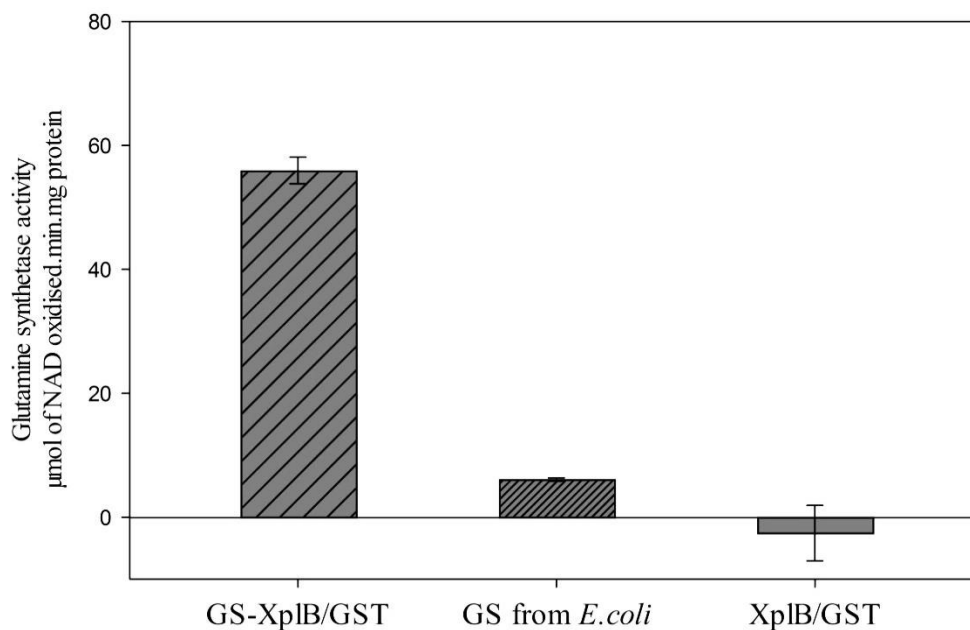


Figure 5.72: Glutamine synthetase activity assay of purified GS-XplB. The activity of the GS-XplB/GST tagged was examined spectrophotometrically based on the oxidation rate of the β -NADH at A340. The commercial GS of *E. coli* K12 (Sigma-Aldrich) was used as a positive control. Background interference of the XplB-GST, fused with GS enzyme in KTR9, was studied by using the purified XplB-GS from *R. rhodochrous* 11Y.

5.4 Discussion

In summary, the analysis of the XplB-GS fusion from *Gordonia* sp. KTR9 presented here demonstrates that XplB is inactive, but even though the GS portion of the protein is truncated it still demonstrates glutamine synthetase activity. The XplB is inactive mainly as a result of having Ser-385 in place of highly conserved Trp that is present in the FAD containing proteins.

5.4.1 The XplB portion of the XplB-GS fusion

The level of soluble XplB-GS was very low when it was expressed as a N-terminally His-tagged protein, however an advantage of the pET-28(+)a system, if it had worked, would have been that the His-tag is a relatively small percentage of the overall protein when compared to the GST-tag encoded by the pGEX2T vector. This poor solubility of the protein is in agreement with the protein previously reported [95, 164]. The expression of soluble XplB-GS was greatly enhanced when it was expressed as a GST-tagged protein, as seen with XplB from *R. rhodochrous* 11Y [95], and several other low soluble proteins [165].

Sequence comparison of the *xplB* part of *xplB-glnA* with *xplB* from *R. rhodochrous* 11Y revealed two nucleotides substitution in *xplB-glnA*: first mutation is neutral and results in the formation of a silent mutation; however the second substitution is appeared to have a deleterious effect on the reductase activity of the XplB protein through the formation of Ser-385 in the place of Trp386 in XplB. It has been proposed that most gene mutations are having neutral or deleterious effect on the growth of microorganism [6, 14]. As shown in Figure 5.14, the XplB of XplB-GS is inactive as a reductase part for XplA. Less RDX removal by purified XplA in the cell lysate expressing XplB-GS in comparison to the empty vector could be due to less availability of the endogenous reductase in the *E. coli* cell as the result of over expressed XplB-GS. Previously it was shown that plant or bacterial endogenous reductase can supply electrons to XplA [96, 98, 105, 144]. The deleterious effect of the second mutation and the importance of the Trp residue for the functionality of the XplB was shown by creating a XplB(W386S) mutant, which resulted in the loss of reductase activity. Additionally, the FAD was not detected in the purified XplB(W386S) mutant, whereas purified XplB contained 25 % of its potential FAD. Previous reports have also indicated that FAD binds weakly to

XplB; Jackson *et al.* (2007) reported that only 50 % of FAD was found bound in purified XplB [95], while a recent study of XplB from *R. rhodochrous* 11Y yielded no detectable FAD [164]. The corresponding tryptophan residue to Trp-386 in XplB could be important for the functionality of other FAD containing proteins as it is found to be conserved in all the FAD-containing proteins examined, but no other protein was tested here.

Although Trp has a dramatic influence on the FAD binding and functionality of the XplB protein, homology modelling of the XplB protein showed that this residue is not located in the FAD-binding site. Multiple sequence alignments of XplB with other reductases revealed that the Trp-386 is ubiquitous in all reductases, with the sole exception of XplB-GS. The importance of Trp-386 in FAD binding was further demonstrated by the observation that lysate expressing the XplB (S385W)-GS mutant had increased activity when compared to the endogenous reductase activity of *E. coli* expressing empty vector. The purified XplB(S385W)-GS, which has identical sequence like XplB from *R. rhodochrous* 11Y, was inactive which suggest in addition of the effect of Ser in the place of Trp, the reductase activity of the XplB(S385W)-GS was strongly, but not totally, inhibited by the GS protein fused to it. Considering that *Gordonia* sp. KTR9 was isolated from the soil without any detectable amount of explosive [114], then perhaps the lack of selective pressure is the reason for losing reductase activity of XplB-GS or the recombination and reduction of the genomic island which resulted in the fusion of the XplB to GS. As there was low reductase activity detected for the XplB(S386W)-GS in comparison to the empty vector in the whole cell assay, thus recombination in the genomic island, which resulted of the fusing XplB to GS, could be the reason for the deleterious mutation in XplB from *Gordonia* sp., KTR9. It has already been proposed that a useless gene can be deactivated through sequence mutation [21].

5.4.2 The GS portion of the XplB-GS fusion

Despite the fact that the GS component of the XplB-GS fusion is truncated, it was found to be active, demonstrating that the purified protein is correctly folded and the missing residues are not essential for the functionality of the GS protein.

Due to very low yields of proteins, enzyme kinetics of the XplB-GS fusion was not carried, and thus the activity of the enzyme could not be compared with other GS from the same class.

Finding GS fused with XplB to be active is in agreement with the homology model where the module shows all the residues located on the active sites of the protein are conserved, apart from an incomplete Tyr loop. Importantly, activity assays demonstrate that the incomplete Tyr loop, including missing catalytic tyrosine residue, does not affect the functionality GS fused to XplB. The Tyr loop is involved in the regulation of the GSI- β by adenylation of the catalytic Tyr in the active site, however GS from XplB-GS is belong to GSI- α .

The GS from the GS-XplB fusion belongs to GSI- α and is in the same operon with *xplB/A* this may suggests a potential involvement of GS in RDX degradation, possibly regulation of nitrite levels in the cell through regulating the expression of the GlnR. It is already known that GSI- α from *B. subtilis* plays an important role in regulating nitrogen levels by controlling the expression of GlnR and TnrA in the cell through feedback-inhibition of glutamine mechanism [156, 158, 166], in which Glu flap [166] and Arg62 in GSI- α are shown to be involved [156]. Mutation in GS of *B. subtilis* resulted in the constitutive expression of both proteins [166].

In the *Gordonia* sp. KTR9, *glnR* is shown to be important in the assimilation of the nitrite in the cell. A knock-out mutant of *glnR* in *Gordonia* sp. KTR9 resulted in the accumulating of nitrite [167] and down-regulation of the nitrite reductase gene locus KTR9_1306 and KTR9_1307 [168]. Additionally, the *glnA* mutant from KTR9 lost the ability to utilise RDX, nitrite and nitrate as a sole source of nitrogen, but not ammonium or glutamine. Similarly, deleting of the *tnrA* gene, which has a similar C-terminal to GlnR [169], in the *nrgAB* operon of the *B. subtilis* impaired the ability of the bacterium to use allantoin, γ -aminobutyrate, isoleucine, nitrate, urea and valine as nitrogen sources [160].

Chapter 6: Expression, Purification and Characterisation of XplA- homologues from non-RDX degrading bacteria

6.1 Introduction

The cytochrome P450 XplA (CYP1771A1) is an unusual P450 that consists of a heme domain C-terminally fused to a native flavodox domain. This enzyme, with its reductase partner XplB, catalyses the reductive denitration of the recalcitrant pollutant RDX (Chapter 1) [1, 2].

Unusually for a P450, the biodegradation of RDX by XplA is not an oxygen dependent reaction and can occur both aerobically and anaerobically; however, while oxygen is not required for activity it influences the level of denitration of RDX. In both conditions, the ring structure of RDX is cleaved to produce nitrite and formaldehyde with either 4-nitro-2,4-diazabutanal (NDAB) under aerobic conditions, or methylene dinitramine (MEDINA) under anaerobic conditions (Figure 6.1).

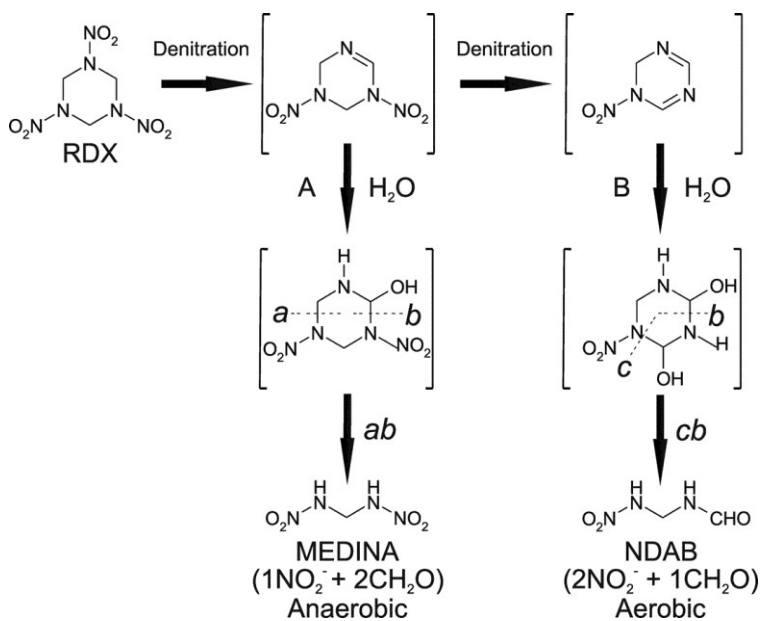


Figure 6.73: Biodegradation pathway of RDX catalysed by XplA from *R. rhodochrous* 11Y. (A) is the anaerobic pathway, in which the RDX structure is cleaved after denitration and hydration to produce one mole of nitrite, two moles of formaldehyde, and methylene dinitramine (MEDINA). (B) is the aerobic biodegradation pathway of RDX; the RDX is double denitrated, then hydrated to form two moles of nitrite, formaldehyde and 4-nitro-2,4-diazabutanal (NDAB). Reproduced from Jackson *et al.* (2007) [95].

The crystal structure of the XplA-heme domain has been solved and shown to share the same overall structure with other P450 enzymes, but with three differences: The first

and most significantly, is that the I-helix in the XplA-heme domain is broken above the iron heme in the region which is usually occupied by the highly conserved Glu/Asp-Thr/Ser residues. These acidic residues, that are essential for oxidation activities in other P450s, have been replaced by Met-394 and Ala-395 in XplA. The second difference is that the D-helix is distorted in the middle of the helix between Asp-262 and Arg-266. Third and lastly, is the addition of a short helix near the N-terminal of the protein (Figure 6.2).

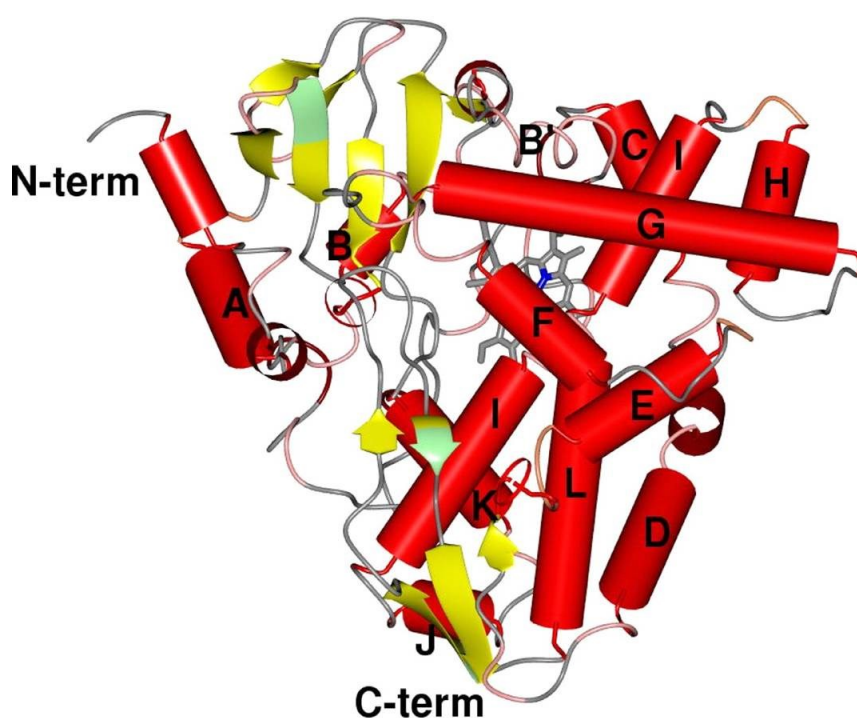


Figure 6.74: Topology of the XplA-heme (pdb: 2wiy). Overall structure of the XplA-heme domain has a canonical structure, like other P450s. The α -helix and β -sheet components of the protein are shown in red cylinders and yellow arrows, respectively. Heme cofactor is shown in silver and buried at the center of the protein. N-term refers to the N-terminal; C-term refers to C-terminal part in the protein structure. Reproduced from Sabbadin *et al.* (2009) [99].

The XplA-heme has a hydrophobic active site, characterised by having three clustered methionine residues (Met-318, Met-322, Met-394) above the heme iron ring. Additionally, Trp-230, Trp-224, Phe-540, Leu-238, Val-387, Val-391, Ala-395, Gln-438, Cys-503 and Pro-437 are also found in the active site of the protein (Figure 6.3).

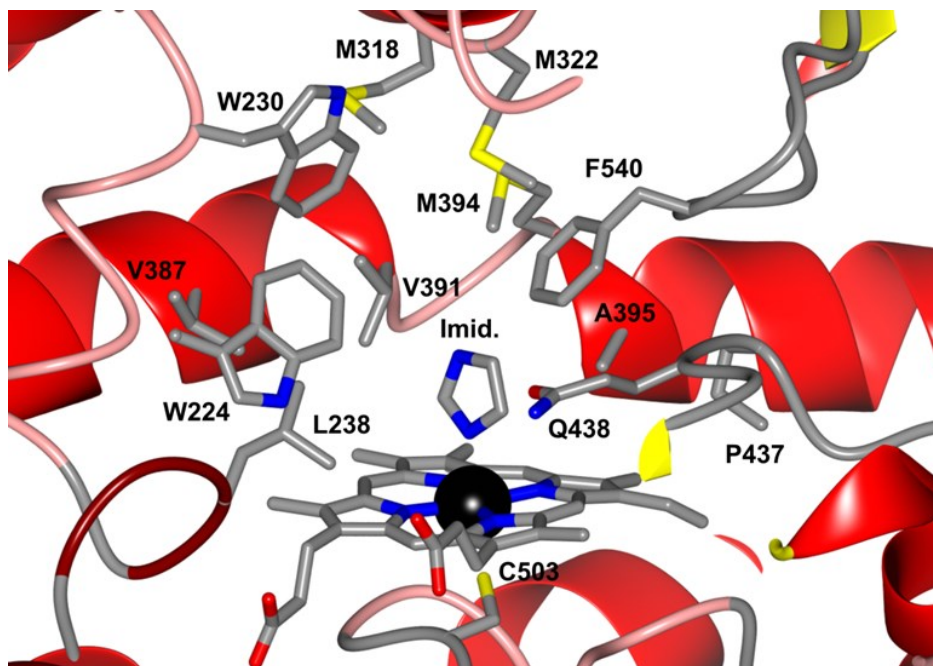


Figure 6.75: The XplA-heme active site. The residues located in the heme binding site are shown, including characteristic three methionines (Met-394, Met-322 and Met-318) above the heme iron ring. The ligand imidazole (labelled as Imid) is bound to the active site. Reproduced from Sabbadin *et al.* (2009) [99].

Two putative channels have been identified on the surface of the XplA-heme protein, which were proposed to be involved in ligand transport into the XplA active site. The largest channel is bound by the side chains of Phe-319, Leu-323, Ala-541, Gln-438, and Met-322. The small channel is bound by the two positively charged side chain residues of Arg-288 and Arg-545, and could be responsible for capturing RDX. These channels together make a path to the methionine cluster in the heme active site at the centre of XplA-heme (Figure 6.4) [1].

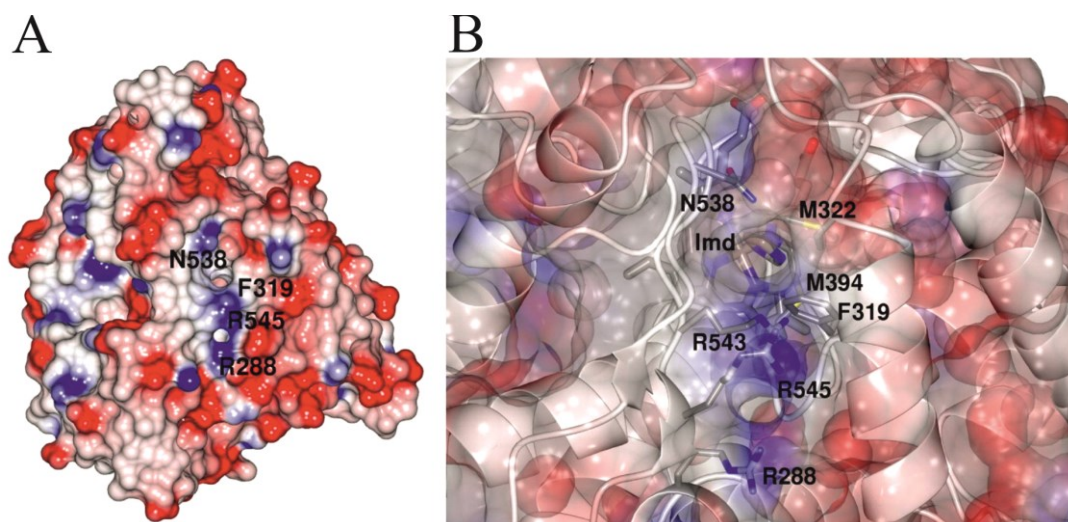


Figure 6. 76: The putative ligand transport channels in the XplA-heme protein. (A) is the electrostatic surface of the XplA heme. The residues Arg-538, Phe-319 contribute to the formation of the large channel, whilst Arg-545 and Arg-288 are located around the small channel. (B) is a magnification of the partially transparent electrostatic surface of the ligand transport channel in XplA. The Arg-543, Arg-288, Arg-545, Gln-538, and Phe-319 residues are making a path for the ligand from the surface to the active site of the protein in the location above methionine cluster. The imidazole ligand (labelled as Imd) can also be seen through the pore from the surface of the XplA-heme. Reproduced from Sabbadin *et al.* (2009) [99].

As described in Chapter 1, the XplA/XplB system has now been characterised in detail and the application of XplA to clean-up RDX contaminated soil is in progress. However, one aspect that remains unclear is the evolutionary origin of *xplA*. Uniquely, XplA is the only cytochrome P450 that has so far been identified that is N-terminally fused to a flavodoxin domain. Nearly identical versions of *xplA* have been identified in all RDX-degrading *Actinomycetales* that have been tested, despite the fact that they have been isolated from distinct geographical locations (Chapter 4) [100, 102, 103]. The gene has not, however, been found in non-RDX degrading bacteria, nor in environmental DNA sequencing projects [98]. The closest homologue of XplA in databases is *Erwinia carotovora* subsp. *atroseptica*. (Uniprot ID Q6D569), a plant pathogen, with 41 % sequence identity [99].

In this chapter, the evolutionary origin of the XplA enzyme was investigated by characterising three, published, putative cytochromes P450 that share sequence homology with XplA. Two of the P450s are from the auto-annotated, whole genome shotgun sequence of *Gordonia polyisoprenivorans* NBRC16320 (Sequence release date:

02/12/2011) and the third one is from the genome shotgun sequencing of *Gordonia terrae* strain NBRC100016 (Sequence released date: 16/02/2012). There is no data currently available regarding the RDX-degrading capability of these two species or whether they had been exposed to explosives. *G. terrae* NBRC100016 was isolated from a soil samples in Japan by Tsukamura (1971) and, interestingly, the bacterium was characterised for the ability to use a wide range of substrates as nitrogen sources including pyrazinamide, serine, methionine, acetamide, nitrate, nitrite, nicotinamide, isonicotinamide, benzamidec [170]. Whereas, *G. polyisoprenivorans* NBRC 16320, which is also called *G. polyisoprenivorans* kd2T DSM=44302T, was isolated for its ability to degrade rubber from fouling water fauna inside a deteriorated automobile tyre in Germany [171].

6.2 Materials and Methods

6.2.1 Cloning of the cytochrome P450 genes

The putative cytochromes P450 used in this study have not previously been characterised. Here the P450 from *G. terrae* strain NBRC 100016 (CYP177B1) (GenBank accession number: GAB46351) is referred to as "GT-XplA", and the two cytochromes P450 of *G. polyisoprenivorans* NBRC 16320, which have accession numbers GAB24219 and GAB24226, as "CYPA" and "CYPB", respectively. CYPA and CYPB have been also officially named as CYP177C1 and CYP1051A1, respectively.

All sequence analyses of the genes encoding the three cytochrome P450s were carried out using the NCBI database (<http://www.ncbi.nlm.nih.gov/>).

The *G. terrae* strain NBRC 100016 and *G. polyisoprenivorans* NBRC 16320 were provided by The Biological Resource Centre (NBRC), the National Institute of Technology and Evaluation (NITE) in Japan.

The *gt-xplA* was amplified from the total genome of *G. terrae* and cloned into a pET-28(a)+ at the restriction sites *EcoRI* and *XhoI* to be expressed as an N-terminally His-tagged protein (Chapter 2.6.12).

The genes encoding CYPA, engineered to contain an ATG as a start codon instead of GTG which express in *E.coli* as valine and CYPB were amplified from the total DNA genome of *G. polyisoprenivorans*. The genes were cloned into *NdeI* and *BamHI* restriction sites of a pET-16b vector, allowing the protein to express as an N-terminally His-tagged protein (Chapter 2.6.12).

Expression of soluble CYPA in pET-16b was problematic. To overcome this, *cypA* was re-cloned into pET-28(+), and then later into pET-16b as truncated CYPA as follows: Cloning of *cypA* into pET-28(+), was carried out by amplifying the gene from the *cypA*-pET-16b construct, then cloning into pET-28(+), at the *NcoI* and *SalI* restriction sites of the vector to achieve a C-terminally His-tagged protein. A truncated version of the *cypA* gene was constructed by cloning the *cypA* gene, missing the 60 bp at the 5' region, into pET-16b at the *NdeI* and *BamHI* restriction site.

6.2.2 Expression of the cytochromes P450

The putative P450s were expressed in an *E. coli* expression strain. For protein expression trials, freshly transformed *E. coli* cells were used to inoculate 125 ml LB medium in 500 ml flasks while for protein purification purpose cells were used to inoculate larger cultures of 500 mL LB medium in 2 L flasks. The LB medium contained 100 µg/ml of the plasmid specific antibiotic and 34 µg/ml of chloramphenicol was added when *E. coli* Rossetta 2 (DE3) cells were used (strain specific antibiotic resistance). Culture were grown with shaking at 37 °C to OD₆₀₀ ~0.6-08, cooled to 20 °C and gene expression was induced by addition of IPTG. At the same time, ALA (δ-aminolevulinic acid, 0.5 mM), FeCl₃ (0.5 mM), and riboflavin (50 µg/L) were also added. The expression level of the proteins was checked by running the soluble and insoluble fractions of *E. coli* cell lysates on SDS-PAGE. The strain of *E. coli*, concentration of IPTG, induction temperature and time are mentioned in the corresponding result sections.

6.2.3 Purification of the cytochromes P450

The *E. coli* cells expressing the gene of interest were harvested and resuspended in His-binding buffer (50 mM sodium phosphate pH 8, 300 mM NaCl). Cells were lysed by sonication (Chapter 2.7.2). Cell debris and other insoluble components were separated from soluble protein by centrifugation of the total cell lysate at 15,000 rpm for 15 minutes using a Sorval Evolution RC high speed centrifuge (Kendro laboratory products).

The expressed proteins were purified using a 5 ml HisTrap FF crude column containing prepacked Ni sepharose and AKTA purifier UPC10 system (GE-Healthcare). The lysate was loaded into a 50 ml superloop and then injected into the column at a flow rate of 1 ml/minute. Protein was washed with five column volumes of His-washing buffer (His-binding buffer containing 5 mM imidazole, pH 8.0). Elution was carried out using a gradient increasing of imidazole concentration in the buffer through gradual increasing ratio of the His-eluting buffer (His-washing buffed with 300 mM imidazole, pH 8) to the ratio of His-washing buffer. The soluble expressed proteins were generally eluted with ~150 mM imidazole. The purified fractions of the protein were identified from a chromatogram generated by AKTA Unicorn software (version 5.31) and from visual inspection for pink to red colour of the P450 proteins. The eluted fractions of the protein

were pooled and dialysed twice in 5 L dialysis buffer (50 mM potassium phosphate buffer, pH 7.0). The fractions from the protein purification steps were collected and analysed by SDS-PAGE.

6.2.4 Spectra analysis of purified protein

The absorbance for each of the reduced forms of the cytochromes P450 with CO was identified by UV-spectra analysis of the purified protein on a spectrophotometer (Shimadzu Corp., Kyoto, Japan). The purified protein was diluted in 50 mM potassium phosphate buffer pH 7.0 and the UV-visible spectrum of the oxidised form of the P450 protein was recorded in the range of 300 to 600 nm in 1 ml UV cuvettes. The reduced and CO-bound spectra of the P450 were generated by first reducing the protein with sodium dithionite and then bubbling with CO.

UV-Spectra of the protein were also used to investigate if the purified protein can bind to RDX by comparing the UV-spectra of the protein before and after adding of 100 μ M of RDX.

6.2.5 Whole cell assays

E. coli cell cultures expressing the P450s, including the truncated CYPA and mutant forms, as well as the mutant from of GT-XplA were tested for RDX degradation capability. The mutant forms of the CYPA and GT-XplA were constructed as described in Chapter 2.6.13. Freshly transformed *E. coli* Rossetta 2 (DE3) cells were grown in 100 ml flasks containing 10 ml of auto-induction medium with 50 μ g/ml of the plasmid selective antibiotic and 34 μ g/ml of chloramphenicol. Cells were grown at 37 °C to OD_{600} ~0.6-0.8. The cultures were cooled to 20 °C, then 0.5 mM ALA, 0.5 mM FeCl₃, 50 μ g/ml riboflavin, and 100 μ M RDX added. An aliquot of the medium (200 μ l) was taken at different time points and used to detect nitrite released from RDX degradation by using the Griess assay (Chapter 2.8.2). The composition of the auto-induction medium is shown in Table 6.1.

Table 6.8: The composition of the auto induction medium

| Medium component | Ingredients | Quantity |
|-----------------------------------|---|----------|
| ZY solution (in 1 L of water) | Tryptone | 10.0 g |
| | Yeast extract | 5.0 g |
| 50X M solution (in 1 L water) | Na ₂ SO ₄ | 36.0 g |
| | NH ₄ Cl | 134.0 g |
| | KH ₂ PO ₄ | 170.0 g |
| | Na ₂ HPO ₄ | 177.0 g |
| 50X 5052 solution (in L in water) | Glycerol | 250.0 g |
| | Glucose | 25.0 g |
| | α -Lactose | 100.0 g |
| 1000X metals (in 1 L of water) | 0.1 M FeCl ₃ .6H ₂ O (in 0.1 M HCL) | 500 ml |
| | 1.0 M CaCl ₂ | 20 ml |
| | 1.0 M MnCl ₂ .4H ₂ O | 10 ml |
| | 1.0 M ZnSO ₄ . 7H ₂ O | 10 ml |
| | 0.2 M CoCl ₂ .6H ₂ O | 10 ml |
| | 0.1 M CuCl ₂ .2H ₂ O | 20 ml |
| | 0.1 M NiCl ₂ . 6H ₂ O | 10 ml |
| | 0.1 M Na ₂ MoO ₄ .5H ₂ O | 20 ml |
| | 0.1 M Na ₂ SeO ₃ .5H ₂ O | 20 ml |
| | 0.1 M H ₃ BO ₃ | 20 ml |

| Component | Volume (ml in 1 L of solution) |
|-------------------------|--------------------------------|
| ZY solution | 928.0 |
| MgSO ₄ (1 M) | 1.0 |
| 1000X metals | 1.0 |
| 50X 5052 solution | 20.0 |
| 50X M Solution | 50.0 |

6.3 Results

6.3.1 Sequence analysis of the XplA homologues

An NCBI database scan for the XplA homologues revealed three putative cytochrome P450s (GT-XplA, CYPA and CYPB) sharing sequence homology to XplA.

The sequence comparison showed that the cytochrome P450 domain of *Gordonia terrae* (GT-XplA) shares 44 % amino acid sequence identity with the heme domain of XplA. Additionally, GT-XplA was found to have a putative flavodoxin fused with the heme domain of the protein with 51 % sequence identity to the flavodoxin domain of XplA. Moreover, sequence analysis of the contig where *gt-xplA* is located (contig: GOTRE150, GenBank accession number: NZ_BAFD01000115.1) revealed that the gene is located in a region sharing sequence similarity to the *xplA* gene cluster in RDX-degrading *Rhodococcus* spp. and *Microbacterium* sp. MA1. The gene located directly upstream of *gt-xplA* encodes a ferredoxin- NADP reductase with 37 % amino acid sequence identity with XplB; *xplB* is directly upstream of *xplA* in *Rhodococcus* spp and *Microbacterium* sp. MA1. The C-terminal of the succinate-semialdehyde dehydrogenase encoded by *gabD* gene, located downstream of *gt-xplA*, also shares 47 % sequence identity with the succinate-semialdehyde dehydrogenase encoded by the gene downstream of *xplA* (Figure 6.5A and B).

The genes encoding the putative cytochromes P450 (CYPA and CYPB) are located in a 143,465 bp contig: GOPIP064 (GenBank accession number: BAEI01000064.1) from the shotgun genome sequence of *G. polyisoprenivorans* NBRC 16320. The *cypB* is located in an ~8.0 kbp region upstream of *cypA* and there is also a similar gene arrangement to the *xplA* gene cluster in RDX-degrading bacteria. The CYPB has only 37 % amino acid sequence identity with the heme domain of XplA. The gene upstream of *cypB* encodes a putative FMN binding protein, which shares 55 % sequence identity to the entire sequence of the flavodoxin domain of XplA. Interestingly, there is also a gene encoding an XplB-like reductase upstream of the gene encoding FMN binding protein, sharing 40 % identity to > 96 % of the XplB protein (Figure 6.5C).

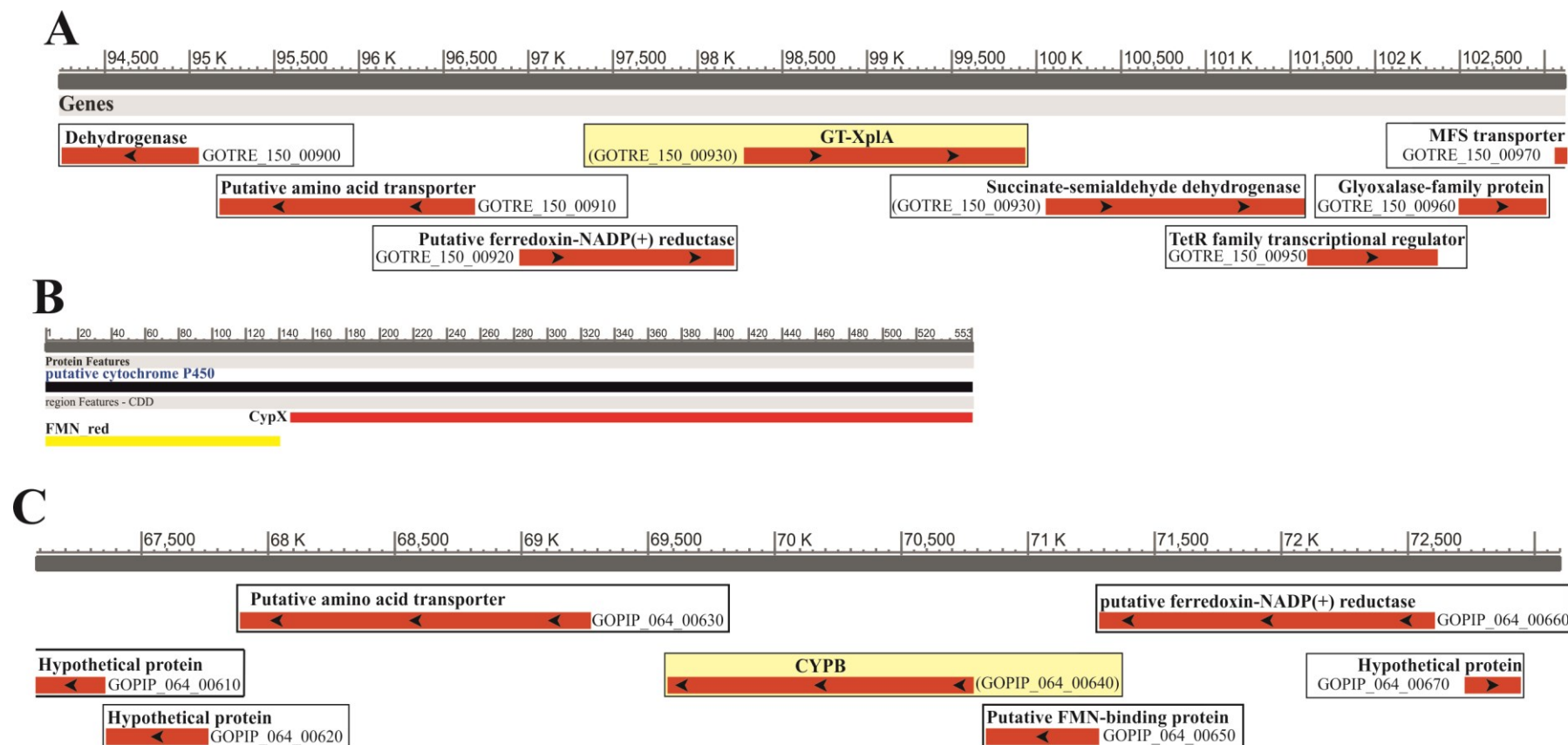


Figure 6.77: (A) The 8.9 kbp region flanking the *gt-xplA* in *G. terrae* strain NBRC 100016. The yellow highlighted box is *gt-xplA*. B- is the graphic view for GT-XplA; the residues Met-1 to Trp-140 encompass the flavodoxin domain and Pro-147 to Ser-553 contains the cytochrome P450 domain. C-The 8.0 kbp region surrounding *cypB* in *G. polyisoprenivorans* NBRC 16320; *cypB* is highlighted in yellow. In both (A) and (C), the red bar represents the genes and black arrows represent the direction of transcription. Name of the proteins encoded by each gene is written above the gene, and each gene locus

is written next to the bar. The graph is a modified version of that downloaded from the graphic view of the contig from NCBI database (<http://www.ncbi.nlm.nih.gov>).

CYPA was shown to have the highest overall sequence identity (51 %) with XplA, but the genes flanking *cypA* do not share sequence homology with those flanking *xplA* in RDX-degrading bacteria (Data not shown).

Homology modelling shows that CYPA has a similar architecture to the XplA-heme domain (pdb: 2WIY), and several residues in the putative active of CYPA identical to those in XplA-heme structure including three methionine residues (Met-255, 179 and 183) forming a cluster above the heme, similar to those in XplA-heme domain (Figure 6.6).

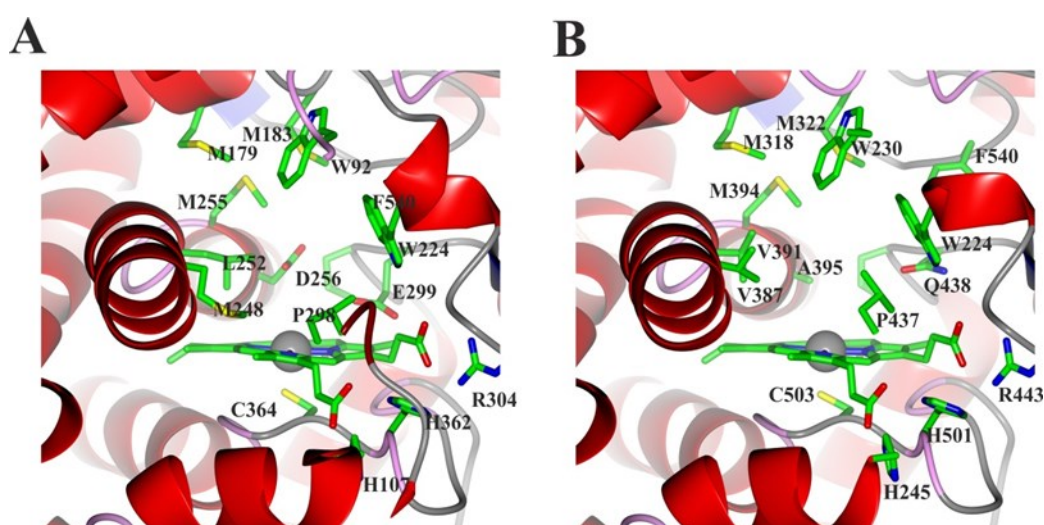


Figure 6.78: A model structure comparing the CYPA and XplA-heme active sites (pdb: 2WIY). The model indicates that most of the residues located in the active site of XplA-heme domain are also conserved in the active site of CYPA. The Root Mean Square Deviation (RMSD) = 0.194 °Å.

The sequence alignments of the GT-XplA, CYPA, and CYPB to XplA revealed that most of the residues located in the active site of the XplA-heme are also conserved in CYPA, including Met-255 that breaks the I-helix in XplA-heme structure. Interestingly, codon sequence analysis of the gene shows that the adjacent residue, that is essential for XplA activity[99], (Ala-395), is replaced by Asp-256 as a result of a single nucleotide variation (GCC is Ala, GAC is Asp). A comparison of the XplA active sites residues to those in GT-XplA, CYPA and CYPB is shown in Table 6.2.

Table 6.9: The corresponding residues of XplA-heme active site in CYPA, CYPB and GT-XplA. Identical residues are shown in Bold. Information on the effect of mutation in the residues were obtained from the study taken by Sabbadin *et al.* (2009) [99].

| XplA | CYPA | CYPB | GT-XplA | Note |
|----------------|----------------|----------------|----------------|--|
| Trp-224 | Trp-86 | Gly-73 | Asn-224 | Heme Binding Pocket |
| Trp-230 | Trp-92 | Trp-79 | Phe-230 | Heme Binding Pocket |
| Leu-238 | Ile-100 | Leu-87 | Leu-239 | Heme Binding Pocket |
| Val-387 | Met-248 | Ile-237 | Leu-239 | Heme Binding Pocket |
| Val-391 | Leu-252 | Ser-241 | Ser-392 | Heme Binding Pocket |
| Met-394 | Met-255 | His-244 | Pro-395 | Heme Binding Pocket. Met394Leu mutant decreased k_{cat}/K_M by 2 fold. |
| Ala-395 | Asp-256 | Asn-245 | Asn-396 | Heme Binding Pocket. Ala395Thr has the most remarkable effect, decreased the k_{cat}/K_M of the enzyme approximately 200 fold. |
| Pro-437 | Pro-298 | Pro-287 | Val-438 | Heme Binding Pocket |
| Gln-438 | Glu-299 | Glu-288 | Glu-439 | Heme Binding Pocket and bounded the largest channel in XplA. Gln438Ala mutant decreased k_{cat}/K_M value 17 times. |
| Cys-503 | Cys-364 | Cys-353 | Cys-504 | Heme Binding Pocket |
| Phe-540 | Phe-401 | Arg-390 | Arg-541 | Heme Binding Pocket |
| Met-318 | Met-179 | Thr-167 | Leu-319 | Met318Leu mutant decreased the k_{cat}/K_M of the enzyme 20 times. |
| Met-322 | Met-183 | Met-171 | Met-323 | Met322Leu mutant decreased k_{cat}/K_M value just one time. |

6.3.2 Cloning and expression of putative ancestral XplA cytochromes P450

The gene encoding GT-XplA was cloned into pET-28(+)_a to be expressed as N-terminally his-tagged protein (Figure 6.7).

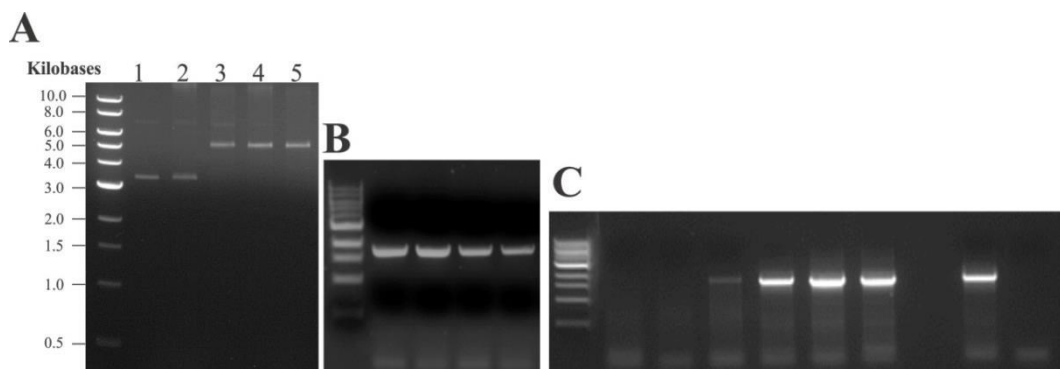


Figure 6.79: Cloning of the *gt-xplA* gene into pET-28(a)₊ vector. (A) is the pET-28a(+) vector digestion; 1 and 2 are undigested plasmid; 3 and 4 are single digested plasmid with *EcoRI* and *XhoI*, respectively; 5 is the double digested plasmid with both restriction enzymes. (B) PCR amplification of the insert (*gt-xplA*), expected PCR product = ~1.7 kbp. (C) Colony PCR of the different transformed colonies using gene specific primers.

The gene *gt-xplA* was expressed in *E. coli* Rossetta 2 (DE3), and protein production induced with 1 mM IPTG. The cells were harvested 16 hours after induction and GT-XplA purified using a 5 ml HisTrap FF crude column and AKTA-purifier UPC10 system. A band corresponding to the expected protein size was found on SDS-PAGE in the eluted fraction (Figure 6.8). This band was cut from the gel and identified as GT-XplA by MALDI-MS.

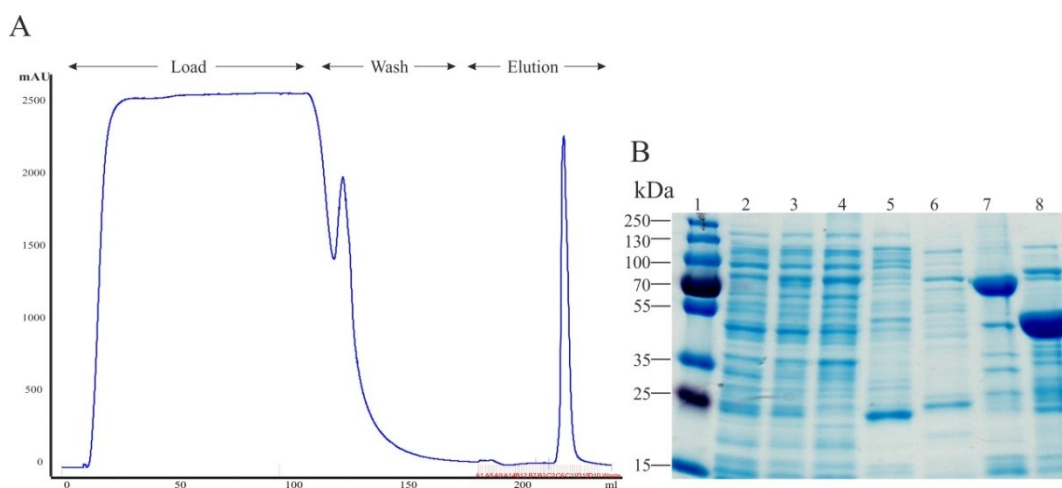


Figure 6.80: (A) Example of a typical chromatogram of GT-XplA purification on Ni-affinity column using an AKTA-purifier. The chromatogram was generated using Unicorn 5.31 software. (B) SDS-PAGE of the purification fractions of the GT-XplA proteins using HisTrap purification column. From left to right: molecular marker (1), lysate of *E. coli* expressing an empty vector (2), lysate of the *E. coli* cells expressing GT-XplA (3), flow-through (4), washed proteins (5 and 6), purified GT-XplA (7), and XplA-heme domain (8). The predicted size of the GT-XplA= 65 kDa.

The genes encoding both CYP_A and CYP_B were cloned into pET-16b and expressed as N-terminally His-tagged proteins (Figure 6.9).

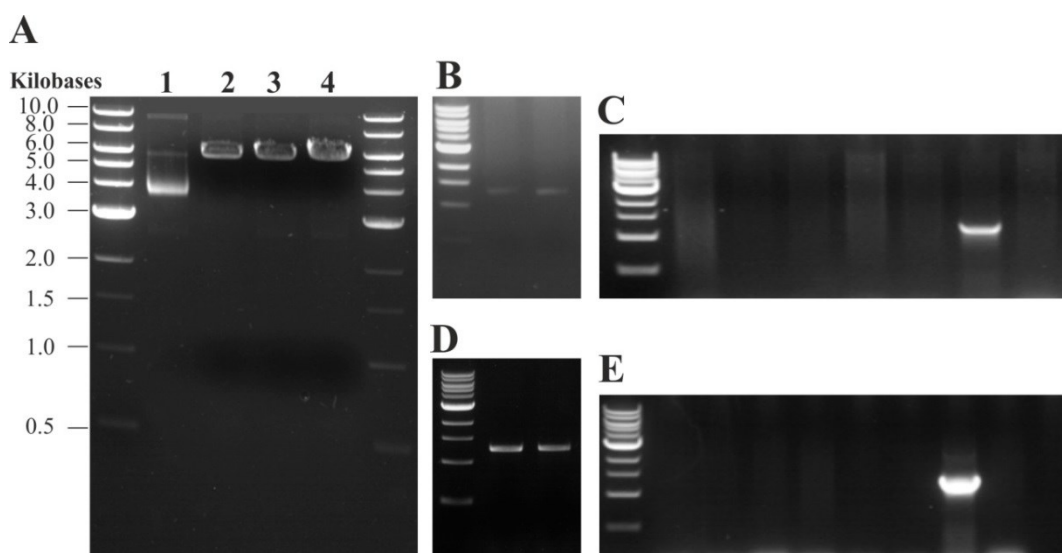


Figure 6.81: Cloning of *cypA* and *cypB* genes into pET-16b vector. (A) Digestion of the pET16b vector; 1 is uncut plasmid; 2 and 3 are single digested plasmid with *NdeI* and *BamHI*, respectively; 4 is a double digested plasmid with both *NdeI* and *BamHI*. (B) PCR amplification of the *cypA*, product size = 1,245 bp. (C) Colony PCR of the different transformed colonies with *cypA* using gene specific primers. (D) PCR amplification of the insert *cypB*, product size = 1,209 bp. (E) Colony PCR of the different transformed colonies with *cypB* using gene specific primers.

The *cypA* and *cypB* genes were expressed in *E. coli* Rossetta 2 (DE3) cells, by inducing with 1 mM IPTG. The proteins were purified using an AKTA purifier (see section 6.2.3). The expected band for the CYPA was not visualised by SDS-PAGE in the fractions from purification steps, while a single band, matching the expected size of the protein, was found for CYPB (Figure 6.10).

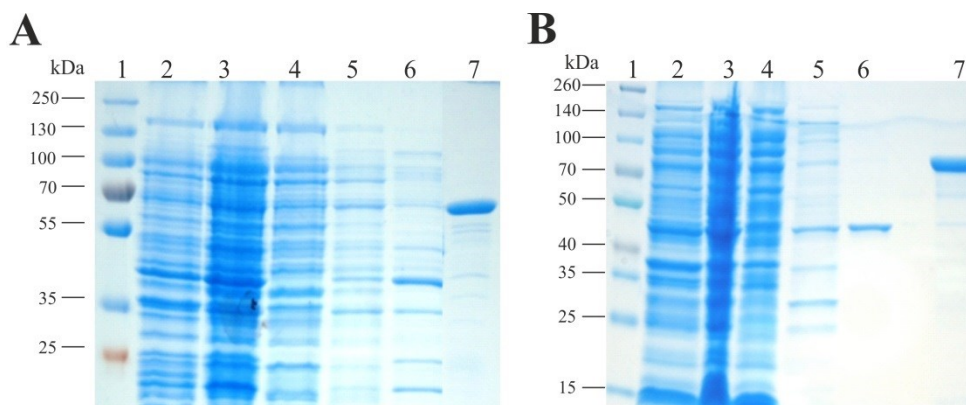


Figure 6.82: SDS-PAGE of the fractions from purification steps of the CYPA (A) and CYPB (B) using AKTA purifier. In both gels, 1 is the molecular markers, 2 is the lysate from empty vector, 3 is the lysate from *E. coli* expressing the gene; 4 and 5 and from the washing steps, 6 is the elution fraction, 7 is purified His-tagged protein as a positive control for western blot.

Western blot analysis using anti-His antibody failed to detect soluble His-tagged CYPA from cell lysate; however, His-tagged CYPB was detected in both crude cell lysate and the eluted fraction after purification (Figure 6.11). The identity of eluted His-tagged CYPB was confirmed by MALDI-MS analysis.

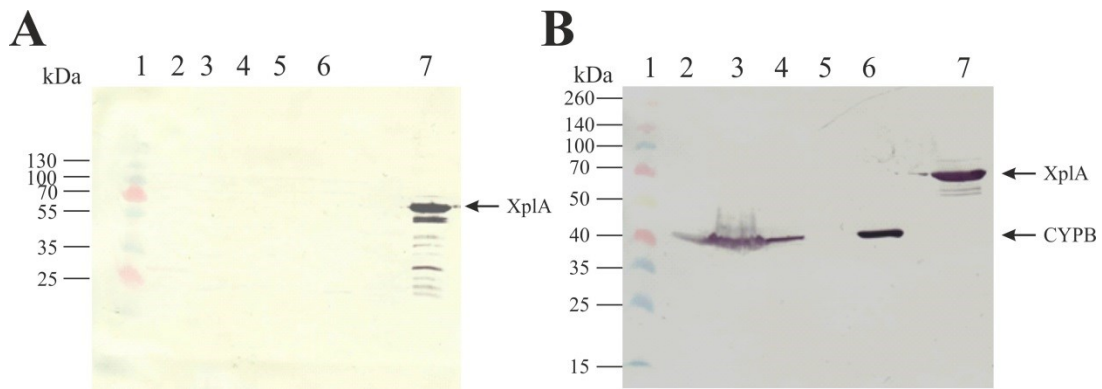


Figure 6.83: Western blot analysis of the fractions from purification steps of CYPA (A) and CYPB (B) using monoclonal His-antibody. In both membranes, 1 is a molecular markers, 2 is the lysate from empty vector, 3 is the lysate from *E. coli* expressing the *cypA* gene, 4 and 5 are fractions from the washing steps, 6 is the elution fraction, and 7 is purified His-tagged protein as a positive control for western blot.

An attempt was made to express CYPA as a soluble protein by decreasing the concentration of IPTG to 0.1 mM, using *E. coli* Rossetta 2 (DE3) cells expressing the protein at 20 °C for 16 hours. No band was detected using SDS-PAGE or western blot analysis from the soluble fraction of cell lysate expressing the gene, whereas the band matching the expected size of the protein was found in the insoluble fraction (Figure 6.12).

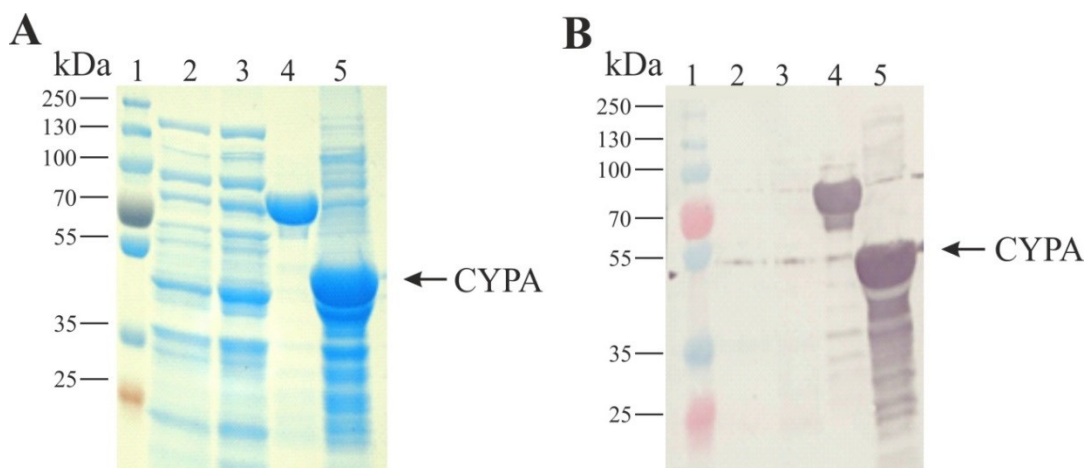


Figure 6.84: SDS-PAGE (A) and western blot (B) analysis of the expression trials of CYPA. In both A and B, 1 refers to protein markers, 2 is the lysate from empty vector, 3 is the lysate of the *E. coli* cells expressing empty vector, 4 is a His-tagged protein as a positive control for western blot, and 5 is the insoluble fraction of the total lysate expressing CYPA gene. The western blot was developed using monoclonal His-antibody.

As the protein appeared to be insoluble when expressed as an N-terminal His-tagged protein, an attempt was made to achieve soluble CYP_A by cloning the gene into pET-28(+)_a, between *Sal*I and *Nco*I restriction sites, to be expressed as a C-terminal His-tagged protein (Figure 6.13).

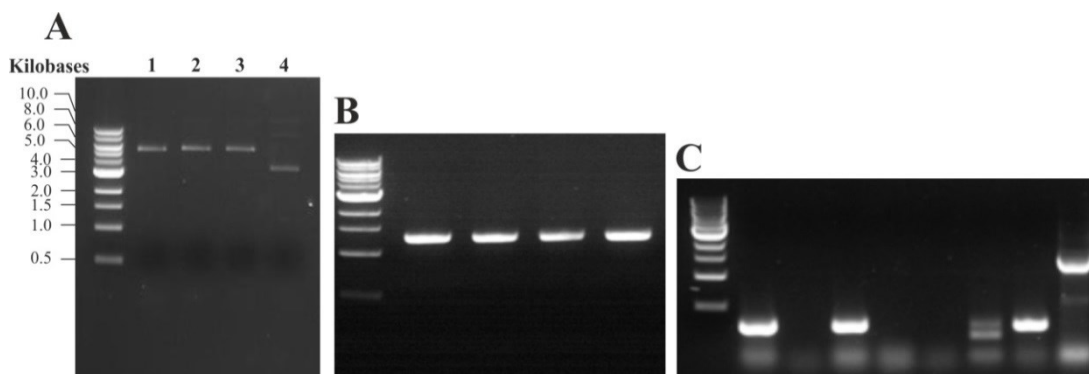


Figure 6.85: Cloning of the *cypA* gene into pET-28(+). (A) is the digestion of the pET-28(a)₊ vector; 1 is double digested plasmid with both *Sal*I and *Nco*I; 2 is the single digested plasmid with *Sal*I; 3 is the single digested plasmid with *Nco*I; 4 is undigested plasmid. (B) PCR amplification of the *cypA* gene; predicted PCR product= 1,245 bp. (C) Colony PCR of the different transformed colonies using universal plasmid primers (T7 F and R).

The *cypA*-pET-28(a)₊ construct was expressed in *E. coli* Rossetta 2 (DE3) cells and induced with 0.1, 0.25 and 0.5 mM IPTG at 20 °C for 11 hours. Soluble expression of the protein was checked by analysing the lysate by SDS-PAGE. The expected protein band was not detected in the soluble fraction of the cell lysate (Figure 6.14).

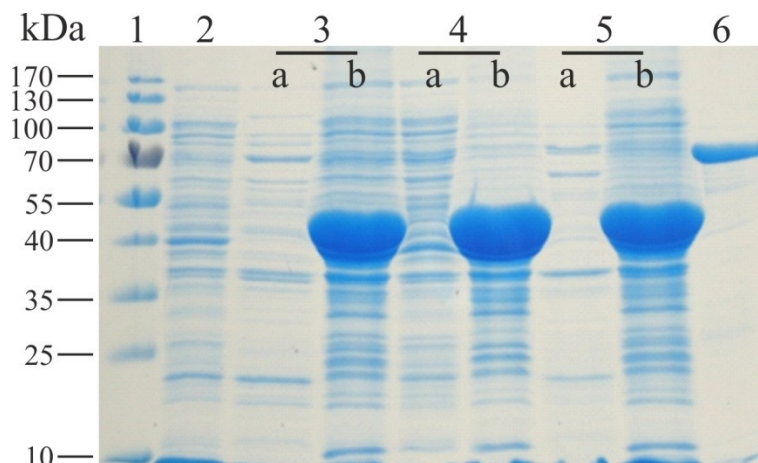


Figure 6.86: SDS-PAGE analysis for the expression trials of CYPA as a C-terminally His-tagged protein. The gel from left to right, protein marker (1), lysate of *E. coli* expressing empty vector (2), the lysate of *E. coli* Rossetta 2 (DE3) cells expressing CYPA and induced with 0.1 mM (3), 0.25 mM (4), 0.5 mM IPTG (5), purified His-tagged protein (6). (a) and (b) refer to the soluble and insoluble fractions, respectively.

Further attempts to achieve soluble expression of CYPA were made by expressing the gene at 15 °C for 21 hours in the *E. coli* Rossetta 2 (DE3) and *E. coli* ArticExpress cells induced with 0.1, 0.25 and 0.5 mM IPTG. Again, no band was detected in the soluble fraction of the cells in SDS-PAGE corresponding to CYPA (Figure 6.15).

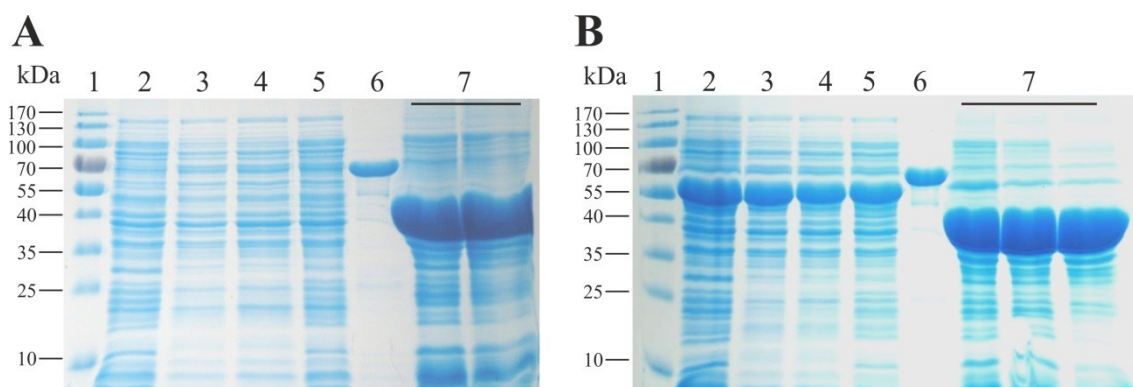


Figure 6.87: SDS-PAGE analysis of expression trials for CYPA in *E. coli* Rossetta 2 (DE3) (A) and ArticExpress (B). In both A and B, 1 refers to protein markers; 2 is the total lysate of *E. coli* expressing empty vector; 3, 4 and 5 are the total lysate of *E. coli* expressing CYPA and induced with 0.1, 0.25 and 0.5 mM IPTG, respectively. Number 6 is the purified His-tag protein, 7 is the insoluble fraction of *E. coli* expressing protein.

Furthermore, soluble CYPA was not detected by SDS-PAGE analysis of the soluble cell lysate of *E. coli* Rossetta 2 (DE3) grown in LB and induced by 0.1, 0.25 and 0.5 mM IPTG at different growth stage (after 3, 5, 7, and 16 hours from induction) (Data not shown).

A bioinformatics approach was taken to investigate if CYPA has transmembrane peptides. Sequence analysis of the protein was carried out using both Dense Alignment Surface (DAS)-Transmembrane prediction [172] and the HMMTOP web service [173, 174]. According to the DAS-Transmembrane prediction web service, residues Ile-261 to Gly-264 encode a transmembrane region in CYPA (Figure 6.16), whereas HMMTOP predicted the Ala-246 to Leu-265 region to be transmembrane helices.

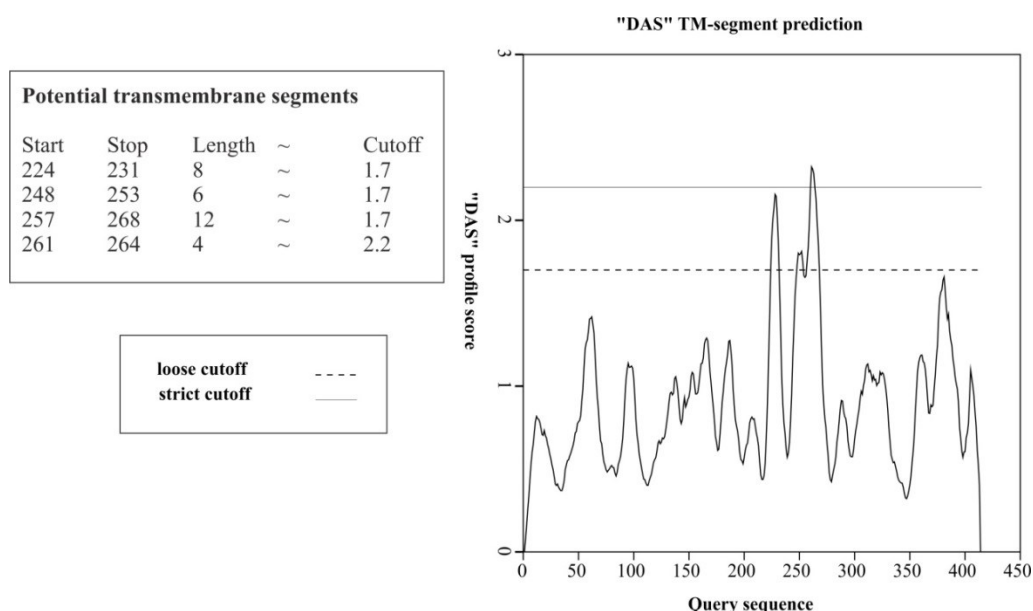


Figure 6.88: Prediction of the transmembrane region in the CYPA protein using DAS-Transmembrane prediction. Reproduced from the DAS-transmembrane website (<http://www.sbc.su.se/~miklos/DAS/>).

Sequence alignment of the CYPA with the XplA-heme domain showed that both predicted transmembrane regions are also conserved in XplA-heme domain (Figure 6.17), suggesting that this is unlikely to be the cause of the insolubility. However, the 20 amino acid sequence at the N-terminus of CYPA was not found in the XplA-heme domain and was therefore identified as the potential cause of insolubility (Figure 6.17).

```

XplA_heme -----MTAASIDRELVPWSDPEFRNPNYPWYRRLQDDHPVHKLED 40
CYPA      MSDIQAAINQEINVTTTRPLEATSTSPTYQHFPWDKPEFTLDPYPWYARALREAFVIYDDL 60
          *:* :.*.*** :***** * : * * :
XplA_heme GTYLVSRYADVSHFAKLPIMSVPEPGWADAGPWAVASDTALGSDPPHHTVLRRTQNKWFTP 100
CYPA      GFYIVSRYEDVMEFGKHPSMSVEPGWQAGPWAVVRDFTVIGKDLDPHTRLRRQTNKWFGP 120
          *:*.*.* * .*. * * * * * * * * * * * * * * * * * * * * * * * * * * * * *
XplA_heme KLVDGWVRTTRELVGDLIDGVEAGQVIEARRDLAVVPTHVTHMARVLQLPEDDADAVMEAM 160
CYPA      KVVDKWTMTTKAVTDELLAARPD-NLLDGWHDL SVLPHTQTMCRVLGVTEAGAGDVQESM 179
          *:* * . * * : : . : * * . : : : : . * * : * * * * * * * * * * * * * * *
XplA_heme FEAMLMQSAEPADGDVDRAAVAFGYLSARVAEMLEDKRVNPGDGLADSLDDAARAGEITE 220
CYPA      FETMPMLAAIPIERGTLGRAEKGFDELTA RLDELIIEKRNPDAGLLSLLSAAANGEISD 239
          *:* * * : * * * * : * * . * . * * * * * * * * * * * * * * * * * * * *
XplA_heme SEAIATILVFYAVGHMAIGYLIASGIELFARRPEVFTAFRNDESARAAINEMVRMDPPQ 280
CYPA      REARATALMLYSLGHMDVGYLIAAGLNIFAARPDYARYRYDGEVRDAVINEIARYDPPE 299
          * * * * * : * : : * * * * * * * * * * * * * * * * * * * * * * * * * *
XplA_heme LSFLRFPTEDEVEIGGVLEAGSPIRFMIGAANRDPEVFDDPDVDFDHTRPPAASRNLSFGL 340
CYPA      LCFYRVAKSDIAIRSVIEIPAGSKVRFMIGAANRDPDVFSDPQEFTHPDRPSRESRNLSFGV 359
          * . * * . . . * : * . * * * * * * * * * * * * * * * * * * * * * * * *
XplA_heme GPHSCAQIISRAEATTVFAVLAERYERIELAEPTVAHNDFARRYRKLPIVLS- 394
CYPA      GSHSCVGQHISRAQARVVFVDVLADHFSGIEFAGAVEMDNTDFSRHFTSLPLRLIP 414
          * . * * * * * * * * * * * * * * * * * * * * * * * * * * * * * * * *

```

Figure 6.89: Sequence alignments of the CYPA and XplA heme domain. The yellow highlighted region is the transmembrane region according to the HMMTOP service, the underlined residues are those predicted to be transmembrane by DAS. Gray highlighted residues are those amino acids which are missing in the XplA-heme domain. Sequence alignments were performed in (<http://www.ebi.ac.uk/Tools/msa/clustalw2/>).

To investigate if removing the 20 amino acids from the N-terminus of CYPA would enhance the solubility of the protein, a truncated version of *cypA* was cloned into pET-16b, at the same previously digested restriction sites, to be expressed as N-terminally His-tagged protein (Figure 6.18).

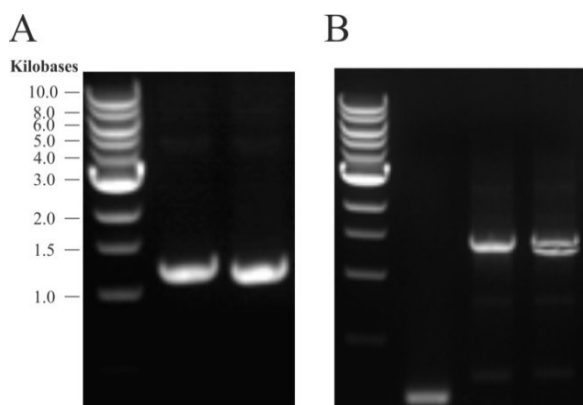


Figure 6.90: Cloning steps of the truncated *cypA* gene into previously digested pET-16b. (A) PCR amplification of the insert (truncated *cypA*); PCR product size= 1,185 bp. (B) Colony PCR of the different transformed colonies using universal plasmid primers.

The truncated-CYPA was expressed in *E. coli* Rossetta 2 (DE3) by inducing with 0.1, 0.5 mM IPTG at 20 °C. Soluble expression of the protein was checked 15 hours after induction. A band at the expected size of the protein was detected by western blot in the soluble lysate using His-antibody (Figure 6.19).

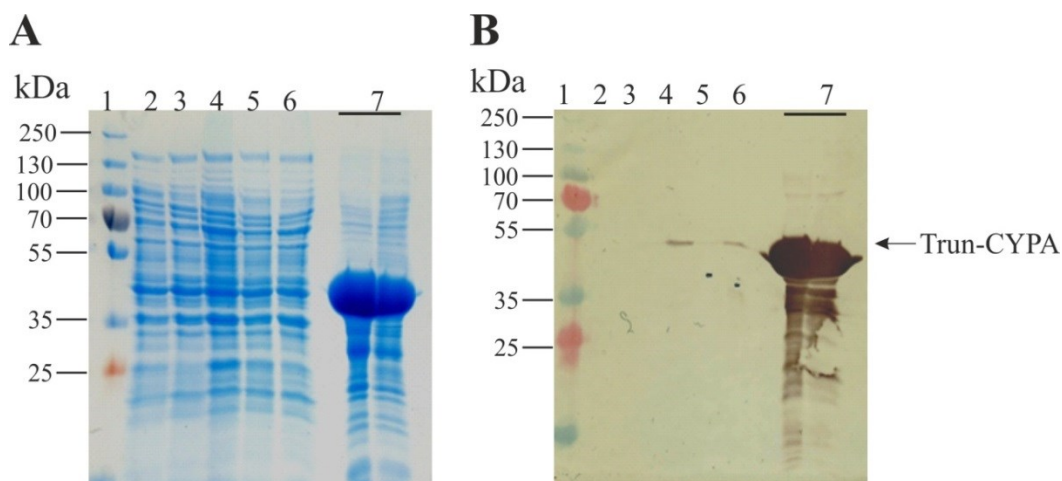


Figure 6.91: Expression of CYPA as a truncated protein in pET-16b. (A) is a SDS-PAGE gel and (B) is a western blot of the expression trial. 1 is protein molecular markers; 2 is the cell lysate before induction; 3 and 4 are the soluble cell lysate induced with 0.1 mM IPTG after 3 hours and 14 hours. 5 and 6 refer to the cells induced with 0.5 mM IPTG after 3 and 15 hours, respectively. 7 is the insoluble fraction of the cell expression line.

In order to increase the amount of soluble protein, expression levels of truncated CYPA were monitored after 12 hours from induction in the *E. coli* Rossetta 2 (DE3) cells with 0.1, 0.5 and 1 mM IPTG at 20 °C. No significant increase in the expression level of the soluble protein was observed in western blot analysis of the cell lysate (Figure 6.20).

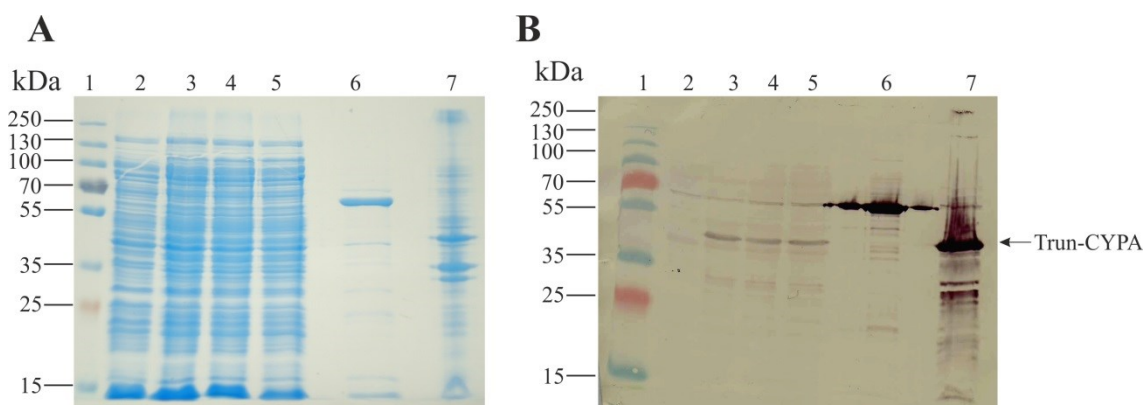


Figure 6.92: SDS-PAGE (A) and western blot (B) analysis for the expression trial of truncated-CYPA in pET-16b. In both (A) and (B), 1 is protein markers; 2 is the lysate from empty vector; 3, 4 and 5 are the lysate from the cells induced with 0.1, 0.5 and 1 mM IPTG, correspondingly. 6 refer to a purified His-tagged protein as a positive control for western blot. 7 is the insoluble fraction of the cells expressing truncated CYPA. The western blot was developed with a His-antibody.

Although the expression level of the protein was very low, an attempt was made to purify the protein using 5 ml HisTrap FF crude column on the AKTA-purifier system. Two bands were present in the SDS-PAGE analysis of the elution fractions, and just one of the bands was detected in western blot analysis using monoclonal His-antibody (Figure 6.21).

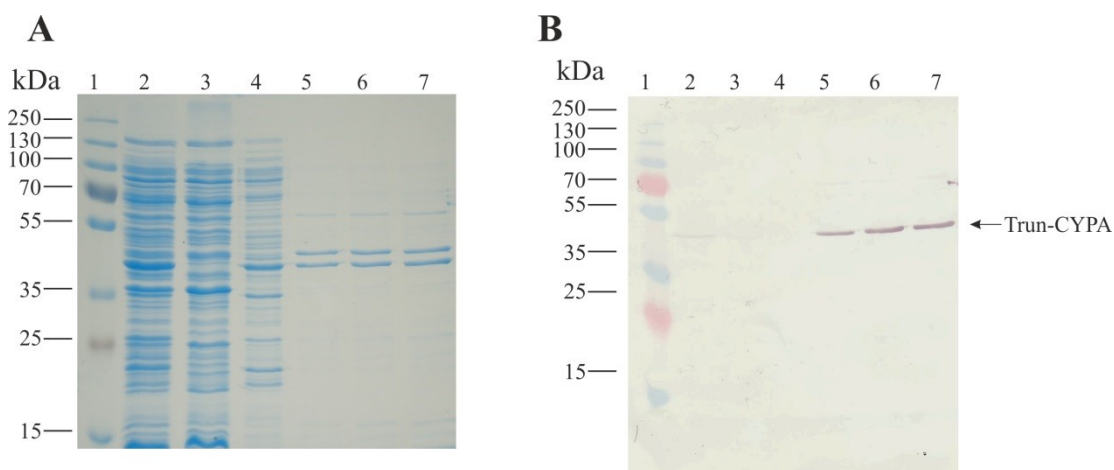


Figure 6.93: SDS-PAGE (A) and western blot analysis (B) for the purification steps of truncated CYPA. In both (A) and (B), 1 is protein markers, 2 is the *E. coli* cell lysate, 3 is flow-through, 4 is unbound proteins, 5, 6 and 7 are purified proteins. The western blot was developed with a His-antibody.

Both bands were sent for MALDI-MS protein identification (Chapter 2.7.5); the top band was identified as CYPA and the lower band as elongation factor Tu from *E. coli*.

6.3.2 Spectrophotometric analysis of the putative cytochromes P450

Spectrophotometric analysis was carried out on the purified GT-XplA, truncated CYPA and CYPB. Absorbance peaks for GT-XplA, truncated-CYPA and CYPB were found at 420, 422 and 416 nm, respectively (Figure 6.22). The spectral shift of the cytochrome P450 from 420 to ~450 nm upon CO binding of the reduced form was seen for GT-XplA and CYPB, but not for the truncated-CYPA (Figure 6.22).

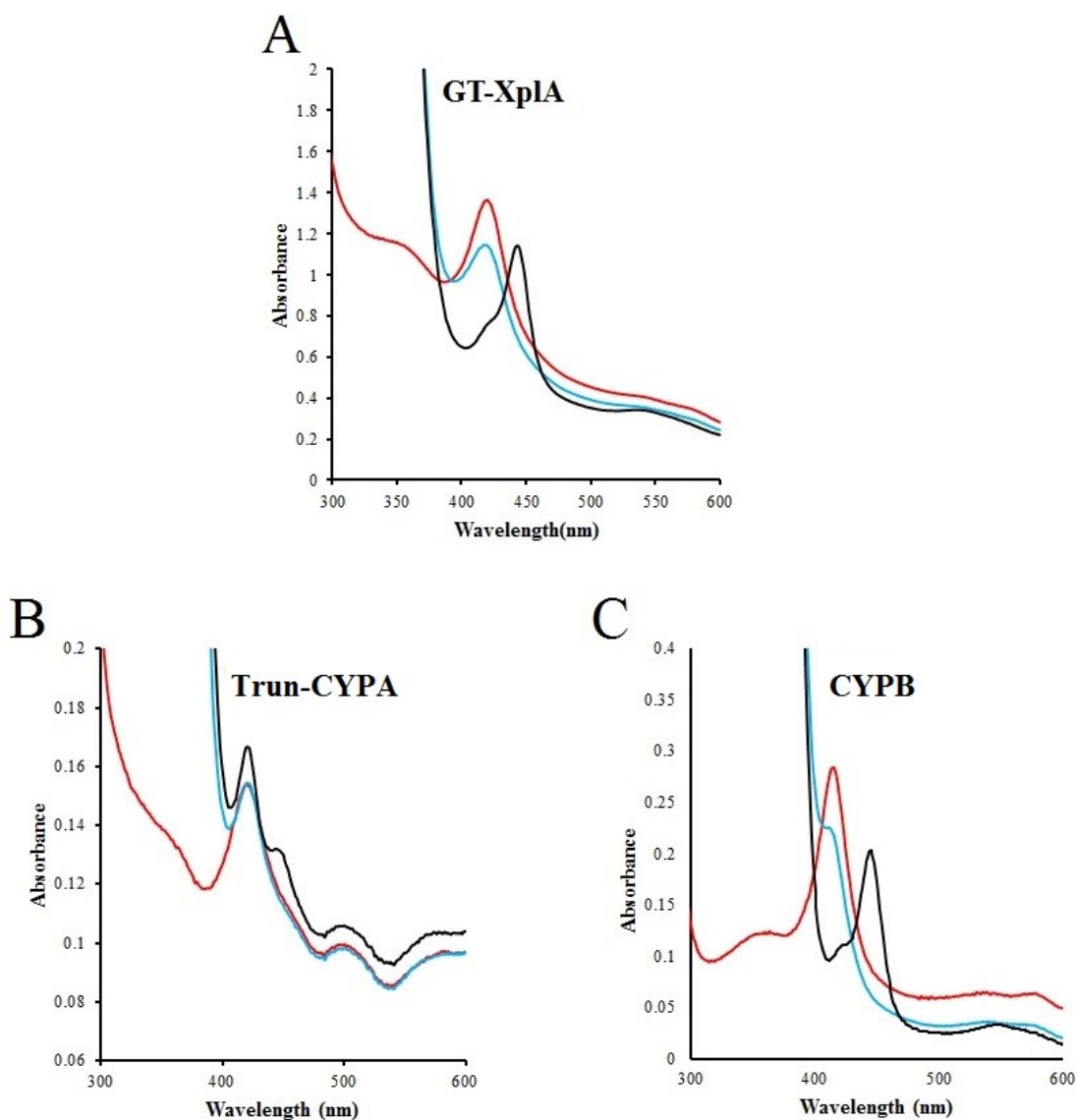


Figure 6.94: UV-visible spectra of the purified GT-XplA, Truncated-CYPA and CYPB proteins in oxidised form (red line), reduced with sodium diethionate (blue line), and reduced CO-bound (black line) forms.

In cytochromes P450, the spectral shift from ~420 (low spin) to 390 nm (high spin) indicates the positive binding of the enzyme to the substrate. However, such a spectral shift was not seen for GT-XplA, truncated-CYPA and CYPB after the addition of 100 μ M RDX (Figure 6.23).

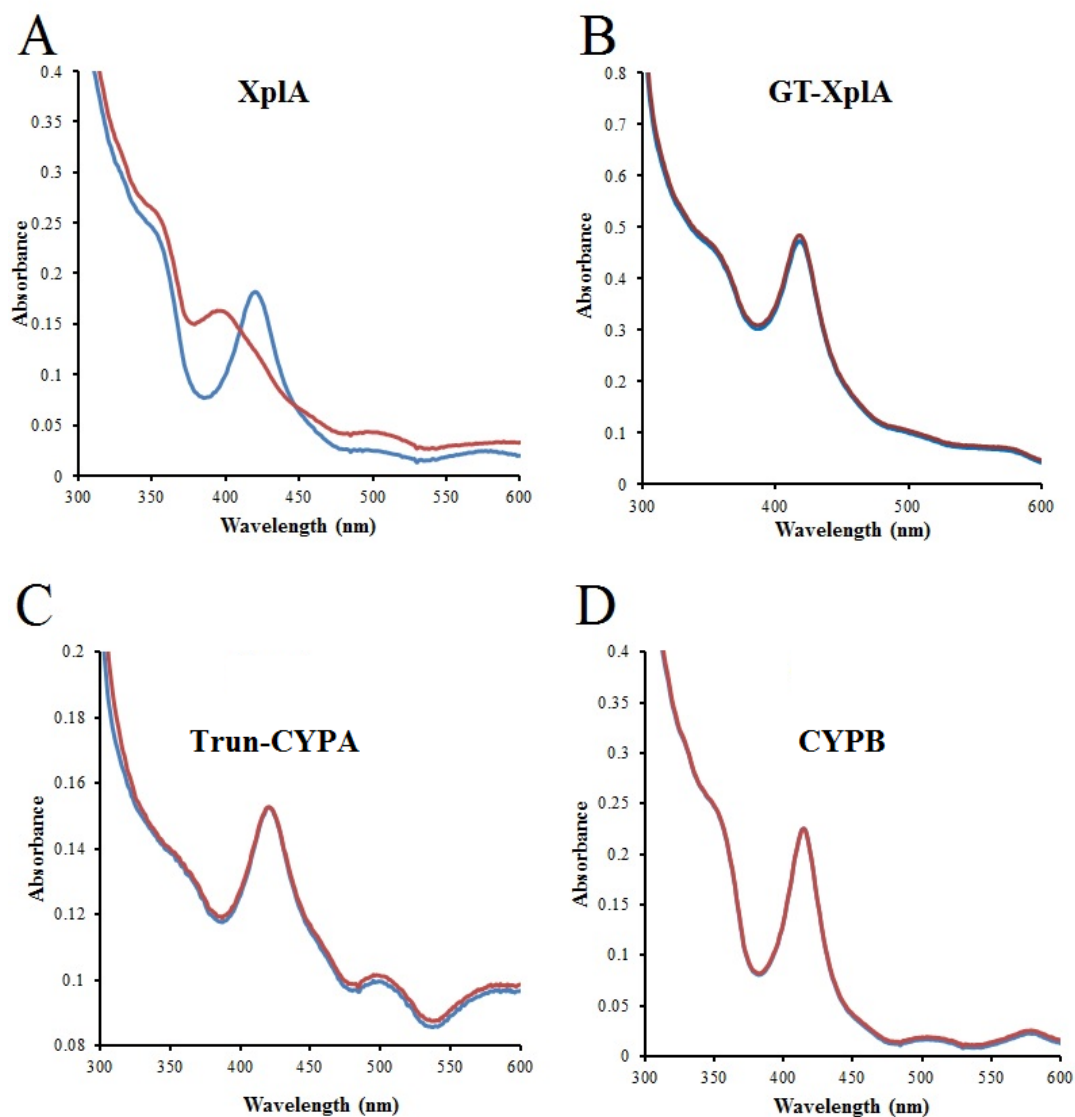


Figure 6.95: UV-visible spectra for RDX-binding of GT-XplA, truncated-CYPA, CYPB and purified XplA (positive control). The red line is the peak of the corresponding protein before adding of RDX, while, blue is the peak of the protein after the addition of 100 μ M RDX.

6.3.3 Mutagenesis study and whole cell activity assay

As spectrophotometric analysis of the purified proteins was suggesting that the putative cytochrome P450s do not have activity toward RDX, site directed mutagenesis was applied to see if targeting specific residues by site directed mutagenesis could produce variants with activity towards RDX. The mutagenesis study was carried out for GT-XplA and truncated-CYPA by substituting residues in the putative active site of each protein with those observed in the active site XplA-heme. The mutant forms of each protein were created as described in Chapter 2.6.13 (Figure 6.24).

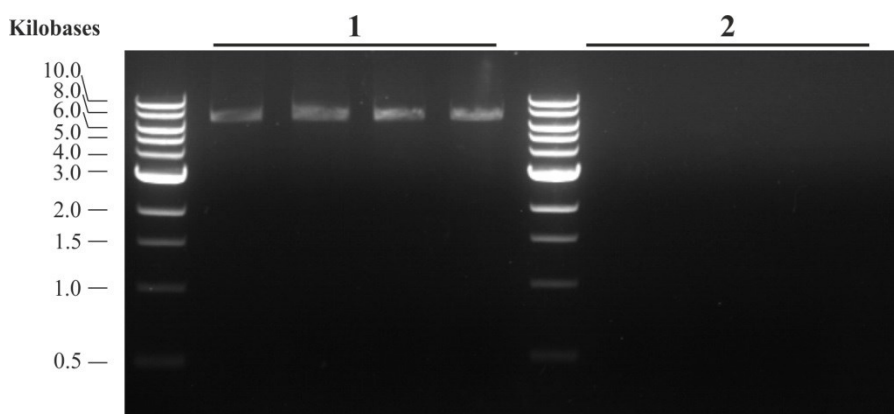


Figure 6.96: Example of an agarose gel from the mutagenesis experiment of the cytochromes P450. Number 1 refers to the PCR products of the mutant strands, 2 is the negative control of the same mutagenesis experiment.

Overall, two mutations in GT-XplA (single mutant and double mutants), with six mutations of truncated-CYPA (single to hextuple mutants) were created by site directed mutagenesis (Table 6.3).

Table 6.10: Mutant constructs generated from truncated *cypA* and *gt-xplA*

| Construct | Mutant forms of the construct | Location of the mutated residue |
|------------------------------|---|--|
| Truncated-<i>cypA</i> | CYPA- D256A | Heme Binding Pocket |
| | CYPA- D256A, E299Q | Heme Binding Pocket |
| | CYPA- D256A, E299Q, P184L | Bounded the large channel of XplA |
| | CYPA- D256A, E299Q, P184L, L252V | Heme Binding Pocket |
| | CYPA- D256A, E299Q, P184L, L52V, M248V | Heme Binding Pocket |
| | CYPA-D254A, E299Q, P184L, L252V, M248V, I100L | Heme Binding Pocket |
| <i>gt-xplA</i> | GT-XplA(N396A) | Heme Binding Pocket |
| | GT-XplA(N396A, P395M) | Heme Binding Pocket |

The first two mutants of Truncated-CYPA (CYPA- D256A and CYPA- D256A, E299Q) were tested to see if the mutation would enhance the solubility of the protein. However, neither of the mutants appeared to more soluble compared to the wild-type of truncated-CYPA (Figure 6.25).

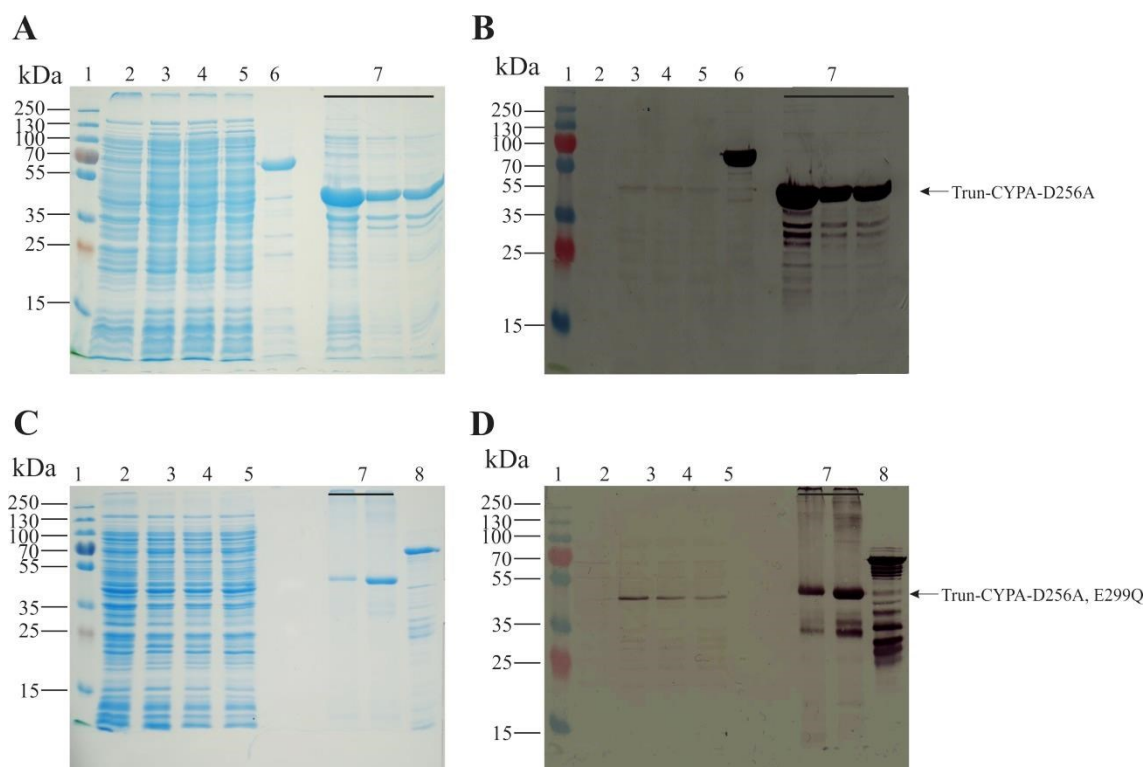





Figure 6.97: Expression trials for single and double mutants of the truncated-CYPA. SDS-PAGE (A) and western blot (B) analysis of the single mutant truncated-CYPA. In both A and B, 1 is a molecular markers; 2 is the lysate of the empty vector; 3,4 and 5 are lysate of the cell induced with 0.1, 0.5 and 1 mM IPTG, respectively; 6 is the positive control and 7 is the insoluble fraction from the lysate expression the mutant. C and D are SDS-PAGE and western blot analysis for the double mutant truncated-CYPA. 1 refers to a protein markers, 2 is the cell lysate expressing the empty vector, 3, 4 and 5 are the cell lysate expressing truncated-CYPA induced with 0.1, 0.5 and 1 mM IPTG. Number 7 is insoluble fraction of the protein. 8 is a His-tagged purified protein as a positive control for the western blot.

Whole cells of *E. coli* expressing the cytochromes P450 and mutant form of GT-XplA and truncated-CYPA were tested for RDX degradation capacity using the whole cell assay. In this assay, *E. coli* Rossetta 2 (DE3) expressing each construct was tested for RDX-degradation capacity using the colorimetric Griess assay to monitor the production of nitrite from RDX. Interestingly, the pink colour indicative of nitrite production in the Griess assay was detected in the quadruple, pentuple and hextuple mutants of truncated-CYPA after 24 hours incubation with RDX. After 48 hours, a strong pink colour was observed for the double, triple and quadruple mutant of CYPA, with a faint colour from a single mutant of Gt-XplA (Table 6.4).

Table 6.11: Preliminary results from the whole cell assay of the XplA-homologues and mutants toward RDX by Griess assay. The pink colour indicates release of nitrite in the culture.

| <u>14 hour</u> | <u>24 hours</u> | <u>48 hours</u> | <u>Constructs</u> |
|--|--|--|---|
|  |  |  | CPYA (C-terminally His-tagged in pET-28(+))a) |
| | | | CYPB(N-terminally His-tagged in pET-16b) |
| | | | CYPA (N-terminally His-tagged in pET-16b) |
| | | | Trun-CYPA (N-terminal His-tagged in PET-16b) |
| | | | Trun-CYPA (D256A) |
| | | | Trun-CYPA (D256A, E299Q) |
| | | | Trun-CYPA (D256A, E299Q, P184L) |
| | | | Trun-CYPA (D256A, E299Q, P184L, P184L, L252V) |
| | | | Trun-CYPA (D256A, E299Q, P184L, P184L, L252V, M248V) |
| | | | Trun-CYPA (D256A, E299Q, P184L, P184L, L252V, M248V, I100L) |
| | | | P450 domain (positive control) |
| | | | GT-XplA |
| | | | GT-XplA (N396A) |
| | | | GT-XplA (N396A, P395M) |
| | | | XplA in pET-16b (positive control) |
| | | | Empty vector (pET-28(+))a) |
| | | | Empty vector (pET-16b) |

6.4 Discussion

Ancestral XplA cytochromes P450

In silico sequence analysis revealed that GT-XplA shares 45 % sequence identity with XplA isolated from RDX-degrading bacteria. Additionally, GT-XplA has a flaxodoxin domain fused N-terminally to the heme domain of the protein, an arrangement that was previously unique to all *xplA*-containing bacteria. Purified GT-XplA did not show the expected spectral shift from 420 to 390 nm after addition of 100 μ M RDX, and nitrite was not detected in the whole cell experiment by Griess assay, suggesting that RDX is not a substrate for GT-XplA. This inability to catalyse denitrify RDX is likely to be due to the overall differences in the GT-XplA sequence, and particularly within the putative heme binding site, when compared to the XplA-heme binding site. A single amino acid residue difference in the active site of an enzyme can have marked effect on activity, for example, melamine deaminase (TriA) has 98 % amino acid sequence identity with the entire sequence of atrazine chlorohydrolase (AtzA) enzyme although neither enzyme has detectable activity with their respective substrate [16]. Site directed mutagenesis, a classical approach to investigate the effect of single mutations on protein function [175], was used to substitute two of the different residues in the putative active site of the GT-XplA to those present in the XplA-heme domain binding pocket. The mutant constructs of GT-XplA, along with the other constructs reported in the work, were tested for RDX-degrading activity using *E. coli* whole cell assays to detect nitrite release from RDX-denitration using the colorimetric Griess assay.

While GT-XplA does not have any RDX-degradation capacity, a pink colour was observed in the medium from *E. coli* cells expressing the single mutant (N396A) of GT-XplA. This result suggests there is an evolutionary relationship between these two proteins, and further supports the importance of A396 (which is equivalent to A395 in XplA) in the denitration step in the active site of the protein. A similar mutagenesis study on the *R. rhodochrous* 11Y XplA-heme also showed that A395 to be important for the activity of the XplA-heme with a A395T mutant of the XplA-heme decreasing the activity of the enzyme ~200 folds [99]. Changing the substrate specificity of an enzyme through a single mutation is not unusual, for example, the activity of *N*-acetylornithine transcarbamylase (AOTCase) can be converted to *N*-succinylornithine transcarbamylase (SOTCase) activity via a single mutation in the active site of E92 to

P, S, V or A. Mutation of the corresponding residue of E92 in SOTCase, (which is P90), to E reversed the activity of the SOTCase to AOTCase [176].

The inability to detect nitrite from whole cell assays on the double mutants (N396A, P395M) of the GT-XplA, under the preliminary experiments conducted, suggests that the second mutation (P to M) impairs the activity of the single GT-XplA (N396A) mutant, i.e. proline is a preferential residue in that position for the RDX-dentritration activity of GT-XplA (N396A). It would be interesting to investigate if XplA activity could be increased in a M394P mutant. In some cases, substituting a residue has enhanced the activity of the protein, for example the hydroxylation activity of the cytochrome P450 monooxygenase (or vitamine D3 hydroxylase, Vdh) is increased by ~80 fold through a single mutation (T107A) in the putative Fdx-binding site of the protein [177]. Mutation of the corresponding residue of P395 in the *R. rhodochrous* 11Y XplA-heme (M394 to L) slightly affected (only by two fold) the activity of the XplA-heme enzyme [99], although it did increase the ability to bind to HMX (with K_D 4.33 μ M).

Of all the cytochromes P450 currently described in the databases, CYPA has the highest sequence identity (> 50 %) with the heme domain of XplA. Additionally, the putative active site of CYPA was shown to have one, which is M255, of the two hydrophobic residues (M394, A395) in common with XplA, in the place of the highly conserved acidic Glu/Asp residues in other P450s. Furthermore, the tertiary structure of the putative heme binding site appears to closely resemble the XplA-heme domain binding site. Although cytochromes P450 from prokaryotic organisms are generally considered to be cytosolic, and expressed as soluble proteins [178, 179], the soluble CYPA could not be produced in *E. coli* under the T7 promoter. Previously, *xplA* from *R. rhodochrous* 11Y also could not be expressed as a soluble protein under the same promoter using pET-11a and pET-16b vectors [180] without supplying the *E. coli* cells with ALA, FeCl₃, and riboflavin as a heme precursors [181]. Soluble XplA protein was obtained in pET-16b after addition heme precursors [98]. Although all expression trials of the CYPA were carried out in the presence of the ALA, riboflavin and FeCl₃, no soluble protein was detectable by either SDS-PAGE or western blot. One commonly known reason for protein insolubility is from over expression of the protein, which can result in the formation of incorrectly folded protein and aggregation in inclusion bodies [182]. However, decreasing the rate of protein expression by lowering temperature, IPTG

concentration and harvesting the cells in the different growth stage were unsuccessful. A different approach to expressing CYPA as a soluble protein was taken by changing the location of the His-tag attached to the CYPA protein sequence. Studies have shown that the location of the His-tag can affect expression [183], as well as the solubility level of the protein [183, 184]. Again the protein was found in the insoluble fraction when CYPA was expressed as a C-terminally His-tagged protein.

A putative transmembrane region [172-174] was considered to be artifactual as it was also conserved in the XplA heme domain, which has been successfully expressed as a soluble protein [98]. Truncating CYPA by deleting the 20 amino acids from the N-terminus in the region which are not present in XplA-heme, resulted in the production of soluble protein, possibly implying that the region is a transmembrane sequence. However, the spectral shift from low spin to high spin was still not observed, and nitrite was not detected after addition of RDX suggesting that the protein does not have activity toward RDX.

While the quadruple, pentatuple and hextuple mutants of truncated-CYPA all had activity towards RDX at 24 hours' time point, as activity was not observed for the triple mutant; adding the fourth mutation (L252 to V) in truncated-CYPA appears to be the key to gaining denitration activity. Although there are no data available on the effect of mutating the corresponding residue (V391) on RDX-degradation by XplA-heme, the structure of the XplA-heme, with the ligand imidazole, shows H-bonding of the residue with A395 to imidazole through a water molecule (Figure 6.26) [99].

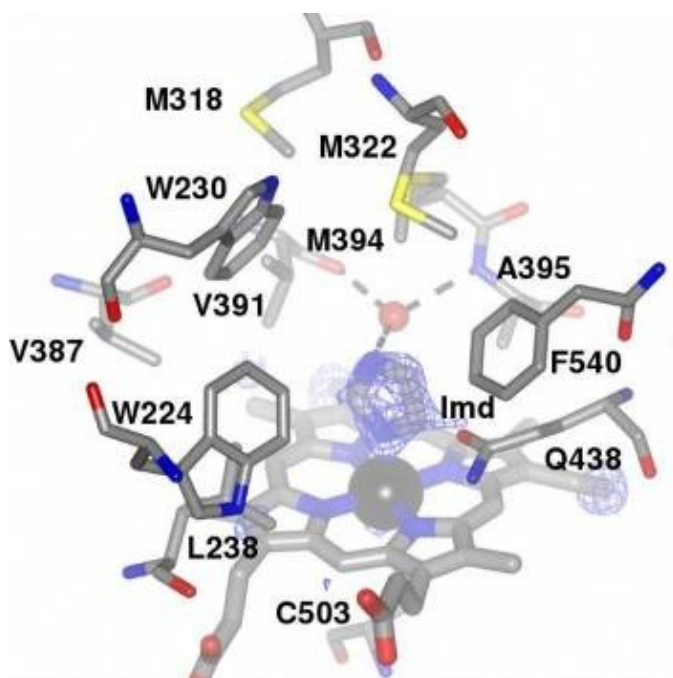


Figure 6.98: The residues located in the heme binding site of XplA. The ligand imidazole (labeled as Imid) is bound to the active site. Reproduced from Sabbadin *et al.* (2009) [99].

The RDX-denitration activity was also detected for the double and triple mutants of truncated-CYPA showing that these two mutations are enough to confer RDX-degrading activity in truncated CYPA. Furthermore, these results show the importance of adding the second mutation (E299Q) in the truncated-CYPA (D256A). The E299 corresponds to Q438 in the XplA-heme, which is located in the heme binding pocket and projects towards the centre of the heme within H bonding distance of the imidazole ligand [99] (Figure 6.26). The Q438A mutant of XplA-heme decreases the k_{cat}/K_M value by 17 times in comparison to the wild-type XplA-heme [99]. The decrease in pink colouration of the Griess assay on the quadruple, pentatuple and hextuple mutants of truncated-CYPA at 48 hour time points may have been due to the reducing of free nitrite in the medium by *E. coli* through the expression of nitrite reductase genes *nrfA* [185].

The CYPB was found to have 36 % identity with XplA-heme domain, but the proteins encoded by the genes upstream of *cypB* also share sequence homology to the flavodoxin domain, and XplB from RDX-degrading bacteria. Although the CYPB was successfully expressed and purified, spectrophotometric analysis and Griess assays indicated that it

was not active towards RDX. Mutagenic studies were not applied to this protein due to the number of differences in the putative active site of the protein in comparison to the XplA-heme binding pocket.

Due to time restrictions, no further experiments or characterisation of the constructs were carried out, however the preliminary results of the whole cell assay for the GT-XplA and truncated CYPB could be further improved by optimising the expression conditions, especially in case of CYPB. Solubility and activity might be increased by co-expression with XplB.

Overall the results presented here, combined with the knowledge that the XplA homologues are from bacteria belonging to *Actinomycetales* order like all the *xplA*-borne RDX-degrading bacteria characterised to date, suggest that these cytochromes P450 could share a common ancestor with the XplA.

Origin of the *xplA* and *xplB* genes

The genes surrounding *gt-xplA* and *cypB* share both sequence similarity and arrangement with those in *xplA* gene cluster in RDX-degrading bacteria. Genes encoding for the XplB like protein and flavodoxin reductase are found in the same operon *cypB* and *gt-xplA* and the gene products share sequence homology with XplB and the flavodoxin domain of RDX-degrading bacteria. Furthermore, the previously identify cytochrome P450 from *Erwinia carotovora subsp. atroseptica*, which has 41 % identity to XplA [99], is also in the operon which have 52 % and 35 % sequence identity to the flavodoxin domain and XplB in RDX-degrading bacteria. Moreover, all RDX-degrading bacteria tested for *xplB* and *xplA* in the same order (Chapter 4). This observation suggests that the genes encoding for the *xplB*, flavodoxin domain and cytochrome P450 domain might have evolutionary relationship, or they were ‘born together’, as the Natal model suggested [186], rather than they became clustered together because of a fitness advantage as postulated by the Fisher model [186].

Chapter 7: Final Discussion

7.1 Final discussion

Previous studies have been performed over recent years to isolate bacteria that can degrade RDX, to elucidate the enzymes involved in RDX degradation, and to explore the potential applications of XplA/XplB to clean up RDX contaminated sites [84, 86-89, 95, 96, 98, 100, 101, 103, 106, 112-114, 128]. This study builds on the knowledge gained so far to gain a further understanding of the mechanisms by which bacteria have evolved to metabolise this novel compound. Focusing mainly on the evolutionary aspects of aerobic RDX degradation by bacteria, the results presented here emphasise the fascinating capacity of bacteria to adapt to previously unseen compounds. Following the rapid evolution of *xplA* from an, as yet, unknown gene, *xplA* and *xplB* have been subsequently distributed around the world within a genomic island through horizontal gene transfer.

Chapter 3 described the selective enrichment procedures that were carried out on explosive-contaminated soil. The soil was collected from distinct geographical locations with the aim of isolating, and further characterising, new RDX-degrading bacteria. The isolates were all identified as *Rhodococcus* spp. and, despite the fact that the soil used was from disparate geographical locations, all contained near identical copies of *xplA*. That only rhodococci were isolated could be either due to the methodology used in the study providing a favourable environment for rhodococci to flourish, or that the results are a true reflection that rhodococci are the dominant aerobic explosive metabolising bacteria in the contaminated soil, and by extrapolation, the military sites. In support of the latter theory, *in situ* studies on microbial communities degrading RDX in contaminated sites, using fully labelled ¹⁵N-RDX, also revealed that rhodococci are the most abundant genus in explosive-polluted soils [113]. The results suggest that *Rhodococcus* has a particularly well-developed adaptive capacity. Indeed members of this Gram positive group are routinely identified for their ability to metabolise organic, xenobiotic compounds [130-133]. In all species tested, the RDX-degrading capacity was found to correlate with the presence of *xplA*; irrespective of the geographical locations from which the bacteria were isolated. Furthermore, *xplA* has been detected in all Gram positive aerobic RDX-degrading bacteria that have been tested to date [100-103, 128]. In addition to XplA, bacterial nitroreductase I [90], XenA and XenB [94] have (albeit slow) activity toward RDX. That new, non-*xplA* dependent, RDX-degrading isolated were not found in this study is perhaps surprising as there are existing nitroreductases

with low activity to RDX already present in many soil species that could be expected to evolve under the selective pressure of RDX.

Type-I oxygen-insensitive nitroreductases with the ability to transform RDX under anaerobic conditions, have been identified in *Morganella morganii* strain B2 and *Enterobacter cloacae* strain 96 [90]. Under either aerobic or anaerobic conditions, the enzyme is also able to transform TNT [90]. In a similar manner, the XenA (from *Pseudomonas putida* II-B) and XenB (from *Pseudomonas fluorescens* I-C) enzymes can also transform RDX along with a number of other explosive compounds including HMX, CL-20 and chemically related compounds [94]. The activity of XenA and XenB is greatly inhibited by oxygen, thus RDX transformation only occurred under anaerobic conditions and under artificially created “anoxic” conditions that supplied with NH_4^+ to grow [94]. In the study by Fuller *et al.* (2009) [94] several factors indicated that the products of RDX transformation have a cytotoxic effect on the cells. Firstly, it was observed that while increasing RDX concentrations negatively affected RDX transformation, increasing RDX concentration increased the RDX transformation rate of purified XenB. Secondly, increasing RDX concentrations did not inhibit the growth rates of the XenA/XenB harbouring strain under aerobic conditions, i.e. when RDX transformation is not occurring [94]. However, the exact cytotoxic mechanism of the RDX-transformation was not described [94]. Cytotoxicity of RDX toward *Pseudomonas* HK-9 has also been reported [126]. It could be concluded therefore, that the cytotoxicity of the products of RDX transformation may have exerted a negative selective pressure on the evolution of endogenous nitroreductase and Xen A/B genes. In Chapter 3, the challenge for RDX-degrading bacteria to successfully colonise explosive-contaminated soil was discussed. The co-contaminating explosive TNT exerts negative effects on RDX-degrading bacteria in two ways: Firstly, TNT directly inhibits the RDX-degrading enzyme, XplA. Secondly, TNT and its transformation products are toxic to the cells themselves. Studies using purified XplA demonstrated that while TNT inhibit the activity of XplA towards RDX, the chemically similar 2- and 4-ADNTs, as well as 2,4- and 2,6-DNT compounds had no inhibitory effect on activity. These results show that the presence of a third nitro functional group is required for inhibition of XplA. Screening of mutated XplA libraries using Griess assays in 96-well formats to track RDX denitration activity in the presence of TNT could be used to find XplA variants

that are resistant to TNT-inhibition. However, it is possible that TNT-inhibition of XplA is intrinsically linked with the RDX-transforming ability of the enzyme.

Although, *R. rhodochrous* 11Y has some TNT-transformation activity and reducing one of the nitro groups into amino groups or removing it is sufficient to stop the inhibitory effect of the compound towards XplA, this did not appear to be enough to overcome the toxicity of TNT towards growth. Therefore, it is likely that *xplA*-carrying bacteria are able to survive in TNT-contaminated sites by living in close association with TNT-detoxifying bacteria such as *Enterobacter cloacae*. The findings presented in Chapter 3 emphasise that TNT is a major environmental pollutant and more research is needed to identify low cost sustainable methods to decontaminate TNT-polluted sites.

Chapter 4 contributes towards reconstructing the evolutionary origin of *xplA* by comparing sequences of *xplA* between eleven RDX-degrading bacteria belonging to four different genera. The bacteria were isolated from distinct geographical sources at different times. Such an approach has successfully been used to estimate the evolutionary origin of the penicillin-binding protein (*pbp*) genes from *Streptococcus pneumoniae* [17]. However, in the case of *xplA*, the gene was found to be so highly conserved that it was not possible to re-construct an ancestral gene. The highly conserved nature of *xplA* strongly supports its recent evolution, and there are many examples where near-identical genes involved in xenobiotic degradation from different bacteria have been reported [146, 148-153]. There are also examples for other highly conserved xenobiotic catabolic genes amongst *Rhodococcus* spp.: the gene encoding for haloalkane dehalogenase (*dhaA*) along with a 12.5 kbp gene cluster flanking *dhla*, has been shown to be highly conserved in six haloalkane-utilising *Rhodococcus* strains isolated in five distinct geographical locations, the Netherlands, the United Kingdom, Japan, Switzerland and the United States [187]. In addition, an operon of genes involved in naphthalene degradation (*narAa, Ab, B*) share greater than 90 % sequence identity between four naphthalene-degrading *Rhodococcus* strains, strains NCIMB12038, P400, P200, CIR2, and indene-converting *Rhodococcus* sp. strain I24 [188]. Janssen *et al.* (2005) [151] proposed that finding near-identical genes either points to the sequence having been acquired originally from a “pre-industrial gene pool” and then distributed by horizontal gene transfer, or that they are continuously acquired from an identical pre-industrial sequence [151]. Mutation might also contribute to the evolution of xenobiotic degrading enzymes from previous functionally related or even

unrelated enzymes. Examples include the proposed evolution of atrazine chlorohydrolase (*atzA*) [16] and haloalkane dehalogenase (*dhlA*) [18]. In addition to highly conserved *xplA/xplB* genes, the other striking observation was that several genes surrounding *xplA/xplB* are almost identical amongst the four different genera examined. This is unusual considering that only *xplA* is required to denitrate RDX [96, 98, 105, 144] and suggests that the whole region has a single evolutionary origin, which has subsequently been distributed by horizontal gene transfer. Up to now the fitness advantage resulting from the transmission of the genes alongside *xplA/xplB* is not well understood. Studies by Chong *et al.* (2014) [144] showed that neither *marR* nor *aroP*, located upstream of *xplA/B* in *R.rhodochrous* 11Y, are directly involved in RDX-degradation [144]. The experimental transfer of RDX-degradation by bacteria via conjugation suggests that conjugation could be a possible transmission route of this gene cluster. Additionally, it is proposed that the gene cluster is part of the genomic island rather than a Class-I transposable element as suggested by Andeer *et al.* (2009) [103]. As the *xplA* gene and its homologues described in Chapter 6 have only been found within the *Actinomycetals* group, this suggests a host-specific feature of the gene and it is tempting to propose that phage might have also had role in the transmission of this gene cluster. Phage have been shown to be involved in the distribution of a 39.4 kb genomic island in *Pseudomonas putida* KT2440 and a 15 kbp pathogenicity island, SaPI1, in *Staphylococcus aureus* has already been reported [48, 189].

One curious observation from the studies presented in Chapter 4 was the finding that the plasmid reduction, intragenomic rearrangement and gene shuffling in the *xplA/xplB* region of *Gordonia* sp. KTR9; particularly, the naturally fusion of *xplB* to *glnA*; a gene encoding glutamine synthetase, a key enzyme in nitrogen metabolism. Although *xplB* from *Gordonia* sp. KTR9 has 99.8 % amino acid sequence identity to XplB from *R. rhodochrous* 11Y, the *Gordonia* XplB was not able to retain the FAD-cofactor and thus was not functional as a reductase to XplA. The importance of the Trp residue in holding FAD in XplB was shown by creation of the XplB(W384S) mutant which resulted in the loss of FAD and subsequent loss of reductase activity. Interestingly, the corresponding residue was found to be conserved in a diverse range of FAD-containing proteins which share as low as 26 % sequence identity to XplB. This indicates that the corresponding Trp is involved in retaining FAD in these other, more distantly-related proteins too. Although homology modelling suggests that Trp does not appear to be directly involved

in FAD-binding in XplB, it would be interesting to have the crystal structure of XplB to gain some insight on the role this residue plays in maintaining FAD in the active site of XplB. However, the poor solubility of XplB would make crystallising this protein challenging [98].

The lack of activity by XplB as a result of single mutation might explain why the enzyme became fused to GS might. As it is proposed by Moran (2002) that “If gene functions are rendered useless, due to redundancy within the host environment, then mutations will inactivate the sequences, and the corresponding DNA will be eroded over time through mutational patterns favoring deletion” [21]. Thus, mutation is perhaps the evolutionary route in the bacterium to further reduce and lose *xplB*. This hypothesis can be further supported by the fact that RDX was not detected in the original ecological niche from which the bacterium was isolated [114]. Furthermore, the inactivity of the XplB portion of the XplB-GS fusion could be at least one of the reasons for low RDX-degrading capacity in *Gordonia* sp. KTR9, although additional factors such as XplA expression level and the ability of the bacterium to uptake RDX could contribute, and have yet to be tested. As discussed in Chapter 4, there is also a single nucleotide substitution which resulted in a mutation from Phe-172 to Iso-172 in *Microbacterium* sp. MA1. *Microbacterium* sp. MA1 also has a lower rate of RDX degradation compared to *R. rhodochrous* 11Y, and the Phe-172 to Iso-172 mutation could be the cause. While beyond the scope of the studies presented here, site-directed mutagenesis studies are underway on *Microbacterium* sp. MA1 to investigate this further.

Sequence analysis of the GS portion of the *Gordonia* sp. KTR9 GS-XplB fusion revealed that it belonged to the Class-I α [155]. Although the truncated protein lacked 15 % of the C-terminal region, spectrophotometric assays revealed that the protein is active. The nitrogen regulatory role of GSI- α from *Bacillus subtilis* through feedback-inhibition of the glutamine mechanism has been reported [156, 158, 166]. Appearance of *glnA* in the same operon as *xplB/xplA* suggests a potential role for GS in the regulation of cellular nitrogen levels, something that could be investigated further by knock-out mutations of *glnA*.

In Chapter 6, the evolutionary origin of *xplA* was further investigated. Three strategies were proposed to study the origin of gene; first, by comparing genes from different

bacterial species. Secondly by searching for homologues of the gene in bacteria lacking the desired ability. Thirdly by searching for homologous genes in metagenomic libraries [151]. Using the first and third strategies was not possible as *xplA* was found to be too highly conserved amongst the studied RDX-degrading isolates (Chapter 4) and in the metagenomic database. However, the sequence analysis of the *xplA* homologues, *gt-xplA* in *Gordonia terrae* strain NBRC 100016 and *cypA* and *cypB* from *Gordonia polyisoprenivorans* NBRC 16320 strongly suggested an evolutionary relationship between these putative cytochromes P450, particularly both GT-XplA and CYPA, with XplA. Despite technical obstacles in the expression of CYPA as a soluble protein, preliminary data from whole cell assays for CYPA as well as Gt-XplA mutant constructs gave an indication that there is indeed an evolutionary relationship between the putative cytochromes P450 and XplA, and that perhaps they share a common ancestor with XplA. It would be interesting to investigate potential natural substrates for GT-XplA and CYPA. Furthermore, the identity between these putative cytochromes P450 and XplA, perhaps not surprisingly, suggests that bacteria acquired RDX-degrading capacity through the modification of *xplA*-like genes which might have had another cellular activity. Moreover, while RDX is a substrate for XplA, it may have activity towards other substrates, although none have yet been discovered despite extensive screening studies. It would not be surprising if closer XplA homologues appear in databases in the future. The question of whether there is a natural substrate for XplA therefore currently remains unanswered: Oxidation activity of XplA towards methyl tolyl and methyl phenyl sulfides, to produce sulfoxides has been reported [95]. XplA was also reported to have activity towards the RDX denitration products MNX and TNX [190].

In conclusion, the originality of the studies presented here can be summarised as follows:

- 1- Although TNT is known to strongly inhibit XplA activity, dinitrotoluenes do not inhibit XplA activity.
- 2- *xplA* is part of a large genomic island and the genomic island has a single evolutionary origin.
- 3- XplB-GS from *Gordonia* sp. KTR9 is inactive as a reductase, as a result of both fusing the protein to GS and substitution of Trp to Ser. However, GS fused with

XplB is active; belong to Class I- α and perhaps works as a nitrogen regulatory protein.

- 4- The evolutionary relationship between CYP_A, Gt-XplA and XplA was shown through site-directed mutagenesis and strongly suggests an evolutionary relationship between all three enzymes, possibly sharing a common ancestor.

List of Abbreviations

| | |
|---------|--|
| °C | degree(s) celsius |
| µg | microgram |
| µL | microlitre |
| µM | micromolar |
| 2,4-DNT | 2,4-dinitrotoluene |
| 2,6-DNT | 2,6-dinitrotoluene |
| 2-ADNT | 2-amino-4,6-dinitrotoluene |
| 4-ADNT | 4-amino-2,6-dinitrotoluene |
| ALA | 5-aminolevulinic acid |
| APS | Ammonium persulphate |
| BLAST | Basic Local Alignment Search Tool |
| BSA | Bovine Serum Albumin |
| CO | Carbon Monoxide |
| DMSO | Dimethyl sulfoxide |
| DNA | Deoxyribonucleic acid |
| dNTP | Deoxyribonucleotide triphosphate |
| DNX | Hexahydro-1,3-dinitroso-5-nitro-1,3,5-triazine |
| FAD | Flavin adenine dinucleotide |
| GST | Glutathione S-transferase |
| His-tag | Polyhistidine tagged |
| HMX | Octahydro-1,3,5,7-tetranitro-1,3,5,7-tetrazocine, High melting explosive |

| | |
|-------|---|
| HMX | High Melting Point eXplosive or Her Majesty's eXplosive |
| HPLC | High Pressure Liquid Chromatography |
| HS | High Spin |
| IPTG | Isopropyl β -D-1-thiogalactopyranoside |
| L | litre |
| LB | Luria-Bertani medium |
| M | molar |
| mM | millimolar |
| MNX | Hexahydro-1-nitroso-3,5-dinitro-1,3,5-triazine |
| NADPH | nicotinamide adenine dinucleotide phosphate, reduced form |
| NCBI | National Center for Biotechnology Information |
| NDAP | 4-nitro-2,4-diazabutanal |
| NED | N-1-naphthylethylenediamine dihydrochloride |
| OD | Optical Density |
| ORF | Open Reading Frame |
| PAGE | Poly-Acrylamide Gel Electrophoresis |
| PBS | Phosphate Buffered Saline |
| PCR | Polymerase Chain Reaction |
| PDB | Protein Data Bank |
| PMSF | Phenyl-Methane-Sulphonyl-Fluoride |
| RDX | Hexahydro-1,3,5-trinitro-1,3,5-triazine, Royal Demolition Explosive |
| RNA | ribonucleic acid |
| rpm | revolutions per minute |

| | |
|-----------|--|
| SDS | Sodium Dodecyl Sulphate |
| SNP | Single Nucleotide Polymorphism |
| SOC | Super Optimal broth with Catabolite repression |
| TCA | Trichloroacetic acid |
| TNT | 2,4,6-trinitrotoluene |
| TNX | hexahydro-1,3,5-trinitroso-1,3,5-triazine |
| TRIS | Tris(hydroxymethyl)aminomethane |
| tRNA | Transfer RNA |
| UV | Ultra Violet |
| v/v | Volume/volume |
| w/v | Weight/volume |
| XplA | Explosive-degrading enzyme A, Cytochrome P450 (CYP177A1) |
| XplA-heme | Heme domain of XplA |
| XplB | Explosive-degrading enzyme B, flavodoxin reductase |

References

1. van der Meer, J.R. and V. Sentchilo, *Genomic islands and the evolution of catabolic pathways in bacteria*. Current Opinion in Biotechnology, 2003. **14**(3): p. 248-254.
2. Sinha, S., et al., *Microbial transformation of xenobiotics for environmental bioremediation*. African Journal of Biotechnology, 2011. **8**(22).
3. Agarwal, S., *Environment Biotechnology*. 2007: APH Publishing. Page 274.
4. Moriarty, F., *Ecotoxicology*. Human & Experimental Toxicology, 1988. **7**(5): p. 437-441.
5. van der Meer, J.R., *Environmental pollution promotes selection of microbial degradation pathways*. Frontiers in Ecology and the Environment, 2006. **4**(1): p. 35-42.
6. Arber, W., *Genetic variation: molecular mechanisms and impact on microbial evolution*. FEMS Microbiol Rev, 2000. **24**(1): p. 1-7.
7. Ochman, H., J.G. Lawrence, and E.A. Groisman, *Lateral gene transfer and the nature of bacterial innovation*. Nature, 2000. **405**(6784): p. 299-304.
8. Hacker, J. and E. Carniel, *Ecological fitness, genomic islands and bacterial pathogenicity*. EMBO reports, 2001. **2**(5): p. 376-381.
9. Horikoshi, K., *Barophiles: deep-sea microorganisms adapted to an extreme environment*. Current Opinion in Microbiology, 1998. **1**(3): p. 291-295.
10. Nojiri, H., M. Shintani, and T. Omori, *Divergence of mobile genetic elements involved in the distribution of xenobiotic-catabolic capacity*. Applied Microbiology and Biotechnology, 2004. **64**(2): p. 154-174.
11. Dobrindt, U., et al., *Genomic islands in pathogenic and environmental microorganisms*. Nat Rev Microbiol, 2004. **2**(5): p. 414-24.
12. Kimura, M., *Evolutionary Rate at the Molecular Level*. Nature, 1968. **217**(5129): p. 624-626.
13. Ohta, T., *Slightly Deleterious Mutant Substitutions in Evolution*. Nature, 1973. **246**(5428): p. 96-98.
14. Eyre-Walker, A. and P.D. Keightley, *The distribution of fitness effects of new mutations*. Nat Rev Genet, 2007. **8**(8): p. 610-618.
15. Endo, T., K. Ikeo, and T. Gojobori, *Large-scale search for genes on which positive selection may operate*. Mol Biol Evol, 1996. **13**(5): p. 685-90.

16. Seffernick, J.L., et al., *Melamine Deaminase and Atrazine Chlorohydrolase: 98 Percent Identical but Functionally Different*. *Journal of Bacteriology*, 2001. **183**(8): p. 2405-2410.
17. Chi, F., et al., *Crossing the barrier: Evolution and spread of a major class of mosaic pbp2x in Streptococcus pneumoniae, S. mitis and S. oralis*. *International Journal of Medical Microbiology*, 2007. **297**(7–8): p. 503-512.
18. Pries, F., et al., *The role of spontaneous cap domain mutations in haloalkane dehalogenase specificity and evolution*. *Journal of Biological Chemistry*, 1994. **269**(26): p. 17490-4.
19. Hughes, D., *Evaluating genome dynamics: the constraints on rearrangements within bacterial genomes*. *Genome Biol*, 2000. **1**(6): p. Reviews0006.
20. Brüssow, H., C. Canchaya, and W.-D. Hardt, *Phages and the evolution of bacterial pathogens: from genomic rearrangements to lysogenic conversion*. *Microbiology and Molecular Biology Reviews*, 2004. **68**(3): p. 560-602.
21. Moran, N.A., *Microbial minimalism: genome reduction in bacterial pathogens*. *Cell*, 2002. **108**(5): p. 583-6.
22. Maurelli, A.T., et al., *“Black holes” and bacterial pathogenicity: A large genomic deletion that enhances the virulence of Shigella spp. and enteroinvasive Escherichia coli*. *Proceedings of the National Academy of Sciences*, 1998. **95**(7): p. 3943-3948.
23. Kresse, A.U., et al., *Impact of large chromosomal inversions on the adaptation and evolution of Pseudomonas aeruginosa chronically colonizing cystic fibrosis lungs*. *Mol Microbiol*, 2003. **47**(1): p. 145-58.
24. Campo, N., et al., *Chromosomal constraints in Gram-positive bacteria revealed by artificial inversions*. *Mol Microbiol*, 2004. **51**(2): p. 511-22.
25. Tsuda, M., et al., *Mobile catabolic genes in bacteria*. *Journal of Bioscience and Bioengineering*, 1999. **87**(4): p. 401-410.
26. Grindley, N.D.F. and R.R. Reed, *Transpositional Recombination in Prokaryotes*. *Annual Review of Biochemistry*, 1985. **54**(1): p. 863-896.
27. Mahillon, J. and M. Chandler, *Insertion Sequences*. *Microbiology and Molecular Biology Reviews*, 1998. **62**(3): p. 725-774.
28. van der Meer, J.R., A.J. Zehnder, and W.M. de Vos, *Identification of a novel composite transposable element, Tn5280, carrying chlorobenzene dioxygenase genes of Pseudomonas sp. strain P51*. *J Bacteriol*, 1991. **173**(22): p. 7077-83.
29. Fong, K.P.Y., C.B.H. Goh, and H.-M. Tan, *The Genes for Benzene Catabolism in Pseudomonas putida ML2 Are Flanked by Two Copies of the Insertion Element IS1489, Forming a Class-I-Type Catabolic Transposon, Tn5542*. *Plasmid*, 2000. **43**(2): p. 103-110.

30. Grindley, N.D.F., *Transposition of Tn3 and related transposons*. Cell, 1983. **32**(1): p. 3-5.
31. Burrus, V., et al., *Conjugative transposons: the tip of the iceberg*. Molecular Microbiology, 2002. **46**(3): p. 601-610.
32. Burrus, V. and M.K. Waldor, *Shaping bacterial genomes with integrative and conjugative elements*. Res Microbiol, 2004. **155**(5): p. 376-86.
33. Wozniak, R.A. and M.K. Waldor, *Integrative and conjugative elements: mosaic mobile genetic elements enabling dynamic lateral gene flow*. Nat Rev Microbiol, 2010. **8**(8): p. 552-63.
34. Hsiao, W.W., et al., *Evidence of a large novel gene pool associated with prokaryotic genomic islands*. PLoS Genet, 2005. **1**(5): p. e62.
35. Ravatn, R., et al., *Chromosomal Integration, Tandem Amplification, and Deamplification in Pseudomonas putida F1 of a 105-Kilobase Genetic Element Containing the Chlorocatechol Degradative Genes from Pseudomonas sp. Strain B13*. Journal of Bacteriology, 1998. **180**(17): p. 4360-4369.
36. Gaillard, M., et al., *The clc element of Pseudomonas sp. strain B13, a genomic island with various catabolic properties*. J Bacteriol, 2006. **188**(5): p. 1999-2013.
37. Toussaint, A., et al., *The Biphenyl- and 4-Chlorobiphenyl-Catabolic Transposon Tn4371, a Member of a New Family of Genomic Islands Related to IncP and Ti Plasmids*. Applied and Environmental Microbiology, 2003. **69**(8): p. 4837-4845.
38. Nishi, A., K. Tominaga, and K. Furukawa, *A 90-kilobase conjugative chromosomal element coding for biphenyl and salicylate catabolism in Pseudomonas putida KF715*. J Bacteriol, 2000. **182**(7): p. 1949-55.
39. Hickey, W.J., S. Chen, and J. Zhao, *The phn Island: A New Genomic Island Encoding Catabolism of Polynuclear Aromatic Hydrocarbons*. Frontiers in microbiology, 2012. **3**: p. 125.
40. Nakamura, Y., et al., *Biased biological functions of horizontally transferred genes in prokaryotic genomes*. Nat Genet, 2004. **36**(7): p. 760-766.
41. Chen, I. and D. Dubnau, *DNA uptake during bacterial transformation*. Nat Rev Microbiol, 2004. **2**(3): p. 241-9.
42. Dubnau, D., *DNA uptake in bacteria*. Annu Rev Microbiol, 1999. **53**: p. 217-44.
43. Lorenz, M.G. and W. Wackernagel, *Bacterial gene transfer by natural genetic transformation in the environment*. Microbiol Rev, 1994. **58**(3): p. 563-602.
44. Johnsborg, O., V. Eldholm, and L.S. Håvarstein, *Natural genetic transformation: prevalence, mechanisms and function*. Research in Microbiology, 2007. **158**(10): p. 767-778.

45. Canchaya, C., et al., *Phage as agents of lateral gene transfer*. Current Opinion in Microbiology, 2003. **6**(4): p. 417-424.
46. Groth, A.C. and M.P. Calos, *Phage Integrases: Biology and Applications*. Journal of Molecular Biology, 2004. **335**(3): p. 667-678.
47. Edlin, G., L. Lin, and R. Bitner, *Reproductive fitness of P1, P2, and Mu lysogens of Escherichia coli*. Journal of Virology, 1977. **21**(2): p. 560-564.
48. Ruzin, A., J. Lindsay, and R.P. Novick, *Molecular genetics of SaPII – a mobile pathogenicity island in Staphylococcus aureus*. Molecular Microbiology, 2001. **41**(2): p. 365-377.
49. Grohmann, E., G. Muth, and M. Espinosa, *Conjugative Plasmid Transfer in Gram-Positive Bacteria*. Microbiology and Molecular Biology Reviews, 2003. **67**(2): p. 277-301.
50. Stuart-Keil, K.G., et al., *Plasmids Responsible for Horizontal Transfer of Naphthalene Catabolism Genes between Bacteria at a Coal Tar-Contaminated Site Are Homologous to pDTG1 from Pseudomonas putida NCIB 9816-4*. Applied and Environmental Microbiology, 1998. **64**(10): p. 3633-3640.
51. Dodge, A.G., L.P. Wackett, and M.J. Sadowsky, *Plasmid Localization and Organization of Melamine Degradation Genes in Rhodococcus sp. Strain Mel*. Applied and Environmental Microbiology, 2012. **78**(5): p. 1397-1403.
52. Smit, E., A. Wolters, and J.D. van Elsas, *Self-Transmissible Mercury Resistance Plasmids with Gene-Mobilizing Capacity in Soil Bacterial Populations: Influence of Wheat Roots and Mercury Addition*. Applied and Environmental Microbiology, 1998. **64**(4): p. 1210-1219.
53. *Introduction of explosives*, in *Chemistry of Explosives (2)*, J. Akhavan, Editor. 2004, The Royal Society of Chemistry. p. 1-20.
54. French, C.E., S.J. Rosser, and N.C. Bruce, *Biotransformations of explosives*. Biotechnology and Genetic Engineering Reviews, 2001. **18**(1): p. 171-217.
55. Rylott, E.L. and N.C. Bruce, *Plants disarm soil: engineering plants for the phytoremediation of explosives*. Trends Biotechnol, 2009. **27**(2): p. 73-81.
56. *Chemsketch*. 2014, Advanced Chemistry Development, Inc.: Toronto, ON, Canada.
57. Chong, C.S., *Biodegradation of RDX in Rhodococcus spp.*, in *Department of Biology*. 2011, University of York.
58. Stenuit, B., et al., *Promising Strategies for the Mineralisation of 2,4,6-trinitrotoluene*. Reviews in Environmental Science and Bio/Technology, 2005. **4**(1-2): p. 39-60.
59. Hannink, N.K., S.J. Rosser, and N.C. Bruce, *Phytoremediation of Explosives*. Critical Reviews in Plant Sciences, 2002. **21**(5): p. 511-538.

60. Clausen, J., et al., *A case study of contaminants on military ranges: Camp Edwards, Massachusetts, USA*. Environmental Pollution, 2004. **129**(1): p. 13-21.
61. Pichtel, J., *Distribution and Fate of Military Explosives and Propellants in Soil: A Review*. Applied and Environmental Soil Science, 2012. **2012**: p. 33.
62. *DOD Operational Ranges. More Reliable Cleanup Cost Estimates and a Proactive Approach to Identifying Contamination Are Needed*. 2004, U.S. Government Accountability Office (GAO).
63. Jenkins, T.F., et al., *Identity and distribution of residues of energetic compounds at army live-fire training ranges*. Chemosphere, 2006. **63**(8): p. 1280-1290.
64. Clausen, J.L., *Range assessment lessons learned*. Federal Facilities Environmental Journal, 2005. **16**(2): p. 49-62.
65. Alavi, G., et al., *The fate and transport of RDX, HMX, TNT and DNT in the volcanic soils of Hawaii: a laboratory and modeling study*. J Hazard Mater, 2011. **185**(2-3): p. 1600-4.
66. USEPA, *Handbook on the management of munitions response actions; EPA 505-B-01-001*, in *Office of Solid Waste and Emergency Response, Washington DC*. 2005.
67. Frische, T., *Screening for soil toxicity and mutagenicity using luminescent bacteria--a case study of the explosive 2,4,6-trinitrotoluene (TNT)*. Ecotoxicol Environ Saf, 2002. **51**(2): p. 133-44.
68. Sunahara, G.I., et al., *Ecotoxicological characterization of energetic substances using a soil extraction procedure*. Ecotoxicology and Environmental Safety, 1999. **43**(2): p. 138-148.
69. Berthe-Corti, L., et al., *Cytotoxicity and mutagenicity of a 2,4,6-trinitrotoluene (TNT) and hexogen contaminated soil in S. typhimurium and mammalian cells*. Chemosphere, 1998. **37**(2): p. 209-218.
70. Pavlostathis, S.G., et al., *Transformaton of 2,4,6-trinitrotoluene by the aquatic plant Myriophyllum spicatum*. Environmental Toxicology and Chemistry, 1998. **17**(11): p. 2266-2273.
71. *Toxicological Profile for 2,4,6-Trinitrotoluene*, in *ATSDR's Toxicological Profiles*. 2002, CRC Press.
72. Kucukardali, Y., et al., *Accidental oral poisoning caused by RDX (cyclonite): a report of 5 cases*. J Intensive Care Med, 2003. **18**(1): p. 42-6.
73. Dilley, J.V., et al., *Short-term oral toxicity of a 2,4,6-trinitrotoluene and hexahydro-1,3,5-trinitro-1,3,5-triazine mixture in mice, rats, and dogs*. J Toxicol Environ Health, 1982. **9**(4): p. 587-610.
74. Winfield, L.E., J.H. Rodgers, Jr., and S.J. D'Surney, *The responses of selected terrestrial plants to short (<12 days) and long term (2, 4 and 6 weeks)*

- hexahydro-1,3,5-trinitro-1,3,5-triazine (RDX) exposure. Part I: Growth and developmental effects.* *Ecotoxicology*, 2004. **13**(4): p. 335-47.
75. Symons, Z.C. and N.C. Bruce, *Bacterial pathways for degradation of nitroaromatics.* *Natural Product Reports*, 2006. **23**(6): p. 845-850.
 76. Duque, E., et al., *Construction of a Pseudomonas hybrid strain that mineralizes 2,4,6-trinitrotoluene.* *Journal of Bacteriology*, 1993. **175**(8): p. 2278-2283.
 77. French, C.E., S. Nicklin, and N.C. Bruce, *Aerobic Degradation of 2,4,6-Trinitrotoluene by Enterobacter cloacae PB2 and by Pentaerythritol Tetranitrate Reductase.* *Applied and Environmental Microbiology*, 1998. **64**(8): p. 2864-2868.
 78. Pak, J.W., et al., *Transformation of 2,4,6-Trinitrotoluene by Purified Xenobiotic Reductase B from Pseudomonas fluorescens I-C.* *Applied and Environmental Microbiology*, 2000. **66**(11): p. 4742-4750.
 79. Caballero, A., et al., *PnrA, a new nitroreductase-family enzyme in the TNT-degrading strain Pseudomonas putida JLR11.* *Environmental Microbiology*, 2005. **7**(8): p. 1211-1219.
 80. Esteve-Núñez, A., A. Caballero, and J.L. Ramos, *Biological Degradation of 2,4,6-Trinitrotoluene.* *Microbiology and Molecular Biology Reviews*, 2001. **65**(3): p. 335-352.
 81. Rylott, E.L., A. Lorenz, and N.C. Bruce, *Biodegradation and biotransformation of explosives.* *Curr Opin Biotechnol*, 2010.
 82. Bryant, C. and M. DeLuca, *Purification and characterization of an oxygen-insensitive NAD(P)H nitroreductase from Enterobacter cloacae.* *Journal of Biological Chemistry*, 1991. **266**(7): p. 4119-25.
 83. Vorbeck, C., et al., *Initial Reductive Reactions in Aerobic Microbial Metabolism of 2,4,6-Trinitrotoluene.* *Applied and Environmental Microbiology*, 1998. **64**(1): p. 246-252.
 84. Rylott, E.L., et al., *Engineering plants for the phytoremediation of RDX in the presence of the co-contaminating explosive TNT.* *New Phytologist*, 2011. **192**(2): p. 405-413.
 85. Bhushan, B., et al., *Biotransformation of hexahydro-1,3,5-trinitro-1,3,5-triazine (RDX) by a rabbit liver cytochrome P450: insight into the mechanism of RDX biodegradation by Rhodococcus sp. strain DN22.* *Appl Environ Microbiol*, 2003. **69**(3): p. 1347-51.
 86. McCormick, N.G., J.H. Cornell, and A.M. Kaplan, *Biodegradation of hexahydro-1,3,5-trinitro-1,3,5-triazine.* *Appl Environ Microbiol*, 1981. **42**(5): p. 817-23.

87. Hawari, J., et al., *Characterization of metabolites during biodegradation of hexahydro-1, 3,5-trinitro-1,3,5-triazine (RDX) with municipal anaerobic sludge*. Appl Environ Microbiol, 2000. **66**(6): p. 2652-7.
88. Annamaria, H., et al., *Biodegradation of RDX and MNX with Rhodococcus sp. Strain DN22: New Insights into the Degradation Pathway*. Environmental Science & Technology, 2010. **44**(24): p. 9330-9336.
89. Fournier, D., et al., *Determination of key metabolites during biodegradation of hexahydro-1,3,5-trinitro-1,3,5-triazine with Rhodococcus sp. strain DN22*. Appl Environ Microbiol, 2002. **68**(1): p. 166-72.
90. Kitts, C.L., et al., *Type I nitroreductases in soil enterobacteria reduce TNT (2,4,6-trinitrotoluene) and RDX (hexahydro-1,3,5-trinitro-1,3,5-triazine)*. Canadian Journal of Microbiology, 2000. **46**(3): p. 278-282.
91. Bhushan, B., et al., *Biotransformation of Hexahydro-1,3,5-trinitro-1,3,5-triazine Catalyzed by a NAD(P)H: Nitrate Oxidoreductase from Aspergillus niger*. Environmental Science & Technology, 2002. **36**(14): p. 3104-3108.
92. Kitts, C.L., D.P. Cunningham, and P.J. Unkefer, *Isolation of three hexahydro-1,3,5-trinitro-1,3,5-triazine-degrading species of the family Enterobacteriaceae from nitramine explosive-contaminated soil*. Applied and Environmental Microbiology, 1994. **60**(12): p. 4608-4611.
93. Zhao, J.S., et al., *Metabolism of hexahydro-1,3,5-trinitro-1,3,5-triazine through initial reduction to hexahydro-1-nitroso-3,5-dinitro-1,3,5-triazine followed by denitration in Clostridium bifermentans HAW-1*. Applied Microbiology and Biotechnology, 2003. **63**(2): p. 187-193.
94. Fuller, M.E., et al., *Transformation of RDX and other energetic compounds by xenobiotic reductases XenA and XenB*. Applied Microbiology and Biotechnology, 2009. **84**(3): p. 535-544.
95. Jackson, R.G., et al., *Exploring the biochemical properties and remediation applications of the unusual explosive-degrading P450 system XplA/B*. Proc Natl Acad Sci U S A, 2007. **104**(43): p. 16822-7.
96. Seth-Smith, H.M.B., et al., *Cloning, Sequencing, and Characterization of the Hexahydro-1,3,5-Trinitro-1,3,5-Triazine Degradation Gene Cluster from Rhodococcus rhodochrous*. Applied and Environmental Microbiology, 2002. **68**(10): p. 4764-4771.
97. Bhushan, B., et al., *Diaphorase catalyzed biotransformation of RDX via N-denitration mechanism*. Biochemical and Biophysical Research Communications, 2002. **296**(4): p. 779-784.
98. Rylott, E.L., et al., *An explosive-degrading cytochrome P450 activity and its targeted application for the phytoremediation of RDX*. Nat Biotech, 2006. **24**(2): p. 216-219.

99. Sabbadin, F., et al., *The 1.5-angstrom Structure of XplA-heme, an Unusual Cytochrome P450 Heme Domain That Catalyzes Reductive Biotransformation of Royal Demolition Explosive*. Journal of Biological Chemistry, 2009. **284**(41): p. 28467-28475.
100. Seth-Smith, H.M.B., et al., *The explosive-degrading cytochrome P450 system is highly conserved among strains of Rhodococcus spp.* Applied and Environmental Microbiology, 2008. **74**(14): p. 4550-4552.
101. Bernstein, A., et al., *Isolation and characterization of RDX-degrading Rhodococcus species from a contaminated aquifer*. Biodegradation, 2011. **22**(5): p. 997-1005.
102. Indest, K.J., F.H. Crocker, and R. Athow, *A TaqMan polymerase chain reaction method for monitoring RDX-degrading bacteria based on the xplA functional gene*. J Microbiol Methods, 2007. **68**(2): p. 267-74.
103. Andeer, P.F., et al., *Lateral Transfer of Genes for Hexahydro-1,3,5-Trinitro-1,3,5-Triazine (RDX) Degradation*. Applied and Environmental Microbiology, 2009. **75**(10): p. 3258-3262.
104. Jung, C.M., et al., *Horizontal gene transfer (HGT) as a mechanism of disseminating RDX-degrading activity among Actinomycete bacteria*. J Appl Microbiol, 2011.
105. Indest, K.J., et al., *Functional Characterization of pGKT2, a 182-Kilobase Plasmid Containing the xplAB Genes, Which Are Involved in the Degradation of Hexahydro-1,3,5-Trinitro-1,3,5-Triazine by Gordonia sp. Strain KTR9*. Applied and Environmental Microbiology, 2010. **76**(19): p. 6329-6337.
106. Nejidat, A., et al., *Effect of organic and inorganic nitrogenous compounds on RDX degradation and cytochrome P-450 expression in Rhodococcus strain YH1*. Biodegradation, 2008. **19**(3): p. 313-320.
107. Untergasser, A., et al., *Primer3--new capabilities and interfaces*. Nucleic Acids Res, 2012. **40**(15): p. e115.
108. Koressaar, T. and M. Remm, *Enhancements and modifications of primer design program Primer3*. Bioinformatics, 2007. **23**(10): p. 1289-91.
109. Satokari, R.M., et al., *Bifidobacterial Diversity in Human Feces Detected by Genus-Specific PCR and Denaturing Gradient Gel Electrophoresis*. Applied and Environmental Microbiology, 2001. **67**(2): p. 504-513.
110. Seth-Smith, H.M., et al., *Cloning, sequencing, and characterization of the hexahydro-1,3,5-Trinitro-1,3,5-triazine degradation gene cluster from Rhodococcus rhodochrous*. Appl Environ Microbiol, 2002. **68**(10): p. 4764-71.
111. Brenner, A., et al., *Use of Hexahydro-1,3,5-Trinitro-1,3,5-Triazine as a Nitrogen Source in Biological Treatment of Munitions Wastes*. Water Environment Research, 2000. **72**(4): p. 469-475.

112. Coleman, N.V., D.R. Nelson, and T. Duxbury, *Aerobic biodegradation of hexahydro-1,3,5-trinitro-1,3,5-triazine (RDX) as a nitrogen source by a Rhodococcus sp., strain DN22*. *Soil Biology & Biochemistry*, 1998. **30**(8-9): p. 1159-1167.
113. Andeer, P., et al., *Identification of microbial populations assimilating nitrogen from RDX in munitions contaminated military training range soils by high sensitivity stable isotope probing*. *Environ Sci Technol*, 2013. **47**(18): p. 10356-63.
114. Thompson, K.T., F.H. Crocker, and H.L. Fredrickson, *Mineralization of the cyclic nitramine explosive hexahydro-1,3,5-trinitro-1,3,5-triazine by Gordonia and Williamsia spp.* *Applied and Environmental Microbiology*, 2005. **71**(12): p. 8265-8272.
115. Rosenberger, R.F. and S.R. Elsdén, *The yields of Streptococcus faecalis grown in continuous culture*. *J Gen Microbiol*, 1960. **22**: p. 726-39.
116. Lynch, J.C., et al., *Effects of pH and Temperature on the Aqueous Solubility and Dissolution Rate of 2,4,6-Trinitrotoluene (TNT), Hexahydro-1,3,5-trinitro-1,3,5-triazine (RDX), and Octahydro-1,3,5,7-tetranitro-1,3,5,7-tetrazocine (HMX)*. *Journal of Chemical & Engineering Data*, 2001. **46**(6): p. 1549-1555.
117. Quail, M.A., et al., *A tale of three next generation sequencing platforms: comparison of Ion Torrent, Pacific Biosciences and Illumina MiSeq sequencers*. *BMC Genomics*, 2012. **13**: p. 341-341.
118. Tamura, K., et al., *MEGA4: Molecular Evolutionary Genetics Analysis (MEGA) Software Version 4.0*. *Molecular Biology and Evolution*, 2007. **24**(8): p. 1596-1599.
119. Laemmli, U.K., *Cleavage of Structural Proteins during the Assembly of the Head of Bacteriophage T4*. *Nature*, 1970. **227**(5259): p. 680-685.
120. Pettersen, E.F., et al., *UCSF Chimera--a visualization system for exploratory research and analysis*. *J Comput Chem*, 2004. **25**(13): p. 1605-12.
121. Jackson, R.G., et al., *Exploring the biochemical properties and remediation applications of the unusual explosive-degrading P450 system XpIA/B*. *Proceedings of the National Academy of Sciences of the United States of America*, 2007. **104**(43): p. 16822-16827.
122. Sagi-Ben Moshe, S., et al., *Sequential biodegradation of TNT, RDX and HMX in a mixture*. *Environmental Pollution*, 2009. **157**(8-9): p. 2231-2238.
123. Wawrik, B., et al., *Effect of different carbon sources on community composition of bacterial enrichments from soil*. *Appl Environ Microbiol*, 2005. **71**(11): p. 6776-83.
124. Kimura, N. and Y. Urushigawa, *Metabolism of dibenzo-p-dioxin and chlorinated dibenzo-p-dioxin by a gram-positive bacterium, Rhodococcus opacus SAO101*. *J Biosci Bioeng*, 2001. **92**(2): p. 138-43.

125. Binks, P.R., S. Nicklin, and N.C. Bruce, *Degradation of hexahydro-1,3,5-trinitro-1,3,5-triazine (RDX) by Stenotrophomonas maltophilia PBI*. Applied and Environmental Microbiology, 1995. **61**(4): p. 1318-22.
126. Chang, H.W., et al., *Characterization of Pseudomonas sp. HK-6 cells responding to explosive RDX (hexahydro-1,3,5-trinitro-1,3,5-triazine)*. Applied Microbiology and Biotechnology, 2004. **65**(3): p. 323-329.
127. Wawrik, B., et al., *Effect of different carbon sources on community composition of bacterial enrichments from soil*. Applied and Environmental Microbiology, 2005. **71**(11): p. 6776-6783.
128. Rylott, E.L., et al., *The explosive-degrading cytochrome P450 XplA: biochemistry, structural features and prospects for bioremediation*. Biochim Biophys Acta, 2011. **1814**(1): p. 230-6.
129. Sumbali, G. and R.S. Mehrotra, *Principles Of Microbiology*. 2009: New Delhi : Tata McGraw-Hill. Page 99-100.
130. Sekine, M., et al., *Sequence analysis of three plasmids harboured in Rhodococcus erythropolis strain PR4*. Environ Microbiol, 2006. **8**(2): p. 334-46.
131. Zampolli, J., et al., *Biodegradation of variable-chain-length n-alkanes in Rhodococcus opacus R7 and the involvement of an alkane hydroxylase system in the metabolism*. AMB Express, 2014. **4**(1): p. 73.
132. Asturias, J.A. and K.N. Timmis, *Three different 2,3-dihydroxybiphenyl-1,2-dioxygenase genes in the gram-positive polychlorobiphenyl-degrading bacterium Rhodococcus globerulus P6*. J Bacteriol, 1993. **175**(15): p. 4631-40.
133. Saeki, H., et al., *Degradation of trichloroethene by a linear-plasmid-encoded alkene monooxygenase in Rhodococcus corallinus (Nocardia corallina) B-276*. Microbiology, 1999. **145** (Pt 7): p. 1721-30.
134. Li, R.W., et al., *Metagenomic Insights into the RDX-Degrading Potential of the Ovine Rumen Microbiome*. PLoS ONE, 2014. **9**(11): p. e110505.
135. Hwang, P., T. Chow, and N.R. Adrian, *Transformation of trinitrotoluene to triaminotoluene by mixed cultures incubated under methanogenic conditions*. Environmental Toxicology and Chemistry, 2000. **19**(4): p. 836-841.
136. Oh, B.-T., et al., *TNT Biotransformation and Detoxification by a Pseudomonas Aeruginosa Strain*. Biodegradation, 2003. **14**(5): p. 309-319.
137. Boopathy, R. and C.F. Kulpa, *Biotransformation of 2,4,6-trinitrotoluene (TNT) by a Methanococcus sp. (strain B) isolated from a lake sediment*. Can J Microbiol, 1994. **40**(4): p. 273-8.
138. Hoehamer, C.F., N.L. Wolfe, and K.E.L. Eriksson, *Biotransformation of 2,4,6-Trinitrotoluene (TNT) by the Fungus Fusarium Oxysporum*. International Journal of Phytoremediation, 2006. **8**(2): p. 95-105.

139. Fernando, T., J.A. Bumpus, and S.D. Aust, *Biodegradation of TNT (2,4,6-trinitrotoluene) by Phanerochaete chrysosporium*. Applied and Environmental Microbiology, 1990. **56**(6): p. 1666-1671.
140. Maeda, T., K. Kadokami, and H.I. Ogawa, *Characterization of 2,4,6-trinitrotoluene (TNT)-metabolizing bacteria isolated from TNT-polluted soils in the Yamada Green Zone, Kitakyushu, Japan*. Journal of environmental biotechnology, 2006. **6**(1): p. 33-39.
141. Fuller, M.E. and J.F. Manning, Jr., *Aerobic gram-positive and gram-negative bacteria exhibit differential sensitivity to and transformation of 2,4,6-trinitrotoluene (TNT)*. Curr Microbiol, 1997. **35**(2): p. 77-83.
142. Young, D.M., P.J. Unkefer, and K.L. Ogden, *Biotransformation of hexahydro-1,3,5-trinitro-1,3,5-triazine (RDX) by a prospective consortium and its most effective isolate Serratia marcescens*. Biotechnol Bioeng, 1997. **53**(5): p. 515-22.
143. Regan, K.M. and R.L. Crawford, *CHARACTERIZATION OF CLOSTRIDIUM-BIFERMENTANS AND ITS BIOTRANSFORMATION OF 2,4,6-TRINITROTOLUENE (TNT) AND 1,3,5-TRIAZA-1,3,5-TRINITROCYCLOHEXANE (RDX)*. Biotechnology Letters, 1994. **16**(10): p. 1081-1086.
144. Chong, C.S., et al., *Analysis of the xplAB-Containing Gene Cluster Involved in the Bacterial Degradation of the Explosive Hexahydro-1,3,5-Trinitro-1,3,5-Triazine*. Applied and Environmental Microbiology, 2014. **80**(21): p. 6601-6610.
145. Van Domselaar, G.H., et al., *BASys: a web server for automated bacterial genome annotation*. Nucleic Acids Res, 2005. **33**(Web Server issue): p. W455-9.
146. van den Wijngaard, A.J., et al., *Degradation of 1,2-dichloroethane by Ancylobacter aquaticus and other facultative methylotrophs*. Appl Environ Microbiol, 1992. **58**(3): p. 976-83.
147. Clark, I.C., et al., *Structure and evolution of chlorate reduction composite transposons*. MBio, 2013. **4**(4).
148. Herrick, J.B., et al., *Natural horizontal transfer of a naphthalene dioxygenase gene between bacteria native to a coal tar-contaminated field site*. Applied and Environmental Microbiology, 1997. **63**(6): p. 2330-7.
149. Sielaff, B. and J.R. Andreesen, *Analysis of the nearly identical morpholine monooxygenase-encoding mor genes from different Mycobacterium strains and characterization of the specific NADH:ferredoxin oxidoreductase of this cytochrome P450 system*. Microbiology, 2005. **151**(8): p. 2593-2603.
150. de Souza, M.L., et al., *The Atrazine Catabolism Genes atzABC Are Widespread and Highly Conserved*. Journal of Bacteriology, 1998. **180**(7): p. 1951-1954.

151. Janssen, D.B., et al., *Bacterial degradation of xenobiotic compounds: evolution and distribution of novel enzyme activities*. Environmental Microbiology, 2005. **7**(12): p. 1868-1882.
152. Springael, D., et al., *Occurrence of Tn4371-related mobile elements and sequences in (chloro)biphenyl-degrading bacteria*. Appl Environ Microbiol, 2001. **67**(1): p. 42-50.
153. Song, J.S., et al., *Genetic organization of the dhlA gene encoding 1,2-dichloroethane dechlorinase from Xanthobacter flavus UE15*. J Microbiol, 2004. **42**(3): p. 188-93.
154. Chen, H.-P., et al., *Genomic and Transcriptomic Studies of an RDX (Hexahydro-1,3,5-Trinitro-1,3,5-Triazine)-Degrading Actinobacterium*. Applied and Environmental Microbiology, 2012. **78**(21): p. 7798-7800.
155. Brown, J.R., et al., *Evolutionary relationships of bacterial and archaeal glutamine synthetase genes*. Journal of Molecular Evolution, 1994. **38**(6): p. 566-576.
156. Murray, D.S., et al., *Structures of the Bacillus subtilis Glutamine Synthetase Dodecamer Reveal Large Intersubunit Catalytic Conformational Changes Linked to a Unique Feedback Inhibition Mechanism*. Journal of Biological Chemistry, 2013. **288**(50): p. 35801-35811.
157. Hayward, D., P. van Helden, and I. Wiid, *Glutamine synthetase sequence evolution in the mycobacteria and their use as molecular markers for Actinobacteria speciation*. BMC Evolutionary Biology, 2009. **9**(1): p. 48.
158. Fisher, S.H. and L.V. Wray, *Bacillus subtilis glutamine synthetase regulates its own synthesis by acting as a chaperone to stabilize GlnR–DNA complexes*. Proceedings of the National Academy of Sciences, 2008. **105**(3): p. 1014-1019.
159. Wray, L.V., Jr., J.M. Zalieckas, and S.H. Fisher, *Bacillus subtilis glutamine synthetase controls gene expression through a protein-protein interaction with transcription factor TnrA*. Cell, 2001. **107**(4): p. 427-35.
160. Wray, L.V., Jr., et al., *TnrA, a transcription factor required for global nitrogen regulation in Bacillus subtilis*. Proc Natl Acad Sci U S A, 1996. **93**(17): p. 8841-5.
161. Aliverti, A., B. Curti, and M.A. Vanoni, *Identifying and quantitating FAD and FMN in simple and in iron-sulfur-containing flavoproteins*. Methods Mol Biol, 1999. **131**: p. 9-23.
162. Kingdon, H.S., J.S. Hubbard, and E.R. Stadtman, *Regulation of glutamine synthetase. XI. The nature and implications of a lag phase in the Escherichia coli glutamine synthetase reaction*. Biochemistry, 1968. **7**(6): p. 2136-42.
163. Muller, J.J., et al., *Adrenodoxin reductase-adrenodoxin complex structure suggests electron transfer path in steroid biosynthesis*. J Biol Chem, 2001. **276**(4): p. 2786-9.

164. Bui, S.H., *Characterisation of the RDX-degrading XplA/XplB Redox System from Rhodococcus rhodochrous*. 2012, University of Manchester.
165. Smith, D.B. and K.S. Johnson, *Single-step purification of polypeptides expressed in Escherichia coli as fusions with glutathione S-transferase*. *Gene*, 1988. **67**(1): p. 31-40.
166. Wray, L.V., Jr. and S.H. Fisher, *Functional roles of the conserved Glu304 loop of Bacillus subtilis glutamine synthetase*. *J Bacteriol*, 2010. **192**(19): p. 5018-25.
167. Zhu, S.H., et al., *The essential role of nitrogen limitation in expression of xplA and degradation of hexahydro-1,3,5-trinitro-1,3,5-triazine (RDX) in Gordonia sp. strain KTR9*. *Appl Microbiol Biotechnol*, 2015. **99**(1): p. 459-67.
168. Indest, K.J., et al., *Role of nitrogen limitation in transformation of RDX (hexahydro-1,3,5-trinitro-1,3,5-triazine) by Gordonia sp. strain KTR9*. *Appl Environ Microbiol*, 2013. **79**(5): p. 1746-50.
169. Fisher, S.H., *Regulation of nitrogen metabolism in Bacillus subtilis: vive la différence!* *Molecular Microbiology*, 1999. **32**(2): p. 223-232.
170. TSUKAMURA, M., *Proposal of a New Genus, Gordona, for Slightly Acid-fast Organisms Occurring in Sputa of Patients With Pulmonary Disease and in Soil*. *Journal of General Microbiology*, 1971. **68**(1): p. 15-26.
171. Linos, A., et al., *Gordonia polyisoprenivorans sp. nov., a rubber-degrading actinomycete isolated from an automobile tyre*. *Int J Syst Bacteriol*, 1999. **49 Pt 4**: p. 1785-91.
172. Cserző, M., et al., *Prediction of transmembrane alpha-helices in prokaryotic membrane proteins: the dense alignment surface method*. *Protein Engineering*, 1997. **10**(6): p. 673-676.
173. Tusnady, G.E. and I. Simon, *Principles governing amino acid composition of integral membrane proteins: application to topology prediction*. *J Mol Biol*, 1998. **283**(2): p. 489-506.
174. Tusnady, G.E. and I. Simon, *The HMMTOP transmembrane topology prediction server*. *Bioinformatics*, 2001. **17**(9): p. 849-850.
175. Wallace, R.B., et al., *Oligonucleotide directed mutagenesis of the human beta-globin gene: a general method for producing specific point mutations in cloned DNA*. *Nucleic Acids Res*, 1981. **9**(15): p. 3647-56.
176. Dashuang, S., et al., *A single mutation in the active site swaps the substrate specificity of N-acetyl-L-ornithine transcarbamylase and N-succinyl-L-ornithine transcarbamylase*. *Protein Science*, 2007. **16**(8): p. 1689-1699.
177. Yasutake, Y., et al., *A single mutation at the ferredoxin binding site of P450 Vdh enables efficient biocatalytic production of 25-hydroxyvitamin D(3)*. *Chembiochem*, 2013. **14**(17): p. 2284-91.

178. Danielson, P.B., *The cytochrome P450 superfamily: biochemistry, evolution and drug metabolism in humans*. Curr Drug Metab, 2002. **3**(6): p. 561-97.
179. Bracco, P., D. Janssen, and A. Schallmeyer, *Selective steroid oxyfunctionalisation by CYP154C5, a bacterial cytochrome P450*. Microbial Cell Factories, 2013. **12**(1): p. 95.
180. Seth-Smith, H.M.B., *Microbial degradation of RDX*. 2002, University of Cambridge.
181. Hussain, H.A. and J.M. Ward, *Enhanced Heterologous Expression of Two Streptomyces griseolus Cytochrome P450s and Streptomyces coelicolor Ferredoxin Reductase as Potentially Efficient Hydroxylation Catalysts*. Applied and Environmental Microbiology, 2003. **69**(1): p. 373-382.
182. Terpe, K., *Overview of bacterial expression systems for heterologous protein production: from molecular and biochemical fundamentals to commercial systems*. Applied Microbiology and Biotechnology, 2006. **72**(2): p. 211-222.
183. Woestenenk, E.A., et al., *His tag effect on solubility of human proteins produced in Escherichia coli: a comparison between four expression vectors*. J Struct Funct Genomics, 2004. **5**(3): p. 217-29.
184. Busso, D., R. Kim, and S.-H. Kim, *Expression of soluble recombinant proteins in a cell-free system using a 96-well format*. Journal of Biochemical and Biophysical Methods, 2003. **55**(3): p. 233-240.
185. Einsle, O., et al., *Mechanism of the Six-Electron Reduction of Nitrite to Ammonia by Cytochrome c Nitrite Reductase*. Journal of the American Chemical Society, 2002. **124**(39): p. 11737-11745.
186. Lawrence, J.G. and J.R. Roth, *Selfish operons: horizontal transfer may drive the evolution of gene clusters*. Genetics, 1996. **143**(4): p. 1843-60.
187. Poelarends, G.J., et al., *Haloalkane-utilizing Rhodococcus strains isolated from geographically distinct locations possess a highly conserved gene cluster encoding haloalkane catabolism*. J Bacteriol, 2000. **182**(10): p. 2725-31.
188. Kulakov, L.A., et al., *Web-Type Evolution of Rhodococcus Gene Clusters Associated with Utilization of Naphthalene*. Applied and Environmental Microbiology, 2005. **71**(4): p. 1754-1764.
189. Quesada, J.M., M.I. Soriano, and M. Espinosa-Urgel, *Stability of a Pseudomonas putida KT2440 bacteriophage-carried genomic island and its impact on rhizosphere fitness*. Appl Environ Microbiol, 2012. **78**(19): p. 6963-74.
190. Halasz, A., et al., *Biodegradation of RDX nitroso products MNX and TNX by cytochrome P450 XplA*. Environ Sci Technol, 2012. **46**(13): p. 7245-51.